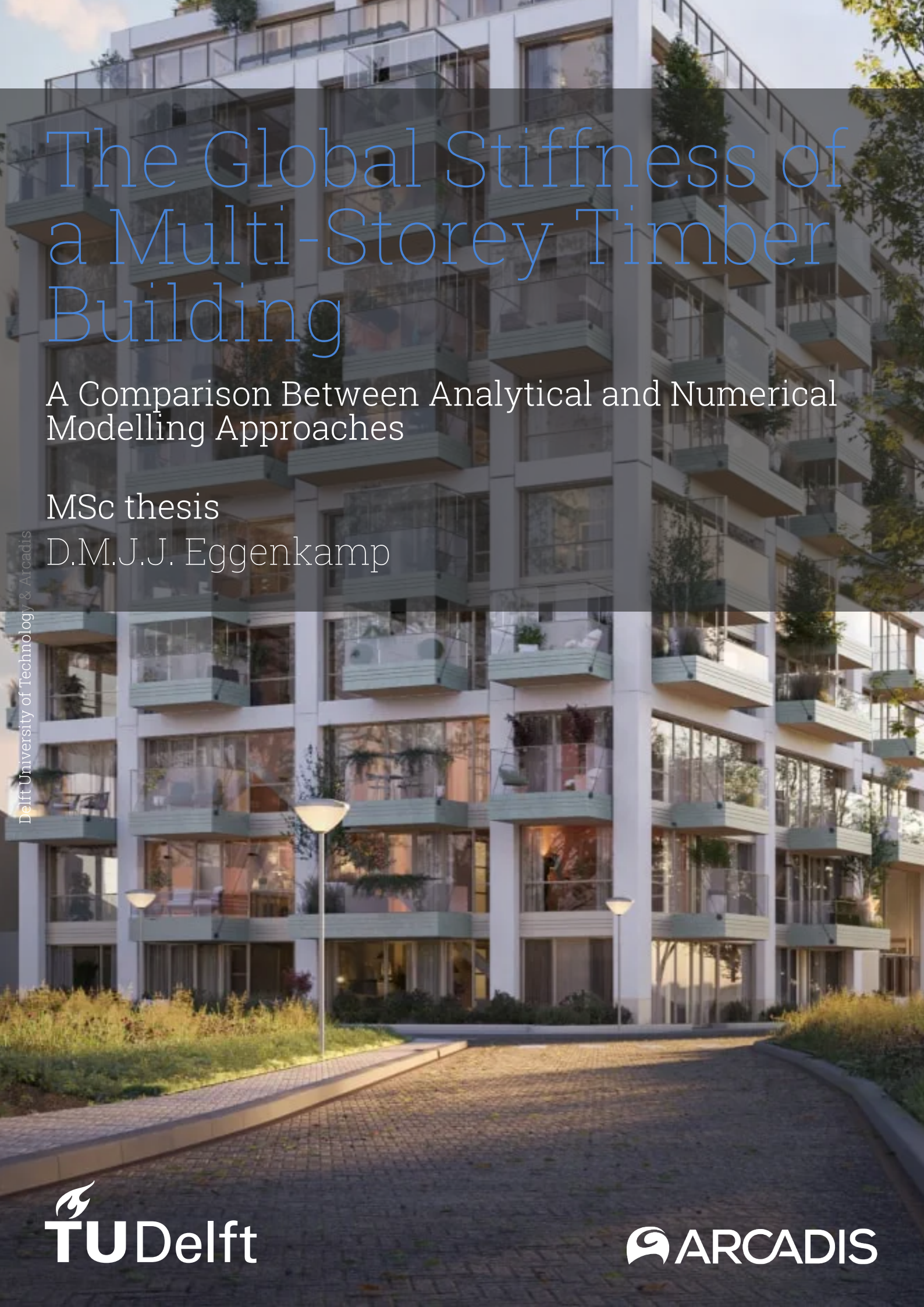

The Global Stiffness of a Multi-Storey Timber Building

A Comparison Between Analytical and Numerical Modelling Approaches

MSc thesis

D.M.J.J. Eggenkamp

Delft University of Technology & Arcadis

TU Delft

ARCADIS

The Global Stiffness of a Multi-Storey Timber Building

A Comparison Between Analytical and Numerical Modelling Approaches

by

D.M.J.J. Eggenkamp

Master of Science

in Civil Engineering at the Delft University of Technology

To be defended publicly on Friday Juli 3, 2026 at 11:00 AM.

Thesis Committee:	Dr.ir. H.R. Schipper	TU Delft, Chair
	Dr.ir. G.J.P. Ravenshorst	TU Delft, Supervisor
	Dr.ir. G. Pagella	TU Delft, Supervisor
	Ir. M. Smith	Arcadis, Supervisor
Project Duration:	November, 2025 - April, 2026	
Faculty:	Faculty of Civil Engineering and Geosciences, Delft	
Student Number:	5145341	

Cover:	Render of the Urban Woods building in Delft (Arcadis)
Style:	TU Delft Report Style, with modifications by Daan Zwaneveld

An electronic version of this thesis is available at `http://repository.tudelft.nl/`.

TU Delft ARCADIS

Preface

Throughout my studies at the Delft University of Technology I have learned from courses with a high variety in topics with the aim to become a structural engineer. The most fascinating topics for me were those related to either the structural integrity of buildings or the environmental impact of the building sector. For the completion of my Master's degree in Structural Engineering, I successfully combined these interests into this thesis, by researching the global behaviour of a multi-storey timber building, which has a CO2-negative footprint. My hope is that this thesis contributes in improving the understanding of using timber as the main structural material in multi-storey buildings, and thereby helps in the current trend of creating more environmental structures.

I was able to find the topic and case study of my thesis via a quest lecture of Meint Smith from Arcadis, which team I was fortunate to join over the last seven months. The case study is the Urban Woods building in Delft, which is the first building of The Urban Woods (name of the contractor, architect and developer). As a starting engineer it is inspiring to have studied this building and see the project being extended with new buildings incoming.

This research expanded my knowledge on stability systems and timber as a construction material, as well as my expertise in creating the types of analytical and numerical models used in this thesis. I would like to thank both Giorgio Pagella and Meint Smith for their continuous support through the whole, from helping me find a topic to being part of my graduation committee. My appreciation also extends to Roel Schipper, for being the head of my committee, and Geert Ravenshorst, for adding his expertise in timber to my committee. CLT-s, the structural engineers behind the design of the timber structure, have my gratitude giving me their drawings, model, and help when needed.

To conclude, I would like to thank my family, friends, professors, and fellow students for the time I have experienced at the university in Delft.

D.M.J.J. Eggenkamp
Delft, June 2026

Abstract

This thesis investigates the global stiffness of cross-laminated timber (CLT) buildings. A case study is conducted on the 10-storey Urban Woods building in Delft, in which the lateral load-resisting system consists of façade bracing supported by a central CLT core. The study evaluates the accuracy of early-stage analytical and numerical models in predicting global stiffness and examines the influence of uncertainty in the slip modulus of dowel-type connections. The objective is to improve the understanding of the applicability of early-stage modelling approaches for estimating the global stiffness of timber structures, and to quantify the impact of uncertainties in connection stiffness on the global structural response.

Assessing the global stiffness of timber buildings is critical, as their lower stiffness and self-weight compared to conventional concrete, masonry, and steel structures make them more susceptible to global deformations. The global stiffness is governed by both the configuration of the structural system and the stiffness of its connections, particularly within the lateral load-resisting system. During the preliminary design phase, engineers must estimate global stiffness and the associated horizontal deformations of a proposed structure. However, due to the relatively limited number of timber high-rise buildings and the associated lack of practical experience, these estimations remain uncertain and need to be supported by complex numerical models. In addition, recent studies have reported discrepancies between experimentally obtained slip moduli and analytical predictions according to Eurocode 5 for dowel-type connections. As these fasteners are widely used in timber lateral load-resisting systems, this introduces additional uncertainty in predicting global structural deformations.

The translational stiffness of the connections was determined using the analytical serviceability approach prescribed in Eurocode 5. These stiffness values were implemented in both analytical models based on the method of Virtual Work and numerical models developed in RFEM. The models were subjected to self-weight and wind loads according to serviceability limit state combinations. To assess the influence of connection stiffness, the translational stiffness values were varied, and the resulting maximum horizontal deflection was used as the primary response parameter.

The results show that analytical models based on the method of Virtual Work systematically overestimate the global stiffness of timber structures by approximately 10–40% compared to numerical models developed in RFEM, primarily due to simplifying the structure. A key difference between the modelling approaches lies in their sensitivity to changes in connection stiffness. For moderate reductions in connection stiffness (up to approximately 50–60%), the overestimation remains relatively constant. However, beyond this threshold, a significant divergence emerges: the numerical models exhibit a non-linear decrease in global stiffness, whereas the analytical models predict a linear reduction. For the global structural model, a reduction of 60% in connection stiffness results in an average decrease in global stiffness of approximately 20%. These findings are supported by literature, which reports that analytical estimates of connection stiffness based on Eurocode 5 can overestimate stiffness by up to approximately 60%, indicating that such reductions are feasible in practice.[GP1.1] Therefore, it is advised to increase the estimation of the horizontal deflection by up to 20%, if the lateral load-resisting system is dependent on the stiffness dowel-type connections.

The results further indicate that the accuracy of analytical and numerical models depend on the structural complexity, with better agreement observed for simpler configurations. In addition, the importance of form stability in the lateral load-resisting system is highlighted: structures with a higher degree of form stability are less sensitive to the stiffness of connections. [GP2.1]For systems made out of simple and form stable configurations an analytical model can provide reliable estimations of the global stiffness. However, numerical models tend to perform better and are therefore preferred for the analysis of more complex and non-form stable structures.

Contents

Preface i

Abstract ii

1 Introduction 1
- 1.1 Research context . . . 1
- 1.2 Case study . . . 1
- 1.3 Research problem and objective . . . 1
- 1.4 Research questions . . . 2
- 1.5 Scope . . . 2
- 1.6 Methodology . . . 3
  - 1.6.1 Conceptual framework . . . 3
  - 1.6.2 Research Outline . . . 3
- 1.7 Analysis of the structure . . . 5

2 Literature review 7
- 2.1 Stiffness of dowel connections . . . 7
- 2.2 Structural systems and lateral stiffness in tall buildings . . . 11
- 2.3 Diaphragms . . . 12

3 Calculation methods 14
- 3.1 Stiffness of the connections . . . 14
  - 3.1.1 Translational stiffness . . . 14
  - 3.1.2 Refined translational stiffness calculation of dowel groups . . . 15
  - 3.1.3 Axial stiffness and behaviour of inclined screws . . . 16
  - 3.1.4 Range of stiffness per connection . . . 17
- 3.2 Virtual Work method . . . 17
- 3.3 RFEM models . . . 18
  - 3.3.1 Finite Element Analysis . . . 19
  - 3.3.2 RFEM methods . . . 19
- 3.4 Verification of the wind load distribution . . . 20

4 Implementation to the case study 21
- 4.1 Schematization of the facades . . . 21
  - 4.1.1 Illustrations per connection . . . 22
- 4.2 Structural restraints . . . 29
- 4.3 Load cases and combinations . . . 30
  - 4.3.1 Self weight . . . 30
  - 4.3.2 Wind load . . . 31

5 Results 34
- 5.1 Calculation of connection stiffness . . . 34
- 5.2 Global response . . . 35
  - 5.2.1 Overview of the models . . . 35
  - 5.2.2 Deformed shapes . . . 36
  - 5.2.3 Horizontal deflection . . . 41
- 5.3 Influence of connection stiffness . . . 41
  - 5.3.1 Global model . . . 41
  - 5.3.2 Façade / 2D models . . . 45
  - 5.3.3 Core model . . . 46
- 5.4 Role of subsystems in global stiffness . . . 47

5.4.1 Influence of the stiffness of dowels vs screws . . . 47
5.4.2 Relative change in deflection . . . 48
5.5 Comparison of modelling approaches . . . 48
5.5.1 Horizontal deflection of the façades . . . 48
5.5.2 Influence of the foundation . . . 50
5.5.3 Core connections . . . 51
5.6 Model validation and verification . . . 52
5.6.1 Wind load distribution . . . 52
5.6.2 Dowel connection validation . . . 53

6 Discussion **57**
6.1 Influence of connection stiffness on global stiffness . . . 57
6.2 Load distribution and structural interaction . . . 57
6.3 Importance of a form stable structure . . . 58
6.4 Evaluation of modelling approaches . . . 59
6.4.1 Horizontal deflection of the façades . . . 59
6.4.2 Influence of foundation . . . 61
6.4.3 Core connections . . . 61
6.5 Comparison of stiffness per fastener . . . 61
6.6 Verification of the dowel connections . . . 62
6.7 Limitations of the study . . . 63

7 Conclusion and Recommendations **64**
7.1 Conclusions . . . 64
7.2 Recommendations . . . 66
7.2.1 Structural advice . . . 66
7.2.2 Future research . . . 67

References **69**

A Stiffness of connections **71**
A.1 Slotted-in steel plates in the façades . . . 71
A.2 Slotted-in steel plate in the core . . . 73
A.3 WHT Plates . . . 73
A.4 TTP1200 . . . 75
A.5 VGZ . . . 76
A.6 TBS . . . 78
A.7 VGS . . . 79
A.8 Summary and results . . . 79

B Virtual Work method **82**

C RFEM models **90**
C.1 2D models of the facades . . . 90
C.2 Core model . . . 91
C.3 Urban Woods model . . . 95
C.3.1 Floor system . . . 95
C.3.2 10th storey . . . 98
C.4 Additional results . . . 99
C.4.1 Deformed shapes . . . 99
C.4.2 Influence of connection stiffness . . . 99

D Load cases and combinations **105**
D.1 Wind load . . . 105
D.1.1 Peak velocity pressure . . . 105
D.1.2 Wind pressure per zone . . . 107
D.1.3 Wind load 2D and core models . . . 113
D.2 Self weight . . . 117

1

Introduction

1.1. Research context

Timber construction is among the earliest forms of structural engineering, with archaeological evidence indicating that primitive shelters attributed to Peking Man existed between one million and 300,000 years ago in what is now China. Due to its natural abundance, ease of processing, and favourable strength-to-weight ratio, timber remained a widely used construction material for centuries (Smith and Snow 2008).

However, timber also exhibits inherent limitations that influence its structural performance, including sensitivity to moisture, vulnerability to biological degradation and fire, and natural variability in material properties. As the demand for larger and taller multi-storey buildings increased, these characteristics constrained the structural application of timber, particularly in comparison to industrial construction materials such as steel and reinforced concrete (Smith and Snow 2008).

In recent decades, timber has re-emerged as a viable construction material, largely driven by the need for more sustainable alternatives to conventional materials. In addition, the development of engineered timber products such as cross-laminated timber (CLT) and glued laminated timber (glulam) has enabled the construction of increasingly tall and structurally complex timber buildings worldwide (Tupenaite et al. 2023).

1.2. Case study

The Urban Woods project is the current front runner in the Netherlands for the trend of using timber as its main construction material for the load-resisting system of a multi-storey timber building. With the building in Delft being the first in a series of timber buildings, the project focuses on sustainability. This focus is seen not only in the construction phase of the building, by using timber, but also in its operational phase, by designing the building partly modular and optimizing the usage of energy and water. The developer, architect, and contractor of the building are the same company named The Urban Woods, and the structural engineers of the project are Arcadis and CLT-s (Woods 2023).

The Urban Woods building in Delft is a 10 storey high timber building resting on a concrete basement and foundation. The timber part of the building is made out of CLT panels, for the floors and core walls, and glulam members as the beams, columns and diagonal elements, as braces in the façades. The bracing system and the core function as the lateral load-resisting systems of the building. The structure is further explained later on in the Introduction in Section 1.7.

1.3. Research problem and objective

A key challenge in multi-story timber buildings is predicting their global behaviour, as their performance depends not only on the strength and stiffness of the members but also on the properties of their connections. This results into that an uncertainty for the stiffness values of the connections, affects the

accuracy of other estimations, such as the estimation for global stiffness. In recent years, advances have been made in researching the stiffness of connections used in timber buildings; however, the number of examples and research these advances are used in is still limited (Kjell Arne Malo et al. 2023) (Tao et al. 2021). This thesis addresses these advances in recent research by showcasing the importance of being able to accurately estimate the connection stiffness, by looking into how this uncertainty influences the global stiffness of the Urban Woods project in Delft. The second objective is to improve the general understanding for estimating the global stiffness in the early stages of the design process.

1.4. Research questions

To achieve the objectives of this research, the following main research question is addressed:

How accurately can Eurocode-based hand calculations predict the global stiffness of a multi-story timber building, and how sensitive is this estimation to variations in connection stiffness compared to RFEM 6 results?

The main question is supported by four sub-questions:

1. **What are the stiffness values of the connections (in or between the core, floors and bracings) used in the Urban Woods building in Delft, how are they determined, and which design parameters have the most influence on the stiffness?**
   Introduces the case study and explains the calculation methods used for the connections and the influence of the parameters, from the design of the connections, on the stiffness values. This makes it possible to get a better understanding for why there is wide range of values between the calculation methods.
2. **According to the literature, how accurate are the Eurocode-based calculations of connection stiffness for the dowel connections used in the Urban Woods project, and which parameters influence this accuracy the most?**
   This question investigates the current state of the literature related to the topic and focuses on whether the analytical approach of the Eurocode is accurate enough for dowel connections. This provides context to the range of change in connection stiffness that is later applied in the models.
3. **How does a variation in connection stiffness influence the global stiffness of the Urban Woods project in Delft, according to an RFEM 6 model?**
   To answer this question a numerical model of the complete building is made and analysed with the stiffness values form the first research question. By altering the stiffness values the influence of their change can be analysed.
4. **How can insights from Eurocode calculations, RFEM simulations, and the Method of Virtual Work be integrated to improve early-stage global stiffness estimation for multi storey CLT buildings?**
   This question examines the conditions under which the Method of Virtual Work provides reliable stiffness estimates and where it doesn't.The goal is not to combine the methods, but to clarify the underlying assumptions of Virtual Work, identify the reasons it may succeed or fail for this specific building type, and assess whether it can be meaningfully generalized to similar multi storey CLT structures.

Global stiffness refers to the effective lateral rigidity of the entire structural system, determined by the combined stiffness contributions of its vertical elements (columns and core walls), horizontal elements (beams and diaphragms), diagonal elements, and the connections between them. It represents how much the building deforms as a whole under lateral loading and is in this research quantified as the applied horizontal force divided by the corresponding maximum displacement.

1.5. Scope

This research is limited to the design of the Urban Woods building in Delft. As such, only the structural members and connection types present in this project are considered, and the results are specific to this case study.

The structural models include only the timber structure. The influence of the concrete basement and foundation is incorporated through support stiffness values, based on existing design assumptions. Although previous research has shown that foundation stiffness can significantly affect the global stiffness of a building, its influence is included in a simplified manner and analysed only qualitatively, without a detailed parametric investigation.

The modelling of connections is limited to their translational stiffness. Rotational stiffness, slip behaviour, and the potential presence of gaps between connected members are not included. Furthermore, only fasteners designed to transfer structural loads under normal conditions are considered. Fasteners that primarily serve to ensure proper assembly, improve robustness, or provide performance under accidental or fire conditions are excluded. As a result, the overall stiffness of the structure in this research is expected to be lower than in reality.

Additional factors that may contribute to the global stiffness of the structure, such as the presence of façade elements (e.g. windows), geometric details (e.g. notches in columns), and friction between timber components, are also neglected.

Steel-to-steel connections, such as pin and welded connections, are assumed to be infinitely stiff. This assumption is justified by their significantly higher stiffness compared to the timber connections with which they are combined in series.

All analyses in this research are carried out at the Serviceability Limit State (SLS). The stiffness of both members and connections is therefore determined in accordance with SLS conditions, not accounting for factors such as moisture content, load duration, and creep. Which are found in the Ultimate Limit State, and therefore not in the scope of this study

1.6. Methodology

1.6.1. Conceptual framework

The conceptual framework of this research is based on the relationship between the local stiffness of timber connections and the global stiffness of a multi-story timber building. The stiffness of the connections, together with the stiffness of the structural elements, governs the transfer of forces and moments throughout the structure and thereby influences its overall lateral deformation and dynamic response.

The independent variable in this study is the connection stiffness, which can be determined using analytical methods such as those in Eurocode 5 or more detailed finite element models. The dependent variable is the global stiffness of the building, which can be expressed through bending stiffness (EI) or lateral stiffness (K).

The relationship between these variables is influenced by several intervening factors, including the stiffness of structural elements (the core, floors and bracings) and the present load transfer mechanisms, and the rigidity of floor diaphragms. Moderating factors such as building geometry, the number of stories, and connection layout affect how local stiffness variations propagate to the global structural response.

The conceptual framework is illustrated using the Urban Woods project in Delft as a case study. By systematically varying the connection stiffness within realistic ranges and analysing the resulting changes in global stiffness, the study demonstrates how assumptions at the connection level influence the overall structural behaviour. This thesis thus connects micro-scale (connection) behaviour to macro-scale (building) stiffness and enables evaluation of the accuracy of simplified Eurocode-based estimation methods for the global stiffness of a timber building.

1.6.2. Research Outline

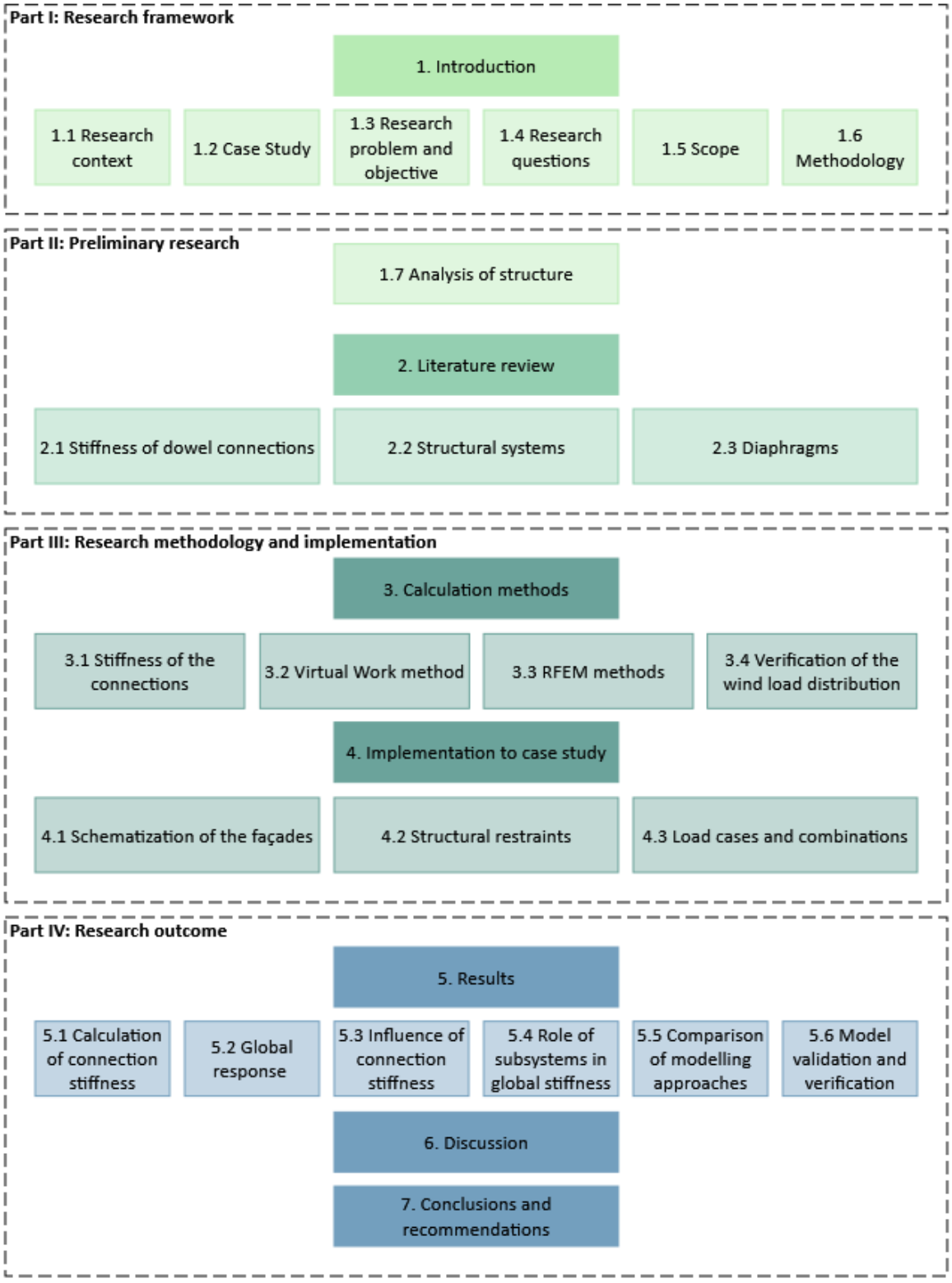

Figure 1.1: Outline of the research with corresponding chapter and sub-chapter numbers

1.7. Analysis of the structure

This section explains the structure of the Urban Woods building in Delft, it mentions what elements are used and how they are connected. The information provided in this section is then used in rest of the chapters, either for relevancy (Literature review) or as an example for the research. More detail on the modelled parts of the building can be found in Appendix C and the complete technical drawings at CLT-S NV (2024).

The building is a 10 storey timber structure with an overall height of 31.85 m and plan dimensions of 20.06 by 30.24 m. The primary structural system consists of glulam beams, columns, and diagonal bracing elements made out of GL24h, while the floor plates and core walls are constructed from CLT panels (C24).

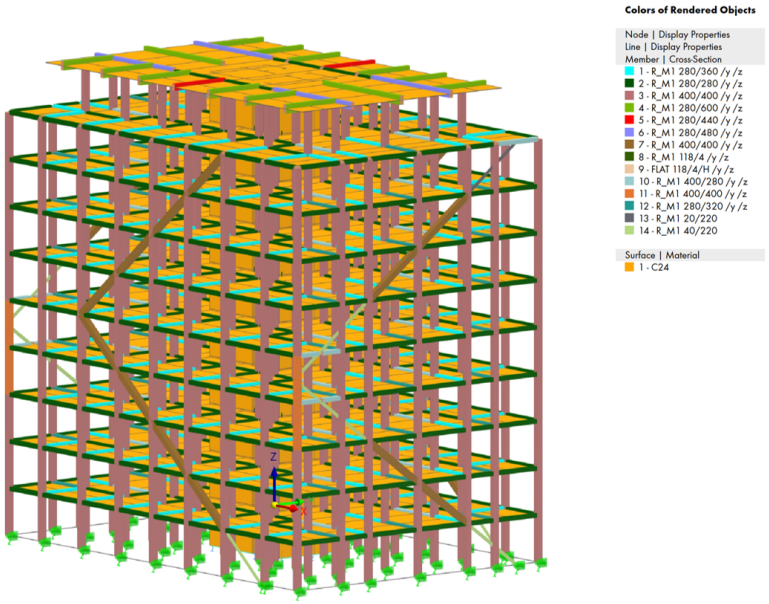

Figure 1.2: General overview of the structure in RFEM 6

All standard columns have a cross-section of 400 by 400 mm and typically span one storey (3.04 m). Exceptions occur at the locations where the diagonal members change direction and at the columns directly below these points. These columns extend over 2 or 3 storeys and, in some cases, utilize a higher strength class (GL30h instead of GL24h). The increased length minimizes the number of connection interfaces and thus reduces cumulative deformations, while the higher strength class is required to carry the concentrated loads transferred through the diagonal elements.

Column to column and column to beam connections are typically made using pairs of VGZ screws. For the highly loaded locations mentioned above, two slotted-in steel plates with dowels are used instead to ensure adequate stiffness and load transfer capacity. Variants of dowel connections with slotted-in steel plates are also found in the diagonals, with the amount of dowels going as high as 50 for one connection. It is noteworthy, that in some diagonals the steel plates run through the whole length. Resulting in structurally it being more of a steel element with the support of some timber.

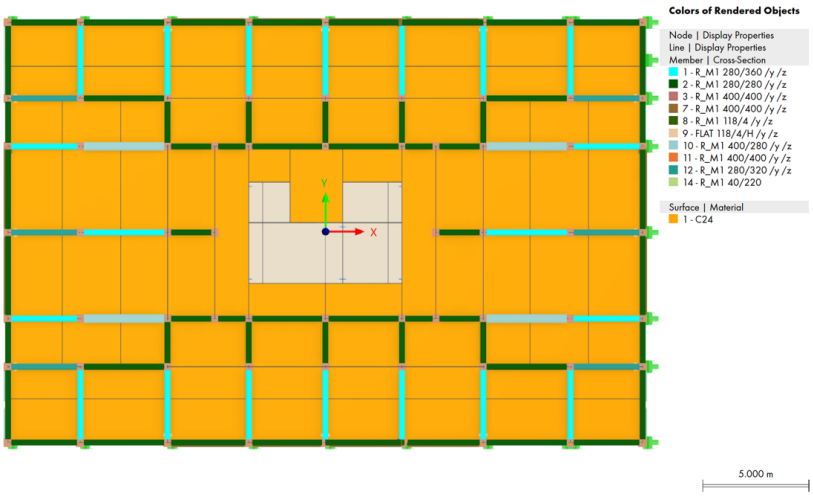

Figure 1.3: Layout beams and columns, with the core at the center

Each floor level contains beams spanning between the columns, as seen in Figure 1.3. Their dimensions vary depending on their position within the frame, but their primary function is consistent: supporting the CLT floor panels and transferring loads toward the diagonal bracing system. Straight TBS screws are used to connect the CLT floor slabs to the beams. Notably, beams do not connect directly to the core walls; instead, only the floor slabs are connected to the core. This highlights that the floor slabs work as rigid diaphragms, distributing the lateral loads based on the relative stiffness of the structural parts. The general layout of the floor slabs is as shown in Figure 1.4. There are slight changes to 1st floor, due to the a part being left out near the entrance, and the floor and ceiling of the 10th floor are slightly different.

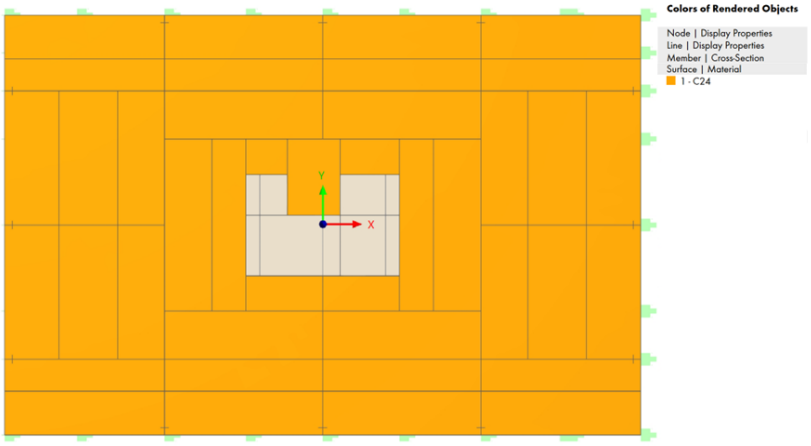

Figure 1.4: General layout CLT floor slabs and the core at the center

The CLT floor slabs are generally 180 mm thick, except for several roof panels on the 10th storey, which are 220 mm thick. The CLT core walls have a thickness of 200 mm and are installed as 3□storey□high segments, meaning they are connected at the 3rd, 6th, and 9th floors.

The lateral load-resisting system exists out of a combination of the core and the diagonal bracing elements found in each facade. With the beams and floor slabs distributing the lateral loads to these parts. In the beginning phase of the design of the building it was assumed that 25% of the wind load on the wide side of the building is taken up by the core and 35% for the narrow side. The vertical load paths exist out of the 66 columns for each floor, the core and the diagonals.

2

Literature review

The literature reviewed is divided into multiple categories. In the first part the focus is on the recent developments in estimating the stiffness of timber connections. The second part looks into the structural systems of high-rise buildings in general and how that translates to timber buildings. Finally, the influence of diaphragms on the stability of the structure is further analysed.

2.1. Stiffness of dowel connections

For a little more than a decade, several high-rise buildings have been realized with structural systems made entirely of timber. Notable examples include the 14-storey “Treet” and the 18-storey “Mjøstårnet”, both of which rely on large glulam trusses with dowel-type connections and slotted-in steel plates (K. A. Malo, R. B. Abrahamsen, and Bjertnæs 2016) (R. Abrahamsen 2017). The Urban Woods project in the Netherlands continues this trend by delivering multi-storey timber buildings, with the first being a 10-storey structure in Delft (Woods 2023). However, because only a limited number of such buildings have been constructed to date, experience with their serviceability limit states, such as wind-induced vibrations, deflections, and lateral drift, remains scarce. A major reason for this knowledge gap lies in the difficulty of reliably estimating the stiffness of mechanical connections, which are decisive for these behaviours (Kjell Arne Malo et al. 2023)(Jockwer and Jorissen 2018). As Gui, Ying Hei Chui, and Salenikovich (2025) emphasize, connection stiffness not only governs serviceability aspects like vibration and drift but also controls load redistribution in statically indeterminate systems at the ultimate limit state. Nevertheless, current timber design standards, including Eurocode 5 and CSA O86, still rely on simplified empirical formulas based only on timber density (ρ) and fastener diameter (d). While easy to apply, these expressions tend to be conservative for single dowels and lack sufficient generality across different joint types and configurations, limiting their accuracy for modern tall timber structures (Kjell Arne Malo et al. 2023).

$$k_{ser} = \rho_{mean}^{1,5} \frac{d}{23} \tag{2.1}$$

Connections exist of fasteners and the connected members, both their properties, such as geometry, elastic modulus, and material characteristics, all influence the performance of the connection. Consequently, the density of the timber is often a key parameter in empirical models, as seen in the equation from the Eurocode for the lateral slip modulus per shear plane per fastener (Equation: 2.1). Experimental studies have demonstrated a clear relationship between timber density and connection stiffness during initial loading, which is represented by the density exponent of 1.5 in the Eurocode formulation. In contrast, during unloading, the stiffness of the connection has been shown to be largely independent of timber density (Dorn, Borst, and Eberhardsteiner 2013). The moisture content can also play a significant role in determining the stiffness of timber connections. Studies have demonstrated that wetting of the timber post-fabrication can lead to a notable reduction in the stiffness (Kiwelu 2019). Studies focused on the parameters of the fasteners, such as the diameter and the penetration length, generally

highlight a positive relationship between these parameters and the connection stiffness (Gui, Ying Hei Chui, and Salenikovich 2025).

In addition, the arrangement and spacing of dowels have been shown to significantly influence the overall behaviour of the joint. Eurocode 5 assumes a linear superposition of the stiffness contributions of individual shear planes and prescribes a reduction by a factor of two when loading is applied perpendicular to the grain. Research by Kjell Arne Malo et al. (2023) confirms the latter but questions the former. Their study demonstrates that Eurocode 5 underestimates the stiffness of a single dowel by a factor of 2.5, accurately estimates the stiffness of a connection with ten dowels , but then overestimates for bigger joints. The overestimation reaches an asymptotic value of 0.225 for joints with a hundred dowels (ten rows and ten columns of dowels). The result of their research is Equation 2.2, which takes the method of the Eurocode by multiplying the stiffness of a single shear plane (k_{ser}) with the amount of shear planes per dowel (n_{spd}), amount of rows of dowels along the grain (n_0), and the amount of columns of dowels perpendicular to the grain (n_{90}). This is then multiplied by the calibration factor of a single dowel (m) and an additional part that takes into account the amount of rows and columns of dowels. The values for $q_{i,j}$ and r_i are retrieved from tests performed with 12 mm dowels embedded in GL30c members. The results for the part related to the layout of the dowels is visualized in Figure 2.1. The minimum value of this graph is 0.09 for a joint with a layout of ten by ten dowels. Multiplying this value by a factor of 2.5 (m) for the underestimation of a single dowel, one retrieves the previously mentioned asymptotic value of 0.225. Meaning their modelled stiffness for a joint of ten by ten dowels is 22.5% of the stiffness calculated via the Eurocode 5 methods.

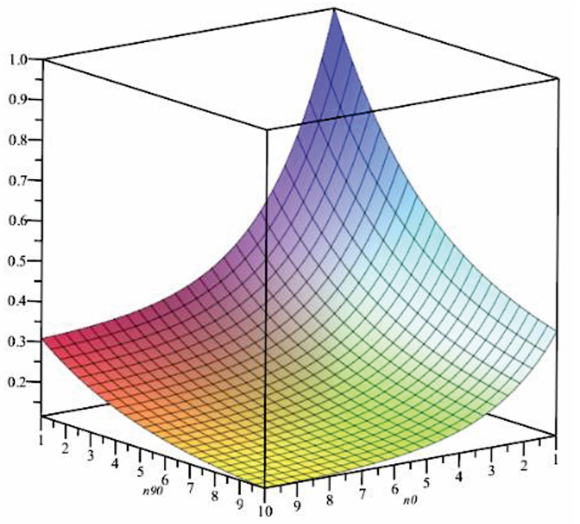

Figure 2.1: Average relative stiffness dependent on number of dowels in the two directions (Kjell Arne Malo et al. 2023)

$$K_{ser,mod} = k_{ser} \cdot m \cdot n_{spd} \cdot n_0 \cdot \left(q_{0,1} + q_{0,2} e^{\frac{1-n_0}{r_0}}\right) \cdot n_{90} \cdot \left(q_{90,1} + q_{90,2} e^{\frac{1-n_{90}}{r_{90}}}\right) \tag{2.2}$$

Beyond material properties and connection geometry, the mechanical response of timber connections is also strongly influenced by the applied loading conditions. Loading conditions, such as cyclic loading, long-term loading, and loading rate, have been studied to assess their impact on the mechanical behaviour of timber connections. Compared to static loading, cyclic loading has been found to cause a considerably increase in initial connection stiffness, which may be attributed to the associated increase in loading rate (Ying H. Chui and Ni 1997). However in the long run, under repeated loading cycles, the connections stiffness tends to degrade with increasing displacements, primarily due to hysteretic pinching. Experimental evidence indicates that after approximately 200,000 to 300,000 loading cycles, the stiffness decline plateaus and stabilizes, indicating a transition to a steady-state behaviour (Gui, Ying Hei Chui, and Salenikovich 2025).

Finally, to improve the estimation of the connection stiffness of timber structures new empirical and mechanical formulas are presented. In general, mechanical models provide a theoretical foundation for understanding connection behaviour, while empirical formulae offer practical approximations derived from experimental testing. Eurocode 5 (Equation: 2.1) and the research by Kjell Arne Malo et al. (2023) (Equation: 2.2) are examples of the empirical approach. One of

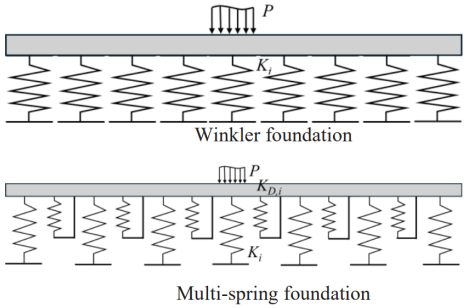

Figure 2.2: Foundation theories used for estimating the stiffness of one dowel (Gui, Ying Hei Chui, and Salenikovich 2025)

the early mechanical approaches is the Beam on Elastic Foundation (BoEF) theory (Winkler foundation), which treats a dowel or bolt as a beam supported by independent springs representing the surrounding timber. However, this theory is limited by its assumption that the reaction at any point on the foundation depends solely on the settlement of its own location, being completely independent from its neighbouring points. Alternative theories have been developed to address this limitation. The Semi-infinite elastic foundation theory, or more commonly known as the Half-space foundation theory, sees the foundation as an isotropic, homogeneous, and semi-infinite elastic medium. Another theory, called the Multi-spring foundation theory, addresses the discontinuity issue of the Winkler model by adding shear springs between the embedment springs, thereby adding a coupling effect between the embedment springs. Recent studies, where BoEF theories were applied, confirm that these approaches significantly improve the accuracy of stiffness predictions when compared to experimental results, reducing the discrepancy from over 60 % in Eurocode 5 to less than 20 % in refined models (Gui, Ying Hei Chui, and Salenikovich 2025)(Tao et al. 2021).

Overall, the literature indicates that the Eurocode 5 formulation provides a practical but simplified estimate of dowel connection stiffness, with its accuracy strongly dependent on the connection configuration. While it tends to underestimate the stiffness of single dowels and may reasonably approximate medium-sized joints, it can significantly overestimate stiffness for larger, multi-fastener connections due to its assumption of linear superposition. The accuracy of the estimation is primarily influenced by the number and arrangement of dowels, which govern interaction effects between fasteners that are not captured in the Eurocode model. In addition, timber density, fastener diameter, moisture content, and loading conditions affect stiffness, although these parameters are only partially accounted for or simplified in current formulations. Consequently, more advanced empirical or mechanical models are required to reliably predict connection stiffness in modern multi-storey timber structures. An overview of all experimental findings on the accuracy of Eurocode 5 slip-modulus expressions for dowel-type timber connections found are presented in Table 2.1.

Table 2.1: Overview of experimental findings on the accuracy of Eurocode 5 slip-modulus expressions for dowel-type timber connections

Experimental scope	Key findings	Source
Tests with 12 mm dowels in GL30c to improve the EC5 stiffness equation for groups of dowels	EC5 underestimates single-dowel stiffness by a factor of 2.5, while group stiffness is overestimated, with measured stiffness reduced to approximately 22.5% of the EC5 prediction for 100-dowel connections	Kjell Arne Malo et al. (2023)
Tests on multi-dowel timber connections with two dowel diameters, hardwood and softwood specimens, and dowel groups ranging from 1 to 35	Measured stiffness per dowel decreases with increasing group size; a 35-dowel connection exhibited approximately 50% of the EC5-predicted stiffness	Reynolds et al. (2022)
Experimental data on dowel-type fasteners, bolts, and self-tapping screws used to validate three Beam on Elastic Foundation (BoEF) models	EC5 predictions show a mean relative difference of 61.5% compared to test results, whereas BoEF models reduce the error to approximately 20%	Gui et al. (2025)
Tests with 12 and 14 mm dowels in spruce, beech, and azobé with 1, 3, or 5 dowels per connection	EC5 significantly overestimates stiffness in several configurations, with measured values up to four times lower than predicted; large scatter was observed ($R^2 = 0.634$ and 0.516)	Sandhaas (2012)
Experimental data on steel–wood–steel (SWS) connections with dowels compared with predicted values	EC5 overestimates connection stiffness by factors ranging from 1.00 to 4.14, with an average overestimation factor of 1.90	Nur Liza Binti (2019)
Tests with 16 mm dowels in GL24 made of Scots pine and Northeast China larch, without steel plates; failures following European Yield Modes I and III	EC5 overestimates single-dowel stiffness by an average of 68.7%, while BoEF models predict stiffness within 10% of test results	Wang et al. (2021)
Tests with 12 mm dowels in members with varying wood densities and geometric properties, including an embedded steel plate	EC5 overestimates single-dowel stiffness for 40 mm member width, provides accurate estimates for 100 mm width, and underestimates stiffness for 200 mm width	Dorn et al. (2013)
Tests with 12, 14, and 16 mm dowels in timber with mean density of 467 kg/m^3 (GL28), with varying member thicknesses	EC5 overestimates single-dowel stiffness by an average of 18.2% for loading parallel to the grain and 47.6% for loading perpendicular to the grain; the EC5 slip modulus is not modified for loading angle	J. Cao et al. (2021)
Tests with 12, 16, and 20 mm dowels in GL24 with varying connection geometries and loading angles	Test results range from 85% to 210% of the corresponding EC5 value for single-dowel stiffness; a reduction factor of 0.8 per fastener is proposed for small dowel groups (5–6 dowels)	Kuhlmann and Gauß (2021)
Synthesis of reviewed literature	Across the reviewed studies, EC5 slip-modulus expressions tend to underestimate stiffness for small dowels ($d \leq 12$ [mm]) and overestimate stiffness for larger dowels and groups of dowels. Beam on Elastic Foundation models consistently reduce prediction error	This study

2.2. Structural systems and lateral stiffness in tall buildings

A bit more than a century ago the race for height began, as taller and taller skyscrapers were being built. Which in the end resulted in the completion of the 102-storey tall Empire State Building in 1931. The majority of the buildings from this race had structural systems existing out of steel rigid frames with wind bracings and were able to reach their heights through excessive use of structural materials. Since then, the development of lateral load resisting systems in tall buildings has significantly increased. Ali and Moon classify tall building structures into interior and exterior systems depending on the location of the primary stiffness components in the building (Ali and Moon 2007). Interior systems, such as outrigger and shear wall frame interactions systems, rely on central cores and connected columns to control lateral drift. On the other hand, exterior systems, such as tubes and diagrids, mobilize the building perimeter to achieve stiffness through three-dimensional action. Fazlur Khan introduced a concept called the “premium for height”, which says that as buildings become taller, stiffness rather than strength governs the design, since lateral deformations increase disproportionately with height. Efficient structural systems therefore minimize material use by distributing stiffness where it is most effective.

Due to the century long development of structural systems for high-rise buildings and the recent advances in structural timber products, it is possible to use timber as the main material for the structure of a high-rise building. For example, the tube-in-tube concept, traditionally applied in reinforced concrete and steel structures, has been reinterpreted in timber design to enhance global rigidity (e.g., floor diaphragms linking an inner shear core and outer frame). The study by Binck, A. S. Cao, and Frangi (2022) extends this concept by proposing hybrid tube-in-tube systems in which the load path between the core and perimeter frames is strengthened using glulam or CLT shear walls and rigid diaphragm action. These systems improve both bending and torsional stiffness, enabling timber towers to achieve lateral stiffness comparable to conventional high-rise systems. The study emphasizes that, as in steel and concrete towers, the coupling between the core and perimeter systems is critical: the efficiency of the global system depends on the stiffness of these connections and their ability to transfer shear and bending between subsystems.

Research by Felicita (2021) focused on the influence of the stability system, connection stiffness and building height on the design of a high-rise timber building . The outcome of her research showcased the importance of the stability system in comparison to the other two parameters. This is due to the relationship between the design choice of a structural/ stability system and the global stiffness of the building. Form-stable stability systems, such as a glulam diagrid system with triangular configuration of the diagonal elements, have a higher global stiffness than non-form stable systems. This also directly impacts the influence of the connection stiffness, as it was deemed nearly negligible for form-stable structures, but highly influential for non-form stable structures such as a glulam frame structure. Together, these developments show that global stiffness in tall buildings, regardless of material, depends on the same governing principles of structural hierarchy and interaction. For multi-storey timber buildings, understanding and quantifying how connection stiffness affects this interaction becomes essential, since even small variations in joint stiffness can significantly alter the overall deflection and dynamic response of the structure.

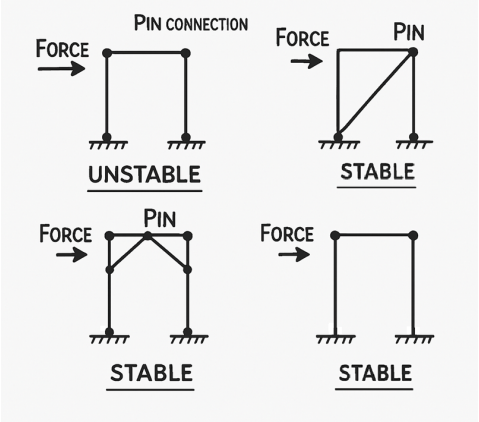

Figure 2.3: Non-form stable and form stable structures

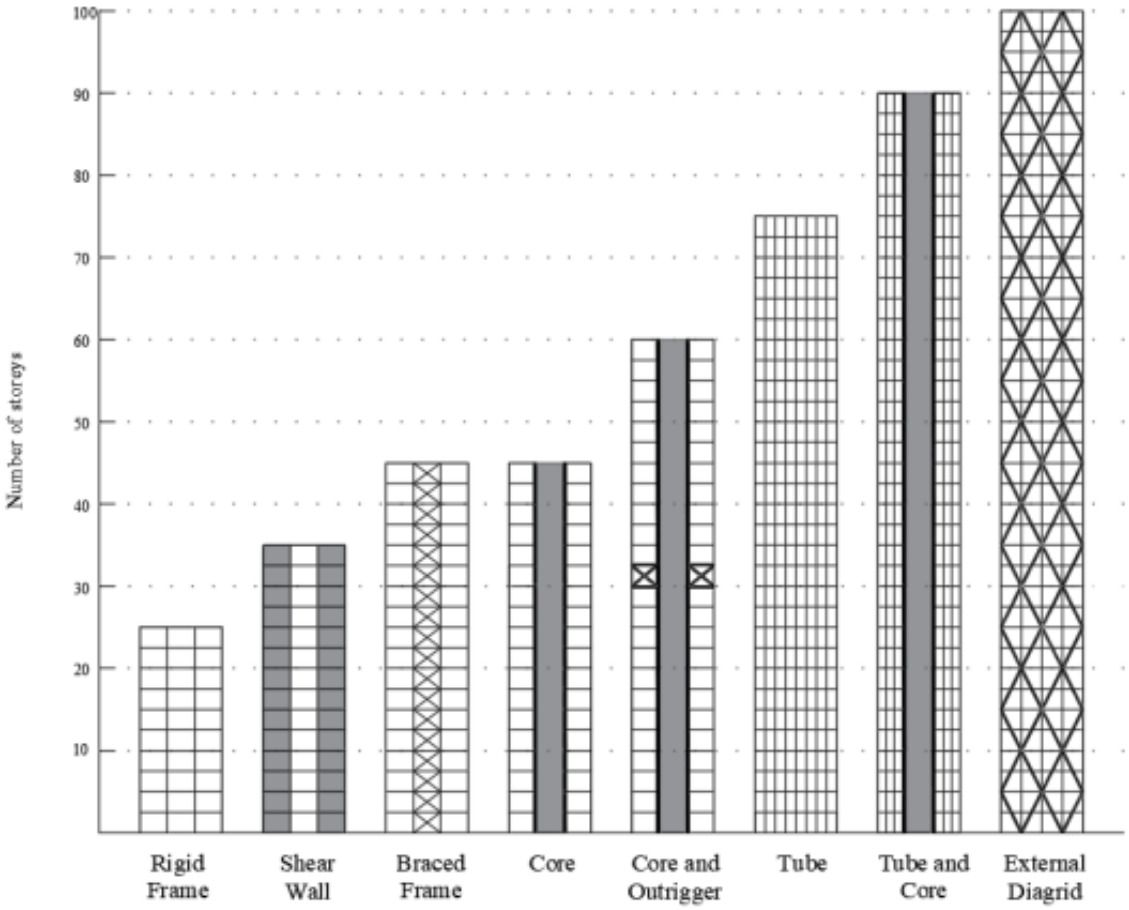

Figure 2.4: Most commonly structural systems for high-rise buildings (Felicita 2021)

2.3. Diaphragms

Among the fundamental parts of any stability system are the diaphragms. Diaphragms are horizontal members (floor, roof, membrame, or horizontal bracing) that transfer horizontal loads to the rest of the members of the stability system, thereby tying together the structural system. To simplify the behaviour of the diaphragm engineers use two categories for analysis purposes: flexible and rigid diaphragms. The general assumption is that flexible diaphragms distribute the lateral loads to the members of the structural system in proportion to tributary areas. On the other hand, rigid diaphragms distribute the loads in proportion to the stiffness of the members. Meaning the stiffness of the diaphragms has a direct influence on the load path and stability of the structure. In timber buildings diaphragms exist out of large and thick timber panels made timber engineered products (D'Arenzo et al. 2024). For floors cross-laminated timber (CLT) is often used, for example, the floors and roof in the Urban Woods building in Delft are CLT panels and function as diaphragms for the structural system.

CLT panels sizes differ by manufacturer, with typical widths ranging from 0.6 to 3 m, lengths can be up to 18 m, and the thickness can go up to 508 mm. Larger dimensions are possible, but are often limited by boundary conditions such as transportation. The CLT diaphragms can be supported by beams, walls and columns. For the latter the design takes advantage of the two-way spanning capability of CLT panels. This is due to the cross-lamination, which also results in good in-plane stiffness in comparison to glulam decking. However, due to the fact that CLT panels are significantly longer than they are wide, the stiffness and strength may differ in the two in-plane orthogonal directions. One of the key aspects that influence this difference is the choice of connection used between the CLT panels (D'Arenzo et al. 2024).

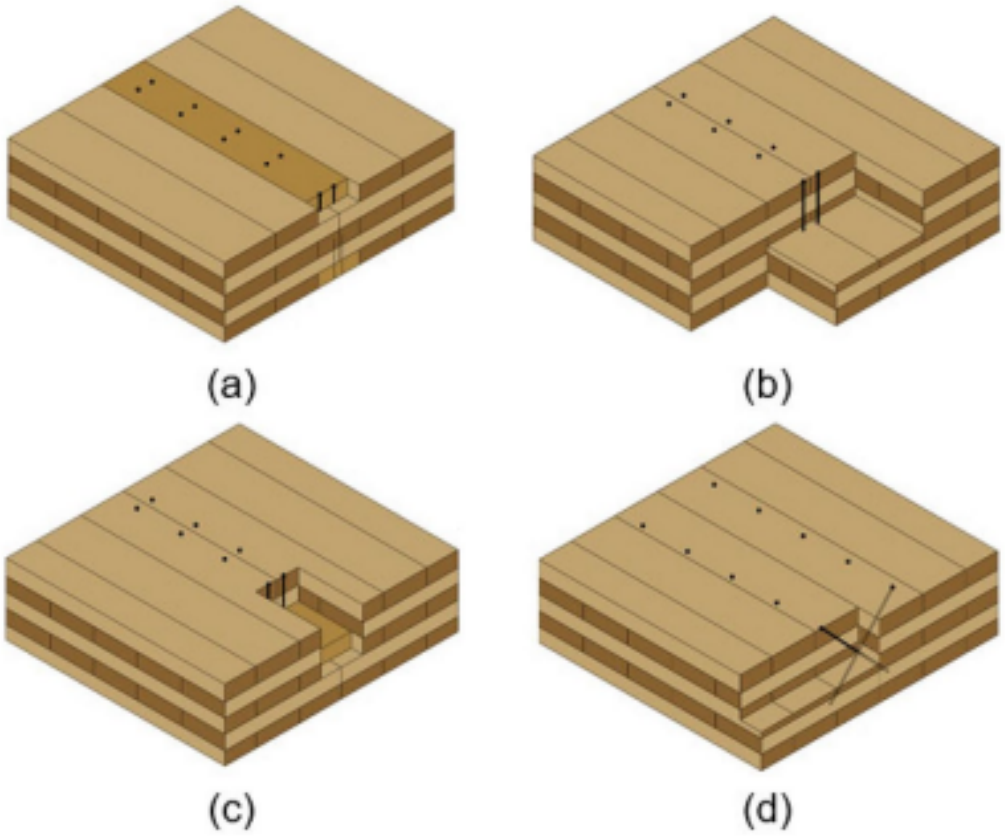

Figure 2.5: Examples of CLT floor panel-to-panel connections: **(a)** outer spline-, **(b)** lap-, **(c)** inner spline- and **(d)** butt-joints (D'Arenzo et al. 2024)

Figure 2.5 shows the four most common types of joints used to connect the CLT floor panels to one-another. These connections can use either nails, partially threaded screws (PTSs), or fully threaded screws (FTSs). In the Urban Woods building in Delft the panels are connected via butt-joints (d), with the usage of fully threaded screws (FTSs). Multiple researchers have tested these connections varying in the lengths of the screws and threads, the diameter and the inclinations. Stiffnesses from these tests vary from 0.40 to 12.20 kN/mm depending on the design, in the case study pairs of 7x220 are used with an inclination of 45° (Loss, Hossain, and Tannert 2018).

To conclude, the CLT panels in the Urban Woods building can be considered as rigid, distributing the loads over the structure in proportion to the stiffness of load-resisting systems. Due to a significant variety in stiffness values between types of connections used for CLT panels, it is deemed valuable to calculate and include the exact values of the stiffness in the models of this research.

3

Calculation methods

This chapter lists the main calculation methods used in this research, all methods are based on Eurocode 5 ((Standardization 2025) and/or the literature from Chapter 2. The actual calculation with the methods are further explained in Appendices A and B.

3.1. Stiffness of the connections

3.1.1. Translational stiffness

The timber structure of the Urban Woods building uses timber and steel connections. The steel connections (pin and weld) are considered to be infinitely stiff translational, with the pin connections having a zero rotational stiffness. For the translational stiffness of the timber connections (dowels, screws) Equations (3.1) and (3.2) from Eurocode 5 are used (Standardization 2011).

$$K_{SLS,v,i} = \rho_{mean}^{1,5} \frac{d}{23} \tag{3.1}$$

$$K_{SLS,v,i} = 60 d_1^{1,7} \left(\frac{\rho_{mean}}{420}\right)^{1,1} \tag{3.2}$$

where

- ρ_{mean} is the mean density in kg/m^3
- d is the diameter of the fastener in mm
- d_1 is the inner thread diameter in mm

Every connection in the Urban Woods building exists out of multiple dowels and or screws. To retrieve the total stiffness of the joint the stiffnesses are linearly added together following Equation (3.3).

$$K_{ser} = K_{SLS} \cdot f_{s/t} \cdot n_{spd} \cdot n_0 \cdot n_{90} \tag{3.3}$$

where

- K_{SLS} is the stiffness per shear plane per fastener according to Equations (3.1) or (3.2) in N/mm
- $f_{s/t}$ is the factor for steel/timber connections, is 2 when a steel plate is used in combination with the fasteners or 1 when there is no plate
- n_{spd} is the number of shear planes per dowel or screw
- n_0 is the number of fasteners along the grain
- n_{90} is the number of fasteners perpendicular to the grain

When the load on a joint is applied under an angle with the fibres of the timber member the stiffness is reduced. The rule is to half the stiffness when the load is applied perpendicular and to interpolate between 0.5 and 1.0 for other angles (Standardization 2011).

A couple of connections (WHTPT and TTP) use a combination of screws and a thin steel plate on the outside of the timber. To calculate the translational stiffness of these connections the connection is divided into three springs, two for the translational stiffness of the screws on either side and one for the stiffness of the steel plate between the two screw groups. The stiffnesses of these springs then need to be added together according to the rule of adding springs in series (Equation (3.4)).

$$Series: \frac{1}{K_i} = \frac{1}{K_{i,1}} + \frac{1}{K_{i,2}} + ... \tag{3.4}$$

$$Parallel: K_i = K_{i,1} + K_{i,2} + ... \tag{3.5}$$

3.1.2. Refined translational stiffness calculation of dowel groups

In Subchapter 2.1 an alternative for calculating the translational stiffness of groups of dowels was introduced. The research performed by Kjell Arne Malo et al. (2023) uses Equation (3.6) , which is an alternative for Equation (3.3).

$$K_{ser,mod} = k_{SLS} \cdot f_{s/t} \cdot m \cdot n_{spd} \cdot n_0 \cdot \left(q_{0,1} + q_{0,2} e^{\frac{1-n_0}{r_0}}\right) \cdot n_{90} \cdot \left(q_{90,1} + q_{90,2} e^{\frac{1-n_{90}}{r_{90}}}\right) \tag{3.6}$$

where

- K_{SLS} is the stiffness per shear plane per fastener according to Equation (3.1) in kN/mm
- $f_{s/t}$ is the factor for steel/timber connections, is 2 when a steel plate is used in combination with the fasteners or 1 when there is no plate
- m is the calibration factor for one dowel
- n_{spd} is the number of shear planes per dowel or screw
- n_0 is the number of dowels along the grain
- n_{90} is the number of dowels perpendicular to the grain
- $q_{i,j}$ and r_i are model parameters based on tested values
- $K_{ser,mod}$ is the modified stiffness of a group of dowels in kN/mm

The additional parameters (m, $q_{i,j}$ and r_i) are obtained from the test results obtained in the same research by Kjell Arne Malo et al. (2023). The parameter m represents the difference found between the Eurocode and test results for the stiffness of one dowel. With the Eurocode underestimating the stiffness by a factor of 2.5 for a dowel loaded perpendicular to the grain (EC5: 9.3 kN/mm vs test: 23 kN/mm) The part between brackets in Equation (3.6) represents the decay in stiffness per dowel when the amount of dowels per connection increases.

Table 3.1: Model parameters for 12 mm dowels embedded in Norway spruce GL30c (Kjell Arne Malo et al. 2023)

	Along grain			**Perpendicular grain**		
Number of dowels	n_0			n_{90}		
Model symbols	$q_{0,1}$	$q_{0,2}$	r_0	$q_{90,1}$	$q_{90,2}$	r_{90}
Model values	0.3	0.7	2	0.3	0.7	4
Loading direction	$m = 2.5$			$m = 1.3$		

The empirical interaction parameters proposed by Kjell Arne Malo et al. (2023) were derived for 12 mm dowels in GL30c. In the present study, however, 16 mm dowels in GL24h and GL30h are used. Due to the lack of experimental results that accurately represent the connection configurations applied in the Urban Woods building, no attempt is made to recalibrate these parameters for the present case study. Instead, the parameter values listed in Table 3.1 are adopted unchanged, acknowledging that this reduces the accuracy of the stiffness estimation. Although the influence of dowel diameter and timber density on the single□dowel stiffness is accounted for through Equation (3.6), these changes also affect the empirical interaction parameters themselves. In addition, geometric characteristics such as dowel spacing and dowel length differ between the experimental configurations reported by Kjell Arne Malo

et al. (2023) and the connections used in the Urban Woods building, further influencing interaction behaviour. Consequently, meaningful adjustment of the interaction parameters would only be justified if experimental tests were available that closely represent the actual connection layout and material properties of the Urban Woods building in Delft.

3.1.3. Axial stiffness and behaviour of inclined screws

In Section 3.1.1 the EC5 method for calculating the translational stiffness of screws is explained. However, a multitude of connections in the Urban Woods building don't load the screws in the translational direction, but in the axial direction or a combination of the two (inclined screws).

$$K_{SLS,ax} = n \cdot \frac{1}{\sum_{i=1}^{j} \frac{1}{K_{SLS,ax,i}}} \tag{3.7}$$

where

- $K_{SLS,ax,i}$ = mean slip modulus of displacement share i
- n = the total number of fasteners
- j = number of connected members (or axial slip components)

The axial stiffness of a screw (Equation (3.7)) is often a combination of multiple springs. The illustration in Figure 3.1 shows a common situation where the total axial stiffness is a summation of three springs. The springs in the first timber element work parallel to one another and work in series with the spring in the second element. $K_{SLS,w,i}$ is the withdrawal resistance of the threaded part in element i of a screw and is calculated with Equation (3.8). The axial resistance related to the head pull-through of a screw is calculated using Equations (3.9) and (3.10).

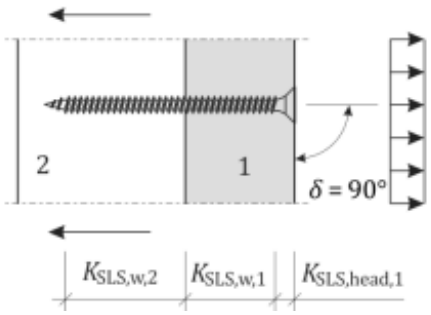

Figure 3.1: General illustration for the axial slip modulus of a screw (Standardization 2025)

$$K_{SLS,w,i} = 2 \cdot d^{0,6} \cdot l_w^{0,6} \cdot \rho_{mean}^{0,9} \tag{3.8}$$

where

- d = diameter of the fastener in mm
- l_w = withdrawal length in mm
- ρ_{mean} = mean density of the timber in kg/m^3

$$K_{SLS,head} = \frac{F_{pull,k}}{15mm} \tag{3.9}$$

$$F_{pull,k} = 15 \cdot e^{\left(-\frac{d_{head}}{50}\right)} \cdot d_{head}^2 \cdot \left(\frac{\rho_k}{350}\right)^{0,8} \tag{3.10}$$

where

- d_{head} = head diameter in mm
- ρ_k = density in kg/m^3

The most common connection in the Urban Woods building in Delft is likely a pair of inclined screws. For these connections the stiffness in 2 out of the 3 directions exists out of a combination of axial and translational stiffness. Standardization (2025) states to use Equation (3.11) in those circumstances.

$$K_{SLS} = K_{SLS,v} \cdot \sin\delta \cdot (\sin\delta - \mu\cos\delta) + K_{SLS,ax} \cdot \cos\delta \cdot (\cos\delta + \mu\sin\delta) \tag{3.11}$$

where

- $K_{SLS,v}$ = lateral mean slip modulus per shear plane according to Equation 3.2
- $K_{SLS,ax}$ = axial mean slip modulus per connection between members according to Equation 3.7
- δ = angle between the fastener axis and the shear plane in degrees
- μ = the friction coefficient between the members = 0,25 -

3.1.4. Range of stiffness per connection

A key objective of this research is to investigate the influence of uncertainty in the estimated stiffness of connections. To enable a systematic sensitivity analysis, a range of stiffness values is introduced by applying multiplicative factors to the calculated connection stiffness. An example for a dowel connection is shown with Equation 3.12

$$K_{ser,\%} = K_{ser} \cdot F_{all} \cdot F_{dowel} \tag{3.12}$$

where

- K_{ser} is the stiffness of a dowel connection in N/mm
- F_{all} is the factor for all connections, standard set to 1
- F_{dowel} is the factor for all dowel connections, standard set to 1
- $K_{ser,\%}$ is the stiffness of a dowel connection with a change of stiffness included in N/mm

3.2. Virtual Work method

The global lateral stiffness of the Urban Woods building is estimated using the Virtual Force method (also referred to as the Virtual Work method), implemented in Microsoft Excel. The lateral load-resisting behaviour of the structure is assumed to be dominated by the stiffness of the façade bracing system, while the core provides a secondary contribution. This assumption was used with the original structural design and is therefore adopted in the present analysis. The façade bracing system of the Urban Woods building exist out of four timber trusses, with two distinct designs (one for each principal direction of the building). By determining the stiffness of these trusses, an estimate of the global lateral stiffness is made.

The Virtual Force method is based on the principle of Virtual Work, in which the displacement at a point is obtained by equating internal and external virtual work. In this research it is used to calculate a desired deflection by a summation of deformations of the members and connections. These deformations arise from axial forces in the members, resulting from the applied permanent loads (self-weight) and wind loads.

$$u_{members} = \sum F_i \frac{F_{1i} l_i}{A_i E_i} \tag{3.13}$$

$$u_{connections} = \sum \frac{F_i F_{1i}}{K_i} \tag{3.14}$$

$$u_H = u_{members} + u_{connections} \tag{3.15}$$

where

- u = desired deflection of structure in mm
- F_i = axial force of member i in N
- F_{1i} = axial force of member i caused by unit load
- l_i = length of member i in mm
- E_i = Modulus of Elasticity of member i in N/mm^2
- A_i = area of the profile of member i in mm^2
- K_i = stiffness value of all connections on member i in N/mm

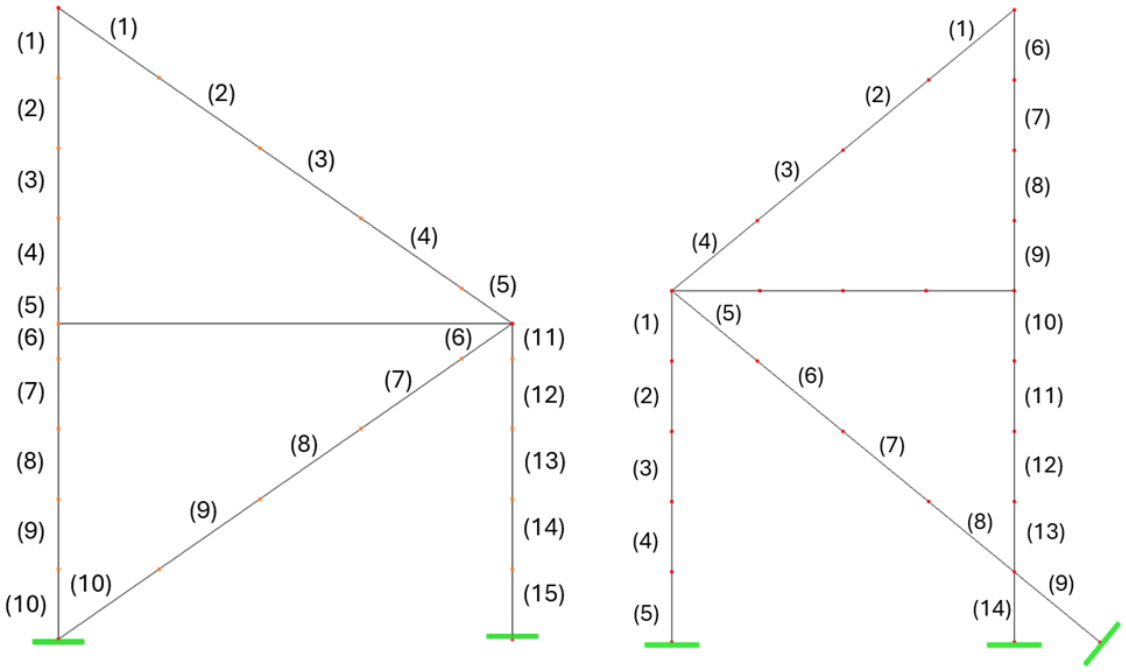

Figure 3.2: Numbering of the two facades

Each façade consists of a large number of beams, columns, and diagonal members. In principle, the Virtual Force method can be applied to the full structural system. However, to reduce the computational effort while maintaining accuracy, a simplified structural model is adopted in which only the members contributing significantly to the primary load path are included. The diagonal members are the dominant elements in resisting lateral loads, as they transfer wind induced forces from the beams towards the supports. Consequently, axial forces in the diagonals increase towards the base of the structure. In addition, the columns located at the nodes where diagonal orientations change are included, as these elements are subjected to high vertical forces resulting directly from the diagonal load transfer. The remaining members experience relatively low axial forces under lateral loading and are therefore neglected in the simplified model. Nevertheless, one additional column per façade is included to ensure overall structural stability. For this purpose, the column located at the end of the upper diagonal is selected.

This results into two reduced structural models of the original façades, as seen in Figure 3.2. For each member in this structural model the values needed for Equation 3.15 need to be determined. The axial force of member i caused by a unit load (F_{1i}) is obtained by loading the structure with a unit load of 1 at the location and in the direction of interest. For the stiffness values of all connections on each member (K_i) the stiffness value of each connection on the members has to be determined. Then these values need to be summed up, taking into account the rules for adding up spring values in series or parallel as described in Equations 3.4 and 3.5.

The presented methodology provides an analytical estimate of the lateral stiffness of the building based on the governing load paths in the façade trusses. By explicitly accounting for both member and connection deformability, the approach captures the key factors influencing the global structural response while remaining computationally efficient. The results obtained using this method are subsequently used as a reference for comparison with the numerical models made in RFEM.

3.3. RFEM models

For the design of the building an RFEM 5 model was made, this is transformed to an RFEM 6 model to improve further use. This new model is the base model on which alterations are made to research the

results. Next to the main model three other RFEM models are made. Two 2D models of the bracings in the façade are made to compare with the results of the virtual force method. These two models have structures that represent both the actual design of the façade and reduced versions that focus on the members in the main load path. The last model is a model of the core, made to analyse specifically the core and the different forms of deformation (sliding, rocking). To explain the process of making an RFEM model first, the numerical method behind RFEM is introduced and followed by the main methods used in RFEM to model the building.

3.3.1. Finite Element Analysis

RFEM is a powerful 3D Finite Element Analysis (FEA) software designed for structural engineering and analysis. FEA is a numerical method used in engineering to analyse and solve complex structural and physical problems by dividing a structure into smaller, manageable pieces called finite elements. These elements approximate the behaviour of the entire structure, allowing the calculation of displacements, stresses, and strains under various loads. In FEA, the structure is discretized into elements connected at nodes, interpolation functions approximate the physical behaviour within each element, and a global system of equations is assembled and solved to provide detailed insight into the structural response. This method is particularly useful for complex geometries, heterogeneous materials, and non-linear behaviours in structures.

3.3.2. RFEM methods

At the start of a model the standard and code are set, in this research Standard group EN 1990 and National annex NEN | 2019-11 are used. Then the geometry of the building is made using nodes, lines, members and surfaces. The members and surfaces are prescribed a material and cross-section or thickness and in case of the main model of this research eccentricities are used on the members to better represent the actual building (prevents overlapping of members). At the base of the building supports are added and to analyse the behaviour of the building load cases and load combinations are added and generated.

To implement the stiffness values of the connections for the members and surfaces Hinges (an RFEM function) are introduced for the members and Line Releases for the surfaces. These give options to set translational and rotational stiffness in the x, y and z directions, via a multitude of options as visible in Figure 3.3.

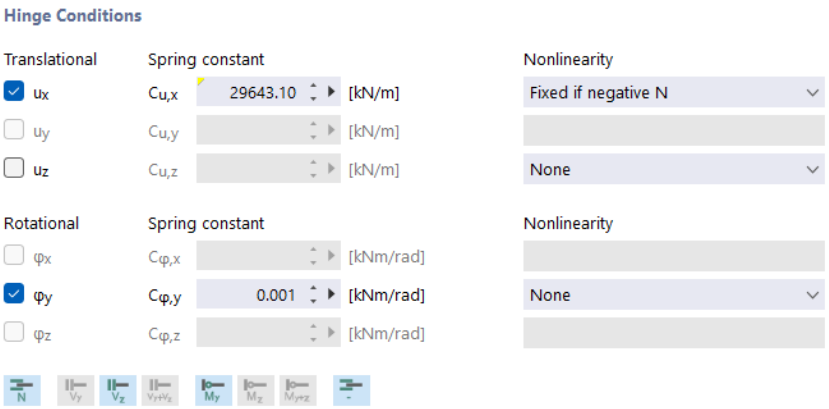

Figure 3.3: Example of stiffness options for hinges in RFEM 6

The values can be set as constant or non-linear. For constant one can fill in a value (as is done in Figure 3.3) or a formula or parameter. The formula option in combination with parameters is mainly used in this research. Parameters are easy to use, because one can make a parameter for the stiffness of each connection type. If one then wants to change the stiffness of one or more type of connections, the only action needed is to change the value of the parameter, thereby changing all the stiffnesses of the connections that are related to that parameter. Figure 3.4 shows how the spring constant Cu,x in Figure 3.3 is determined via a formula of parameters. Here the parameter ”VGZ9x480” represents

the stiffness of a connection with VGZ fasteners with a diameter of 9 mm and a length of 480 mm. This parameter is then multiplied by two parameters that each represent a factor. These factors are used to investigate a range of stiffness values as explained in Subchapter 3.1.4. The example given is used in the models were both connections and members transnationally deform. To research how the structures deform without the translational deformation of the connections, all connections are modelled as pinned connections, fully fixed translational and fully released rotational.

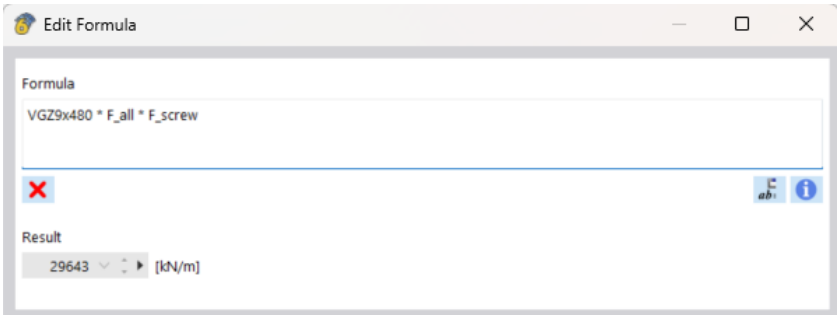

Figure 3.4: Input spring constant Cu,x in figure 3.3

3.4. Verification of the wind load distribution

In the structural design of the building, an assumed distribution of wind load between the core and the façade bracing system was adopted. For wind acting on the wide face of the building, 25% of the total wind load was assumed to be resisted by the core, while for wind acting on the narrow face this share was taken as 35%. The remaining part of the wind load was assumed to be transferred to the bracing systems in the façades. Consequently, each narrow façade (façade X), contributing to resistance of wind on the wide face, was assumed to carry 37.5% of the total wind load, while the wide façade (façade Y), contributing to resistance of wind on the narrow face, was assumed to carry 32.5%.

To verify the plausibility of this assumption, the RFEM model of the core and the 2D RFEM models of the façades were used to estimate their relative lateral stiffness. Each model was subjected to a horizontal point load of 100 kN applied at the top of the structure in the direction corresponding to the considered wind load. This resulted, for each wind direction, in a horizontal top displacement of both the core model and the relevant façade bracing model.

Based on the applied load and the resulting displacements, an equivalent lateral stiffness was estimated for the core and for each façade bracing according to

$$K = \frac{F}{u}, \tag{3.16}$$

where F is the applied horizontal force and u is the corresponding horizontal displacement at the top of the structure.

This procedure results in an estimated stiffness value for the core and for the two façade bracing systems in each wind direction. Assuming infinitely stiff connections between the core and the façade bracings, the total lateral stiffness of the system may be approximated as the sum of the individual stiffness contributions. Under this assumption, the share of the wind load transferred to the core is estimated by dividing the stiffness of the core by the total lateral stiffness of the system.

4

Implementation to the case study

The purpose of this chapter is to explain how the structure from Section 1.7 is combined with the information from Chapter 2 and the methods from Chapter 3. The outcome of the actions prescribed in this Chapter, are shown in Chapter 5.

4.1. Schematization of the facades

To accurately make the models and apply the method of Virtual Work there is the need for a good understanding of the structural elements and their connections. This sub-chapter looks at the two façades and illustrates them as a series of springs.

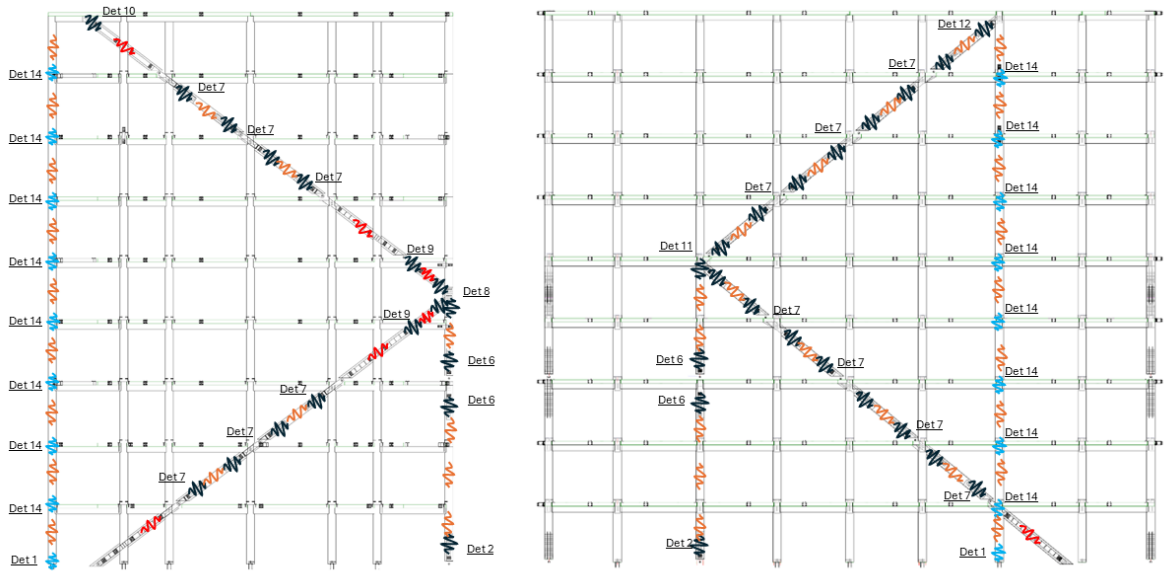

Figure 4.1: Illustrations of Facade X and Y as springs, adapted from CLT-S NV (2024)

Figure 4.1 shows the reduced models, used for the Virtual Work method, as a series of springs. In this research this is done for all structural elements and connections and then applied in all models. The two reduced models show the bulk of the connections and are further explained down bellow. The numbering of the connections is following the original structural drawings made by CLT-s. The connections that are not mentioned in this sub-chapter are mentioned in the



Figure 4.2: Legend for Figure 4.1

calculation of their stiffness in Appendix A.

4.1.1. Illustrations per connection

To get a better understanding of the structure and its connections an illustration is made for each connection (detail). First, the connections following the main load path in the diagonal are shown, starting at the top of the building up to the connection to the concrete basement. Then the heavy loaded column is shown to end with the standard, more common, column. The illustrations for each connection exist out of an image of the detail, a force polygon if deemed helpful, and an illustration of how the connection is modelled as a system of springs. In this system of springs the blue elements deform and the black elements are deemed infinitely stiff. In some cases there is an illustration for both tension and compression in the connection, if there is only one illustration, then the connection behaves the same for both load cases.

Detail 10

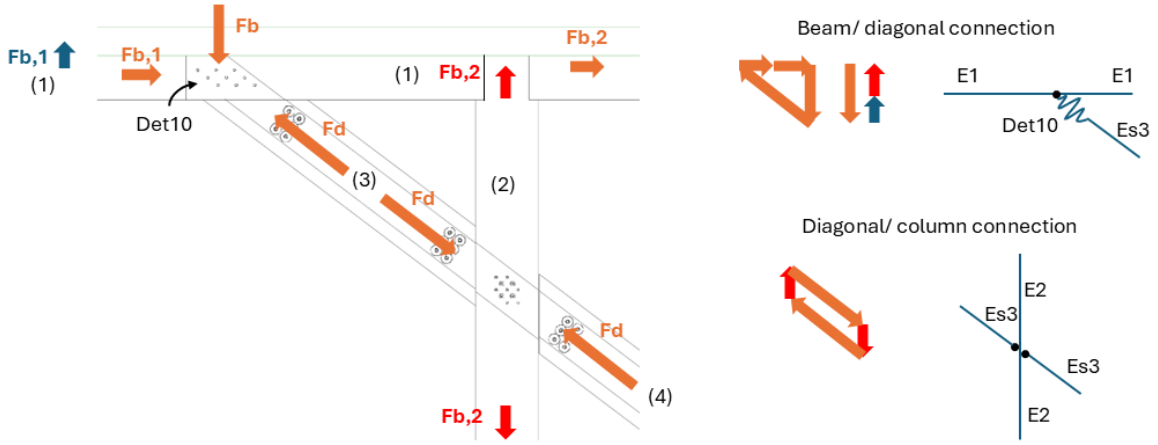

Figure 4.3: Illustration of spring system detail 10, adapted from CLT-S NV (2024)

The load on the structure is a wind load with a pushing load (Fb,1) and a pulling load (Fb,2), as is seen in Figure 4.3, the other loads are a resultant of these two. The connection is modelled as a spring in the direction of the diagonal for the connection with the beam. Next to detail 10 the connection between the column and diagonal is also shown. The connection in the column is about 1.5 times stiffer than the timber, although this sounds significant, compared to other connections this is rather low. Furthermore, if this connection is added to the model it will result into local moments in the diagonal and column. Therefore, it was deemed that the purpose of the connection is mainly to align the timber members and limit the buckling length and not to transfer any load. The result is that in the models this connection is neglected and the timber members cross over one another.

Detail 12

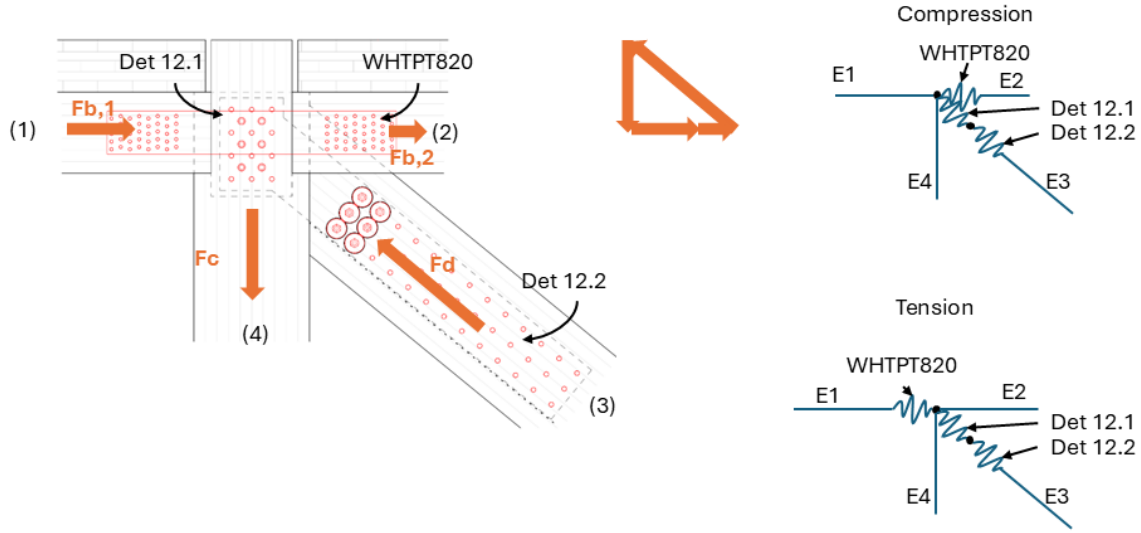

Figure 4.4: Illustration of spring system detail 12, adapted from CLT-S NV (2024)

In detail 12 the diagonal connects to both the beam and column at the same place. Again two loads resulting of the wind load are present in Fb,1 and Fb,2. The difference between the case with compression and tension in the diagonal is whether which load goes through the WHTPT fastener. The path to get the loads into the diagonal is the same for both cases, first the load goes from the timber to the steel with Det 12.1 and then from the steel to the timber diagonal via Det 12.2.

Detail 7

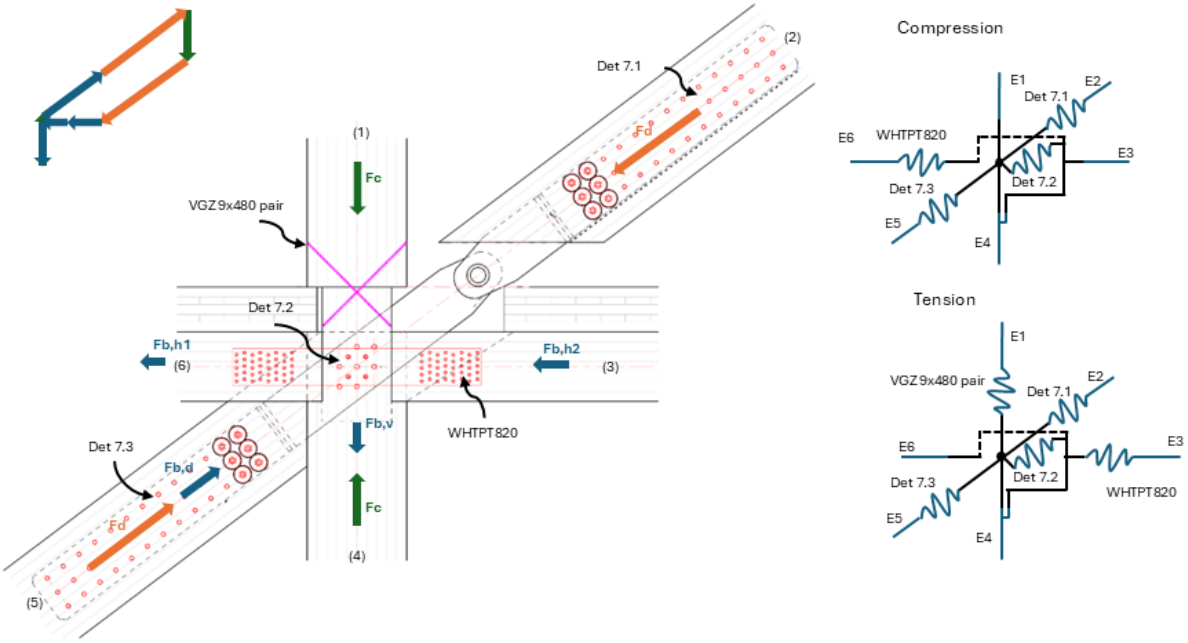

Figure 4.5: Illustration of spring system detail 7, adapted from CLT-S NV (2024)

Detail 7 is the most common connection for the diagonal elements in the facade. The main load going through the diagonals goes from the timber to the steel via Det 7.1 to then go back to the timber via Det

7.3. The column to column connection is timber to timber for the case of compression and via a pair of VGZ fasteners when there is tension. The loads coming from the beams go into the bottom diagonal and column, the resultant force that goes into the diagonal does that via Det 7.2, which is illustrated as a spring in the direction of the diagonal. When modelling this connection in RFEM no satisfactory method was found to include the part Det 7.2 in the models. Therefore, this connection was simplified by excluding Det 7.2 from the models.

Detail 9

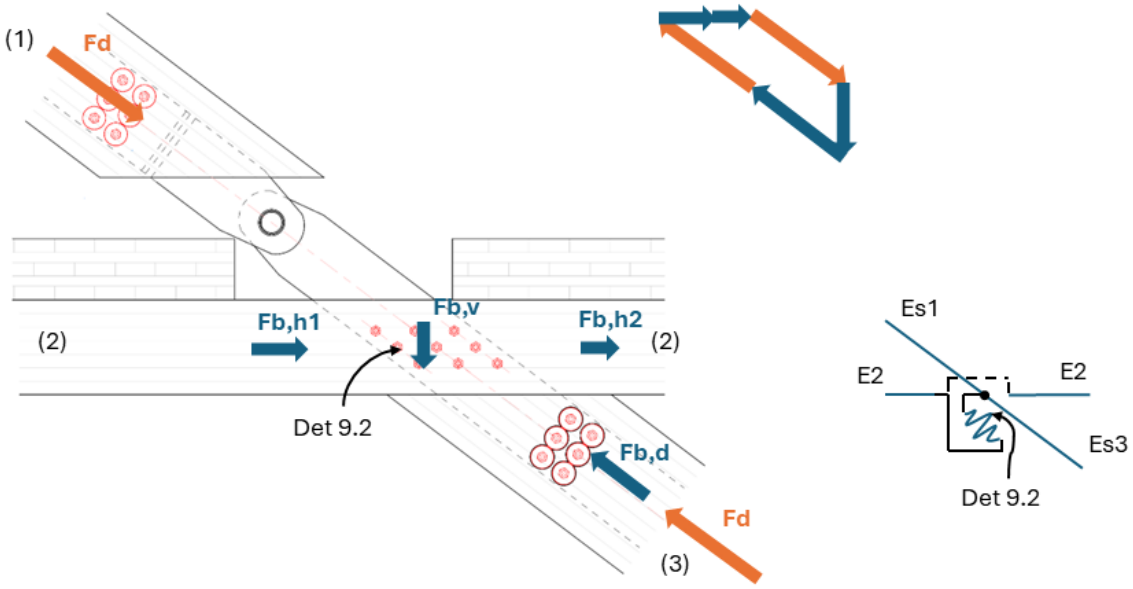

Figure 4.6: Illustration of spring system detail 9, adapted from CLT-S NV (2024)

The diagonal in Facade X at some points goes through beams and columns separately, detail 9 is an example of this. The forces in the beam go into the diagonal via Det 9.2. This results into a shear force and moment in the beam and diagonal. When modelling this connection in RFEM a method was found to add the spring under the angle of the diagonal as an Hinge in the beam. However, a multitude of tests showed no difference between angling the spring to the direction of the diagonal or keeping it straight in the direction of the beam. Therefore, this connection was simplified by modelling spring Det 9.2 in the horizontal direction, but with the stiffness of the connection for a load in the axial direction of the diagonal.

Detail 8

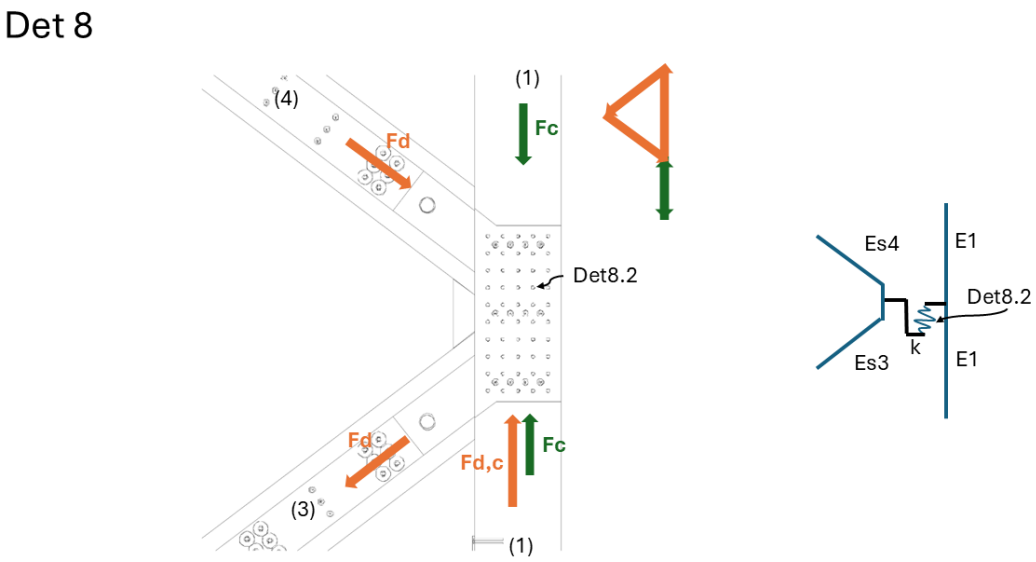

Figure 4.7: Illustration of spring system detail 8, adapted from CLT-S NV (2024)

The diagonal elements connected to dowel group Det 8.2 are made out of steel and transfer back to timber later on in the structure, meaning although there are bolts visible in elements 3 and 4 they are not relevant for the load path. With the steel plates being continuous from diagonal to column to diagonal, although connected steel-to-steel connections, it is assumed that from these steel plates only the resulting vertical force is transferred to the column. This is illustrated via a vertical spring with the stiffness of connection Detail 8.2 in Figure 4.7

Detail 11

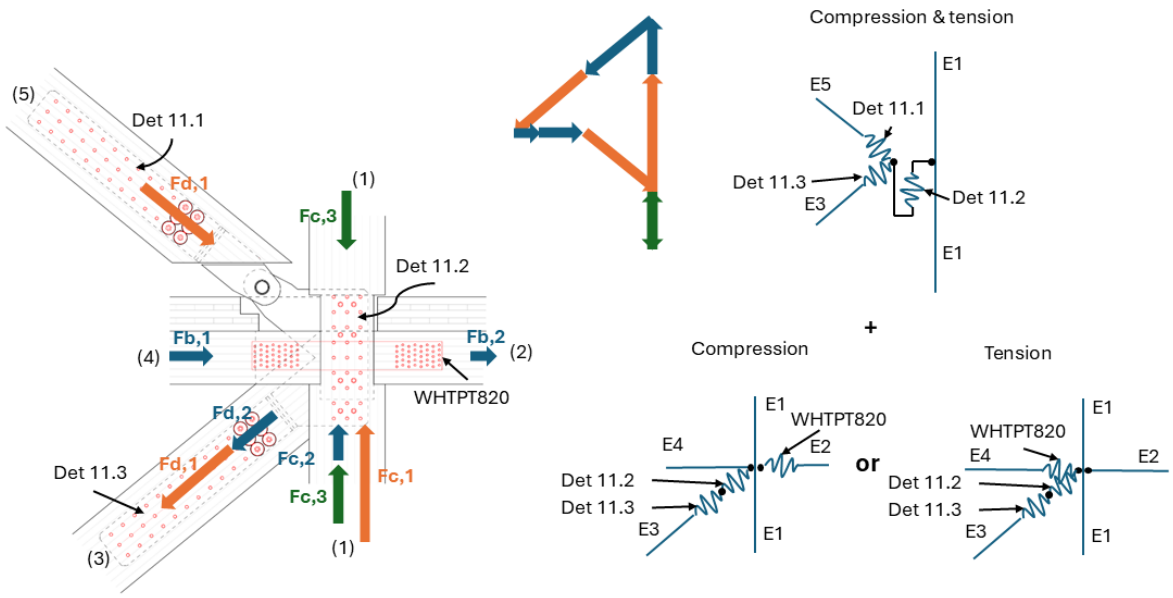

Figure 4.8: Illustration of spring system detail 11, adapted from CLT-S NV (2024)

Detail 11 is the connection where the diagonals change direction in Façade Y. The spring system is for this case separated into two systems that work parallel to one another, one for the load coming from the top diagonal and one for the loads coming through the beams. The system for the load coming from the diagonal is similar to version 2 of Detial 8, but in this case there are bolt groups per member/ direction. The second system running parallel to this is similar to Detail 12, where the loads going through the beams go directly or via fastener WHTPT820 into bolt group Det 11.2, to then go into the diagonal element via Det 11.3. When modelling this connection there was no method found to model the connection so that the loads coming from the beams use Det 11.2 in the direction of the diagonal, while the loads from the diagonals use Det 11.2 in the direction of the columns. The loads coming from the diagonals are significantly higher than the loads coming from the beams. Therefore, Det 11.2 is only modelled as a spring in the vertical direction and excluded from the spring in the angled direction.

Detail 1

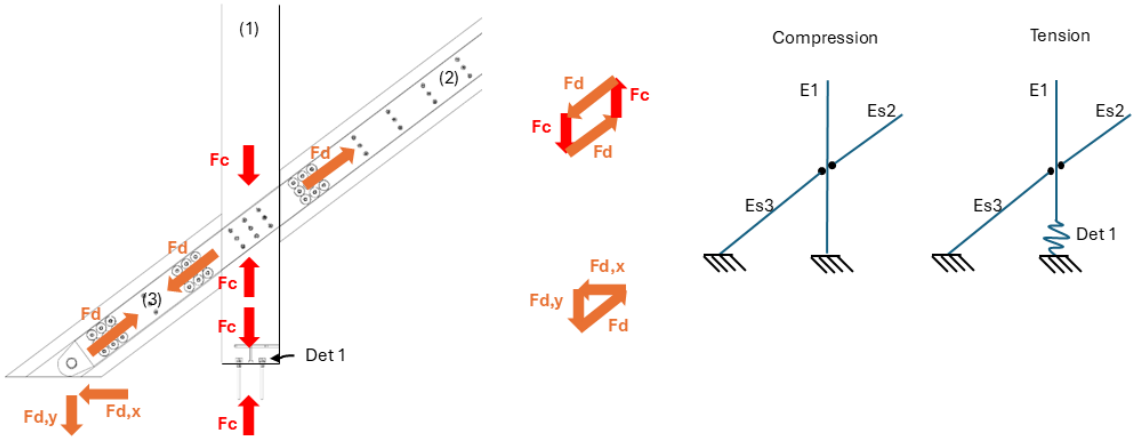

Figure 4.9: Illustration of spring system detail 1, adapted from CLT-S NV (2024)

The illustration in Figure 4.9 shows three connections. First Det 1, which is the most common connection from column to basement. Under compression the load goes from the timber to the concrete directly, while under tension it first passes through connection Det 1. The diagonal elements 2 and 3 are the same steel element and are connected to the basement via a steel connection. Where the column and diagonal meet, 9 screws are used to connect the two, it is assumed that there is no force transfer here, as the stiffness of the 9 screws is eight times lower as the timber column.

Detail 2

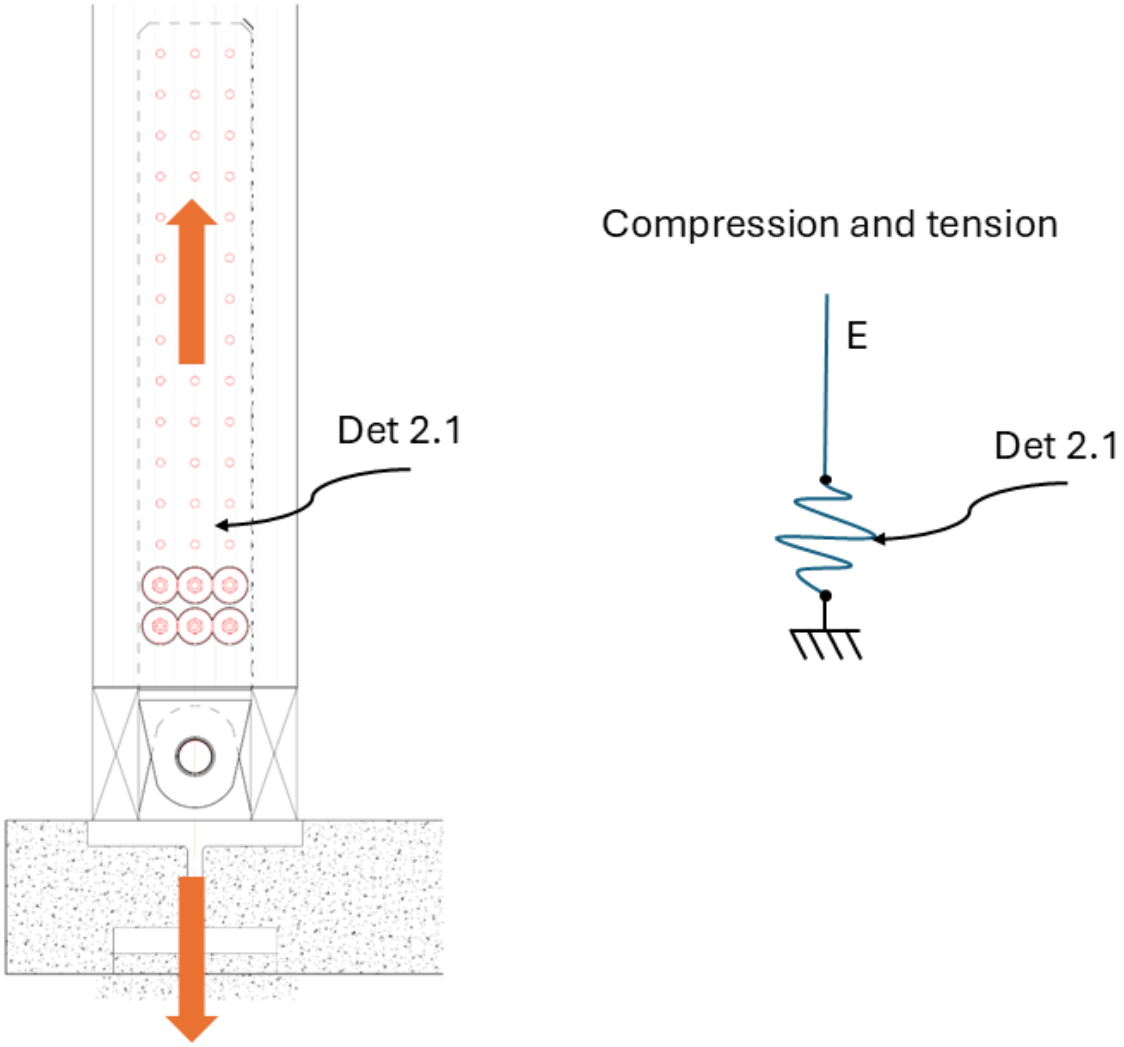

Figure 4.10: Illustration of spring system detail 2, adapted from CLT-S NV (2024)

Detail 2 is the connection used to connect the columns with high loads to the basement. To transfer the load a big dowel and bolt group is used in both compression and tension.

Detail 6

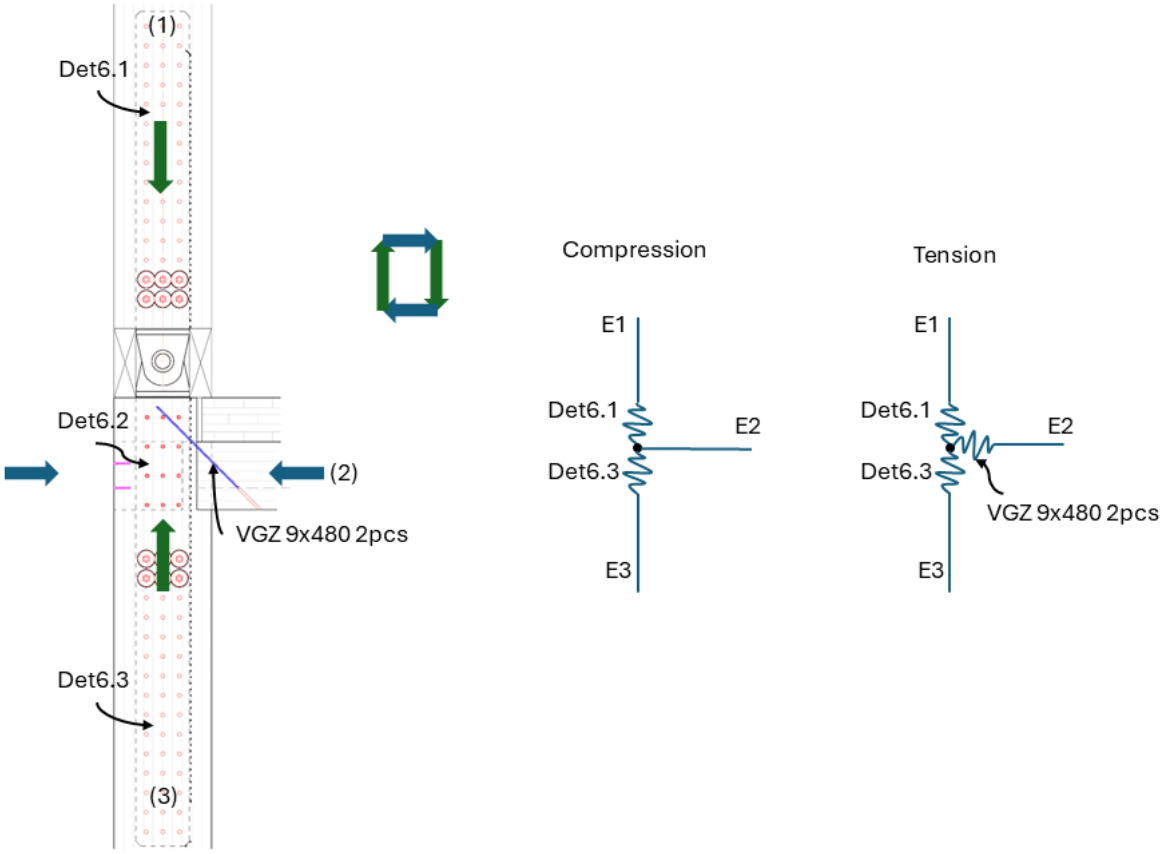

Figure 4.11: Illustration of spring system detail 6, adapted from CLT-S NV (2024)

The same column in Detail 2 is seen in Figure 4.11 as element 3. Here, the column to column connection is modelled as a series of springs (Det 6.1 and Det 6.3), while the beam is connected via VGZ fasteners. Det 6.2 connects the beam, perpendicular to the view, to the column and is irrelevant for the load transfer of the illustrated loads.

Detail 14

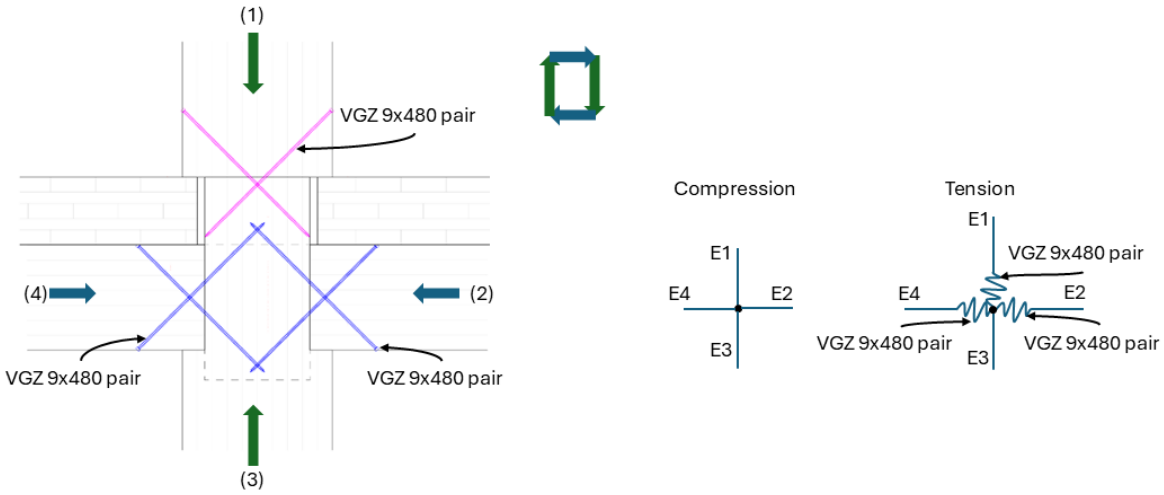

Figure 4.12: Illustration of spring system detail 14, adapted from CLT-S NV (2024)

The most common connection of the timber members in the façade and the rest of the structure is illustrated in Figure 4.12. Pairs of VGZ fasteners transfer the tension loads over from member to member, while under compression the loads go directly from timber to timber.

4.2. Structural restraints

The timber part of the building is supported by a two story concrete basement, the basement is then supported by concrete pads and foundation piles. To include the influence of the concrete basement and the ground, supports are added on each part where the timber goes over into concrete. In RFEM this results into nodal supports underneath each column and a combination of line and nodal supports underneath the core walls.

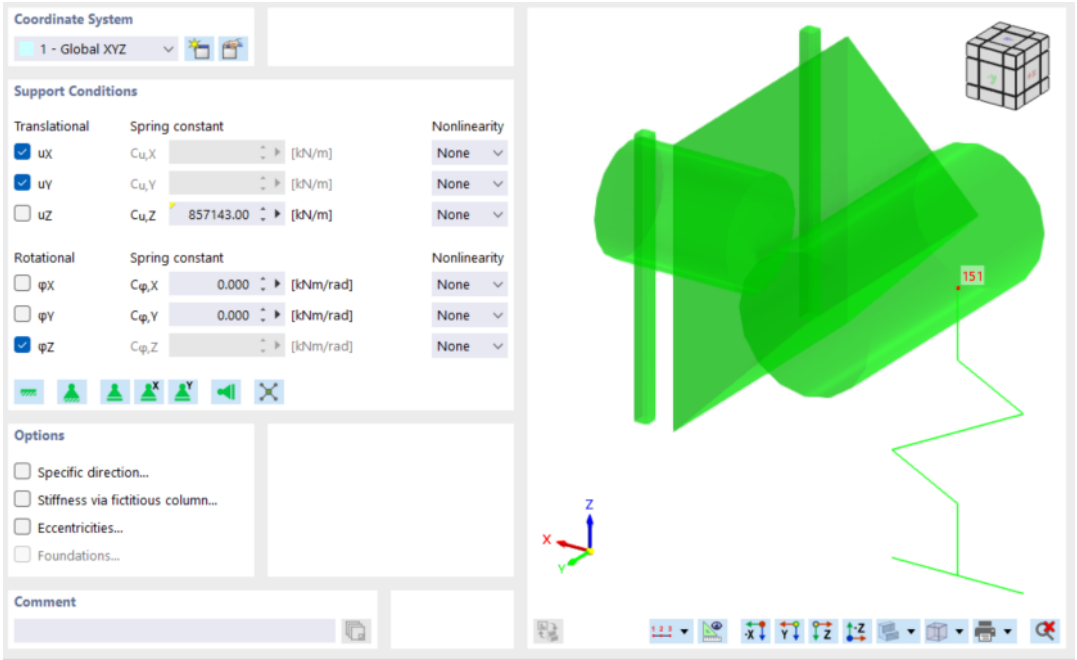

Figure 4.13: Input of the Nodal Supports in RFEM

Figure 4.13 shows the edit screen of the nodal supports beneath the columns in the main model. The supports are free to rotate about the x- and y-axes and are modelled with a translational spring in the z-direction with a stiffness of 857,143.00 kN/m. This stiffness value was derived from an existing RFEM 5 model of the basement structure developed by Arcadis. In that model, the basement was subjected to point loads corresponding to the maximum support reactions obtained from the timber structure under wind loading. The resulting vertical displacements of the most heavily loaded nodes were evaluated. On average, a node subjected to a vertical point load of 600 kN exhibited a vertical displacement of approximately 0.7 mm. Dividing the applied load by the corresponding displacement results in the adopted spring stiffness.

The supports under the core in the RFEM models exists out of two variants, nodal and line supports. Of which the layout is presented in Figure 4.14. The nodal supports are big groups of dowels (40 pcs) at 11 specific locations in the core walls. Between these big groups of dowels a single line of dowels connect the CLT walls to the basement, for which a line support is used in the RFEM models. For these supports the stiffness of the dowels work in series with the stiffness of the foundation. For the stiffness of the dowels Appendix A.2 provides more information. The stiffness of the foundation for the nodal supports is identical to the stiffness gives for the columns (857,143.00 kN/m), as mentioned above. For the foundation stiffness of the line supports a smeared stiffness is calculated. This is done by adding up all the stiffness values for the nodal supports, as parallel springs, and divide it by the total width of all the core walls that connect to the basement. This can be done because the two type of supports never work at the same time, in case of compression the line supports resist the loads and in case of tension the nodal supports resist. The eleven nodal supports add up to a total stiffness of 9,428,571.43 kN/m, and the total width of the walls is 30.95 m. Dividing the two values result into a smeared stiffness of 304,638.82 kN/m^2 for the line supports.

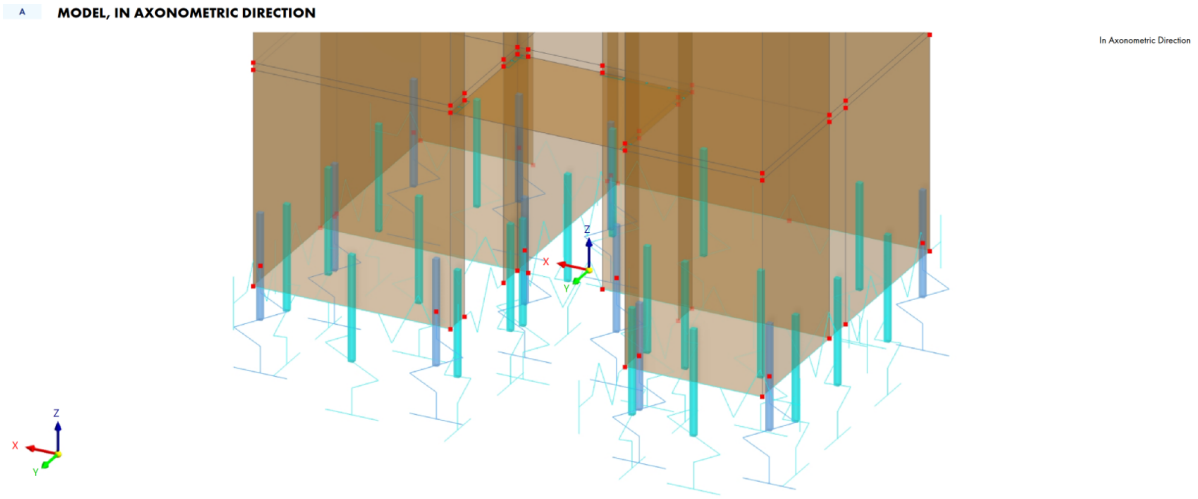

Figure 4.14: The layout of the two types of supports in the core, nodal supports (blue) and line supports (light blue)

4.3. Load cases and combinations

The relevant load combinations used for this research exist out of a wind load in one of the four directions and the self weight in the serviceability limit state.

4.3.1. Self weight

The self weight used in the RFEM 6 models originates from the RFEM 5 model used in the design of the building and is in correspondence with code NEN-EN 1991-1-1:2002. It exists out of surface loads 1.50 kN/m^2 (outside) and 2.75 kN/m^2 (inside), line loads 1.0 kN/m and 3.0 kN/m depending on the facade, and point loads for the balconies. Figures on how these loads are applied in the model are visible in Appendix D.

4.3.2. Wind load

The wind loads are calculated using codes NEN-EN 1991-1-4:2005 and
NEN-EN 1991-1-4+A1+C2:2011/NB:2019+C2:2023, the first one explains the formulas used and the second is a national annex with the values for parameters specifically for the Netherlands. The whole calculation process is explained in the Appendix D, in this sub-chapter the wind load per model is showcased.

Wind load global model

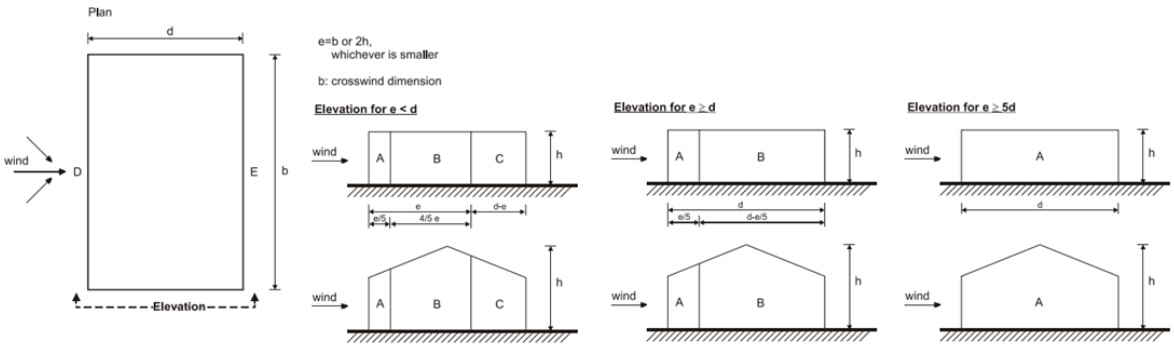

Figure 4.15: Wind zones

Zone	$c_{pe,10}$	w_e [kN/m^2]	q [kN/m]	Comments
A	-1.20	-1.47	-4.46	Length of Zone A = 6.05 m
B	-0.80	-0.98	-2.97	Length of Zone B = 14.01 m
C				
D	0.80	0.98	2.97	Full height, one zone
D’				
E	-0.53	-0.65	-1.97	

Table 4.1: Wind loads per zone for the wide face of the building

Zone	$c_{pe,10}$	w_e [kN/m^2]	q [kN/m]	Comments
A	-1.20	-1.47	-4.46	Length of Zone A = 4.01 m
B	-0.80	-0.98	-2.97	Length of Zone B = 16.05 m
C	-0.50	-0.61	-1.86	Length of Zone C = 10.18 m
D	0.80	0.98	2.97	Starts from h = 20.06 up to h = 31.85
D’	0.80	0.85	2.60	Starts from h = 0 up to h = 20.06
E	-0.50	-0.61	-1.87	

Table 4.2: Wind loads per zone for the wide narrow face of the building

The q-loads that represent the wind load are halved for the roof and ground floor, as the surface area the wind load is applied on is halved. The roof has additional wind loads for a 1.5 m high fence, to account for what is placed on the roof. This is further explained in Appendix D. Figure 4.16 shows the application of the wind load for the load case +X on the global structure.

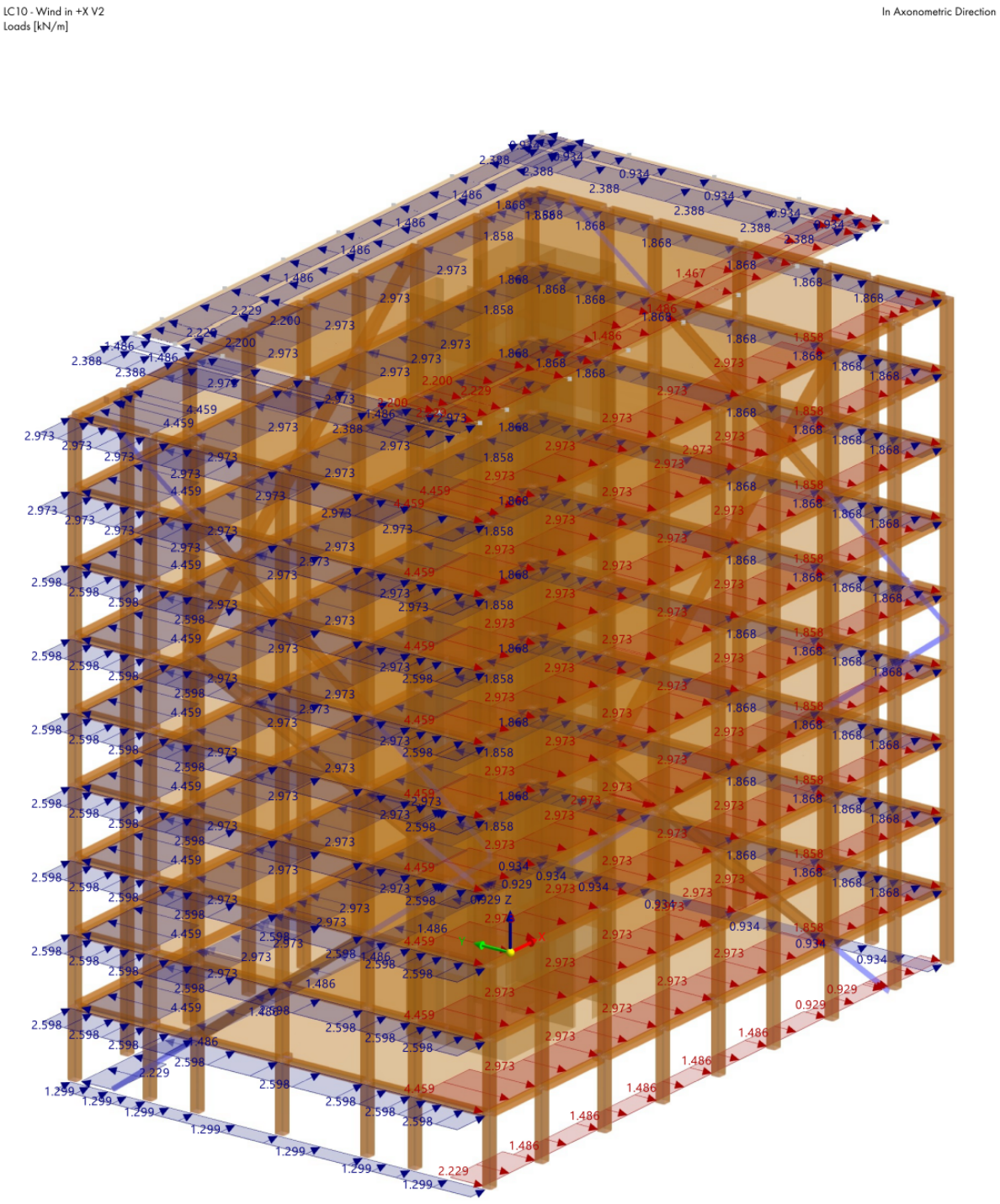

Figure 4.16: Wind loads in the +X direction [kN/m]

Wind load 2D and core models

The Tables 4.1 and 4.2 give the values for the wind loads in the model for the whole building, to get the values for the other models (façades and core) further calculation is needed, which is illustrated in Figure 4.17. The illustration is a top view on how the wind load (q_w) is applied on one level of the façade. This q-load is multiplied by the width of the façade and the percentage of what each part takes up. The building was designed with the idea that for the wide face 25% goes to the core and for the narrow face 35%. Meaning each narrow façade (Façade X) takes up 37.5% and wide façade (Façade Y) 32.5% of the wind pressure on the façade perpendicular to theirs. In the model of the core the structure is subjected to a distributed load instead of a point load for the façades. The calculation process is similar with the addition that the whole value needs to be divided by the effective width of the core for that direction. Not just the width of the core, but the effective width. This is because of the openings in the core on which no load can be applied. The effective width (b_{eff}) is 4.74 m for the narrow side and 6.15 or 7.2 m for the wide side, depending on which wide side the load is applied on. The loads on the roof for the model of the core are higher than listed in the Table, mainly due to the bracing system not continuing up to the roof. This is further explained in Appendix D.

Zone	X-façade [kN]	Y-façade [kN]	Core, Y-direction [kN/m]	Core, X-direction [kN/m]
D	33.71	19.38	3.65 or 3.12	4.40
D'		16.94		3.85
E	-22.31	-12.18	-2.07 or -2.42	-2.77

Note: Core, Y-direction values differ depending on the effective width of the core (b_{eff}).

Table 4.3: Wind loads for models of the facades and core

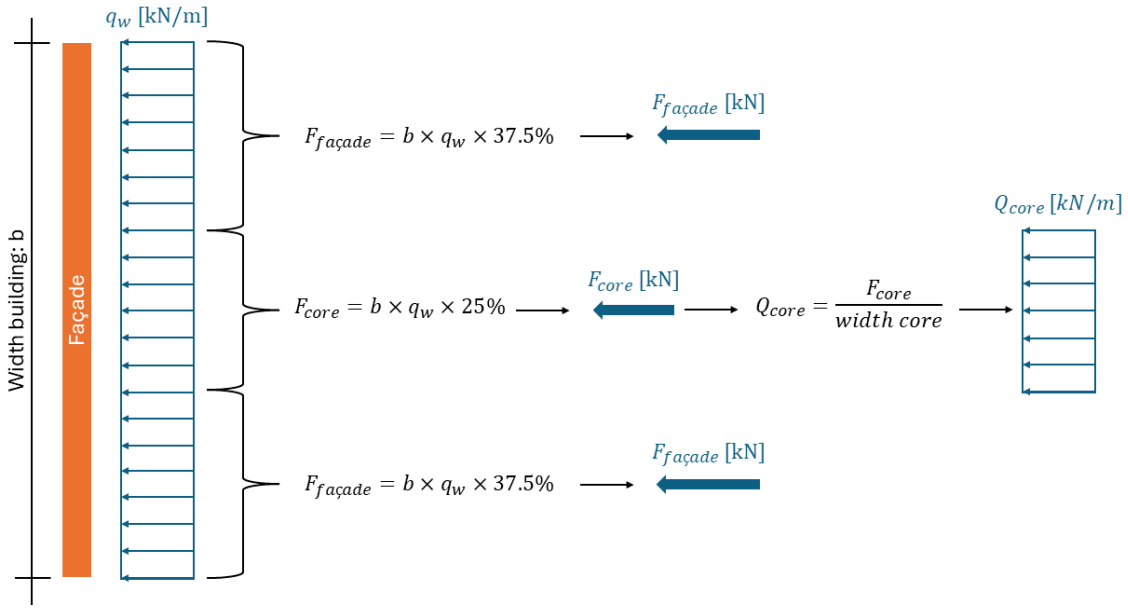

Figure 4.17: Illustration on how the wind load on the 2D and core models is based on the load on the global model (Top view)

5

Results

In this Chapter the results of a multitude of calculations and models are presented. The methods for obtaining the results are described in Chapter 3 and their implementation to the case study in Chapter 4. First, the results of the calculations of the stiffness of the relevant connections is showcased. This is followed by results from all the models categorized per type of results. At the end, results relating to validating or verifying assumptions are presented.

5.1. Calculation of connection stiffness

The stiffness of all relevant timber connections (with relevance defined in Section 1.5) are calculated according to Eurocode 5 (EC5) (Standardization (2025)). In this section, the stiffness values of the connections that govern the global stiffness are presented. The underlying calculation approaches, as well as the stiffness values of secondary connections, are described in Chapter 3 and Appendix A.

Stiffness of governing connections

The most significant connections with respect to global stiffness are those in the diagonals of the façade, as these connections transfer the majority of the lateral loads acting on the building. These connections consist of groups of M16 bolts and dowels, as well as TBS MAX 8$\times$360 screws. According to EC5, the slip modulus of an individual fastener depends on the timber density, the angle between the load and the fibres and the fastener diameter or threaded diameter.

For bolts and dowels, the stiffness per shear plane and an angle of zero is 11.98 kN/mm or 14.63 kN/mm for timber densities of 420 kg/m^3 and 480 kg/m^3, respectively. For the screws, corresponding stiffness values of 2.11 kN/mm and 2.44 kN/mm are obtained. Each fastener has four shear planes due to the presence of two embedded steel plates, resulting in a fourfold increase of the effective fastener stiffness. Consequently, the total stiffness per fastener amounts to 47.90 kN/mm and 58.53 kN/mm for bolts and dowels, and 8.44 kN/mm and 9.77 kN/mm for screws. Meaning of the fasteners used in these connections of the Urban Woods building in Delft, one dowel is 5 to 6 times as stiff as one screw. Table 5.1 presents the total stiffness values of the whole group of fasteners for the governing connections with the highest amount of fasteners. More detailed information on these connections is found in Section 4.1 and a complete table with the stiffness of all dowel connections is found in the Appendix (Table A.3).

Table 5.1: Stiffness of governing diagonal connections

Connection	# bolts/dowels	K_{ser} [kN/mm]	# screws	K_{ser} [N/mm]	Total [kN/mm]
Det 2, 6	45	2155,60	0	0,00	2155,60
Det 7, 11, 12	39	1868,19	0	0,00	1868,19
Det 8	50	2926,27	12	117,30	3043,56

Reduction in stiffness for groups of dowels

In the the Literature review (Chapter 2) an alternative empirical method was introduced by Kjell Arne Malo et al. (2023) to calculate the stiffness for groups of dowels. This method takes into account an underappreciation for the stiffness of a single dowel when using the Eurocode and the over-appreciation of the stiffness for groups of dowels. Using their parameters, based on different but comparable circumstances, a reduction in stiffness is calculated for the connections listed in Table 5.1. The reduction factor for both the connections of Details 2, 6 and Details 7, 11 and 12 are 0.55 and for Detail 8 the factor is 0.43. A connection of around 10 dowels is accurately estimated using this method (meaning factor is around 1.0)

Stiffness of secondary connections

In addition to the governing connections of the dowels in the bracings, the stiffness of secondary connections are calculated. These connections are needed to make the building and model structurally sound, but are not individually pivotal for the resistance of the lateral loads. All these connections mainly use screws of different forms and sizes. A complete overview of the stiffness of each fastener is presented in Table A.2 in the appendix, in this section a short overview is given.

Most common are pairs of inclined VGZ fasteners, five different variants are used to connect timber members and surfaces. These pairs have a high stiffness for the directions in plain and are weak out of plain, their high stiffness varies from 16.04 kN/mm for a pair of VGZ 7x220 to 30.99 kN/mm for a pair of VGZ 9x520. Next to the inclined screws there are single fasteners placed straight, either for their lateral or axial resistance. The most common of these is the TBS fastener connecting CLT panels to the beams. The TBS 8x280 are relatively small but are placed at a frequent interval (200 or 300 mm), these have a lateral resistance of 1.05 kN/mm and axial of 0.36 kN/mm. On the opposite side of the spectrum there are VGS 13x600 fasteners, connecting the top layer of beams to the top of the columns. Their lateral resistance is only double the value of the TBS fasteners, with a value of 2.06 kN/mm, but their axial resistance is significantly higher at 21.75 kN/mm.

The last variant of connections used in this research use a thin steel plate on the outside of the joint, connecting the steel plate to the timber via groups of screws. The stiffness of this type of connection is calculated as a series of springs. With the smallest total stiffness of a value of 7.27 kN/mm for the WHTPT300 and the largest at 45.37 kN/mm for the WHTPT820.

5.2. Global response

This section presents an overview of the different modelling approaches used in this research, including their deformed shapes under the combination of wind load and self-weight, as well as the resulting maximum horizontal deflections at the top of the structure.

5.2.1. Overview of the models

A brief overview of the different models used in this research is provided below; a more detailed description can be found in Chapter 3. The analytical models provide estimates of the deformation of members, connections, and the total structure, whereas the numerical RFEM models provide more detailed and varied results in both magnitude and deformation patterns.

Analytical

- **Method of Virtual Work:** two models based on the method of Virtual Work are implemented in Excel, one for each façade design.

Numerical

- **Global modal:** a complete three-dimensional model of the timber structure developed in RFEM.
- **RFEM Virtual Work:** two two-dimensional models of simplified façade structures, corresponding to those used in the method of virtual work. These models are used to directly compare the results with the analytical approach.
- **RFEM façades:** two two-dimensional models representing the complete structures of the façades.
- **RFEM core:** a three-dimensional model of the core structure.

5.2.2. Deformed shapes

The numerical models provide deformed shapes of the structures when subjected to the load combination of their own self-weight and wind load. From the four wind directions, two are chosen to present the deformed shapes of in this section, the positive X and Y directions. The stiffness of the connections are as presented in Section 5.1.

The following observations are made on the deformed shapes of the structures in Figures 5.2-5.8:

- The deformed shapes of the global model with wind in both directions are identical to that of the core when looking at the roof of the structure, Figures 5.3, 5.5 and 5.8. For both wind directions the maximum horizontal deflection is not found along the side on which the main wind load is applied on but on the side perpendicular to it.
- On the right side of Figure 5.8 the core is subjected to the self weight and a wind load in the positive Y-direction. The maximum horizontal deformation is not found at the top of the building but along a connection running vertically, connecting two core walls (the dark red area).
- The horizontal deformations for both the RFEM VW models are big at the midspan of members, and become smaller at the joints.
- From the side-views of the global model and the RFEM façade models a linear trend is seen for the horizontal deflection along the height of the structure for the first levels. For the global model subjected to wind in the X direction, Figure 5.2, this linear trend is observed along the whole height of the bracing system, and for the last storey the trend becomes non-linear. The linear trend for the deflection in the façade model subjected to the same wind load, Figure 5.6, ends at the fifth level. On the fifth level a significant increase in lateral deflection is observed, after which an oscillating pattern follows for the lateral deflection over the remaining floors (the deflection increases, then decreases, then increases , etc)
  For the models subjected to wind in the Y direction, Figures 5.4 and 5.7, this linear trend stops at the fifth floor, the floor above the change in direction of the diagonals. On that floor a significant increase in horizontal deflection is observed, after which a linear trend is again observed for the horizontal deflection of the floors above. This sudden increase in lateral deflection is more extreme for the façade model, as the maximum horizontal deflection is not found at the top but at the fifth floor, while for the global model the increase is noticeable, but smaller, and afterward the deflection keeps increasing for higher floors.

For the façade subjected to the wind in Y direction, the narrow façade, the area with the sudden increase in deflection is presented in Figure 5.1. In the figure it can be observed that the horizontal deflection at the crossing of the bottom beam and the diagonal is 5.58 mm. Half a level higher at the connection of the diagonal and the outer column the deflection is doubled to a value of 11.44 mm. In this connection at the outer column the value increases to a value of 15.64 mm and, to then again increase to 27.83 mm at the crossing of the diagonal and the second beam in the figure. At the next connection of the diagonal the lateral deflection has decreased to a value of 22.00 mm.

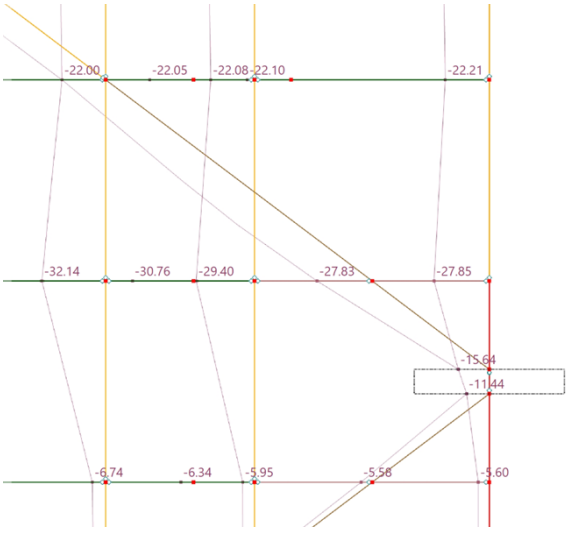

Figure 5.1: Complications in the design of the façade subjected to wind in the Y direction (narrow façade)

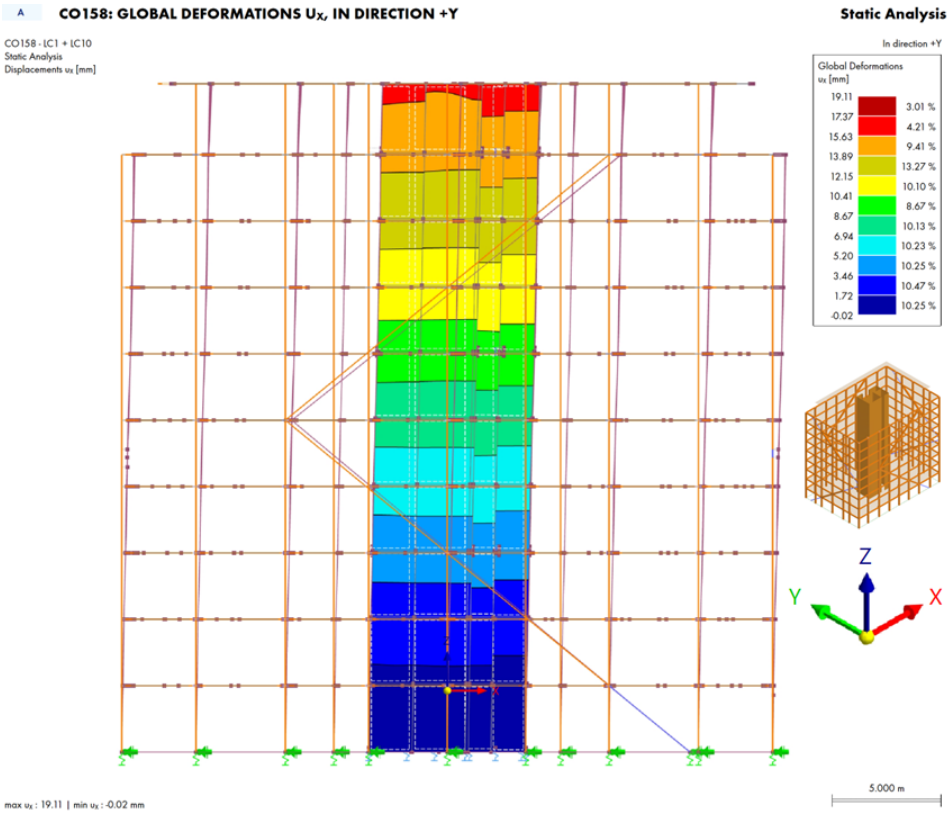

Figure 5.2: Side view of the displacement due to wind load X+ and self weight, deformation shape scaled by 40

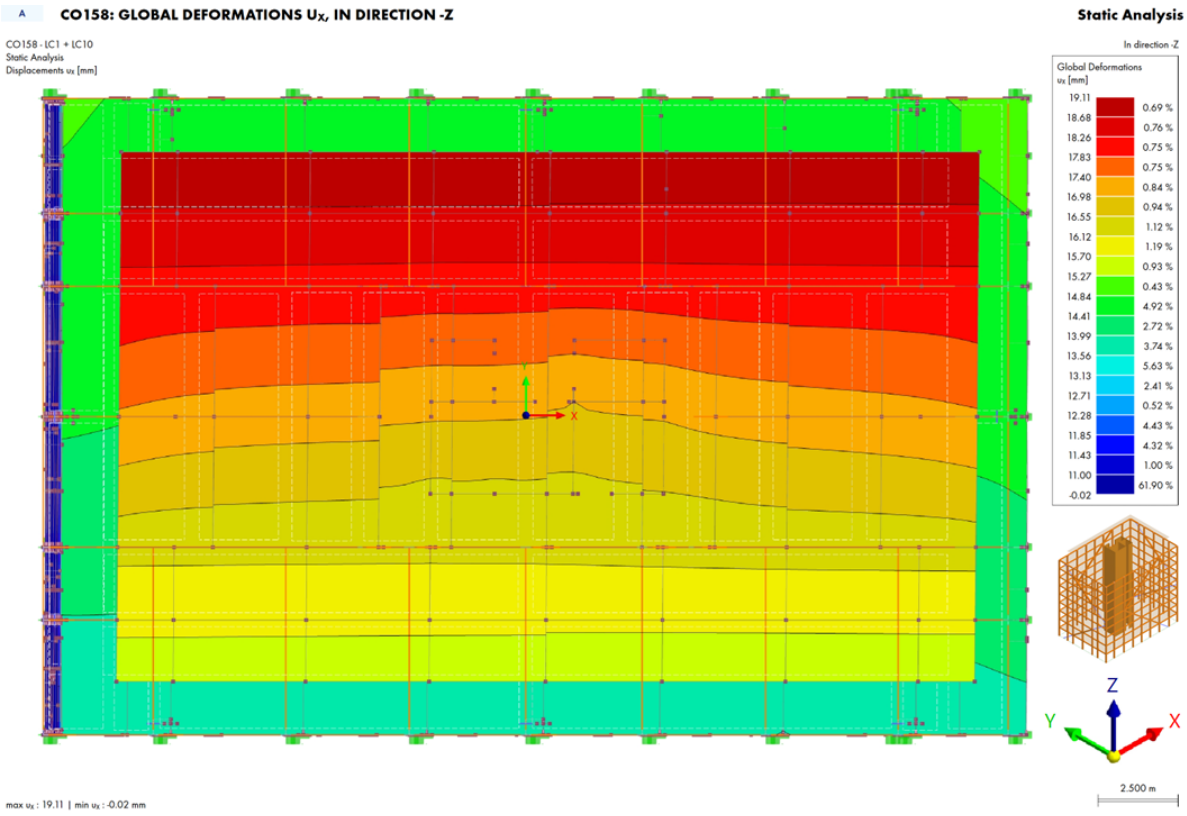

Figure 5.3: Top view of the displacement due to wind load X+ and self weight, deformation shape scaled by 40

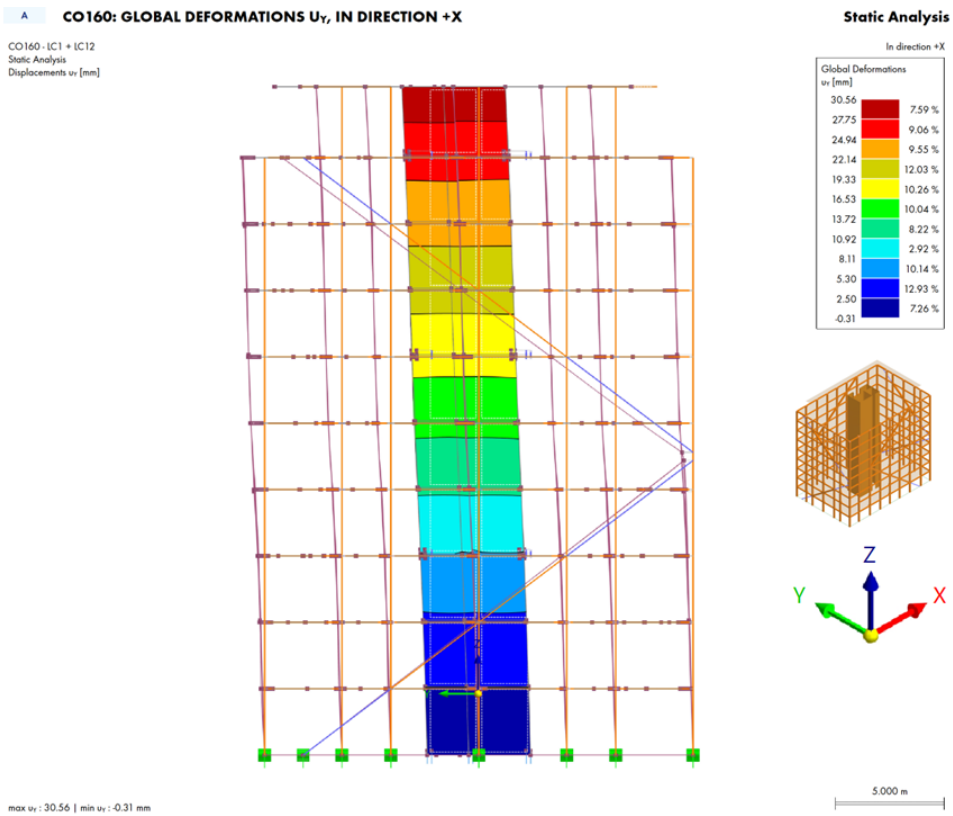

Figure 5.4: Side view of the displacement due to wind load Y+ and self weight, deformation shape scaled by 40

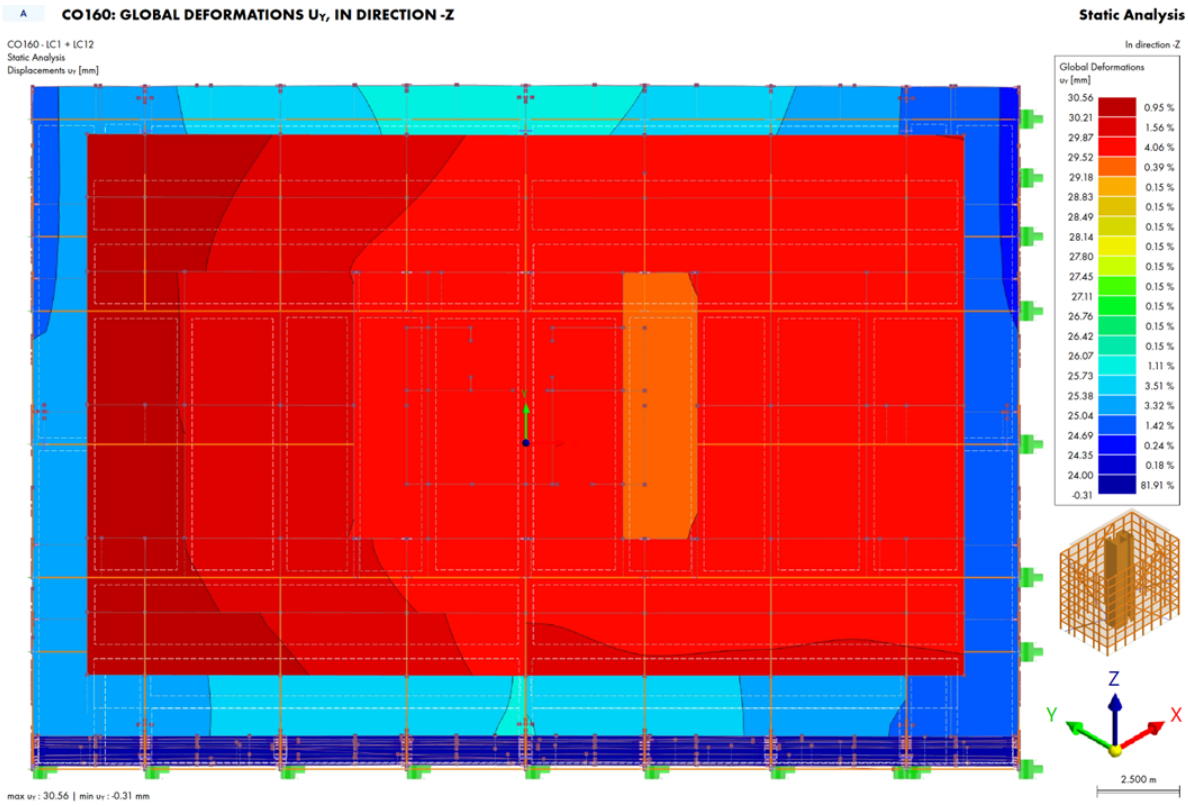

Figure 5.5: Top view of the displacement due to wind load Y+ and self weight, deformation shape scaled by 40

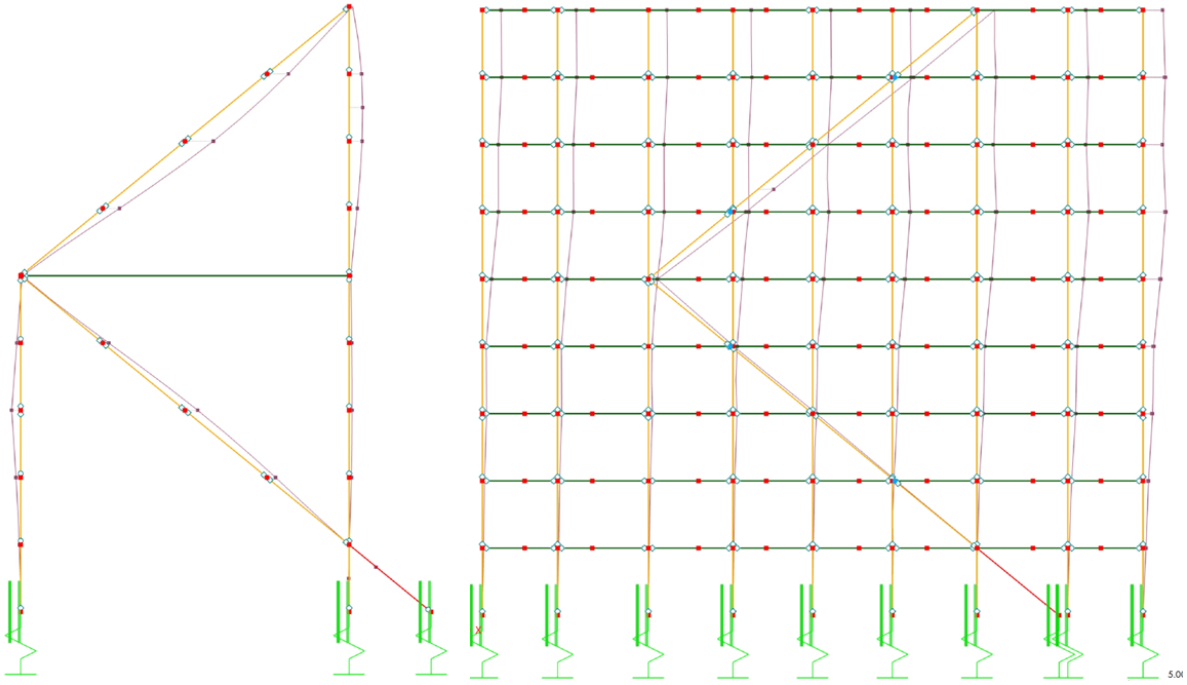

Figure 5.6: Horizontally deformed shapes of the RFEM VW model (left) and the RFEM 2D model (right) of the wide facade loaded by the self weight and the wind in direction X+

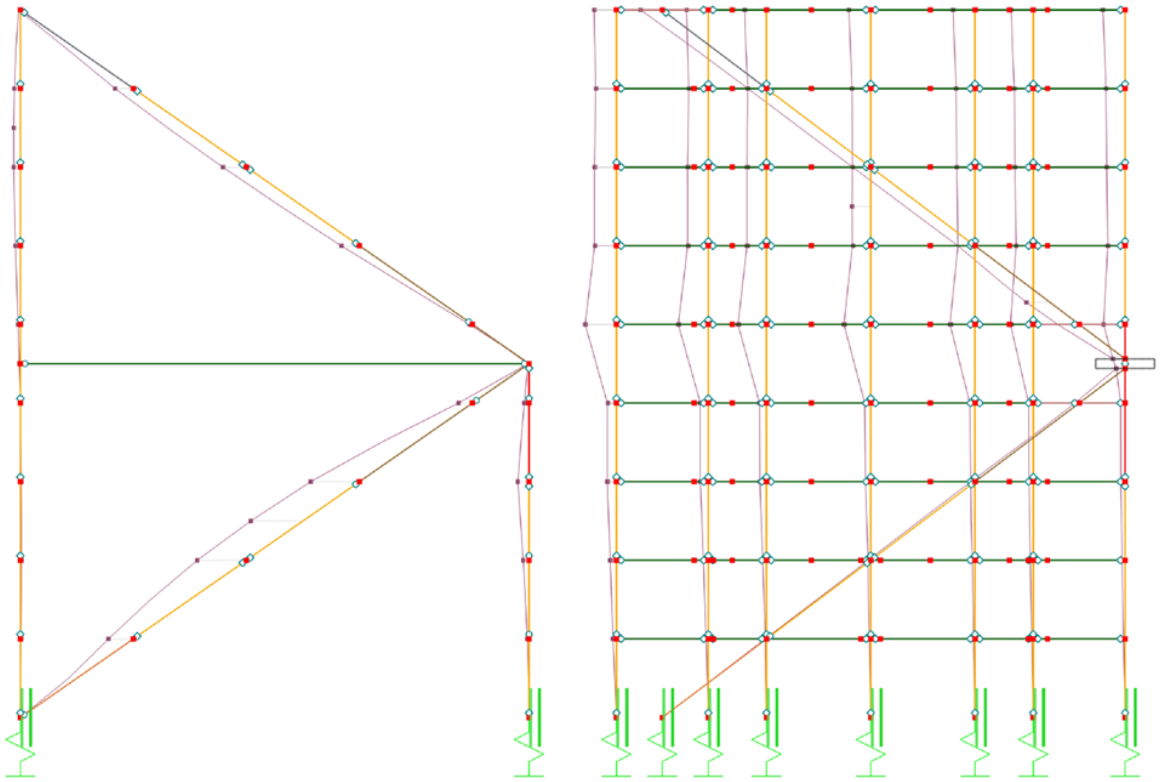

Figure 5.7: Horizontally deformed shapes of the RFEM VW model (left) and the RFEM 2D model (right) of the narrow facade loaded by the self weight and the wind in direction Y+

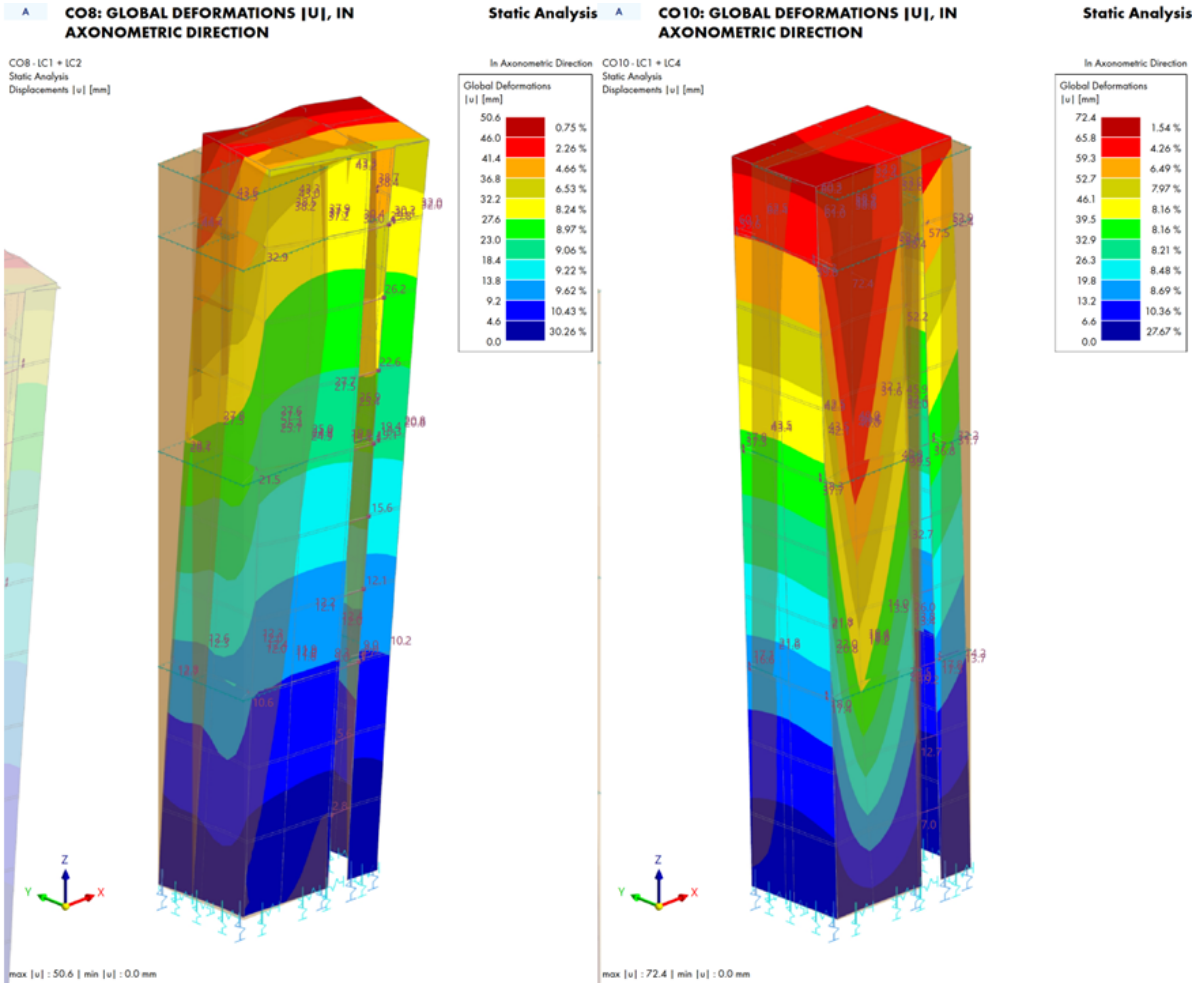

Figure 5.8: Maximum horizontal deflection of the core model, for the wind load in X+-direction (left) and Y+-direction (right)

5.2.3. Horizontal deflection

Table 5.2 presents the values of the maximum horizontal deflection corresponding to the deformed shapes. The global modal is in this research set as the most realistic. Therefore, along the deflection values, of the other models, the relative difference to the results from the global modal are added. Due to the façades not continuing till the roof of the structure (the 10th floor) a separation was made between the results from the 9th and 10th floor.

It is important to note that the loading on the different models is distributed according to an estimation on what each part of the building takes up. This is in more detail explained in Section 3.4 and the distribution it self is tested, of which the results are shown in Section 5.6.1. What it entails is that the values for the different models in Table 5.2 can be directly compared to one another.

Table 5.2: Maximum horizontal deflection at the 9th and 10th floor and the relative difference to the global model per model per wind direction [mm]

		Wind direction							
Floor	Model	X+	Δ	X-	Δ	Y+	Δ	Y-	Δ
9th floor									
	Global	15.31	–	19.44	–	26.42	–	27.84	–
	Virtual Work	9.21	-39.86%	17.36	-10.72%	17.81	-32.59%	23.78	-14.59%
	RFEM VW	9.01	-41.15%	17.13	-11.88%	18.55	-29.79%	25.17	-9.59%
	RFEM façade	11.00	-28.15%	18.48	-4.94%	28.74	8.78%	28.30	1.65%
10th floor									
	Global	19.11	–	22.82	–	30.56	–	33.15	–
	Core	48.20	152.22%	43.64	91.24%	68.18	123.10%	53.02	59.94%

The following observations are based on the results presented in Table 5.2:

- Higher deflection values are found for wind in negative direction than for positive direction and for wind in Y direction than for X direction.
- The results of the global model present a smaller difference between negative and positive wind directions than the other models.
- The results of the Virtual Work model and RFEM VW are close to identical, underestimating the horizontal deflection by 10.72 to 39.86%. With the better estimation for the negative wind directions.
- The models RFEM façade provide better estimation of the deflection than the models based on Virtual Work. With the relative difference to the global model varying from 1.65 to 28.15%.
- The model of the core presents the biggest difference to the results from the global model, as the horizontal deflection is overestimated by 59.94 to 152.22%.

5.3. Influence of connection stiffness

This section presents the results needed to research the influence the stiffness of the connections have on the horizontal deflection of the building. This is done by altering the stiffness parameters as explained in Section 3.1.4. The boundary conditions (load combination and supports) are calibrated to each model, so that the results can be directly compared, as is explained in Chapter 4.

First the focus is placed on only the global model, this is then followed up by the results from the models of the façades (Virtual Work, RFEM VW, and RFEM façades) and the model of the core separately.

5.3.1. Global model

Maximum horizontal deflection

The graphs in Figures 5.9 and 5.10 present the maximum horizontal deflection of the 9th and 10th storey per change in connection stiffness. At 0% change in connection stiffness, the translational stiffness values following the analytical approach explained in Chapter 3.1.1 are used. These values are then

changed for increments of 10%. Straight lines are added on top of the curves to give more context. First, the purple dashed line, labelled ”Kjell Arne Malo et al. (2023)”, shows the reduction in stiffness for the biggest group of dowels (50 dowels) in the Urban Woods building, when using the equation from the research done by Kjell Arne Malo et al. (2023). Secondly, the black dashed, labelled ”h/500”, shows the limit for the maximum horizontal deflection used in the early stages of the design process of the building, it has a value of 64 mm. Lastly, the horizontal asymptotes, of the curves are added to the graphs, labelled ”Y asym” & ”X asym”. Their values are obtained by making the translational stiffnesses in the model infinitely stiff.

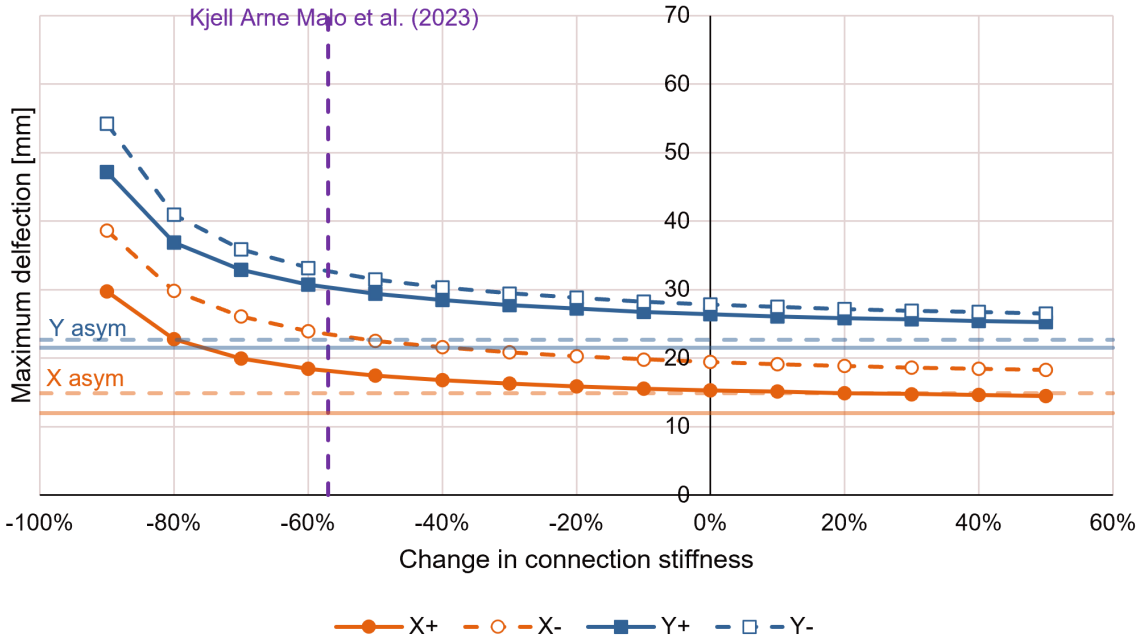

Figure 5.9: Maximum horizontal deflection of the 9th storey for four wind directions (X+, X-, Y+ & Y-) per change in connection stiffness

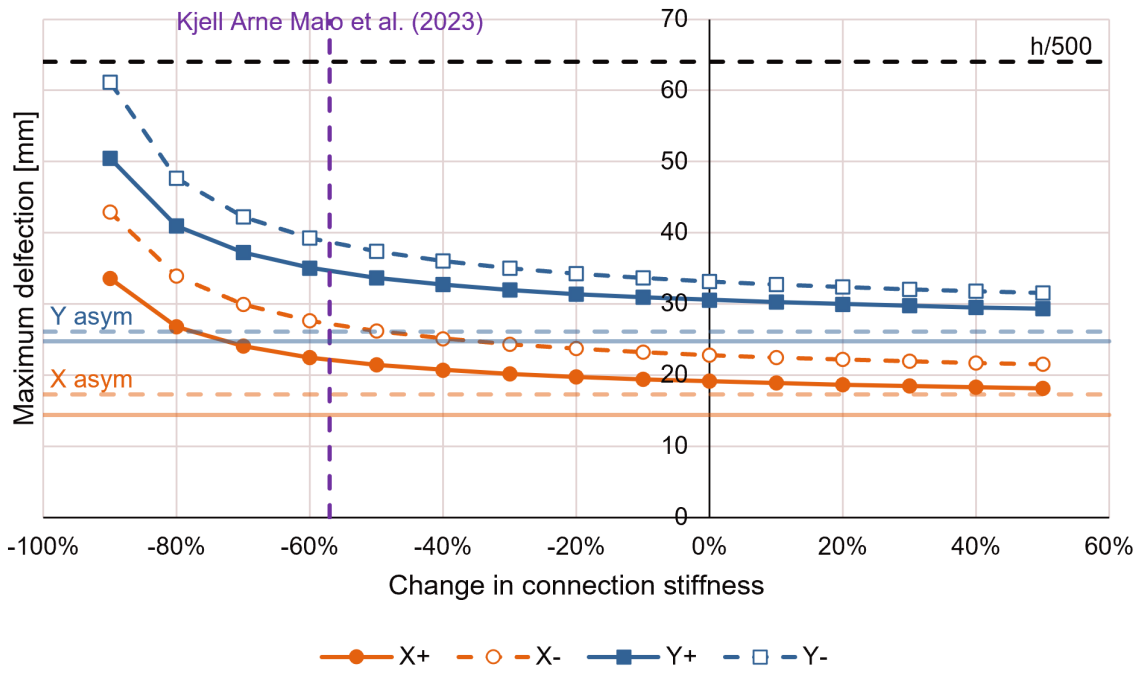

Figure 5.10: Maximum horizontal deflection of the 10th storey for four wind directions (X+, X-, Y+ & Y-) per change in connection stiffness

The following observations can be made from the graphs in Figures 5.9 and 5.10:

- In both graphs the shape of the lines for the four wind directions are similar, highlighting the presence of a general trend for the influence of the connection stiffness on the maximum horizontal deflection.
- The deflections in the Y directions are always higher than their counterparts in the X directions. Similarly, this is also seen for the negative direction (X- & Y-) compared to the positive directions (X+ & Y+).
- Up until 50% reduction in connection stiffness, around the (Kjell Arne Malo et al. 2023) line, the change in maximum deflection appears to follow a linear trend. From 50% up the trend becomes non-linear, for all wind directions in both graphs. This rate of change is further highlighted in the graphs of the following Figures 5.11 and 5.12.
- There is no value measured above the early stage design limit for the maximum horizontal deflection of the building (black dashed line labelled ”h/500”).
- With the range of change observed for the maximum deflection per increase of the connection stiffness it appears that the asymptotes will not be reached any time soon.

Relative change in maximum deflection

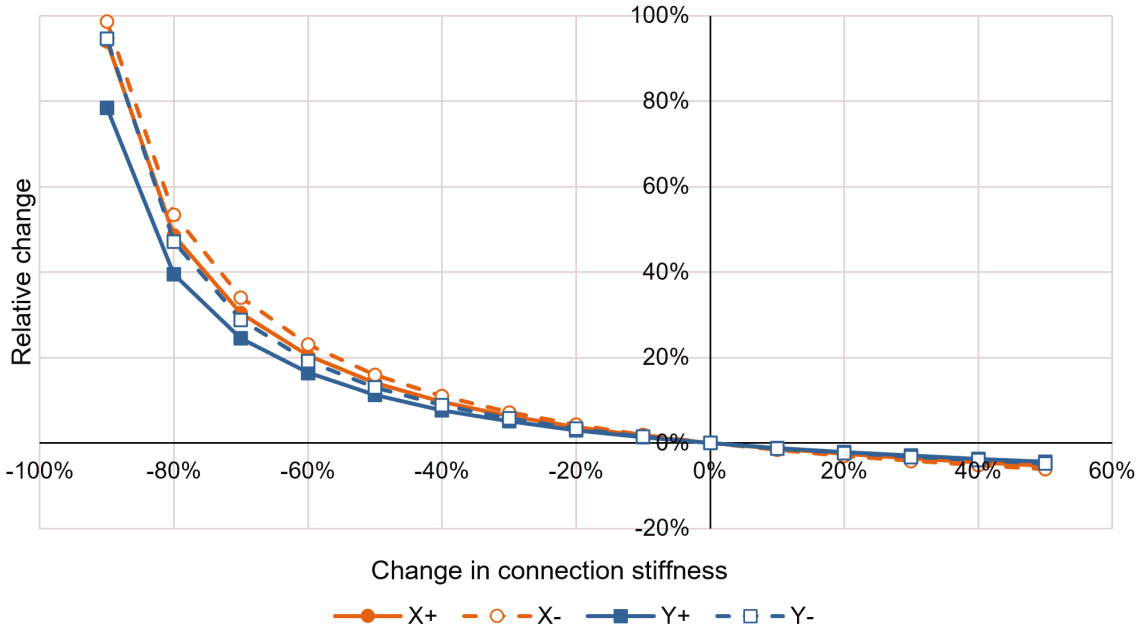

Figure 5.11: Relative change calculated with respect to the 0% change in connection stiffness case for the 9th storey of the data in Figure 5.9 for the four wind directions (X+, X-, Y+ & Y-)

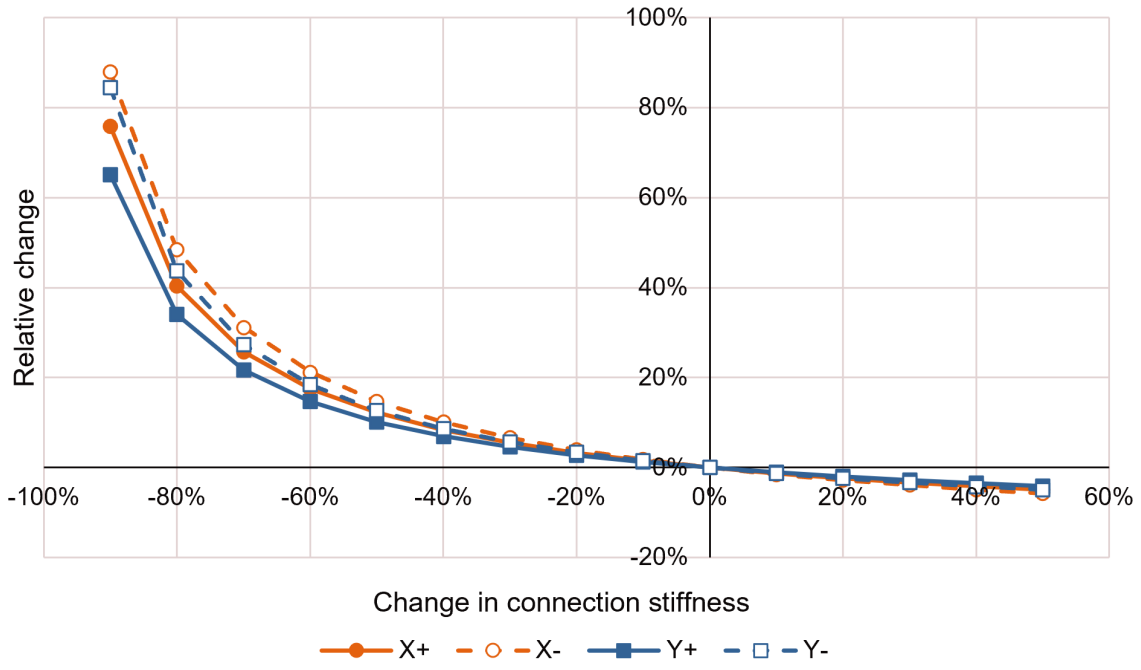

Figure 5.12: Relative change calculated with respect to the 0% change in connection stiffness case for the 10th storey of the data in Figure 5.10 for the four wind directions (X+, X-, Y+ & Y-)

The following observations can be made from the graphs in Figures 5.11 and 5.12:

- Similarly to the previous graphs in Figures 5.9 and 5.10 a linear trend is seen for the positive and low negative change in connection stiffness (50% to -50%), which then slowly turns exponential/ non-linear, starting around 50% reduction.
- The relative change in maximum deflection is close to identical for the four wind directions. However, from the small differences seen between the curves for the highest values in reduction of connection stiffness, it can be observed that the structure subjected to wind loads in the X direction has a higher relative change than the structure subjected to wind loads in the Y direction. A similar observation can be made for negative and positive wind loads, with negative wind loads having the higher values for the relative change.

5.3.2. Façade / 2D models

In Section 5.3.1 the connection stiffness is altered to research the influence of this stiffness on the global stiffness of the building. Similarly to the global model the stiffness of the connections is also altered for the other models. The boundary conditions (load combination and supports) are calibrated to each model, so that the results can be directly compared, as is explained in Chapter 4. Figure 5.13 presents four graphs that show the maximum horizontal deflection of the 9th storey per reduction of the connection stiffness for the four models, with each graph being a different wind direction. Specifically the deflection at the 9th storey is shown as all models go up to the 9th and only the global model goes higher to the 10th storey.

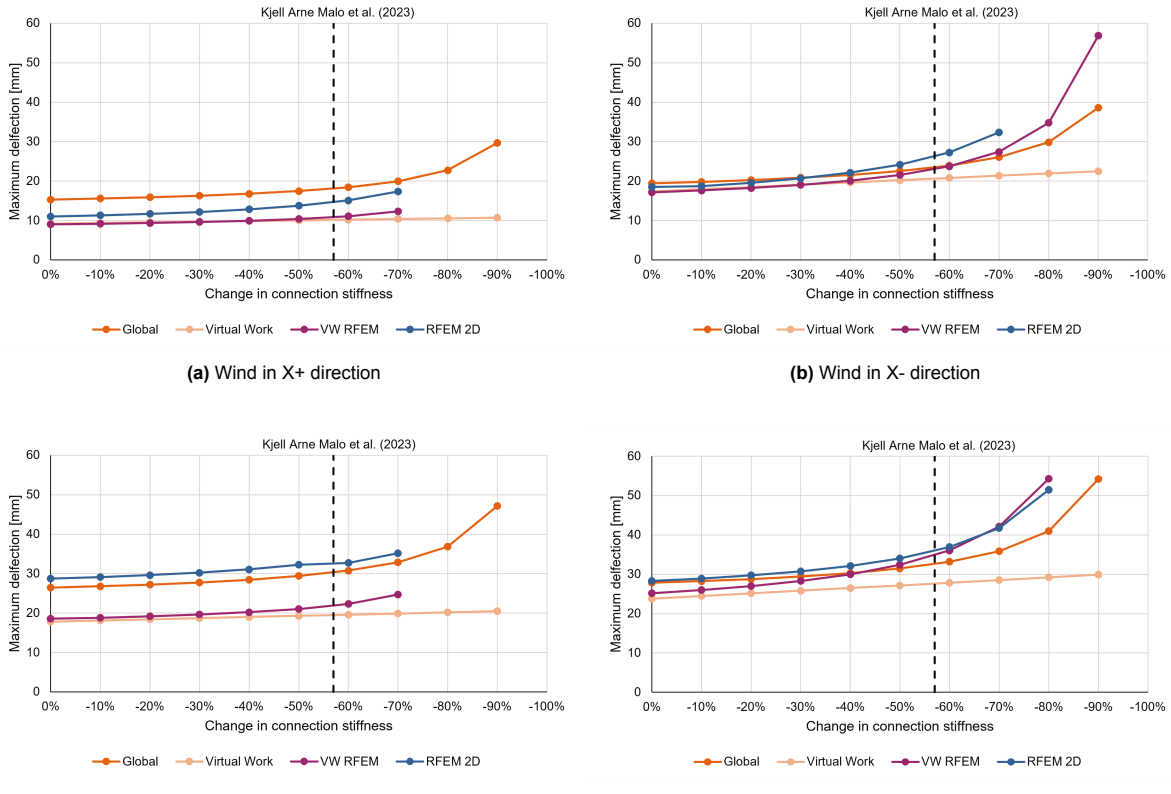

(a) Wind in X+ direction

(b) Wind in X- direction

(c) Wind in Y+ direction

(d) Wind in Y- direction

Figure 5.13: Maximum horizontal deflection of the 9th storey per reduction of the connection stiffness for the global model, Virtual Work in Excel, Virtual Work in RFEM and 2D model of the complete façades in RFEM

The following observations are made on the graphs in Figure 5.13:

- The curve of the Virtual Work model is in each graph a linear line with a small rate of change. The shape of the curves of the VW RFEM and RFEM 2D models are more similar to the curves of the Global model. For low percentages the curves seem linear, but the higher the change in connection stiffness goes, it becomes more clear that the curves are non-linear. Often showing

this non-linear trend earlier than the Global model, resulting into higher relative increase per change in connection stiffness than the Global model.

- The curves for the VW RFEM and RFEM 2D models are shaped more identical for the load cases with the wind in the X-directions than when compared to the load cases with the wind in the Y-directions. Specifically the load case with the wind in the negative Y direction presents an outlier for a result with the VW RFEM model overtaking the RFEM 2D model for the maximum deflection the higher the change in connection stiffness is. This is seen for only this particular load case, as for the other graphs the two models either stay at a similar distance from one another, or even move away slightly.

5.3.3. Core model

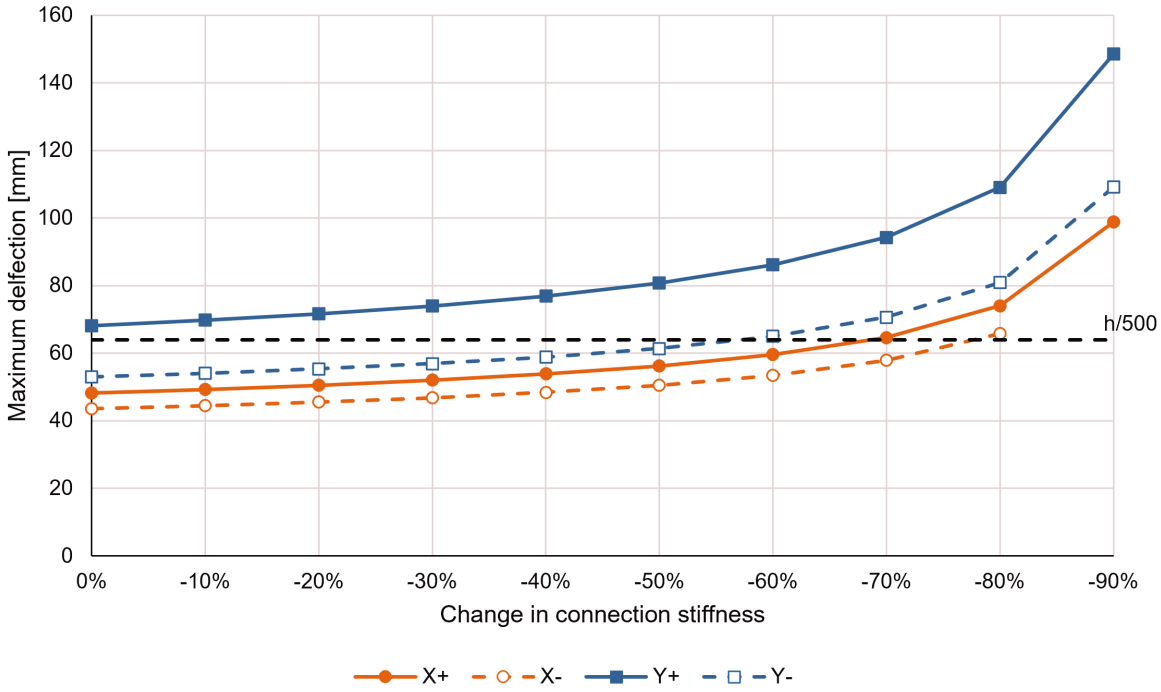

Figure 5.14: Maximum horizontal deflection of the core model for four wind directions

To research the influence of reducing the stiffness of the connections in the core the graph in Figure 5.14 is obtained from values from the numerical model. The maximum horizontal deflection is plotted on the vertical axis and the change in connection stiffness of the horizontal axis, in increments of 10%. The model from which these values are obtained is the core model with all connections added. A horizontally stripped line, labelled ”h/500”, is added to illustrate the SLS limit for the maximum deflection at 64 mm. The following observations are made on the graph in Figure 5.14:

- The curves for the four different wind directions are shaped identical. A non-linear trend is seen for the maximum horizontal deflection as the relative increase of the values gradually increases for higher reductions in connection stiffness.
- The maximum deflection of the core is lower for load combinations with wind loads in the X-direction, when compared to the Y-direction. Similarly, the load combinations with wind loads in negative direction result in lower deflection values than the combinations with wind loads in positive direction.
- The maximum horizontal deflection with the wind load in the negative Y-direction is higher than the maximum allowed horizontal deflection used in the design (h/500 line). The other wind directions also cross the line, but only with significant reductions in connection stiffness.

5.4. Role of subsystems in global stiffness

To investigate the influence of the different lateral load resisting systems (core and the façades) on the global stiffness of the building, this section presents two different types of results. First, horizontal deflection values of the global model, with altering the stiffness of the fasteners used in either the façades or the core. Second, by plotting the relative change in horizontal deflection per change in connection stiffness for the numerical models of the two lateral load resisting systems.

5.4.1. Influence of the stiffness of dowels vs screws

To obtain a clearer understanding of the contribution of the two lateral load-resisting systems in the Urban Woods building, a sensitivity analysis was performed in which only the stiffness of either the dowel-type or screw-type connections was varied in the global model. The rationale for this approach is that the bracing systems in the façades predominantly consist of dowel connections, whereas those in the core are primarily composed of screw connections. By modifying the stiffness of only one fastener type at a time, the relative influence of each lateral load-resisting system on the global stiffness can be isolated and evaluated.

The procedure used to alter the connection stiffness is described in Section 3.1.4. For this analysis, the global model is subjected to load combinations including self-weight and wind loads acting in both the X- and Y-directions. For each reduction in stiffness, the resulting maximum horizontal deflection is determined and presented in Figure 5.15.

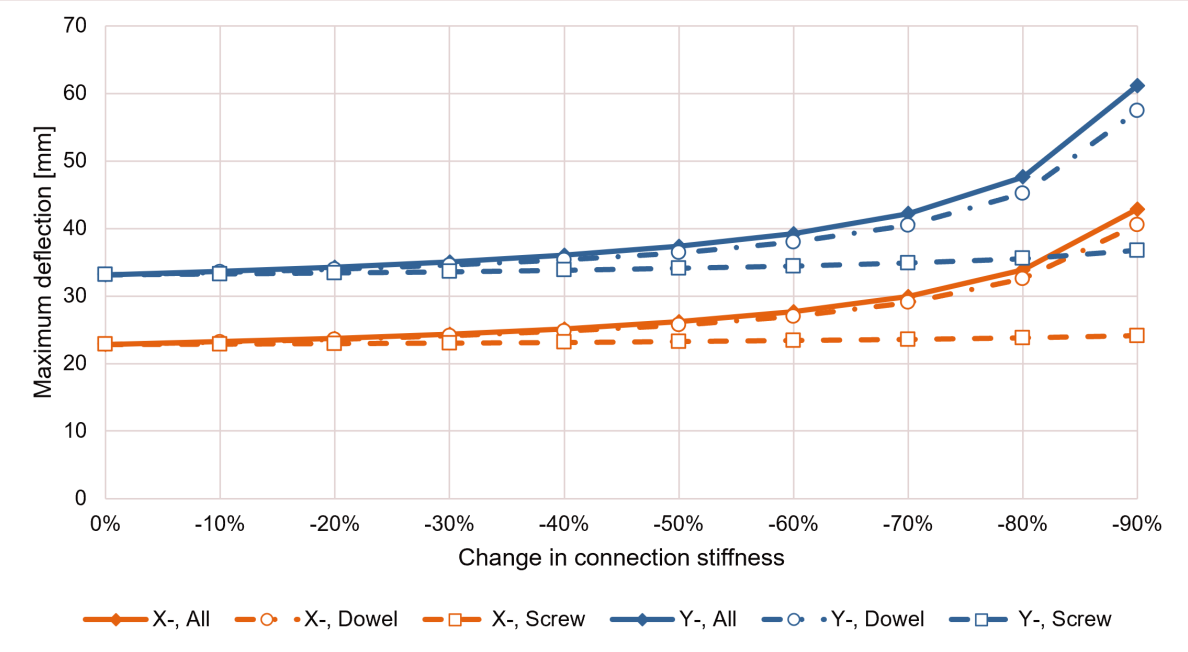

Figure 5.15: Maximum horizontal deflection per reduction of the connection stiffness of all connections, only the dowels and only the screws, for the wind directions X- and Y-

The following observations can be made from Figure 5.15:

- All six curves start with a linear trend and the curves for the reduction of the stiffness of the screws stay linear. The curves for the reduction in stiffness of all connections and only the dowel connections transfer from a linear trend in the lower percentages to a non-linear trend around 60% in reduction.
- The curves for the reduction in stiffness of the dowel connections have an identical shape as the curves for all connections, but with slightly lower values. The difference between the two types of curves increases over the change in connection stiffness. This difference is bigger than the increase in horizontal deflection caused by the change in connection stiffness of the screwed connections. For example, at 90% reduction the maximum horizontal deflection of the ”Y-, Screw”

curve has increased by 3.6 mm and the difference between the curves ”Y-, All” and ”Y-, Dowel” is 3.9 mm.

5.4.2. Relative change in deflection

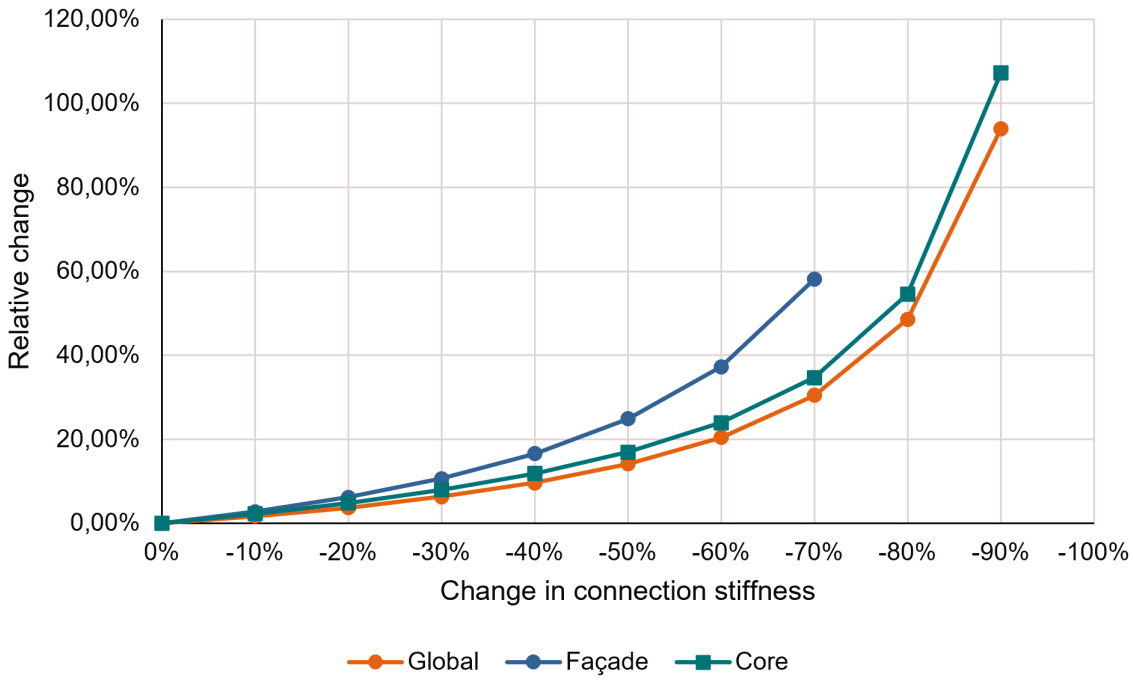

Figure 5.16: Relative increase of the maximum horizontal deflection of the 9th storey for the lateral load resisting systems, while subjected to the self weight and the wind load in X+ direction

To further research the influence of the lateral load-resiting systems on the global stiffness, their relative change in maximum horizontal deflection is plotted in Figure 5.16. The Figure presents the results for the different numerical models subjected to the self-weight and the wind load in X+ direction, the results for the other wind directions are displayed in the Appendix, but the general trend can be observed from this single graph.

The main observation from the graph in Figure 5.16 is that the curve for the 2D model of the façade (RFEM 2D) has the highest values and increases the most per change in connection stiffness. Second is the curve for the model of the core and the least influenced by the change in connection stiffness is the curve for the global model.

5.5. Comparison of modelling approaches

This section presents the results for different modelling approaches used throughout the research. The first subsection focusses on more detailed deflection values of the models of the façades and the global model, then previously presented in Section 5.2.3. This is follow up by exhibiting the influence of adding the foundation to all the different models used in this research. Lastly, deflection values per inclusion of different types of connections are presented for the core model.

5.5.1. Horizontal deflection of the façades

The main lateral load-resisting systems in the Urban Woods building in Delft are the bracing systems in the two types of façades. To estimate the horizontal deflection of the façades both numerical (RFEM) and analytical (method of Virtual Work) are used in this research. Both methods are introduced in Chapter 3 and their application is further explained in Appendices B and C.

When using the method of Virtual Work the total deformation (u,total) exists out of the axial deformation of the members (u,members) and the deformation of the connections between the members

(u,connections). Multiple types of RFEM models are made of which the results can be compared to the results of the Virtual Work. First is a 2D model made as closely as possible to method of Virtual Work (RFEM VW), meaning it exists out of the same members and uses the same connections. Secondly, 2D models of the full façades are made (RFEM façade). the Virtual Work method simplifies the structure of the façades, this simplification is left out in this model, meaning it is a complete 2D model of the façades of the building. Lastly, the Virtual Work method is compared to the Global model, of which the results are shown in the previous Section 5.2.3. It is important to note that all models have identical boundary conditions, as they have the same supports and are all subjected to the SLS combinations of the self-weight and the four different wind directions. The loading on the four models is distributed according to an estimation on what each part of the building takes up. This is in more detail explained in Section 3.4 and the distribution it self is tested, of which the results are shown in Section 5.6.1. What it entails is that the values for the different models in Table 5.3 can be directly compared to one another.

Table 5.3: Comparison of deflections obtained from the virtual work method and RFEM analyses for four wind directions (X+, X-, Y+ and Y-)

Deflection	Virtual Work [mm]	RFEM VW [mm]	RFEM façade [mm]	Global [mm]
u_{X+}, members	7.54	7.55	8.47	11.96
u_{X+}, connections	1.67	1.46	2.53	3.35
u_{X+}, total	9.21	9.01	11.00	15.31
u_{X-}, members	11.62	11.62	11.02	14.93
u_{X-}, connections	5.74	5.51	7.46	4.51
u_{X-}, total	17.36	17.13	18.48	19.44
u_{Y+}, members	14.85	14.83	24.77	21.52
u_{Y+}, connections	2.96	3.72	3.97	4.90
u_{Y+}, total	17.81	18.55	28.74	26.42
u_{Y-}, members	16.98	16.26	21.44	22.65
u_{Y-}, connections	6.80	8.91	6.86	5.19
u_{Y-}, total	23.78	25.17	28.30	27.84

The total deflection per wind direction consists of the deflection caused by axial deformation of the members and the deflection caused by deformation of the connections between the members.

Table 5.4: Contribution of member and connection deformation to the total lateral deflection for different modelling approaches.

Deflection component	Virtual Work [%]	RFEM façade [%]	Global [%]
Wind direction X+			
Members	81.89	77.00	78.12
Connections	18.11	23.00	21.88
Wind direction X-			
Members	66.94	59.63	76.80
Connections	33.06	40.37	23.20
Wind direction Y+			
Members	83.37	86.19	81.45
Connections	16.63	13.81	18.55
Wind direction Y-			
Members	71.40	75.76	81.36
Connections	28.60	24.24	18.64

Table 5.5: Percentage difference in deflection relative to the RFEM 3D results ($\Delta = (u_{\text{method}} - u_{\text{global}})/u_{global} \cdot 100$).

Deflection (baseline: Global)	Virtual Work [%]	RFEM façade [%]
u_{X+}, members	-36.96	-29.18
u_{X+}, connections	-50.22	-24.48
u_{X+}, total	-39.86	-28.15
u_{X-}, members	-22.19	-26.19
u_{X-}, connections	27.23	65.41
u_{X-}, total	-10.72	-4.94
u_{Y+}, members	-31.00	15.10
u_{Y+}, connections	-39.57	-18.98
u_{Y+}, total	-32.59	8.78
u_{Y-}, members	-25.04	-5.34
u_{Y-}, connections	31.02	32.18
u_{Y-}, total	-14.59	1.65

The following observations are made on the results listed in Tables 5.3 and 5.5:

- The results of the Virtual Work method and the RFEM VW models are close to identical. Especially the deflection caused by the deformation of the members is the same, with some slight differences for the deformation of the connections.
- Comparing the values for the models of Virtual Work with those from the RFEM façade models it can be noticed that there is a small discrepancy (approximately 2 mm) for the structures subjected to wind loads in X directions. While for the Y directions a larger discrepancy is observed (10 mm at maximum).
- A clear trend visible over the results of all the models is that the contribution to the total deflection of the connections is lower than the contribution by the members. The contribution of the connections ranges from 13.81% to 40.37%, with the lower contribution percentages found when the models are subjected to positive wind loads.
- The global model shows limit sensitivity to whether the wind direction is positive (X+ and Y+) or negative (X- and Y-), in the absolute values displayed in Table 5.3 and the contribution values in Table 5.4. The other models do show differences between the positive and negative test results.
- Considering the total deflection, the 2D models (Virtual Work and RFEM façade) provide better agreement with the global model for the negative wind directions (X− and Y−) than for the positive directions (X+ and Y+). This is reflected in substantially smaller percentage differences, with the most extreme case showing a reduction from 28.15% to 4.94% (Table 5.5).
- Another difference between the results for the negative (X- and Y-) and positive (X+ and Y+) wind directions is that for the 2D models the contribution of the connections to the total deflection for the positive wind directions is approximately half of that for the negative wind directions, see Table 5.4. However, this trend is not seen for the global model. The trend that is observed over the three models is that the contribution of the connections is higher for the wind loads in X directions than it is for loads in Y directions.
- For the total deflection the Virtual Work method consistently produces the lowest values for all wind directions, underestimating the deflection in the best case by 10.72% and in the worst case by 39.86% (Table 5.5. The RFEM façade models perform better with the estimations for the total horizontal deflection varying from underestimation by 28.15% to overestimation by 1.65%

5.5.2. Influence of the foundation

Chapter 4 lists in Section 4.2 how the influence of the foundation and the basement is included in the models. In short, the influence is taken into account by adding vertical springs in the nodal and line supports of the models. To research this influence the maximum horizontal deflection is taken for the four wind directions from the models with and without the vertical springs for the foundation. In case

of no influence of the foundation the supports are modelled as fully rigid. Arcadis also researched the influence of the foundation and the basement by making a numerical model in RFEM, their results are added to validate the values obtained from the models in this research. The different results on the influence of the foundation are listed in Table 5.6.

Table 5.6: Absolute and relative increase in the maximum horizontal deflection of the models subjected to the self weight and the four different wind loads

Models	Wind directions							
	X+		X-		Y+		Y-	
	[mm]	[Δ%]	[mm]	[Δ%]	[mm]	[Δ%]	[mm]	[Δ%]
Global	2,38	14,23%	3,58	18,61%	5,45	21,70%	5,86	21,47%
RFEM façade	0,21	1,95%	1,49	8,77%	1,09	3,94%	1,28	4,74%
RFEM VW	0,10	1,12%	1,17	7,33%	1,27	7,35%	1,27	5,31%
VW	0,22	2,50%	1,31	8,14%	0,99	5,87%	1,38	6,18%
Core	17,35	56,24%	15,42	54,64%	26,38	63,11%	19,27	57,10%
Arcadis	3,20	11,47%	3,20	11,47%	7,70	16,49%	7,70	16,49%

The following observations are made on the results in Table 5.6:

- The façade bracing models, implemented in Excel (VW) and RFEM (façade and VW), consistently yield the lowest additional deflection, both in absolute and relative terms. The global model exhibits moderately higher values, whereas the core model shows by far the largest increase in both measures, with differences reaching up to approximately 20 mm and 40%.
- For the 2D (façade and VW) and global models, the increase in deflection for wind in the X+ direction is consistently lower compared to the other wind directions.
- The results of the global model and the Arcadis model are of comparable magnitude for both the absolute and relative increases. Both models also exhibit a clear trend, with higher increases observed for wind loading in the Y-direction compared to the X-direction.

5.5.3. Core connections

Five different models of the core are made, of which their build-up is explained in Appendix C. In short, the first model has no connections modelled into the structure of the core and is supported by nodal and line supports. The second model is an upgrade of the basic model, the vertical joints connecting the core walls are added to the basic model. The third model is made to investigate sliding of the core walls, by taking the second model and add horizontal connections that can only deform by sliding of the walls. The forth model is similar to the third, but instead of focussing on the sliding of the core walls, rocking is focused on. The last model, has all the connections of the previous models and is also a direct representation of the core in the global model of the whole building. Table 5.7 contains the maximum horizontal deflection of each model for the load combinations of the self weight and the four different wind loads. Figure 5.8 shows the deflection shape for the highest value of the table.

Table 5.7: Maximum horizontal deflection of the core model for different wind directions with self-weight added and connection configurations

Added connections	Wind direction							
	X+ [mm]	Δ [%]	X- [mm]	Δ [%]	Y+ [mm]	Δ [%]	Y- [mm]	Δ [%]
None	38.98	–	35.73	–	56.34	–	43.92	–
Vertical	42.39	8.75	38.49	7.72	61.83	9.74	46.80	6.56
Sliding	45.69	17.21	40.88	14.41	63.97	13.54	48.48	10.38
Rocking	47.29	21.32	43.01	20.38	67.33	19.51	52.31	19.10
All	48.20	23.65	43.64	22.14	68.18	21.02	53.02	20.72

The following observations are made based on the results from Table 5.7:

- By adding the vertical connections and those for resisting the sliding or rocking of the core walls an increase in horizontal deflection is found. The addition of the vertical connections increases the maximum deflection by 6 to 10%. With pure sliding of the walls increasing these percentage to 10 to 17% in horizontal deflection and rocking to 19 to 21%. By adding all the connections in the core the maximum horizontal deflection increases by 20 to 24%, when compared to a model with no connections.
- In general, the core deforms more when the wind comes from the Y-directions than it does for the wind in the X-directions.

5.6. Model validation and verification

The results needed to validate and or verify, the wind load distribution over the different parts of the structure and assumptions made on certain dowel connections, are presented in this section.

5.6.1. Wind load distribution

This subsection presents the results of the verification of the assumed wind load distribution between the core and the façade bracing systems. Using the verification method described in Section 3.4, the relative contribution of the core and the façades to the total lateral stiffness is evaluated for both wind directions. The resulting load shares are compared with the originally assumed distribution to assess the quality of the adopted assumptions.

Table 5.8: Load–displacement results used for stiffness estimation

	Wide face		Narrow face		
Quantity	Façade X	Core (X)	Façade Y	Core (Y)	Units
F	100	100	100	100	kN
u^+	16.4	20.6	12.2	22.5	mm
u^-	21.3	18.2	21.8	19.3	mm
K^+	6097.6	4854.4	8196.7	4444.4	kN/m
K^-	4694.8	5494.5	4587.2	5181.4	kN/m

Table 5.9: Estimated wind load distribution based on stiffness ratios

Quantity	Wide face	Narrow face	Units
K^+_{total}	17049.5	20837.9	kN/m
Core share $^+$	28.5	21.3	%
K^-_{total}	14884.2	14355.7	kN/m
Core share $^-$	36.9	36.1	%
Assumed core share	25.0	35.0	%

The following observations are made based on the Tables 5.8 and 5.9:

- The stiffnesses of the core in both the wide face and narrow face of the building are significantly more uniform for both wind directions (+ & -), when compared to the façades. The core has a maximum difference of around 800 kN/m, while the façade supporting the narrow face of the building has a difference in stiffness of around 3600 kN/m depending on the wind direction.
- The estimated core share for the positive wind direction is significantly lower than for the negative wind direction for both the wide face and narrow face of the building. This can be explained by that the façades have a higher stiffness for the positive wind direction, while the cores have lower value, when compared to the negative wind direction.
- The assumed core share for the wide face appear to be to low as it is lower than the estimation for both wind directions. On the other hand, the assumptions for the narrow face seems to be appropriate, as it is between the two values for the different wind directions, leaning towards the higher of the two.

5.6.2. Dowel connection validation

In Section 3.3 it is explained how a connection is modelled in RFEM and in Chapter 4 it is illustrated how the input for the different dowel connections is determined. In this subsection for four of these connections the results in RFEM are shown, with the purpose to identify the quality of the assumptions made in modelling the connections. The connections discussed in this Section are Detail 7, 8, 9, and 11. To verify the quality of the connections the 2D RFEM façade models are used, with the structures subjected to a wind load that pushes the building to the right in the figures. Table 5.10 provides the translational stiffness of the connection ($C_{u,x}$ a.k.a K_{ser}), the normal force in the connection (N), the deformation according to RFEM (U_{RFEM}), the test deformation following the analytical Equation 3.16 (U_{test}), and the absolute difference between the two deformation values. For the rotational parameters the Table provides values for the rotational stiffness ($C_{\varphi,y}$), the moment (M_y), and the rotational deformation (φ_y). Table 5.10 is supported by figures for each connection displaying the internal forces in the members near the connections, limited to those displaying non-zero values. To research what the difference in results is for the structures when the connections can or cannot transnationally deform, additional numerical models were made with all connections as standard pinned connections. Table 5.11 presents values for the same parameters as Table 5.10, with the only difference in the models being the input in the connections.

Table 5.10: Comparison of translational and rotational spring behaviour in RFEM and test results

	Det 7	Det 8	Det 9	Det 11 diag.	Det 11 col.	Units
$C_{u,x}$ (K_{ser})	1868.19	3043.56	336.92	1868.19	1344.00	kN/mm
N	-140.13	-43.41	-34.42	158.53	222.45	kN
U_{RFEM}	-0.08	-0.01	-0.10	0.08	0.17	mm
U_{test}	-0.07501	-0.01426	-0.10216	0.08486	0.16551	mm
ΔU	-0.00499	0.00426	0.00216	-0.00486	0.00449	mm
$C_{\varphi,y}$	0	0	0	0	0	kNm/rad
M_y	0	0	0	0	0	kNm
φ_y	-0.3	-3.8	-7.6	0.1	0	mrad

Table 5.11: Deformation of pinned member hinges in RFEM

	Det 7	Det 8	Det 9	Det 11 diag.	Det 11 col.	Units
$C_{u,x}$ (K_{ser})	∞	∞	∞	∞	∞	kN/m
N	-140.13	-82.65	-35.19	158.94	222.45	kN
U_{RFEM}	0	0	0	0	0	mm
$C_{\varphi,y}$	0	0	0	0	0	kNm/rad
M_y	0	0	0	0	0	kNm
φ_y	0	-3.8	-7.9	-0.1	0.2	mrad

The following observations are made on the results from Tables 5.10 and 5.11:

- The translational deformation values from RFEM (U_{RFEM}) are as expected for the normal forces found in the hinges, proven by a small ΔU value for non-fixed hinges and a value U_{RFEM} value of 0 for pinned connections
- The values for the parameters related to the rotation of the hinge are similar for the two tables. With values of 0 for the stiffness ($C_{\varphi,y}$) and moment (M_y).

Detail 7

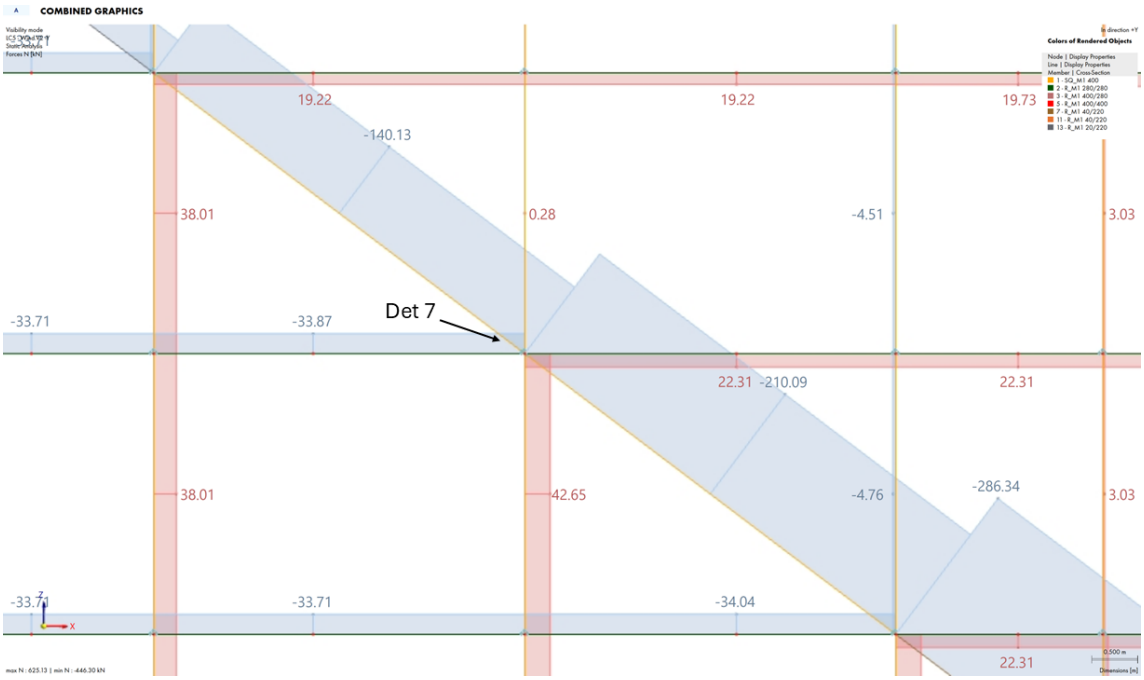

Figure 5.17: Normal forces (kN) in the members surrounding connection Detail 7, when structure is subjected to wind loads pushing/pulling in the right direction

The following observation are made on the results in Figure 5.17 and Table 5.10:

- At connection Detail 7, the wind loads coming through the beams result into an increase of the compression in the diagonal and a tension force in the column bellow the connection.
- The Member Hinge in RFEM for Detail 7 works as intended, it has the correct internal force and deformation value.

Detail 8 & 9

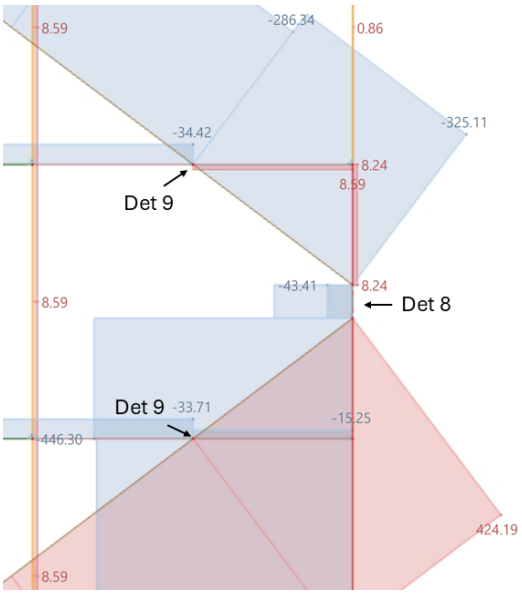

Figure 5.18: Normal forces (kN) in the members surrounding connections Detail 8 and 9, when structure is subjected to wind loads pushing/pulling in the right direction

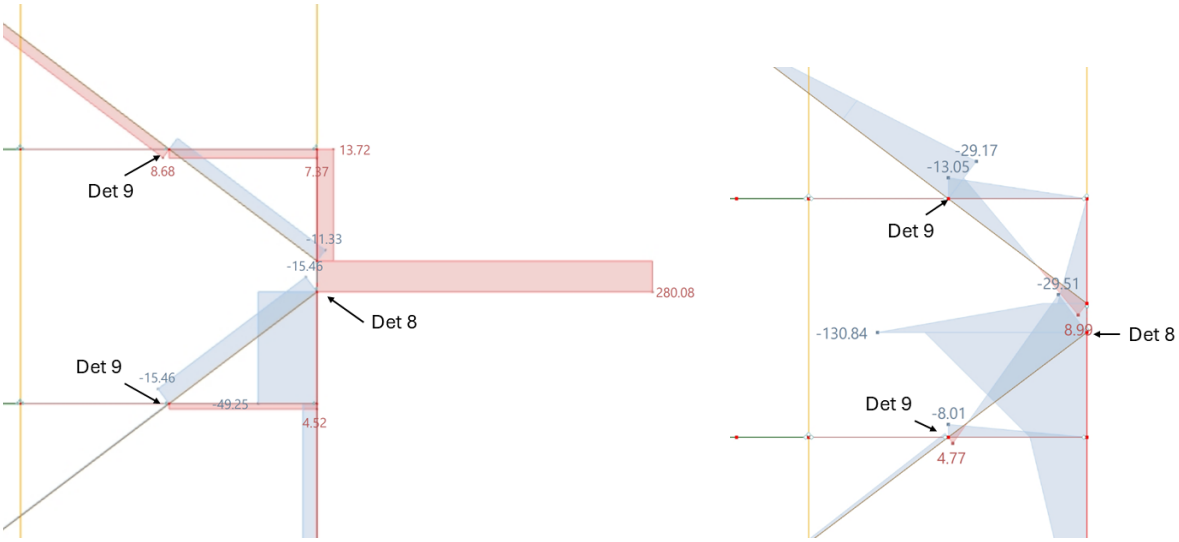

(a) Shear forces **(b)** Moments

Figure 5.19: Internal forces in the members surrounding connections Detail 8 and 9 under wind loading (pushing/pulling in the right direction)

The following observations are made on the results in Figures 5.18 and 5.19 and Table 5.10:

- At connection Detail 8 the diagonal elements change direction and thereby the type of normal force (tension or compression). This causes a high normal force in the column beneath Detail 8 and high local shear forces. The compression force in the top diagonal is around 100 kN smaller than the tension in the bottom diagonal. The shear forces in the column coming from the connections with the beams, subsequently combine to about a 100 kN.
- The results in the Table show that the Member Hinge for connection Detail 8 takes up the wrong normal force, causing it to deform less than it should. With the current modelling approach the normal force in the connection is -43.41 kN, while it should be the increase in normal at the connection of around -400 kN.

- At the connections with Detail 9 the normal forces in the diagonal elements increase. The upper connection causes an increase of around 40 kN in the diagonal element, while the lower connection an creates increase of around 12 kN.
- The results in the Table show that the Member Hinge for connection Detail 9 takes up the wrong normal force, causing it to deform less than it should. With the current modelling approach the normal force in the connection is -34.42 kN, while it should be the change in normal at the connection of 34.42 + 8.59 = 43.01 kN.
- For both Details 8 and 9 there are moments in the members and nodes near/connected to the connections, while the values for the moments in the Member Hinges in Table 5.10 are zero. The moments in the Member Hinges in the figure are also zero, however, it has not resulted in no moments in the nodes and members, only in the members on which the hinge is modelled.

Detail 11

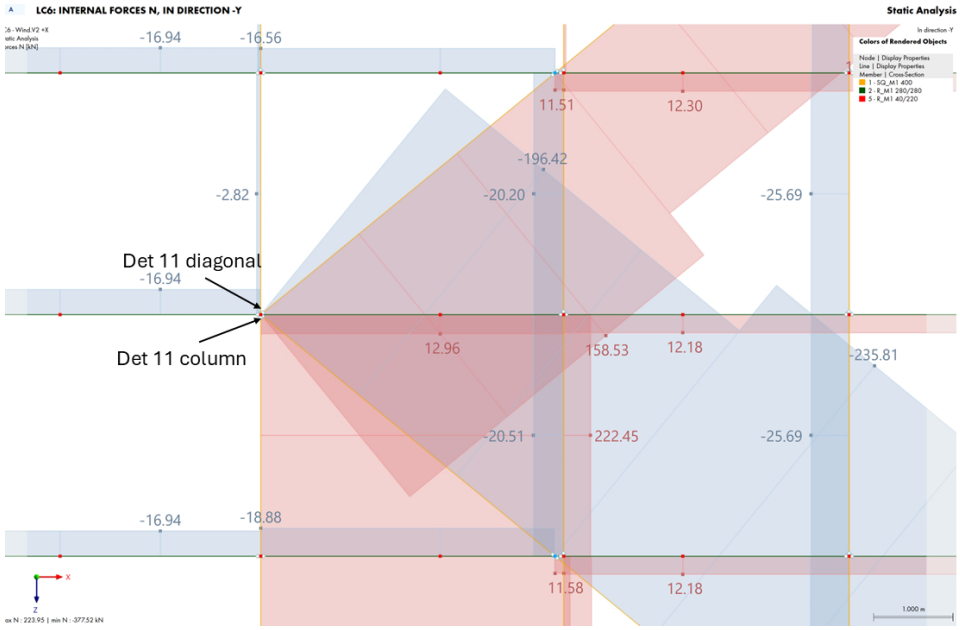

Figure 5.20: Normal forces (kN) in the members surrounding connection Detail 11, when structure is subjected to wind loads pushing/pulling in the right direction

The following observations are based on the results obtained from Figure 5.20 and Table 5.10:

- At the connection Detail 11, the normal forces in the diagonal members increases proportionally with the added force coming through the beams and the column bellow the connection retrieves the vertical resultant of the normal forces in the two diagonals.
- For both the connection in the diagonal and the column the Member Hinge retrieves the correct normal force, resulting in the expected deformation.

6

Discussion

This chapter focusses on discussing the results and observations presented in Chapter 5, with the purpose to find the answers to the research questions and other conclusions or recommendations.

6.1. Influence of connection stiffness on global stiffness

From the results of the numerical models, such as Figure 5.10, it is observed that there is a non-linear trend for the maximum horizontal deflection per change in connection stiffness. For the smaller changes in connections stiffness (-50% to +50%) the influence is relatively small (max 15% at 50% reduction). However, above the threshold of approximately 50–60% reduction, the horizontal deflection starts to ramp up (on the order of 20% increase in deflection with a decrease of 60% in connection stiffness). This behaviour indicates a transition in the structural response, where the global deformation becomes increasingly governed by the stiffness of the connections rather than the stiffness of the structural members and the geometry of the structure.

This threshold coincides with the reduction range reported by Kjell Arne Malo et al. (2023), illustrated by the vertically striped line in Figure 5.10. In addition, the literature review (Chapter 2) highlights that Eurocode 5 formulations tend to overestimate the slip modulus of dowel-type connections by approximately 60%, corresponding to a reduction in stiffness of around 40%. For larger dowel groups, such as those present in the Urban Woods building, this discrepancy is expected to be even more pronounced due to group effects and load redistribution between fasteners.

As a result, the global stiffness of the structure may be systematically overestimated when using analytical stiffness values, leading to an underestimation of the expected horizontal deflections in the serviceability limit state. The results suggest that this underestimation may be on the order of 20%, particularly in systems where the structural response is highly dependent on connection behaviour.

6.2. Load distribution and structural interaction

Within the structure of the Urban Woods building, two distinct lateral load-resisting systems can be identified: the bracing systems in the façades, consisting primarily of dowel-type connections, and the CLT core, in which screw-type fasteners are used. During the design phase and throughout this research, the façade systems were assumed to function as the primary lateral load-resisting systems, with the core acting as a secondary system. The results presented in Section 5.4 and Section 5.6.1 confirm this assumption.

The results show that the dowel-type connections, and thereby the façade bracing systems, are more sensitive to reductions in connection stiffness than the screw-based connections in the core. As the stiffness of the façade system decreases, a redistribution of loads occurs, with a larger portion of the lateral load being transferred to less affected parts of the structure, such as the core. This behaviour follows directly from the stiffness dependent load distribution in statically indeterminate systems, where stiffer elements attract a larger share of the load. Consequently, a reduction in façade stiffness decreases its

contribution to the global stiffness of the structure.

In the initial design, it was assumed that 25% of the wind load acting on the wide face of the building (façade Y) is resisted by the core, while a value of 35% was used for the narrow face (façade X). The results indicate that the 25% assumption underestimates the actual contribution of the core, with values closer to 35% being more appropriate.

This discrepancy can be explained by the structural configuration of the core and façades. The core is asymmetrical and, although it has greater dimensions in the X-direction, the presence of multiple openings in the core walls in this direction significantly reduces its effective stiffness. In contrast, the Y-direction contains fewer openings, resulting in a relatively stiffer load path. Additionally, the façade resisting loads in the Y-direction is less stiff than the façade in the X-direction (6097.6 kN/m compared to 8196.7 kN/m for the positive load direction). As a result, a larger portion of the load is transferred to the core in the Y-direction (28.5% compared to 21.3%), further highlighting the dependence of load distribution on the relative stiffness of the structural subsystems.

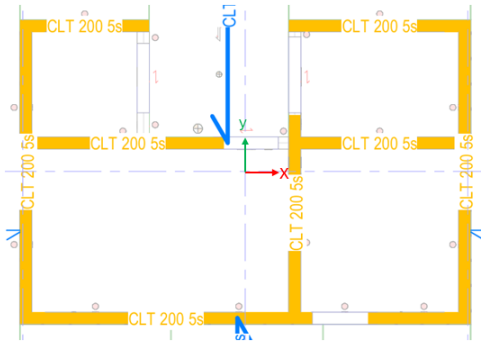

Figure 6.1: Design of the core shows asymmetry in the core walls

The asymmetry of the core does not only influence the global stiffness, but as well the shape of the global deformation. The deformation shapes of the global model presented unexpected deformed shapes for the roof of the building, with the maximum values not being observed on the sides on which the wind is pushing, see Figures 5.3 and 5.5. Similar deformed shapes are found in the core model (Figure 5.8), proving its origin. The lack of influence of the façades in these deformation shapes is due to the façades not continuing until the top of the structure, as for the other floors the deformed shape of the core is not observed in the global model.

These results demonstrate that accurate estimation of subsystem stiffness and their location in the building are essential for predicting load distribution and, consequently, the global structural response.

6.3. Importance of a form stable structure

Results from both the literature and this research indicate that the more form stable the geometry of a structure is, the less dependent its global behaviour is on the stiffness of the connections. In form stable systems, the structural response is primarily governed by the geometry of the system, limiting its deformation and the influence of the connections stiffness.

The lateral load-resisting systems of the Urban Woods building (the façades and the core) provide sufficient stiffness to ensure that the structure remains within serviceability limits. However, both systems are not completely form stable. This is reflected in the observed sensitivity of both systems to changes in connection stiffness (see Figure 5.16), with the façades being the most affected.

Bracing or truss systems, such as those used in the façades, are generally considered to be inherently form stable. However, this is only valid under certain conditions. Firstly, eccentricities in connections must be limited, ensuring that diagonal members connect at nodes where beams and columns coincide, allowing for efficient force transfer. Secondly, the diagonal members must be to the whole structure, to ensure full cooperation. In the façade designs of the Urban Woods building, these assumptions are not fully satisfied, due to the presence of connection eccentricities and parts of the façades not being a part of the bracing systems. As a result, the systems cannot be considered fully form stable.

The observed sensitivity of the façade systems to connection stiffness can therefore be attributed to this lack of full form stability. Consequently, increasing the degree of form stability within the lateral load-resisting systems would reduce the dependency on connection stiffness for the whole building, leading to a more robust and predictable structural behaviour.

6.4. Evaluation of modelling approaches

6.4.1. Horizontal deflection of the façades

Virtual Work vs RFEM VW

The close agreement between the horizontal deflections obtained using the Virtual Work method and the RFEM Virtual Work (RFEM VW) model is both expected and confirms the consistency of the modelling approach. Both models employ identical member properties, connection stiffnesses, and load cases. The only differences arise from the inclusion of an additional stabilizing beam in the RFEM VW model and the ability of RFEM to capture internal forces beyond purely axial effects.

The small discrepancies observed between the two approaches originate exclusively from connection deformation, as confirmed by the identical member-related deflections reported in Table 5.3. This difference can be attributed to the more detailed representation of joint behaviour in RFEM, where rotational deformations, bending moments, and shear forces are implicitly included. Despite the presence of these additional effects, their influence on global nodal displacements remains limited.

The influence in the modelling approaches of the two types of models becomes more apparent when discussing the influence of changing the connection stiffness on horizontal deflection. The graphs in Figure 5.13 demonstrate that the relationship between the deflection and the stiffness of the connections is non-linear for the RFEM models, similar to the global model. While, the curves for the models of Virtual Work are linear, with their slopes depending on the percentage of the deflection that comes from the deformation of the connections.

Influence of the complexity of a structure

The results indicate that the complexity of the façade systems, both in their geometric configuration and in their modelling, has a direct influence on the predicted structural response. In contrast to idealised bracing systems, the façades of the Urban Woods building contain multiple sources of complexity, which introduce additional deformation mechanisms not accounted for in simplified approaches.

This effect is clearly visible in Figures 5.7 and 5.6, where the maximum horizontal deformation does not occur at the top of the façades, but at levels where the diagonals change direction. A similar, although less pronounced, pattern is observed in the global model (Figure 5.4), indicating that this behaviour originates from the structural configuration rather than solely from modelling assumptions.

The primary source of this behaviour lies in the geometric complexity of the façade systems. For the façade resisting wind in the Y-direction, not all connections of the diagonals are at standard beam–column nodes, but at intermediate locations along members. As a result, the load transfer is no longer governed purely by axial forces, and bending moments and shear forces are introduced. Since the connections are primarily designed and modelled to transfer normal forces, these additional effects lead to increased deformation and reduced stiffness.

For the façade resisting wind in the X-direction, the complexity is mainly introduced by eccentricities in a couple of the connections between diagonals, beams, and columns, see Figure 6.2. These eccentricities prevent all members from meeting at a single node, requiring modelling simplifications where connections are represented at different locations. This reduces the effective stiffness of the bracing system at these levels, resulting in local peaks in lateral deformation.

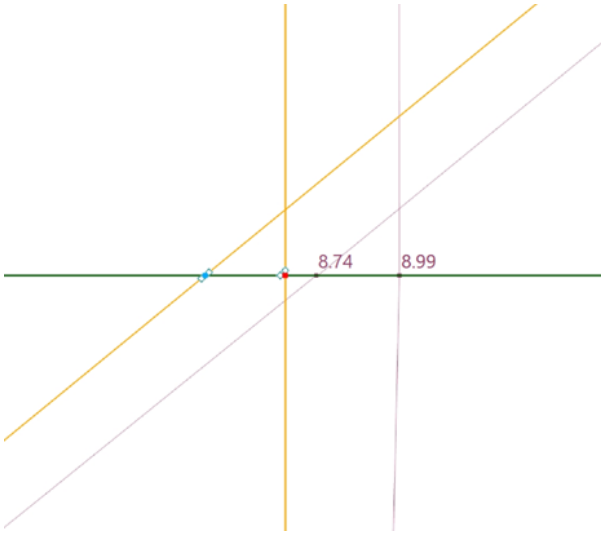

Figure 6.2: Eccentricity in dowel connections of the bracing system in the design of the façade subjected to wind in the X direction (wide façade)

In addition to geometric complexity, modelling simplifications further influence the results. The comparison presented in Table 5.3 shows that the agreement between simplified and numerical approaches is better for the X-direction than for the Y-direction. This can be attributed to the geometric modifications required in the simplified models for the Y-direction, where misaligned diago-

nals were adjusted to fit the analytical framework, effectively increasing the stiffness of the system. Such modifications were not necessary in the X-direction, leading to a closer correspondence between models.

At the system level, the influence of complexity is also reflected in the differences between the global model and the simplified representations. The global model includes additional structural elements that, although not part of the primary lateral load-resisting system, contribute to the overall stiffness and enable load redistribution. By omitting these elements, simplified models neglect secondary load paths, resulting in reduced accuracy and increased sensitivity to modelling assumptions.

Overall, the results demonstrate that structural and modelling complexity significantly affect both the magnitude and distribution of deformations. Simplified approaches are therefore more reliable for structures that more closely resemble idealised, form-stable systems, whereas complex geometries require detailed numerical modelling to accurately capture their behaviour. This behaviour futher explains the sensitivity of the façade systems to connection stiffness, as discussed in Sections 6.1 - 6.3.

Wind direction asymmetry

It is further observed that, for all modelling approaches, deflections resulting from negative wind directions correspond more closely to the results of the global model than those from positive wind directions. This behaviour is directly related to the distribution of axial forces in the diagonal members and adjacent columns.

For negative wind directions, the bottom diagonal is subjected to tension while the top diagonal is in compression, resulting in a significant compressive force in the column where the diagonals change direction. For positive wind directions, this distribution is reversed, leading to substantially lower tensile forces in the same column. This difference is illustrated in Figure 6.3.

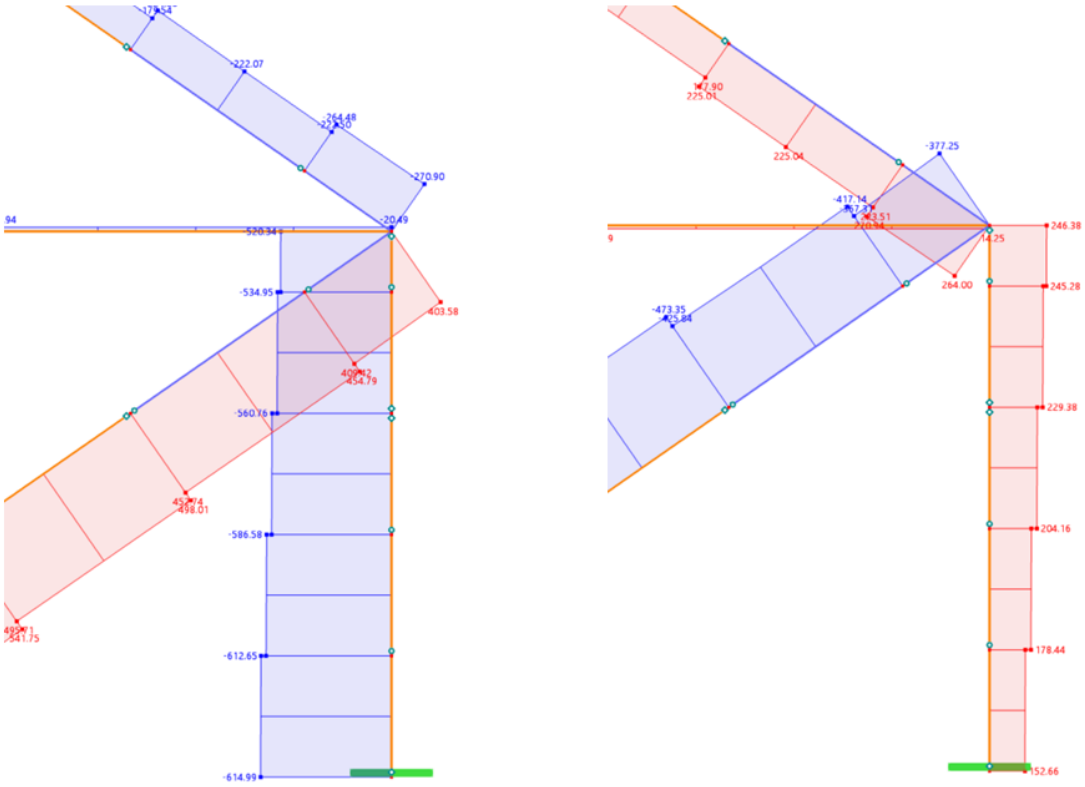

Figure 6.3: Difference in normal force in the column depending on the wind direction

The magnitude of the axial force in this column has a direct influence on the deformation of the associ-

ated connections. As these connections are designed using dowels to accommodate high forces, their deformation increases with the applied load. Consequently, the contribution of connection deformation to the global deflection is significantly larger for negative wind directions, as reflected in Table 5.3, where the contribution is at least twice that of the corresponding positive load cases.

Due to the simplified models (Virtual Work and RFEM façade) having the tendency to underestimate the horizontal deflection, the best estimations are produced for the load combination with the highest deflection, which for this case study is for the wind in the negative directions.

6.4.2. Influence of foundation

Table 5.6 presents the absolute and relative influence of the foundation on the global model, the model of the façades (RFEM 2D, RFEM VW and VW), and the model of the core. This difference can be primarily attributed to the geometry of the structural systems, in particular their width. The façade systems are approximately four times wider than the core. Although the core is continuously connected to the foundation along its entire width, while the façades are supported discretely at column locations, the larger width of the façade systems results in a more distributed support configuration. As a result, the façade systems are less sensitive to local foundation deformations, since the structural response is distributed over a wider base. In contrast, the more concentrated support conditions of the core lead to a stronger dependency on the stiffness of the supports, resulting in a greater influence of foundation deformations on the global response.

A similar reasoning can be used as to why the global model and the results from Arcadis show a higher dependency of the foundation for the structure subjected to loads in Y-direction than for X-direction. The structure is wider in the X-direction and has more supports than in the Y-direction. This means that there is a more distributed support configuration in the X-direction, with the result that the whole building is less sensitive to local foundation deformations in the X-direction.

The relatively low increase observed for wind in the X+ direction can be explained by the interaction between vertical foundation deformations and the global load path. Depending on the wind direction, vertical displacements of individual nodes may either amplify or reduce the overall horizontal deflection. In the X+ load case, the column subjected to the highest normal force contributes to a reduction of the global horizontal deflection, thereby limiting the overall influence of the foundation.

6.4.3. Core connections

The influence of rocking on the horizontal deflection is significantly larger than that of sliding, as is shown in the results from Table 5.7. This is due to the geometry of the core and fundamentally different deformation mechanisms. Sliding introduces a uniform horizontal displacement over the height of the structure per connection, resulting in a constant offset caused by sliding. In contrast, rocking induces a rotation at the base, causing displacements that increase linearly with height. As a result, even small rotational deformations lead to relatively large horizontal displacements at the top of the structure. This is amplified by the geometry of the core, due to the core walls spanning 3 storeys vertically there are only 3 levels with connections in the core (leaving out the connection to the basement and the roof). If the core walls would span only one storey instead, you would expect the discrepancy between the results for sliding and rocking to decrease and possibly have sliding become the primary deformation mechanism. Furthermore, rocking is governed by the axial deformation of the vertical load-bearing elements and the tensile and compressive behaviour of the connections, which are more flexible than the shear mechanisms governing sliding in this structure. This leads to a lower rotational stiffness compared to translational stiffness, thereby amplifying the contribution of rocking to the total horizontal deflection.

6.5. Comparison of stiffness per fastener

In the governing facade connections, a combination of dowels, bolts, and screws is applied. Notably, no connection contains both screws and bolts simultaneously; instead, either bolts and dowels or screws and dowels are used. This choice is directly related to the functional role of bolts and screws within the connection. Their primary purpose is to ensure accurate alignment of the timber members and steel plates during installation, thereby facilitating the subsequent placement of the dowels.

The decision whether to use bolts or screws is governed by two main criteria.

- **Required load transfer and structural contribution.** The bolts used in the Urban Woods building exhibit a stiffness approximately five times higher than that of the screws applied in similar connections. Consequently, the structural contribution of the screws is negligible, restricting their function largely to alignment rather than load transfer. Bolts, on the other hand, provide a significant stiffness and therefore contribute to the overall load bearing capacity of the connection. This results in bolts being applied in connections where additional structural capacity is required, while screws are used where such capacity is not necessary.

  In some locations, load transfer through the connection is intentionally avoided. A clear example is found where a diagonal element passes through a column, visible in Figure 6.4. In these cases, the design intent is for the force in the diagonal to bypass the column and continue through the diagonal member. Here, the connection serves solely as a positioning and alignment detail, for which screws are sufficient and structurally preferable.

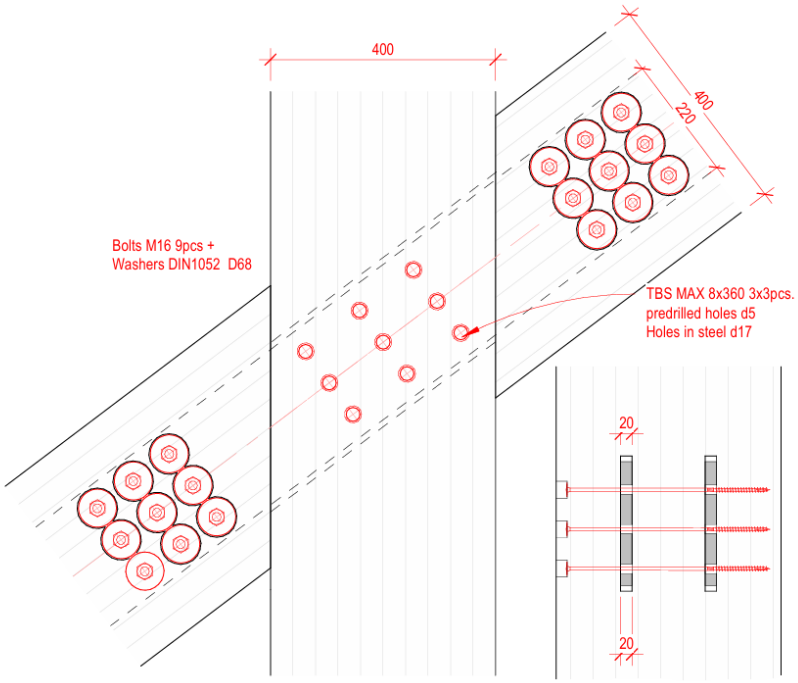

Figure 6.4: Difference in application of screws (in the column) and bolts (in the diagonal) (CLT-S NV 2024)

- **Ease of installation.** The installation of bolts generally requires access to both sides of the timber member, which can be restrictive, particularly in confined or partially enclosed locations. Screws require access from only one side, offering greater flexibility during construction and increasing the range of feasible application locations.

Overall, the connection philosophy adopted for the Urban Woods building in Delft favours the use of a relatively large number of fasteners with low individual stiffness wherever possible, while high-stiffness fasteners and connections are applied only in specific local situations. This approach promotes a more uniform cooperation between structural components and reduces the occurrence of high local stresses, contributing to a more robust and ductile global structural behaviour.

6.6. Verification of the dowel connections

From the different dowel connections in the building four were chosen, based on their relevance to the structure or the results, to verify their functionality in the numerical models. The results for connections Detail 7 and 11 showed no errors, as the normal forces and deformations of the members and connections were as described in Chapter 4. However, connections Detail 8 and 9 did show errors in the results.

In the figures for internal forces The connection of Detail 8 appears to be working as expected with the high normal forces in the diagonals causing a high normal force in the column. There is a difference of a 100 kN between the top diagonal and the bottom diagonal, which was not accounted for in the illustrations and method of modelling of the connection. However, This 100 kN can be traced back to the beams, where on the connection to the column, the wind loads are applied on. It was expected that these wind loads would go as normal forces into the beams. But it appears that the majority of it instead went into the column as a shear force. This is likely due to this load path being more stiff, due to the higher stiffness of the timber members and connections. However, the main error for Detail 8 is not in the values for the normal force, but in the deflection of the Member Hinge, which is the used function to model the connection. Table 5.10 presents that the normal force in the hinge is wrong. Due to modelling complications of this particular connection a significantly lower (10x) normal force is observed in the hinge, resulting in a lower deformation value of the hinge. To conclude, the results of connection Detail 8 show that improvements in the modelling of the connection should be desired.

The connections using the design of Detail 9 are also influenced by the unexpected 100 kN in shear force in column. Due to majority of the wind loads being taken up by the columns instead of the beams a smaller normal force than expected arrives at the connection. Therefore, the increase in normal force in the diagonal elements is smaller than expected. Similar to Detail 8, the Member Hinge used to model Detail 9 has a lower normal force than intended. However, in this case the increase in normal force is limited. Therefore, the desire to improve the modelling of Detail 9 is smaller than Detail 8, but would be beneficial for the quality of the models.

The approach of using Member Hinges shows problems in both Detail 8 and 9, as the values of 0 kNm for the moments in the hinges presented in Table 5.10 do not result in no moments in the nodes and members, on which the Member Hinge is not applied). The moments in the members on which the Member Hinge is applied are zero, but with the current approach that hasn't resulted in no moments in the other member connected to the same node, which is not as desired. Thereby, quantifying the desire for an improvement in the modelling of connections Detail 8 and 9 to improve the numerical models.

6.7. Limitations of the study

Modelling assumptions and simplifications

A key limitation of this study lies in the modelling assumptions and simplifications adopted in both the analytical and numerical approaches. The behaviour of connections is represented using simplified stiffness parameters, while complex phenomena such as non-linear behaviour, slip, and failure mechanisms are not explicitly captured. In addition, geometric simplifications, particularly in the façade models used for the method of Virtual Work, alter the structural configuration and may affect the predicted stiffness. Furthermore, simplified models omit secondary structural elements that contribute to load redistribution, leading to differences compared to the global model. These assumptions influence the accuracy of the results and should be considered when interpreting the findings.

Case study

This research is limited due to only using the design of the Urban Woods building in Delft and from the design only the relevant translational stiffness of the connections that transfer loads in normal circumstances. This limits both the use for comparison to other structures and the quality of the estimations. By adding the translational and rotational stiffness of all connections, a better estimation of the global stiffness is expected. This was not done, due to the expectation that the amount of extra work it would entail would not improve the estimation enough to quantify doing it.

SLS vs ULS

During this research the calculations were performed according to the Serviceability Limit State and not the Ultimate. Apart from the difference in loading combinations, another interesting difference is in the calculation of the stiffness of the connections. When moving from SLS to ULS, aspects as creep, material degradation, moisture, and loading conditions are included in the calculation of the slip modulus of a timber fastener. These same aspects were found in literature to possibly have a significant influence on the stiffness of a dowel.

7

Conclusion and Recommendations

This Chapter concludes the research by answering the four sub research questions and main research question asked in the Chapter 1 in the first section. Follow by the recommendations of this study, categorized in structural advice and future studies.

7.1. Conclusions

Sub-research question 1

What are the stiffness values of the connections (in or between the core, floors and bracings) used in the Urban Woods building in Delft, how are they determined, and which design parameters have the most influence on the stiffness?

The stiffness, for the Serviceability Limit State, of connections in the Urban Woods building varies significantly depending on the connection type, ranging from 1.05 kN/mm for individual screws to 3043.56 kN/mm for the biggest dowel connections with slotted-in steel plates (50 dowels). Screwed connections with steel plates show intermediate stiffness values between 7.27 and 45.37 kN/mm.

These stiffness values are determined using analytical Eurocode 5 formulations for the slip modulus of fasteners, which only depend on the fastener diameter and the timber density. The total stiffness of a connection is obtained by summing the contributions of the individual fasteners and accounting for the number of shear planes. Depending on the size of the connection the quantity of fasteners becomes the most important parameter, as increasing the size of the diameter or timber density can be limited due to contextual restraints.

Sub-research question 2

According to the literature, how accurate are the Eurocode-based calculations of connection stiffness for the dowel connections used in the Urban Woods project, and which parameters influence this accuracy the most?

The Eurocode 5 slip-modulus expressions provide a moderately accurate estimate of connection stiffness, with their accuracy strongly depending on the connection configuration. Across the reviewed studies, EC5 tends to underestimate the stiffness of single small dowels (d ≤ 12 mm), in some cases by a factor of up to 2.5, while it can significantly overestimate the stiffness of larger dowel groups. For these larger configurations, the actual stiffness can be as low as 22.5% of the EC5 prediction. In contrast, other studies report averages of overestimations of up to 60% for single or small amounts of dowels, indicating that the accuracy of EC5 varies considerably between different test conditions and modelling approaches.

These inaccuracies primarily arise from the assumption of linear superposition in the Eurocode formulation, which neglects interaction effects between dowels in a group. As a result, the number and spatial arrangement of dowels are the most influential parameters governing the accuracy of the stiffness estimation. Other influencing parameters include timber density and fastener diameter, which are

explicitly included in the EC5 formulation, as well as moisture content and loading conditions, which affect stiffness but are not directly accounted for in the approach of the Eurocode for the Serviceability Limit State. However, these are accounted for in calculations of the Ultimate Limit State.

Sub-research question 3

How does a variation in connection stiffness influence the global stiffness of the Urban Woods project in Delft, according to an RFEM 6 model?

The influence of connection stiffness on the global stiffness of the Urban Woods is non-linear. For the lower percentages (<50%) in change of connection stiffness a small influences the global stiffness is observed. However, the influence increases significantly for higher reductions in connection stiffness, as a 60% reduction in connection stiffness leads to an increase in deflection of approximately 20%.

This behaviour can be explained by the form-stable structural system, in which lateral resistance is provided by both the CLT core and the façade bracing system. For small reductions in connection stiffness, the façades remain sufficiently stiff to effectively carry lateral loads, resulting in only minor changes in global stiffness. However, beyond a certain reduction level (around 60%), the stiffness of the façade system decreases substantially, leading to a redistribution of forces and a disproportionate increase in global deformations.

Therefore, connection stiffness is not a governing parameter for the global stiffness within a limited variation range, but becomes increasingly critical once the stiffness of the primary load-resisting system is sufficiently reduced.

Sub-research question 4

How can insights from Eurocode calculations, RFEM simulations, and the Method of Virtual Work be integrated to improve early-stage global stiffness estimation for multi storey CLT buildings?

Early-stage global stiffness estimations can be significantly improved by combining simplified analytical methods with insights from numerical models, particularly regarding the representation of connection stiffness. The Method of Virtual Work provides a fast initial estimate but tends to overestimate the global stiffness by approximately 10–40%. In contrast, two-dimensional numerical models of the façades show improved accuracy, with deviations ranging from 1% to 27% when compared to the global three-dimensional numerical model.

The primary source of discrepancy between early-stage methods and detailed numerical models lies in the representation of the stiffness of the connections, whereas the stiffness of the timber members themselves is generally captured accurately. As a result, improving the modelling of connections, especially in terms of their stiffness and configuration within the structural system, offers the greatest potential for increasing prediction accuracy.

Therefore, the method of Virtual Work can be used as an approach for initial estimations of the global stiffness, but a simplified numerical model can be more practical. Due to the higher quality of the results, while a similar amount of time is used to make the model. Special attention should be given to complex bracing configurations, eccentric connections, and non-standard geometries, as these increase modelling uncertainty. Furthermore, the non-linear behaviour of connections, particularly the difference in stiffness between tension and compression, should be considered when making early-stage estimations.

Overall, integrating these methods allows for a more reliable and efficient estimation process, in which simple analytical approaches provide quick bounds and numerical models refine the prediction by capturing critical system interactions.

Main research question

How accurately can Eurocode-based hand calculations predict the global stiffness of a multi-story timber building, and how sensitive is this estimation to variations in connection stiffness compared to RFEM 6 results?

The results indicate that an analytical model (Eurocode-based hand calculations), using the method of Virtual Work, overestimate the global stiffness of a multi-storey timber building when compared to RFEM

6 simulations. The observed overestimation ranges between 10% and 40% for standard connection stiffness values.

A key finding is that this discrepancy is sensitive to reductions in connection stiffness. For moderate reductions in connection stiffness (up to approximately 50–60%), the overestimation remains relatively constant. However, beyond this threshold, a significant divergence emerges. The numerical models, made in RFEM 6, exhibit a non-linear (exponential-like) decrease in global stiffness, whereas the Virtual Work method continues to predict a linear and gradual reduction. This indicates that the analytical approach is unable to capture the non-linear system behaviour associated with reduced connection stiffness.

Although a reduction of 50–60% in connection stiffness may initially appear unrealistic, findings from literature suggest otherwise. Several studies report that an overestimation of 60% of the Eurocode slip-modulus for dowel-type connections is well within expectations, particularly for connections with a large number of fasteners. This implies that the sensitivity observed in this study can realistically occur in practice, especially in multi-storey timber buildings where such connections are common.

The accuracy of estimation when using the method of Virtual Work is highly influenced by the structural configuration of the lateral load-resisting system. The Urban Woods case study demonstrates that the building's global stiffness is strongly governed by façade-based bracing systems. Although the application of the Virtual Work method to these systems required simplifications, the results suggest that the method performs best for structurally simple and form stable bracing systems, while its accuracy decreases as the complexity of the system and/or the complexity of the interaction of the bracings with other parts of the building increases.

Overall, it can be concluded that analytical model using the method of Virtual Work (Eurocode-based hand calculations) provide a reasonable first-order estimation of global stiffness, but they lack the sensitivity required to capture non-linear system behaviour arising from interaction and load redistribution to structural components outside the structure of the model. Consequently, their reliability decreases for systems with reduced connection stiffness or complex load redistribution mechanisms, where advanced numerical modelling (e.g., RFEM 6) becomes essential.

7.2. Recommendations

7.2.1. Structural advice

Higher deflections due to lower connection stiffness

The results of this research indicate that for timber structures in which the global behaviour is significantly governed by dowel-type connections, an increase of approximately 20% in horizontal deflection may be expected when using Eurocode 5 analytical slip modulus equations without reductions for the influence of the configuration of the dowel connections.

The literature review shows that the slip modulus of dowel connections is, on average, overestimated by approximately 60% when calculated according to Eurocode 5 formulations. This discrepancy is expected to be more pronounced for large dowel groups (>10 dowels), where group effects reduce the effective stiffness of the connection.

The numerical results obtained for the global model demonstrate that a 60% reduction in connection stiffness leads to an increase in maximum horizontal deflection of approximately 20%. This highlights the direct relationship between connection stiffness overestimation and underestimation of global structural deformation.

It is therefore recommended to account for a potential increase in horizontal deflection when analysing timber structures with large dowel-type connections, either by applying a reduction factor to the connection stiffness or by explicitly considering the associated increase in deflection in serviceability assessments.

Form stable structures

A solution for making a structure less dependent on the stiffness of its connections, and thereby the uncertainty in the stiffness of dowel connections, is by making the load-resisting systems of the structure more form stable. That is, the stiffness of the systems in the structure should come from the geometry

of members and surfaces and not from the connections. The more form stable a structure is, the less it depends on the stiffness of the connections.

Early-stage estimation methods

In the early stages of the design of timber structures with bracing systems as the primary lateral load-resisting mechanism, both analytical and numerical approaches can be used to estimate the global stiffness.

The method of Virtual Work provides a fast analytical estimation; however, in this case study it consistently overestimates the global stiffness by approximately 10–40%. A more accurate alternative is the use of a two-dimensional numerical model of the complete bracing system in RFEM, which resulted in estimates within 2–28% of those obtained from the full three-dimensional model of the structure.

The accuracy of both approaches is strongly dependent on the complexity of the structure. For relatively simple and form-stable systems, where limited geometric and connection simplifications are required, both methods provide reasonably reliable results. However, as structural complexity increases, the level of simplification required in both analytical and numerical models also increases, leading to a reduction in accuracy.

Both simplified approaches tend to overestimate the global stiffness, and consequently underestimate the horizontal deflections. As a result, the load case that produces the largest deflection generally yields the most reliable estimate when using simplified models.

It is therefore recommended that, for early-stage design, simplified models be used with caution, particularly for complex structures. Where possible, a two-dimensional numerical model of the full bracing system should be preferred over purely analytical methods, and the resulting deflections should be interpreted as lower-bound estimates of the actual structural response.

Influence of non-linearity in connections

Timber connections often exhibit non-linear behaviour, as many fasteners primarily resist loads in tension, while compressive forces are transferred directly through timber-to-timber contact. As a result, the stiffness and deformation of these connections are highly dependent on whether the connection is subjected to tension or compression.

This behaviour must be explicitly considered in both the modelling of connections and the selection of load combinations. When analysing lateral deflection, it is common to consider wind loading only. However, this may lead to unrealistic results, if the resulting force distribution places connections in tension, whereas in practice the inclusion of self-weight would cause these connections to remain in compression.

Neglecting this interaction can lead to an overestimation of connection deformation and, consequently, an inaccurate prediction of the global stiffness. The results of this research demonstrate that the deformation behaviour of connections is strongly influenced by the combination of loads applied.

It is therefore recommended that load cases used for early-stage estimation include at least both wind load and self-weight, particularly when non-linear connection behaviour is relevant. This ensures that the stress state of the connections more closely reflects realistic conditions, resulting in more reliable predictions of global stiffness and deflection.

7.2.2. Future research

Slip-modulus of groups of dowels

Over the past decades, a substantial amount of research has been conducted on the stiffness of dowel-type connections. However, the majority of experimental studies perform tests containing a single dowel or a limited number of fasteners. While these studies provide valuable insights into the fundamental behaviour of timber connections, they do not fully represent the conditions encountered in practice.

In multi-storey timber buildings, connections often consist of a large number of dowels, where interaction effects between fasteners can significantly reduce the effective slip modulus. As a result, current design approaches, including those in the Eurocode, may overestimate connection stiffness when applied to such configurations.

Future research should therefore focus on the experimental and analytical investigation of timber connections with large groups of dowels, specifically with the attention on group effects, load redistribution, and stiffness degradation. Improved models for predicting the slip modulus of these connections would directly contribute to more accurate estimations of global structural stiffness in timber buildings.

Early-stage estimation methods

In this research, the method of Virtual Work was applied as an early-stage estimation method for predicting the global stiffness of a multi-storey timber building. While this method provides a relatively simple and transparent approach, its applicability is limited by its requirements for proper usage. As it needs a structure of which the lateral resistance mainly exists out of a bracing system. Future research should investigate alternative early-stage estimation methods and assess their applicability to different types of timber structures. An example could be the combination of the method of Steiner and a Timoshenko beam to estimate the stiffness of a CLT core system.

Comparative studies between these methods and advanced numerical models, such as finite element analyses, would provide valuable insight into their accuracy, limitations, and suitability for practical design use. Such research could support the development of more reliable and efficient tools for early-stage structural design of timber buildings.

References

Abrahamsen, Rune (2017). “Mjøstårnet - Construction of an 81 m tall timber building”. In: *Internationales Holzbau-Forum* 2017.

Ali, Mir M. and Kyoung Sun Moon (Sept. 2007). “Structural developments in tall Buildings: Current trends and future prospects”. In: *Architectural Science Review* 50.3, pp. 205–223. DOI: 10.3763/asre.2007.5027. URL: https://doi.org/10.3763/asre.2007.5027.

Binck, Charles, Alex Sixie Cao, and Andrea Frangi (June 2022). “Lateral stiffening systems for tall timber buildings – tube-in-tube systems”. In: *Wood Material Science and Engineering* 17.4, pp. 309–316. DOI: 10.1080/17480272.2022.2086066. URL: https://doi.org/10.1080/17480272.2022.2086066.

Cao, Jixing, Haibei Xiong, and Yingyang Liu (Feb. 2021). “Experimental study and analytical model of bolted connections under monotonic loading”. In: *Construction and Building Materials* 270. DOI: https://doi.org/10.1016/j.conbuildmat.2020.121380.

Chui, Ying H. and Chun Ni (1997). “Load-Embedment Response of Timber to Reversed Cyclic Load”. In: *Wood and Fiber Science* 2, pp. 148–160. URL: https://wfs.swst.org/index.php/wfs/article/view/173.

CLT-S NV (2024). *Urban Woods Delft (Project NL21161): Structural execution drawings [Technical drawings]*. URL: https://www.delft.nl/bouwgegevens-inzien.

D’Arenzo, Giuseppe et al. (Nov. 2024). “Characterisation of the rigid diaphragm conditions for cross laminated timber floors”. In: *Bulletin of Earthquake Engineering* 23.4, pp. 1759–1794. DOI: 10.1007/s10518-024-02025-5. URL: https://doi.org/10.1007/s10518-024-02025-5.

Dorn, Michael, Karin de Borst, and Josef Eberhardsteiner (Feb. 2013). “Experiments on dowel-type timber connections”. In: *Engineering Structures* 47, pp. 67–80. DOI: 10.1016/j.engstruct.2012.09.010.

Felicita, Maria (2021). *Timber High-Rise Buildings: Parametric study of the influence of preliminary design parameters on the wind-induced dynamic response of timber high-rise buildings*.

Gui, Tao, Ying Hei Chui, and Alexander Salenikovich (Jan. 2025). “STIFFNESS OF TIMBER CONNECTIONS WITH DOWEL-TYPE FASTENERS UNDER LATERAL LOAD”. In: *World Conference on Timber Engineering* 2025, pp. 3728–3735. DOI: 10.52202/080513-0456. URL: https://doi.org/10.52202/080513-0456.

Jockwer, Robert and André Jorissen (Jan. 2018). “Load-deformation behaviour and stiffness of lateral connections with multiple dowel type fasteners”. In: *INTER* 51.51-07-7, pp. 141–158. URL: https://www.research-collection.ethz.ch/handle/20.500.11850/287636.

Kiwelu, Henry M. (Aug. 2019). “Experimental Study on the Effect of Moisture on Bolt Embedment and Connection Loaded Parallel to Grain for Timber Structures”. In: *Tanzania Journal of Engineering and Technology* 38.1. URL: https://journals.udsm.ac.tz/index.php/tjet/article/view/2935.

Kuhlmann, Ulrike and Julius Gauß (2021). “STIFFNESS OF STEEL-TIMBER DOWEL CONNECTIONS - EXPERIMENTAL AND NUMERICAL RESEARCH”. In: *INTER* 30 (2). URL: https://0cd57cf2-ec4d-4f87-89a6-4df92a7459ea.filesusr.com/ugd/7f6880_c16294a4947c408e93244d93701d5605.pdf.

Loss, Cristiano, Afrin Hossain, and Thomas Tannert (July 2018). “Simple cross-laminated timber shear connections with spatially arranged screws”. In: *Engineering Structures* 173, pp. 340–356. DOI: 10.1016/j.engstruct.2018.07.004. URL: https://doi.org/10.1016/j.engstruct.2018.07.004.

Malo, K. A., R. B. Abrahamsen, and M. A. Bjertnæs (Mar. 2016). “Some structural design issues of the 14-storey timber framed building “Treet” in Norway”. In: *European Journal of Wood and Wood Products* 74.3, pp. 407–424. DOI: 10.1007/s00107-016-1022-5. URL: https://doi.org/10.1007/s00107-016-1022-5.

Malo, Kjell Arne et al. (Jan. 2023). “SERVICEABILITY STIFFNESS OF TIMBER CONNECTIONS WITH DOWELS AND SLOTTED-IN STEEL PLATES”. In: *World Conference on Timber Engineering* 2023, pp. 1136–1145. DOI: 10.52202/069179-0156. URL: https://doi.org/10.52202/069179-0156.

Nur Liza Binti, Rahim (May 2019). *Stiffness of Bolted Timber Connection*. Doctoral thesis.

Reynolds, Thomas P.S. et al. (Aug. 2022). “Stiffness and slip in multi-dowel timber connections with slotted-in steel plates”. In: *Engineering Structures* 268, p. 114723. DOI: 10.1016/j.engstruct.2022.114723. URL: https://doi.org/10.1016/j.engstruct.2022.114723.

Sandhaas, Carmen (June 2012). *MECHANICAL BEHAVIOUR OF TIMBER JOINTS WITH SLOTTED-IN STEEL PLATES*. Doctoral thesis.

Smith, Ian and Monica A Snow (Aug. 2008). “Timber: An ancient construction material with a bright future”. In: *The Forestry Chronicle* 84.4, pp. 504–510. DOI: 10.5558/tfc84504-4. URL: https://doi.org/10.5558/tfc84504-4.

Standardization, European Committee for (Nov. 2011). *Eurocode 5: Design of Timber Structures – Part 1-1: General - Common Rules and Rules for Buildings*. Tech. rep. NEN-EN 1995-1-1+C1+A1. URL: https://connect.nen.nl.

— (Apr. 2025). *Eurocode 5: Design of Timber Structures – Part 1-1: General rules and rules for Buildings*. Tech. rep. FprEN 1995-1-1.

Tao, Haotian et al. (Aug. 2021). “Elastic stiffness of timber joints with dowel-type fasteners and slotted-in steel plate based on the theory of beam on elastic foundation”. In: *Construction and Building Materials* 294. DOI: 10.1016/j.conbuildmat.2021.123569. URL: https://doi.org/10.1016/j.conbuildmat.2021.123569.

Tupenaite, Laura et al. (Apr. 2023). “Timber Construction as a Solution to climate Change: A Systematic Literature review”. In: *MPDI* Buildings 13.4. DOI: https://doi.org/10.3390/buildings13040976.

Wang, X.T. et al. (Oct. 2021). “Analysis and test of stiffness of bolted connections in timber structures”. In: *Construction and Building Materials* 303. DOI: https://doi.org/10.1016/j.conbuildmat.2021.124495.

Woods, The Urban (Mar. 2023). *Onze visie - The Urban Woods*. URL: https://www.theurbanwoods.com/nl/onze-visie/.

A

Stiffness of connections

In this Chapter, the stiffness of the connections is calculated either via information provided by the manufacturer or by estimations via the Eurocode. The code used for the calculations is FprEN 1995-1-1 V0 FV version (Standardization 2025). The last Subchapter of this appendix shows a summary of all the equations used the results per connection.

List of the connections:

- Slotted-in steel plates in the façades
- Slotted-in steel plate in the core
- WHT plates
- TTP1200 (Det 16)
- VGZ pairs at 45°
- TBS
- VGS

A.1. Slotted-in steel plates in the façades

The diagonals in the façades are connected via embedded steel plates with either dowels, bolts, screws or a combination of the three. To show an example of how the stiffness of this type of connection is calculated Detail 7 is taken as an example.

As seen in figure A.1 the diagonal comes from the top right where the timber connects to the steel plates via 33 D16 dowels and 6 M16 bolts. The steel plates split into two by a welded connection to continue to the pin. From there it goes through the column and beams, where it connects to the column via 7 D16 dowels and 4 TBSMAX 8x280 screws. After the column there is a welded connection to change the plates to then have an identical connection as at the start with 33 dowels and 6 bolts.

There are two stiffnesses related to the embedded steel plates that need to be calculated in Detail 7. The connection with 33 dowels and 6 bolts and the connection with 7 dowels and 4 screws.

$$K_{SLS,v,i} = \rho_{mean}^{1,5} \frac{d}{23} \tag{A.1}$$

$$K_{SLS,v,i} = 60 d_1^{1,7} \left(\frac{\rho_{mean}}{420}\right)^{1,1} \tag{A.2}$$

where

- ρ_{mean} = mean density = 420 [kg/m^3]
- d = diameter of the fastener = 16 [mm]

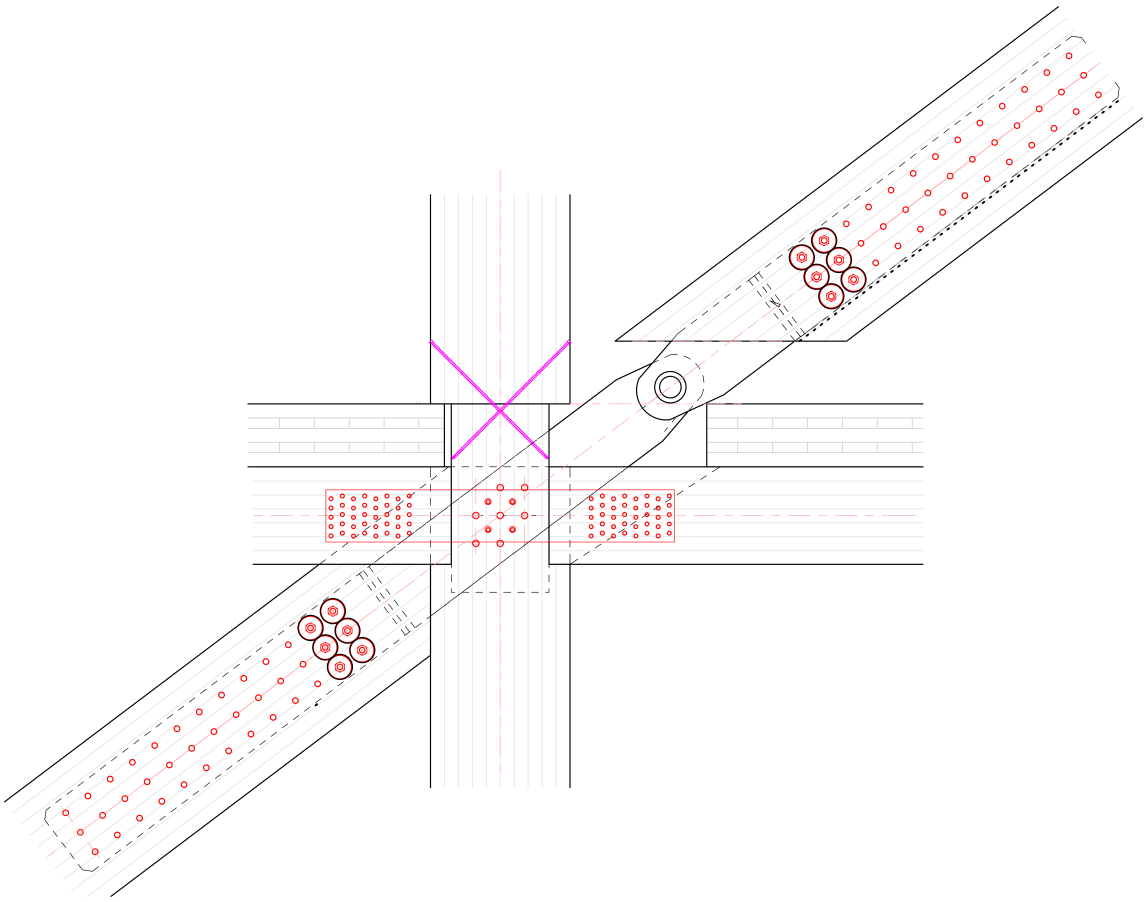

Figure A.1: Connection Urban Woods (Det 7 (CLT-S NV 2024)

- d_1 = inner thread diameter = 5,4 [mm]

For the connection with 33 dowels and 6 bolts the stiffness of one bolt or dowel per shear plane is calculated according to equation A.1. This value is then multiplied by the amount of shear planes, the steel-timber factor and the amount of dowels or bolts. The bolts and dowels work parallel to another, meaning you can add up the stiffnesses of all dowels.

$$K_{ser} = n_{spd} \cdot f_{s/t} \cdot \sum K_{SLS,v,i} \tag{A.3}$$

where

- n_{spd} = number of shear planes per dowel = 4
- $f_{s/t}$ = steel/timber factor = 2

One dowel or bolt with a diameter (d) of 16 [mm] in timber with a mean density (ρ_{mean}) of 420 [kg/m^3] has a stiffness ($K_{SLS,v,i}$) of 47902,27 [N/mm] following equation A.1. There being 33 dowels and 6 bolts result into a K_{ser} value of $1,9 \cdot 10^6$ [N/mm].

The connection with 7 dowels and 4 screws has an identical calculation process for the stiffness, the differences are the amount of connectors, the addition of screws (who have a different stiffness formula), and the angle the force makes with the timber fibres. The fibres in the column are vertical but the direction of the force is along the diagonal. If the angle between the fibres and the force is 90° the stiffness is halved, for any angle between 0 and 90° the stiffness can be interpolated.

A.2. Slotted-in steel plate in the core

To connect the CLT core walls to the concrete basement SBD dowels are used. Two different layouts of the dowels are applied along the walls, at eleven points a group of dowels (4x10) are placed together with three M12 bolts (Figure A.2). The second layout is found in between the big groups of dowels and exists out of a single line of SBD dowels (Figure A.3). The thin steel plate embedded in the CLT core walls is connected to a steal beam, which is then connected to the concrete of the basement. The loads coming from the slotted-in steel plate and end up in the basement/ foundation go through a multitude of connections. These connections are steel to steel or steel to concrete and including the stiffness of these connections falls out of the scope of this research, due to their relative high stiffness. The lateral slip modulus of the dowel connections are calculated in an identical way as to the connections in the façades, explained in the previous Section. Meaning, Equations A.1 and A.3 are used but with different values for the diameter (d is 7,5 or 12 mm instead of 16 mm).

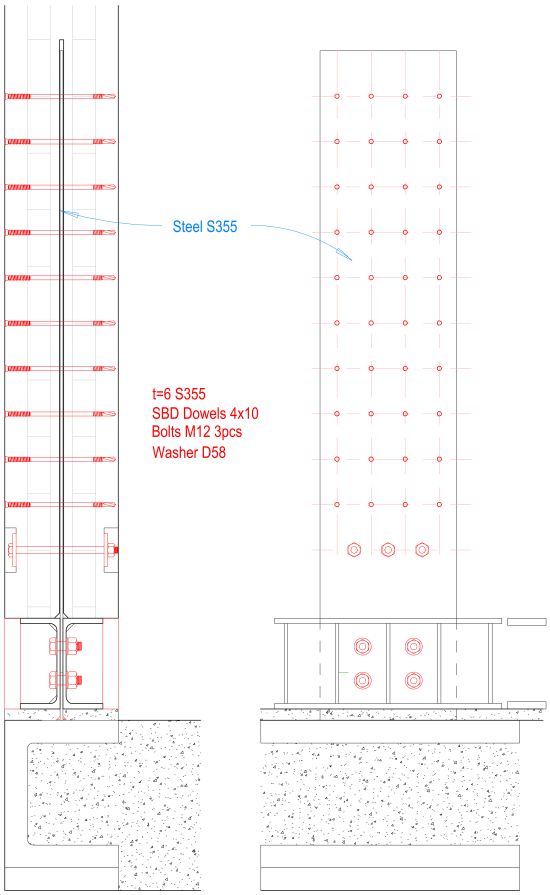

Figure A.2: Detail 3: 4x10 SBD dowels + M12 bolts 3pcs fastened to a t=6 mm S355 plate in a CLT wall (CLT-S NV 2024)

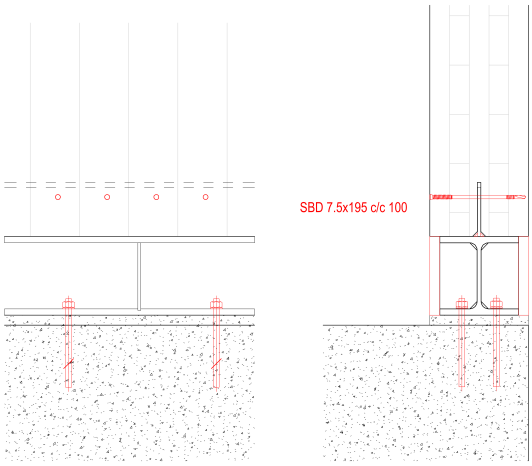

Figure A.3: Detail 4: line of SBD dowels to connect a core wall to the basement (CLT-S NV 2024)

A.3. WHT Plates

The Urban Woods building has three out of the five WHT Plates T, visible in figure A.4, being used in its structure. The 300 and 720 are used between floor slabs and the 820 is used for the vertical connection between the core slabs and in specific beam to beam connections in the façade. The purpose of this connection type is to take up tension, preventing members or slabs from separating.

Rothoblaas, the manufacturer, hasn't publicized any stiffness values for this type of connection. Therefore, an estimation needs to be made. For the estimation one plate is seen as a series of three springs, one spring for each group of screws and one spring for the steel plate between the group of screws, as illustrated in Figure A.5. The screws used are HBSP 8x120 or 8x100, with the 8 being the diameter

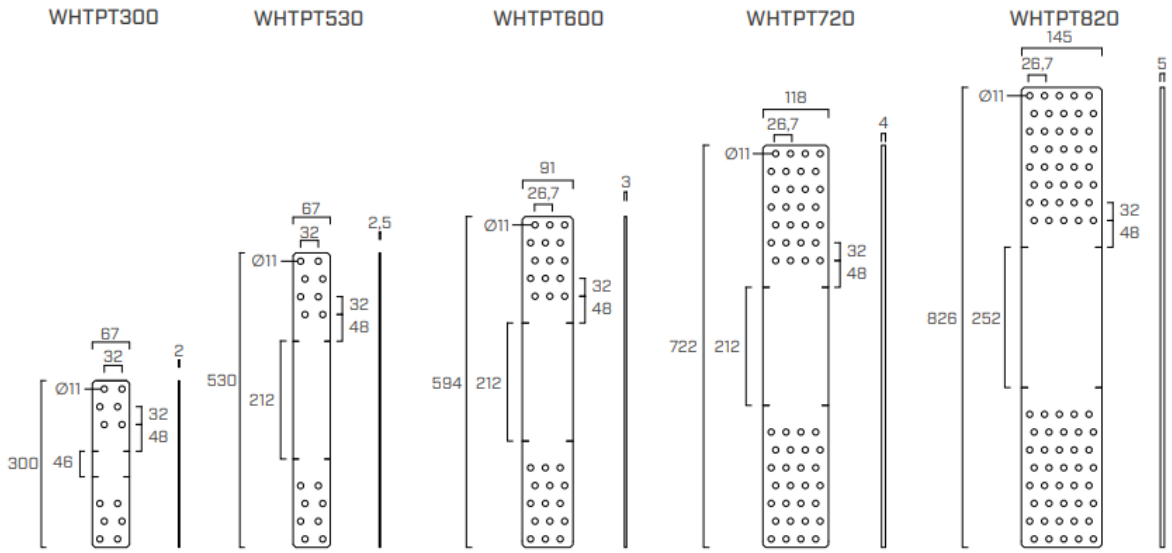

Figure A.4: Geometry of different WHT plates T by Rothoblaas

and the other value the length of the screw. To calculate the stiffness of one screw and the whole group Equations A.2 and A.3 are used. For the stiffness of the steel plate Equation A.4 is used.

$$K_{steel} = \frac{EA}{L} \tag{A.4}$$

where

- E = Modulus of Elasticity = 210000 in N/mm^2
- A = Area in mm^2 of steel plate = B · s
- L = Length, in mm, of steel plate between screw groups

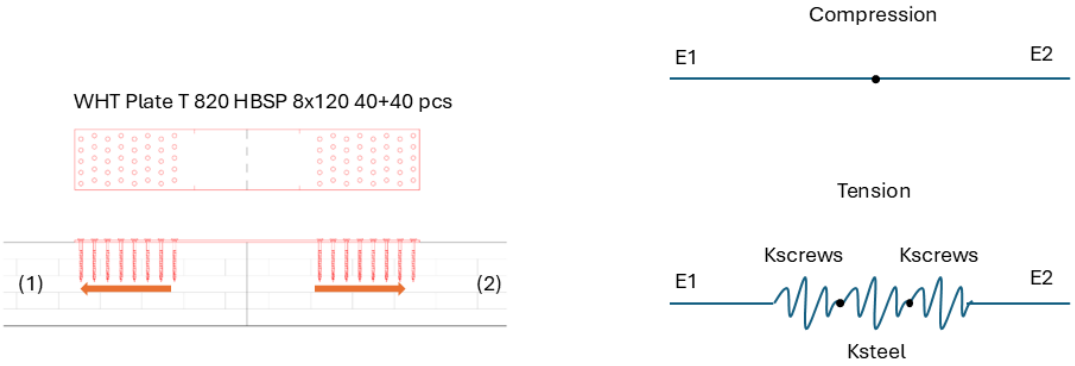

Figure A.5: Illustration of calculation method for WHT plates

Table A.1: Geometrical and stiffness properties for WHTPT series

Parameter	WHTPT300	WHTPT720	WHTPT820
Geometry			
H [mm]	300	722	826

(continued on next page)

(continued) Parameter	WHTPT300	WHTPT720	WHTPT820
B [mm]	67	118	145
s [mm)]	2	4	5
L_{steel} [mm]	48	212	252
Fasteners			
Screw type	HBSP 8x100	HBSP 8x100	HBSP 8x120
Number of screws	6	28	40
d_1 [mm]	5,9	5,9	5,9
Stiffness			
$K_{ser,1}$ [N/mm]	2 452,62	2 452,62	2 452,62
$K_{\text{ser},n}$ [N/mm]	14 715,70	68 673,27	98 104,66
K_{steel} [N/mm]	586 250,00	467 547,20	604 166,67
K_{total} [N/mm]	7 266,65	31 987,47	45 368,83

Table A.1 shows the geometric values, fasteners used and stiffnesses per type. $K_{ser,1}$ is the stiffness of one screw and $K_{ser,n}$ the stiffness of one group of screws.

A.4. TTP1200

With the core slabs being three floors high a connection is needed to continue the core, this connection exists out of pairs of VGZ fasteners, TTP1200 plates and the occasional WHTPT820 (see Section A.3). The TTP1200 has 24 LBS 7x100 fasteners per side at a c/c of 50 mm and its main purpose is to resist shear loads (sliding of the core plates). The stiffness of this shear resistance is calculated as a series of springs, with two of the springs being the rows of screws, and the last one being the shear stiffness of the plate between the two rows. This is illustrated in Figure A.6

$$K_{shear} = \frac{GA}{L} = \frac{GBt}{L} \tag{A.5}$$

where

- G = Shear Modulus = 81000 in N/mm^2
- B = Width of a TTP1200 = 1200 in mm
- t = Thickness of a TTP1200 = 1.5 in mm
- L = vertical spacing between bolt rows = 60 in mm
- K_{shear} = Shear stiffness of one TTP1200 = 177743.9 in N/mm

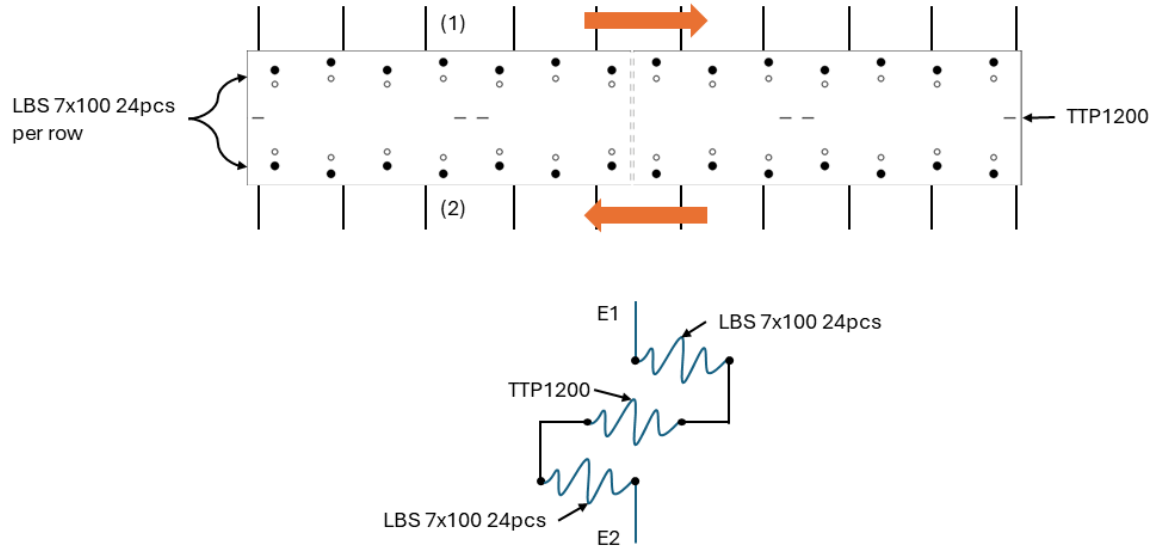

Figure A.6: Illustration of the spring system for the shear stiffness of a TTP1200

A.5. VGZ

VGZ fasteners are used in multiple connections in the structure, with differences in the properties of the screws and the timber parts. However, the calculation process is identical for each connection. The pink VGZ fasteners in Figure A.7 have a stiffness in the vertical direction that exists out of lateral and axial resistance. The lateral resistance can be calculated using Equation A.2, with a value of 5,9 mm for d1 the lateral resistance ($K_{SLS,v,i}$) is 1,23 kN/mm per fastener.

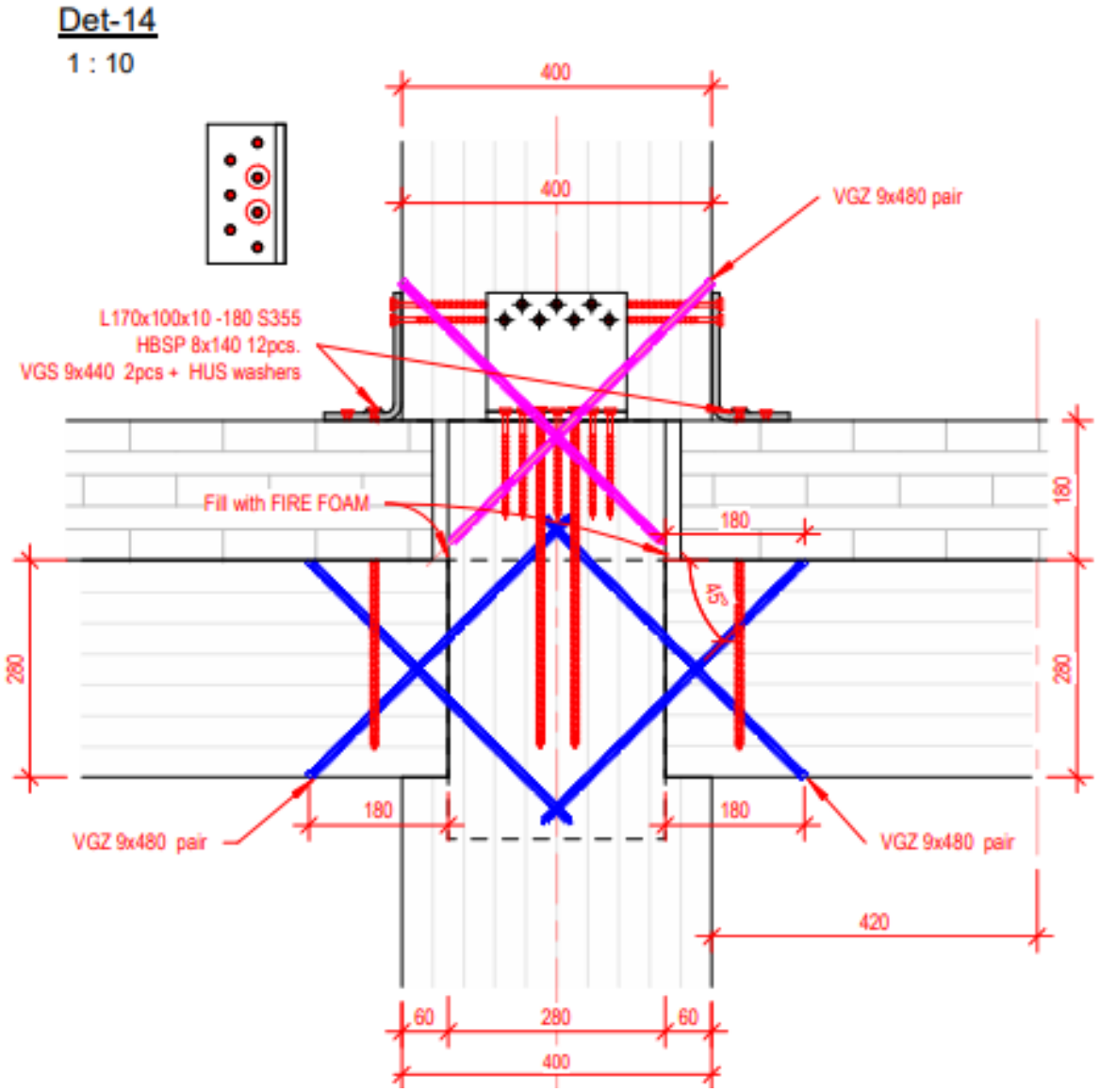

Figure A.7: Connection of columns, beams and floor slabs with angle brackets and pairs of VGZ screws (CLT-S NV 2024)

The axial resistance exists out of three parts: the resistance of the head of the screw against being pulled-through the timber and the two threaded parts, one part for each column. The two threaded parts work in series and the head works parallel to the threaded part of the same column, the illustration of this is shown in Figure A.8 for a δ of 90°.

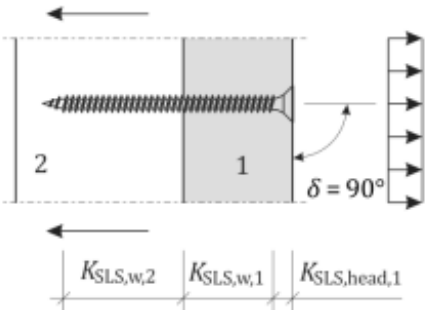

Figure A.8: General illustration for the axial slip modulus of a screw

The withdrawal resistances follows Equation A.6, with the a diameter of 9 mm and a mean density of 420 kg/m^3. The withdrawal length of the top column is 254.56 mm, resulting in a withdrawal resistance of 47.64 kN/mm. The respective values for the bottom column are 225.44 mm and 44.29 kN/mm. The resistance of the head of the screw is calculated following Equations A.7 and A.8. The head diameter of the screws is 11,5 mm and the density of the timber is 385 kg/m^3, resulting in

the values 1701,04 N and 113,40 N/mm for the head pull-through resistance force and slip modulus.

$$K_{SLS,w,i} = 2 \cdot d^{0,6} \cdot l_w^{0,6} \cdot \rho_{mean}^{0,9} \tag{A.6}$$

where

- d = diameter of the fastener in mm
- l_w = withdrawal length in mm
- ρ_{mean} = mean density = 420 kg/m^3

$$F_{pull,k} = 15 \cdot e^{\left(-\frac{d_{head}}{50}\right)} \cdot d_{head}^2 \cdot \left(\frac{\rho_k}{350}\right)^{0,8} \tag{A.7}$$

where

- d_{head} = head diameter in mm
- ρ_k = density in kg/m^3

$$K_{SLS,head} = \frac{F_{pull,k}}{15[mm]} \tag{A.8}$$

The axial resistance of one screw is then calculated according to the rules for springs in parallel and series, resulting in Equation A.9 and a value of 22,98 kN/mm.

$$\frac{1}{K_{SLS,ax}} = \frac{1}{K_{SLS,w,top} + K_{SLS,head}} + \frac{1}{K_{SLS,w,bottom}} \tag{A.9}$$

To combine the axial and lateral resistance Equation A.10 is used. The connection has 2 screws, who work in parallel, meaning the previously provided resistance values need to be multiplied by 2 before filling in Equation A.10. The result is a resistance value of 29,64 kN/mm for the pair of VGZ fasteners in the axial direction of the columns.

$$K_{SLS} = K_{SLS,v} \cdot \sin\delta \cdot (\sin\delta - \mu\cos\delta) + K_{SLS,ax} \cdot \cos\delta \cdot (\cos\delta + \mu\sin\delta) \tag{A.10}$$

where

- $K_{SLS,v}$ = lateral mean slip modulus per shear plane according to Equation A.2
- $K_{SLS,ax}$ = axial mean slip modulus per connection between members according to equation A.9
- δ = angle between the fastener axis and the shear plane in degrees
- μ = the friction coefficient between the members = 0,25 -

A.6. TBS

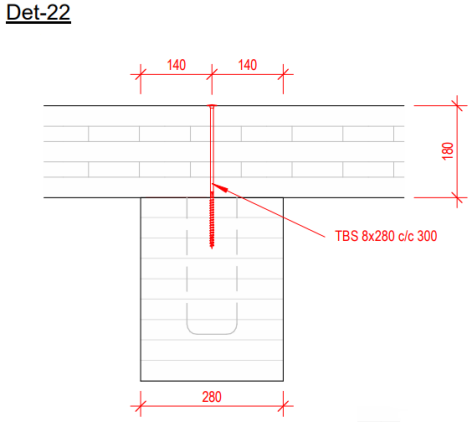

Figure A.9: CLT slab to GL beam by TBS fastener (CLT-S NV 2024)

The TBS fasteners are used to connect the floor slabs to the beams. This type of fastener has a threaded and non-threaded part, the threaded parts are at the ends of the fastener and are only in the beam. This has no influence on the lateral resistance and can therefore be calculated using Equation A.2. However, the axial resistance decreases compared to if it was fully threaded. The axial resistance can still be calculated with Equations A.6, A.7, A.8 and A.9, but there is no withdrawal resistance to go parallel with the head pull-trough resistance in Equation A.9.

A.7. VGS

To connect the beams in the roof to the columns groups of four VGS fasteners are used, this is visualized in Figure A.10. The calculation process for the stiffness of a VGS fastener is similar to the process used for a TBS fastener, but with some key differences. For the lateral slip Equation A.2 is used. The calculation process for the axial slip has an additional complexity. In general the axial slip modulus exists out of the withdrawal resistance of the threaded parts and the head pull through resistance of the head of the fastener. The equations used for calculating these resistances and combinding them are the Equations A.6, A.7, A.8 and A.9 are used. The whole fastener is threaded, meaning there is a withdrawal resistance of the part in the beam and in the column. However, the withdrawal resistance in the column needs to be halved, due to the fibres running parallel to the fastener in the column.

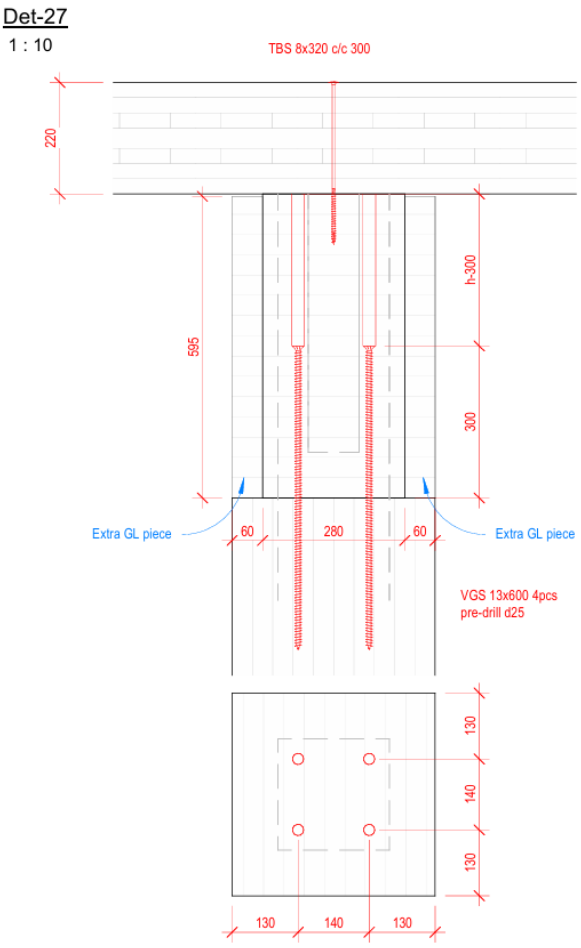

Figure A.10: 4 VGS fasteners used to connect a glulam beam of the highest floor to the glulam column (CLT-S NV 2024)

A.8. Summary and results

The main equations used in this appendix are listed below followed by three tables. Table A.2 summarizes the stiffnesses for all connections except for the embedded in steel plates. The stiffnesses of the latter are listed in Table A.3. The last table (Table A.4) holds the reduced stiffness values of certain connections where the force is under an angle with the fibres.

$$A.1 : K_{SLS,v,i} = \rho_{mean}^{1,5} \frac{d}{23}$$

$$A.2 : K_{SLS,v,i} = 60 d_1^{1,7} \left(\frac{\rho_{mean}}{420}\right)^{1,1}$$

$$A.3 : K_{ser} = n_{spd} \cdot f_{s/t} \cdot \sum K_{SLS,v,i}$$

$$A.4 : K_{steel} = \frac{EA}{L}$$

$$A.5 : K_{SLS,w,i} = 2 \cdot d^{0,6} \cdot l_w^{0,6} \cdot \rho_{mean}^{0,9}$$

$$A,6 : F_{pull,k} = 15 \cdot e^{\left(-\frac{d_{head}}{50}\right)} \cdot d_{head}^2 \cdot \left(\frac{\rho_k}{350}\right)^{0,8}$$

$$A.7 : K_{SLS,head} = \frac{F_{pull,k}}{15(mm)}$$

$$A.9 : K_{SLS} = K_{SLS,v} \cdot \sin\delta \cdot (\sin\delta - \mu\cos\delta) + K_{SLS,ax} \cdot \cos\delta \cdot (\cos\delta + \mu\sin\delta)$$

Table A.2: Stiffness values per type of fastener

Fastener	Detail[a]	Equations	Kser,1 [kN/mm][b]	Kser,2/3 [kN/mm][b]	Kser,4/5 [kN/mm][b]
WHT plates					
WHTPT300	21	A.2, A.3, A.4	7,27		
WHTPT720	8A, 20, 24	A.2, A.3, A.4	31,99		
WHTPT820	7, 11, 12, 17, 30	A.2, A.3, A.4	45,37		
TTP1200	16	A.2, A.3, A.4		17,74	
VGZ pair					
7x220	23	A.2, A.3, A.5, A.6, A.7, A.9	16,04	16,04	2,90
7x260	16	A.2, A.3, A.5, A.6, A.7, A.9	17,73	17,73	2,90
9x280	18	A.2, A.3, A.5, A.6, A.7, A.9	21,75	21,75	4,42
9x480	7, 13, 14, 15	A.2, A.3, A.5, A.6, A.7, A.9	29,64		
9x520	19	A.2, A.3, A.5, A.6, A.7, A.9	30,99	30,99	4,42
TBS					
8x280	21, 22, 25, 28, 31	A.2, A.3, A.5, A.6, A.7	1,05	1,05	0,36
VGS					
13x600	27, 28, 29	A.2, A.3, A.5, A.6, A.7	2,06	2,06	21,75

[a] The numbers in the column *Detail* refer to the technical drawings from (CLT-S NV 2024).

[b] 1 stands for the direction in which the lateral stiffness is the strongest, 2/3 the second lateral stiffness and 4/5 the axial stiffness or the weakest direction.

Table A.3: Stiffnesses of connections with embedded steel plates

Part	# bolts/dowels	Kser [kN/mm]	# screws	Kser [kN/mm]	Total [kN/mm]
Det 1					
Part 1	3	143,71	0	0,00	143,71
Part 2	0	0,00	0	0,00	0,00
Part 3	0	0,00	0	0,00	0,00
Det 2					
Part 1	45	2 155,60	0	0,00	2 155,60
Part 2	0	0,00	0	0,00	0,00
Part 3	0	0,00	0	0,00	0,00
Det 5 (X)					
Part 1	18	862,24	12	101,27	963,51
Part 2	0	0,00	9	75,95	75,95
Part 3	18	862,24	3	25,32	887,56
Det 5 (Y)					
Part 1	18	862,24	30	253,18	1 115,42
Part 2	7	335,32	4	33,76	369,07
Part 3	0	0,00	0	0,00	0,00
Det 6					
Part 1	45	2 155,60	0	0,00	2 155,60

Continued on next page

Part	# bolts/dowels	Kser [kN/mm]	# screws	Kser [kN/mm]	Total [kN/mm]
Part 2	0	0,00	12	101,27	101,27
Part 3	45	2 155,60	0	0,00	2 155,60
Det 7					
Part 1	39	1 868,19	0	0,00	1 868,19
Part 2	7	335,32	4	33,76	369,07
Part 3	39	1 868,19	0	0,00	1 868,19
Det 8					
Part 1	6	287,41	3	25,32	312,73
Part 2	50	2 395,11	12	101,27	2 496,39
Part 3	6	287,41	0	0,00	287,41
Det 9					
Part 1	6	287,41	3	25,32	312,73
Part 2	9	431,12	0	0,00	431,12
Part 3	6	287,41	3	25,32	312,73
Det 10					
Part 1	9	431,12	0	0,00	431,12
Part 2	6	287,41	0	0,00	287,41
Part 3	0	0,00	0	0,00	0,00
Det 11					
Part 1	39	1 868,19	0	0,00	1 868,19
Part 2	27	1 293,36	6	50,64	1 344,00
Part 3	39	1 868,19	0	0,00	1 868,19
Det 12					
Part 1	12	574,83	6	50,64	625,46
Part 2	39	1 868,19	0	0,00	1 868,19
Part 3	0	0,00	0	0,00	0,00

Table A.4: Reduced stiffness values for connections with an angle between the direction of the force and the fibers of the timber it is connected to

Connection	K_{ser} [kN/mm]	$K_{ser,\ reduced}$ [kN/mm]
Det 7.2	369,07	265,18
Det 8.2	2496,39	1793,67
Det 9.2	431,12	336,92
Det 10.1	431,12	336,92
Det 12.1	625,46	449,40

B

Virtual Work method

The Virtual Work method (a.k.a. Virtual Force method) is used on a reduced structure of the two façades with the Equations B.1, B.2 and B.3. Figure B.2 shows the structural model with all its members numbered, the axial forces of the members under the unit load and actual load are shown in Figures B.3, B.4 and B.5. The actual load exists out of a combination of wind load and self weight, combined via SLS standards as further explained in Appendix D. The results of each member and the whole structures are shown in tables B.1, B.2, B.3 and B.4. Table B.5 explains where the stiffnesses (K_{ser}) used in the other tables come from. An important thing to note from Table B.5 are the Non-linear connections, these connections are neglected when a compression force goes through the joint. This is because in these connections the force directly transfers from timber to timber in case of compression, neglecting the steel screws. This is the reason why self weight was included in the Virtual Work method in this research. Without the self weight certain columns would be in tension, resulting in an increase of the total horizontal deflection due to an increase of the deformation of the connections. This is not desired, as the purpose of the application of the model is to get an as close as possible representation of the reality using the Virtual Work method.

$$u_{members} = \sum F_i \frac{F_{1i} l_i}{E_i A_i} \tag{B.1}$$

$$u_{connections} = \sum \frac{F_i F_{1i}}{K_i} \tag{B.2}$$

$$u_H = u_{members} + u_{connections} \tag{B.3}$$

where

- u_H = desired deflection of structure in mm
- F_i = axial force of member i in N
- F_{1i} = axial force of member i caused by unit load
- l_i = length of member i in mm
- E = Modulus of Elasticity in N/mm^2
- A = area of the profile of the members in mm^2
- K_i = stiffness value of all connections on member i combined in N/mm

The majority of the members in the facade are GL24h with an area (A) of 160 000 mm^2 and Modulus of Elasticity (E) of 11 500 N/mm^2. The vertical members 11 and 12 (see figure B.2) of the façade in X-plane have the same area but are made out of GL30h, which has an E of 13 000 N/mm^2. The diagonals are all GL24h members with steel embedded plates, but there is an important differentiation to make between members where the steel plates are only at the connections and members where the steel plates span the whole length of the member.

This is visualized in figure B.1, where the diagonal element connecting to the roof has steel plates that are pinned in DET 07 and continue all the way to DET 10, where they are connected to the beam. On the other hand, the diagonal element between the two DET 07 has only steel plates near the connections. This differentiation has influence on the stiffness of the members and the sum of the stiffnesses of the connections on the members. With steel plates spanning the whole length the stiffness of the member is governed by the stiffness of the steel when in tension and the combined stiffness of the timber and steel when the member is under compression. Furthermore, the connections along this member don't resist the load going through the steel. Therefore, they don't resist the deflection of the whole structure and are not taken into account in the application of the virtual work method.

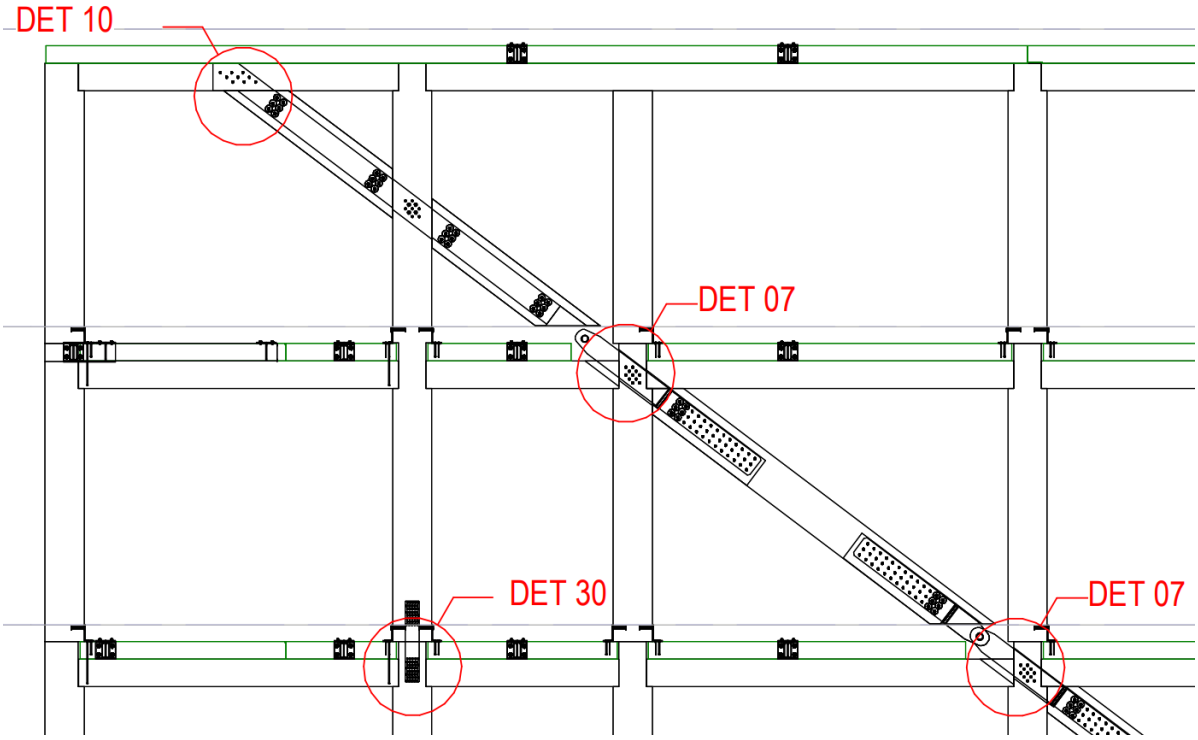

Figure B.1: Two types of diagonals: steel plates spanning the length of the timber element and steel plates only at the connection

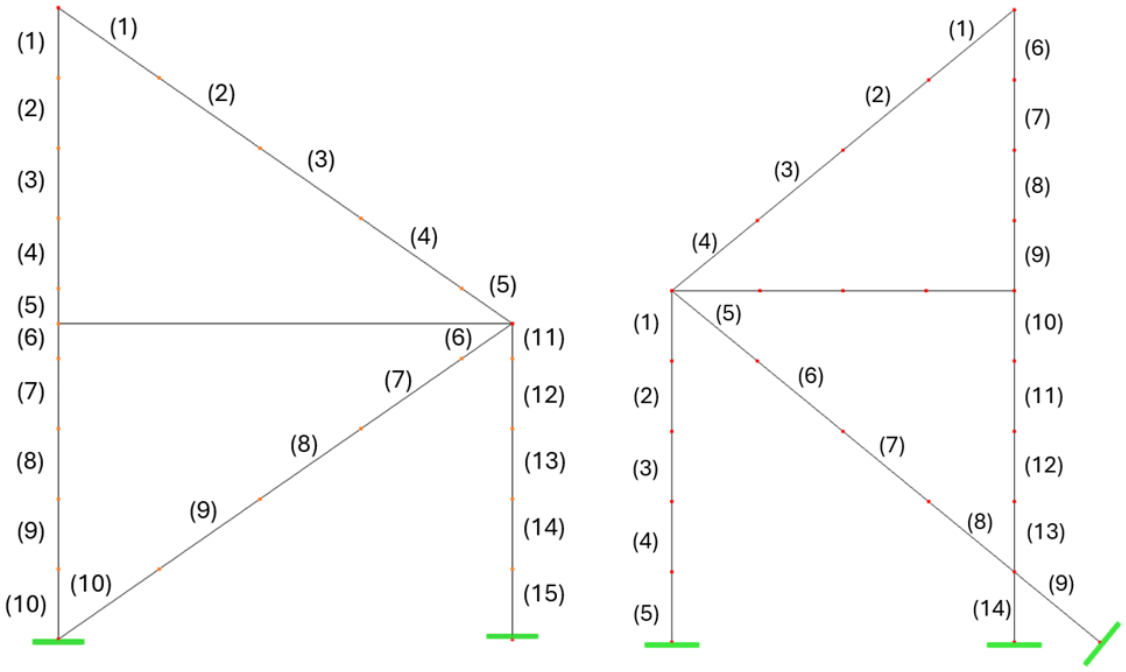

Figure B.2: Numbering of the two facades

Table B.1: Vertical and Diagonal members with forces, displacements, and stiffness of the façade in the X-plane, subjected to self weight and wind load in the negative Y direction

	F_{1i} [-]	F_i [kN]	U_{memb} [mm]	K_{ser} [kN/mm]	U_{con} [mm]	U_H [mm]
Vertical						
1	0,70	82,57	0,10			
2	0,70	57,38	0,07	29,60	1,35	
3	0,70	32,00	0,04	29,60	0,76	
4	0,70	16,48	0,02	29,60	0,39	
5	0,70	−9,18	−0,01			
6	0,70	−10,75	−0,01			
7	0,70	−36,40	−0,04			
8	0,70	−84,36	−0,10			
9	0,70	−132,32	−0,15			
10	0,70	−147,98	−0,17			
Support	0,70	−147,98		857,00	−0,12	
11	−1,39	−533,29	0,52	3 040,00	0,24	
12	−1,39	−548,46	1,07	2 630,00	0,29	
13	−1,39	−575,03	1,32	2 160,00	0,37	
14	−1,39	−602,36	1,38			
15	−1,39	−629,27	1,45	2 160,00	0,41	
Support	−1,39	−629,27		857,00	1,02	
Diagonal						
1	−1,22	−81,54	0,57	337,00	0,30	
2	−1,22	−131,21	0,46	934,00	0,17	
3	−1,22	−180,41	0,64	934,00	0,24	
4	−1,22	−225,41	0,79			

Continues on next page

	F_{1i} [-]	F_i [kN]	U_{memb} [mm]	K_{ser} [kN/mm]	U_{con} [mm]	U_H [mm]
5	−1,22	−267,01	0,47			
6	1,22	419,34	0,74			
7	1,22	466,20	1,64			
8	1,22	509,96	1,80	934,00	0,67	
9	1,22	553,35	1,95	934,00	0,72	
10	1,22	597,99	2,10			
Support	1,22	340,01		857,14	0,48	
Total			16,64		6,80	23,44

Table B.2: Vertical and Diagonal members with forces, displacements, and stiffness of the façade in the X-plane, subjected to self weight and wind load in the positive Y direction

	F_{1i} [-]	F_i [kN]	U_{memb} [mm]	K_{ser} [kN/mm]	U_{con} [mm]	U_H [mm]
Vertical						
1	−0,70	−106,91	0,12			
2	−0,70	−132,45	0,15			
3	−0,70	−158,04	0,18			
4	−0,70	−173,70	0,20			
5	−0,70	−197,32	0,11			
6	−0,70	−202,01	0,12			
7	−0,70	−227,67	0,26			
8	−0,70	−275,63	0,32			
9	−0,70	−323,59	0,37			
10	−0,70	−339,26	0,39			
Support	−0,70	−339,26		857,00	0,28	
11	1,39	245,70	0,24	3 040,00	0,11	
12	1,39	230,99	0,45	2 160,00	0,15	
13	1,39	205,69	0,47	2 630,00	0,11	
14	1,39	180,00	0,41			
15	1,39	154,27	0,35	2 160,00	0,10	
Support	1,39	152,08		857,00	0,25	
Diagonal						
1	1,22	91,43	0,64	431,00	0,26	
2	1,22	135,81	0,48	934,00	0,18	
3	1,22	179,25	0,63	934,00	0,23	
4	1,22	224,87	0,79			
5	1,22	270,67	0,48			
6	−1,22	−375,00	0,66			
7	−1,22	−423,91	1,49			
8	−1,22	−474,71	1,68	934,00	0,62	
9	−1,22	−519,24	1,83	934,00	0,68	
10	−1,22	−570,70	2,01			
Support	−1,22	−325,96		857,00	0,46	
Total			14,85		2,96	17,81

Table B.3: Vertical and Diagonal members with forces, displacements, and stiffness of the façade in the Y-plane, subjected to self weight and wind load in the negative X direction

	F_{1i} [-]	F_i [kN]	U_{memb} [mm]	K_{ser} [kN/mm]	U_{con} [mm]	U_H [mm]
Vertical						
1	−1,64	−532,56	1,44	1 340,00	0,65	
2	−1,64	−606,40	1,64	2 160,00	0,46	
3	−1,64	−680,24	1,84	2 160,00	0,52	
4	−1,64	−749,06	2,03			
5	−1,64	−809,98	2,19	2 160,00	0,62	
Support	−1,64	−809,98		857,00	1,55	
6	0,82	7,47	0,01	75,00	0,08	
7	0,82	−68,37	−0,09			
8	0,82	−142,19	−0,19			
9	0,82	−216,02	−0,29			
10	0,82	−292,49	−0,40			
11	0,82	−361,31	−0,49			
12	0,82	−426,06	−0,58			
13	0,82	−490,17	−0,66			
14	0,82	−634,21	−0,86			
Support	0,82	−634,21		857,00	−0,61	
Diagonal						
1	−1,29	−54,76	0,18	303,00	0,23	
2	−1,29	−81,48	0,27	934,00	0,11	
3	−1,29	−107,77	0,36	934,00	0,15	
4	−1,29	−132,42	0,45	934,00	0,18	
5	1,29	227,72	0,77	934,00	0,31	
6	1,29	248,37	0,84	934,00	0,34	
7	1,29	268,73	0,90	934,00	0,37	
8	1,29	289,48	0,97	934,00	0,40	
9	1,29	380,67	1,27			
Support	1,29	241,29		857,14	0,36	
Total			11,62		5,74	17,36

Table B.4: Vertical and Diagonal members with forces, displacements, and stiffness of the façade in the Y-plane, subjected to self weight and wind load in the positive X direction

	F_{1i} [-]	F_i [kN]	U_{memb} [mm]	K_{ser} [kN/mm]	U_{con} [mm]	U_H [mm]
Vertical						
1	1,64	−90,03	−0,24	1 340,00	−0,11	
2	1,64	−163,87	−0,44	2 160,00	−0,12	
3	1,64	−237,69	−0,64	2 630,00	−0,15	
4	1,64	−306,57	−0,83			
5	1,64	−367,44	−1,00	2 160,00	−0,28	
Support	1,64	−367,44		857,00	−0,70	
6	−0,82	−105,10	0,14			
7	−0,82	−178,90	0,24			
8	−0,82	−252,71	0,34			
9	−0,82	−326,55	0,44			
10	−0,82	−403,87	0,55			

Continues on next page

	F_{1i} [-]	F_i [kN]	U_{memb} [mm]	K_{ser} [kN/mm]	U_{con} [mm]	U_H [mm]
11	−0,82	−472,70	0,64			
12	−0,82	−537,44	0,73			
13	−0,82	−601,56	0,81			
14	−0,82	−589,46	0,80			
Support	−0,82	−589,46		857,00	0,56	
Diagonal						
1	1,29	57,65	0,19	303,00	0,25	
2	1,29	79,75	0,27	934,00	0,11	
3	1,29	102,04	0,34	934,00	0,14	
4	1,29	122,98	0,41	934,00	0,17	
5	−1,29	−223,58	0,75	934,00	0,31	
6	−1,29	−248,35	0,84	934,00	0,34	
7	−1,29	−272,90	0,92	934,00	0,38	
8	−1,29	−297,45	1,00	934,00	0,41	
9	−1,30	−378,18	1,28			
Support	−1,30	−239,71		857,00	0,36	
Total			7,54		1,67	9,21

Table B.5: Kser combinations per member of each facade

Direction / Row	**Kser, X**	**Kser, Y**
Vertical		
1		Det-11.2
2	VGZ 9x480 **Non-linear**	Det-6.1
3	VGZ 9x480 **Non-linear**	Det-6.3
4	VGZ 9x480 **Non-linear**	
5		Det-2.1
6	VGZ 9x480 **Non-linear**	(VGZ 9x480 + WHTPT820) **Non-linear**
7	VGZ 9x480 **Non-linear**	(VGZ 9x480 + WHPT820) **Non-linear**
8	VGZ 9x480 **Non-linear**	VGZ 9x480 **Non-linear**
9	VGZ 9x480 **Non-linear**	VGZ 9x480 **Non-linear**
10	Det-1.1 **Non-linear**	VGZ 9x480 **Non-linear**
11	Det-8.2	VGZ 9x480 **Non-linear**
12	Det-6.1	VGZ 9x480 **Non-linear**
13	Det-6.2	VGZ 9x480 **Non-linear**
14		Det-1.1 **Non-linear**
15	Det-2.1	
Diagonal		
1	Det-10.1-reduced	Det-12.1-reduced + Det-12.2 + Det-7.1
2	Det-7.1 + Det-7.3	Det-7.1 + Det-7.3
3	Det-7.1 + Det-7.3	Det-7.1 + Det-7.3
4		Det-7.3 + Det-11.1
5		Det-11.3 + Det-7.1
6		Det-7.1 + Det-7.3
7		Det-7.1 + Det-7.3
8	Det-7.1 + Det-7.3	Det-7.1 + Det-7.3
9	Det-7.1 + Det-7.3	
10		

-The values corresponding to these parameters are found in tables A.2, A.3 and A.4. Example: Det-12.1 means

the stiffness of Detail 12 part 1.
-Springs are added in series when ”a” + ”b” and parallel when (”a” + ”b”).
-The connections that are **Non-linear** have the stiffness of the connection listed in the table when the member is in tension. Under compression the load doesn’t transfer through the connection, meaning the deformation of it is neglected.

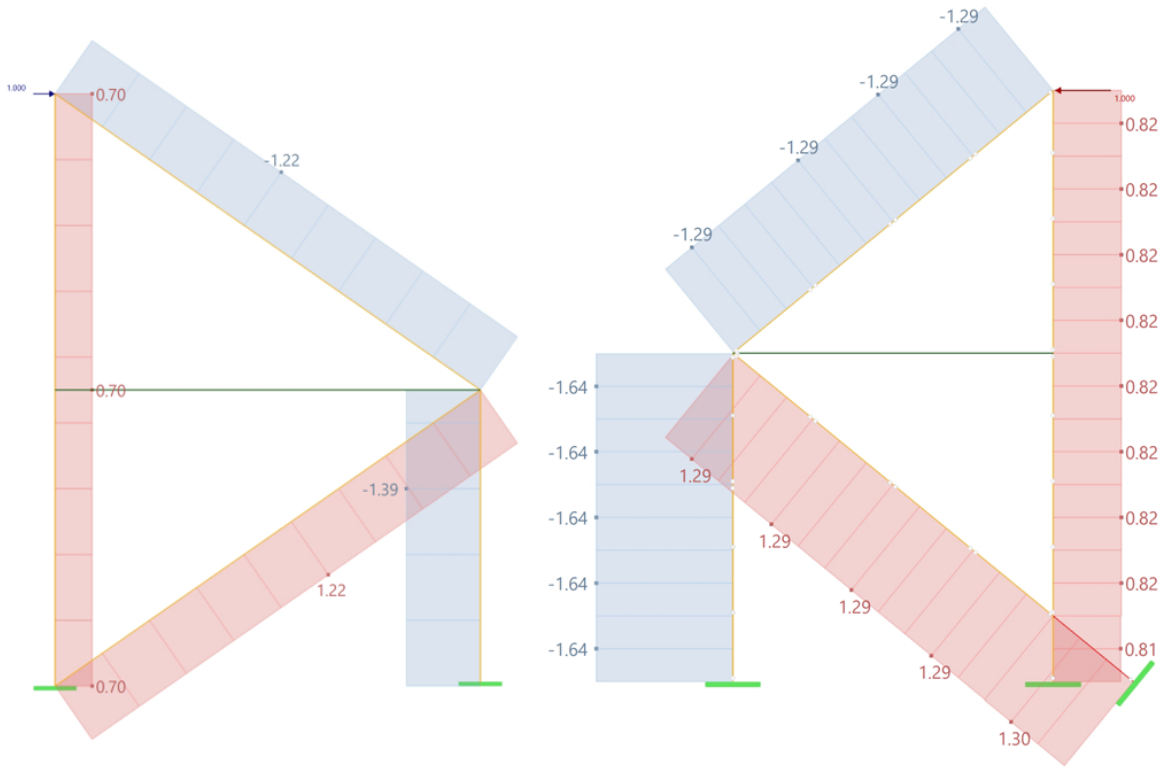

Figure B.3: Axial forces of members due to unit load 1 [-]

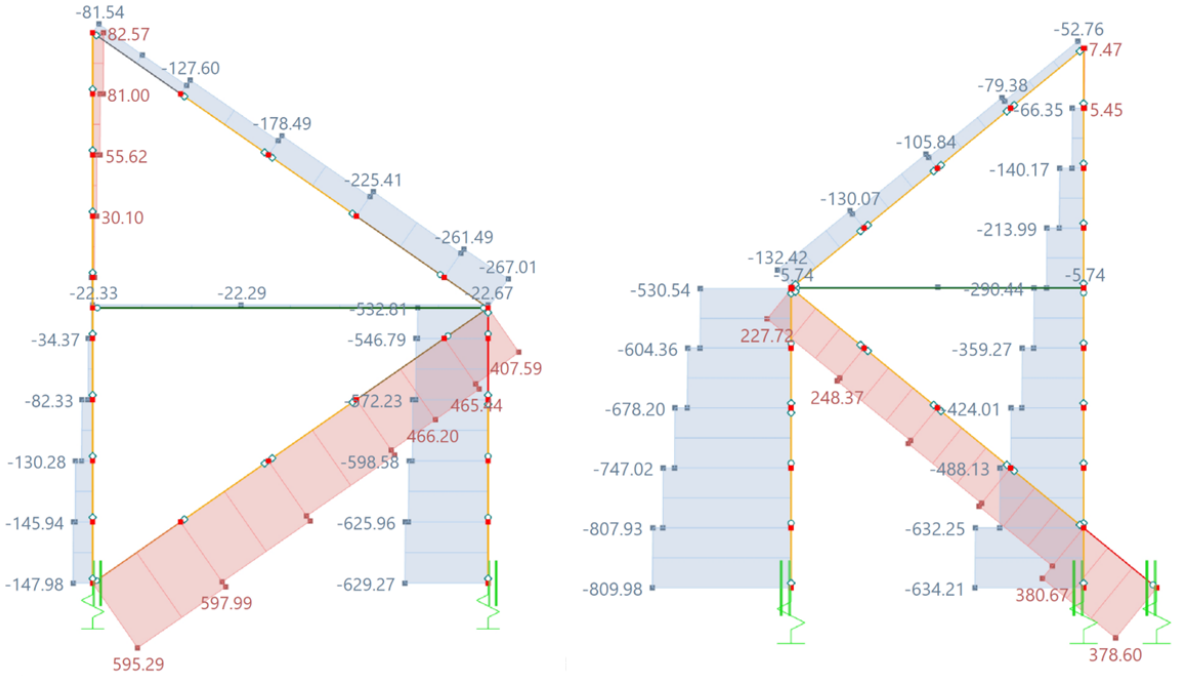

Figure B.4: Axial forces of members due to wind load in negative direction and self weight

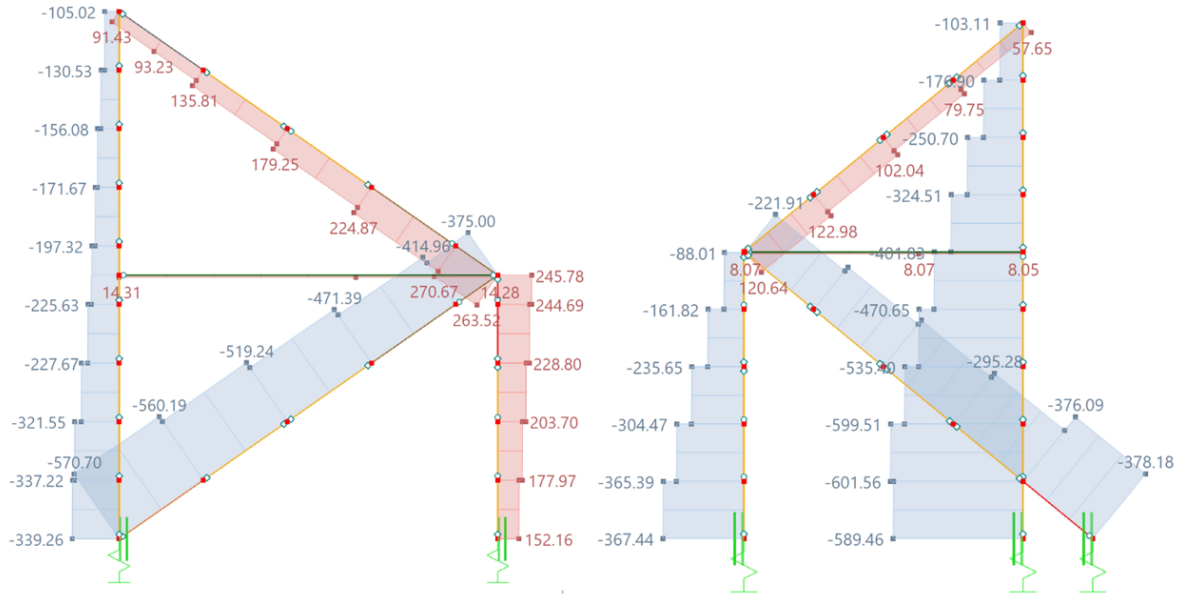

Figure B.5: Axial forces of members due to wind load in positive direction and self weight

C

RFEM models

This appendix holds all information regarding the setup of the six RFEM models made (3D complete building, 3D core, 2 times 2D complete façade and 2 times 2D virtual work model). For every model an additional copy is made with the simplification of having no connections modelled. The dimensions in the models correspond to the technical drawings of the building (CLT-S NV 2024), the stiffness values are found in appendices A and B and the loads are explained in appendix D.

C.1. 2D models of the facades

For both the façades in the X and Y plane two type of 2D models are made, one representing the actual façade as close as possible and one reduced version for the Virtual Work method. The purpose of these models is to compare their results to those of the Virtual Work method and to get an inkling on how stiff the façades are on their own.

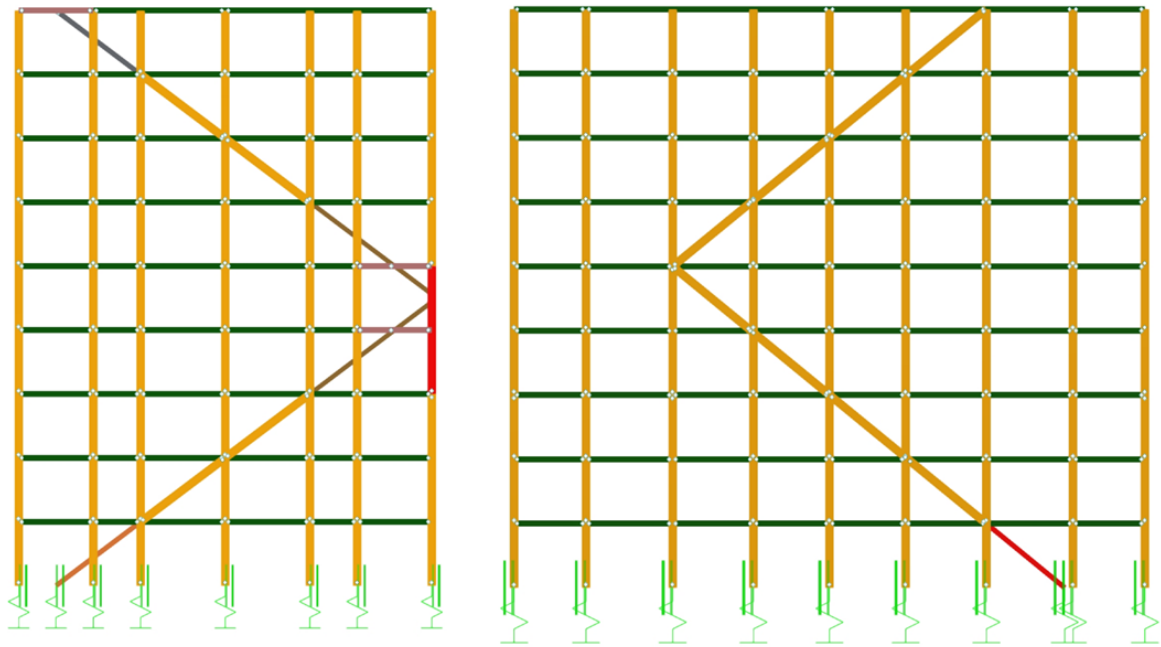

Figure C.1: Structures of the 2D models

Figure C.1 shows the structures of both facades and figure C.2 is a legend added to explain the different cross-sections. In general, the majority of the members have the same cross-section and are made

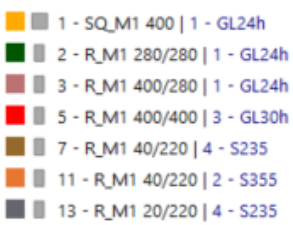

Figure C.2: Legend to figure C.1

out of the same material. There are some special vertical and horizontal members with different dimensions or materials, always at locations with a possibility of high loads. However, the dark blue and brown diagonals are significantly different compared to the standard. This is due to the two steel plates that are embedded in these diagonals and span the entire length of the diagonal. To model these members the ones in tension are modelled as one steel plate with the thicknesses of the two embedded steel plates combined, and the members in compression are modelled as glulam members with twice the amount of area as the standard diagonals. The members in tension are only steel because under tension only the steel will transfer loads due to how the members are and how they are connected. However, under compression both the steel and timber carry the load, as both have (by coincidence) the same EA the area was doubled to implement the higher stiffness.

The stiffnesses of the connections are added to the model by adding hinges on the members with values corresponding to the values found in appendices A and B. The hinges are visualized by the angled hollow blue squares at the joints. The supports are modelled as vertical springs, as explained in Section 4.2.

C.2. Core model

To investigate the influence of the stiffness of the connections in the core, five different structures of the core are made. One is a basic model, one for the vertical joints between the walls, one for sliding of the horizontal joints of the core walls, one for rocking of the core walls and the last one with all connections modelled. The basic model is the basis on which the other models are made, this is then upgraded for the next model that includes the vertical connections between the core walls. The sliding model takes the upgraded model with the vertical connections and adds the horizontal connections to only allow sliding of the core walls additionally to the bending and shear deformation of the core. The rocking model has a similar approach, but then for rocking. The final model combines the sliding and rocking models into one, this model is a direct representation of how the core is modelled in the global model of the whole building.

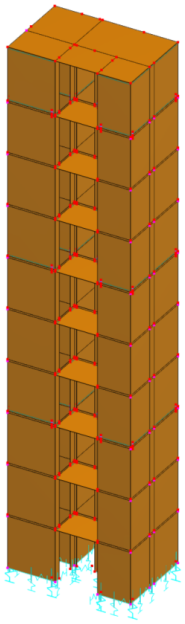

Figure C.3: Basic model of the core

The basic model follows the technical drawings of the building (CLT-S NV 2024), it exists out of core walls, floor slabs, lintels, and supports, as visible in Figure C.3. The core walls are 200 [mm] and the floor slabs and roof are 180 [mm] thick, both are CLT made out off C24. GL24h lintels are added in the openings that are not connected to the floor slabs and can only transfer a normal load. The structure is supported by a combination of eleven nodal supports and line supports running along each part of the core walls.

The core walls are three stories high, meaning that connections are added every three floors to transfer forces in the vertical direction. Figure C.4 shows the technical drawings of the connections and Figure C.5 shows how they are modelled in RFEM. The combination of fasteners in detail 16 is continuous over all walls and is therefore modelled as a line hinge. The WHTPT820 fasteners in detail 17 are only at specific places, therefore they are modelled as steel plates with hinges at the ends to represent the group of screws. What is also visible in the figure for detail 16 is that the floor slabs are connected to the core via pairs of VGZ 7x260 every 500 [mm], this is modelled as a line hinge in RFEM.

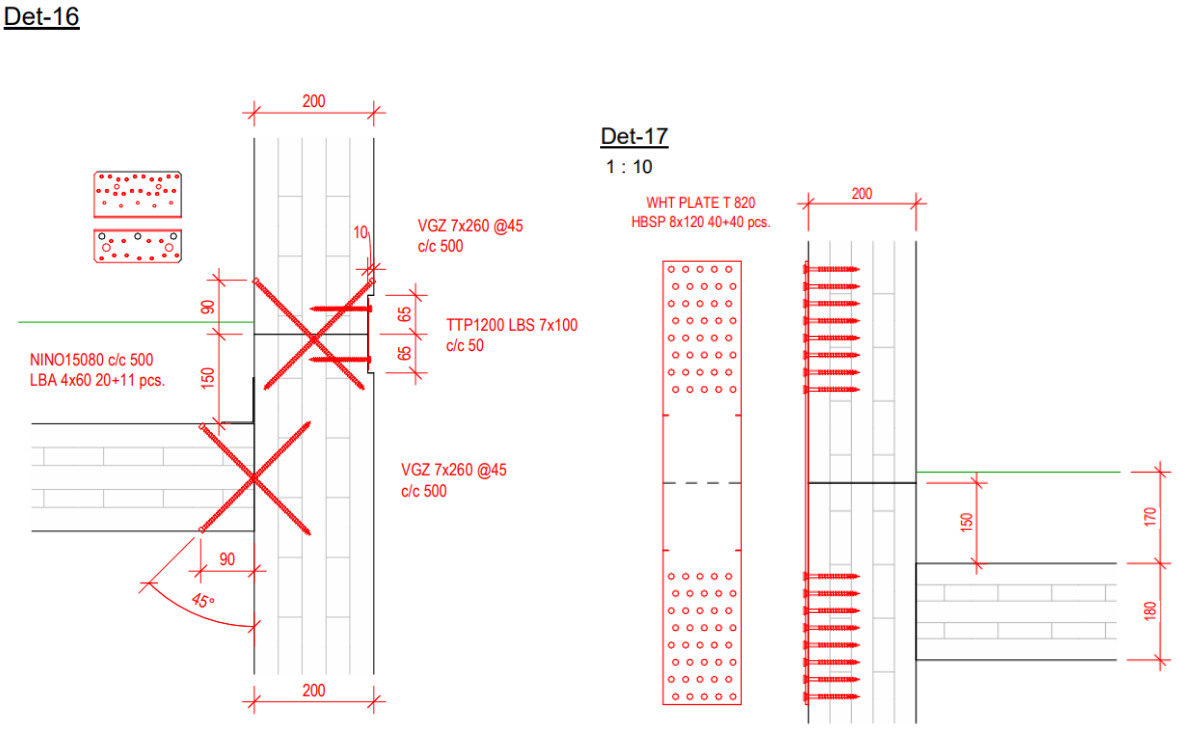

(a) Core connection with TTP1200 and VGZ fasteners

(b) Core connection with WHT Plate T 820

Figure C.4: Vertical core connections Details 16 and 17 from the technical drawings (CLT-S NV 2024)

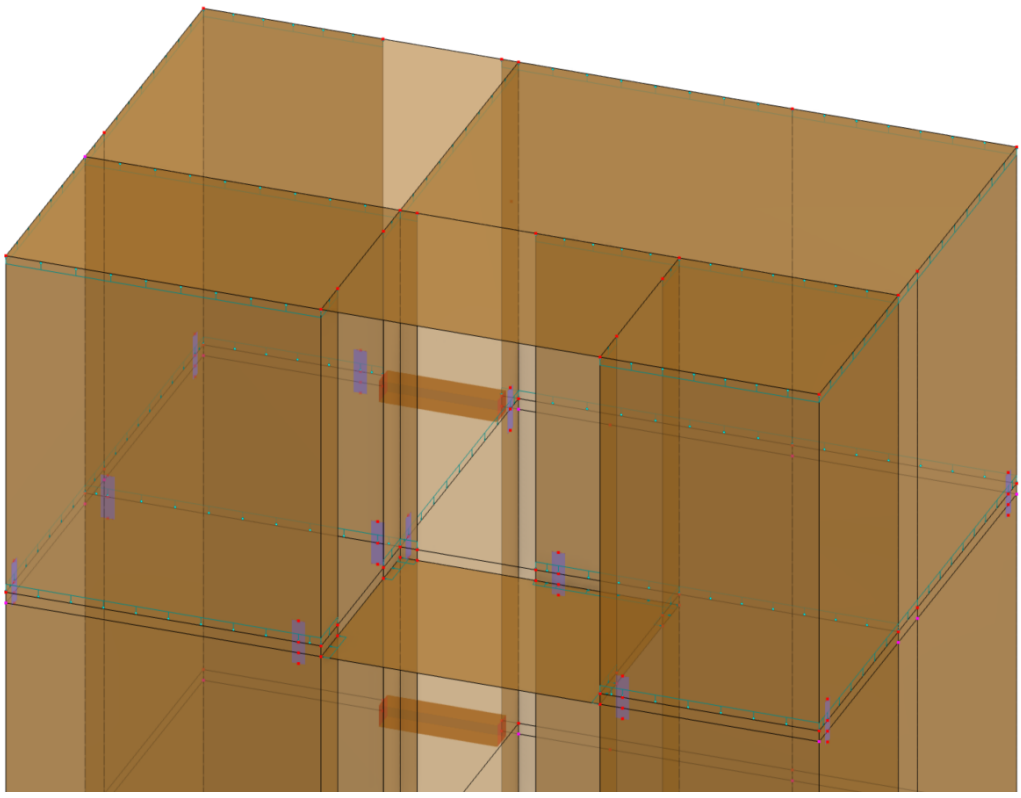

Figure C.5: Core connections modelled in RFEM, green lines are line hinges (Det-16) and the blue surfaces are WHTPT820 fasteners (Det-17)

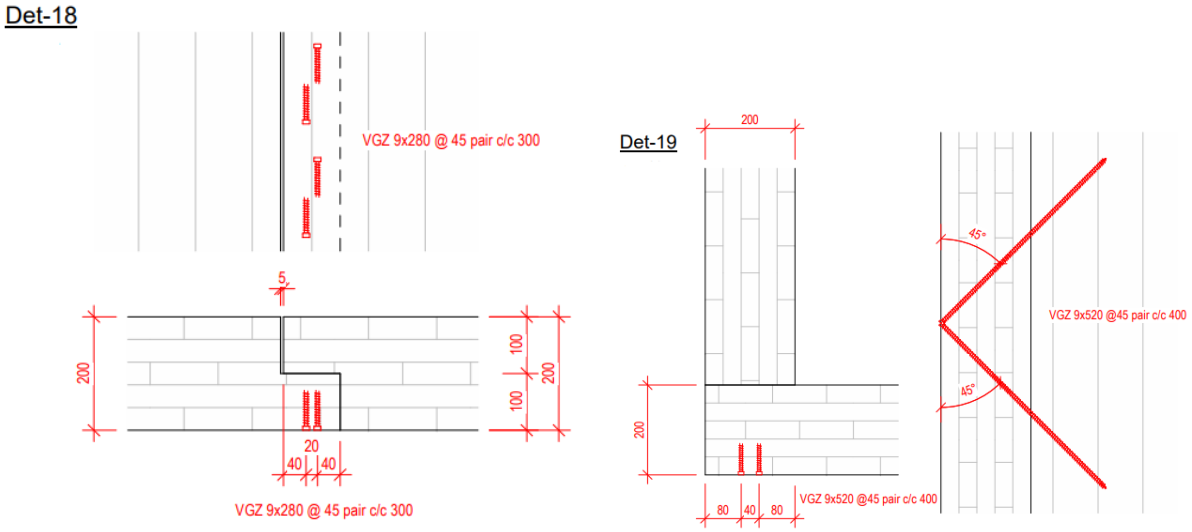

(a) Core connection half-lap joint

(b) Core connection corner joint

Figure C.6: Horizontal core connections Details 18 and 19 from the technical drawings (CLT-S NV 2024)

The core walls are connected to one another in horizontal direction by two types of connections, both use VGZ fasteners as seen in Figure C.6. These connections are modelled in RFEM by adding Line releases to one of the walls of the connection.

The connection of the CLT slab of the roof to the CLT walls of the core is modelled as a TBS8x280 fastener placed every 400 mm, see Figure C.7. The function Line hinge is used to model the connection and it is placed along the top of each wall that is connected to the roof directly.

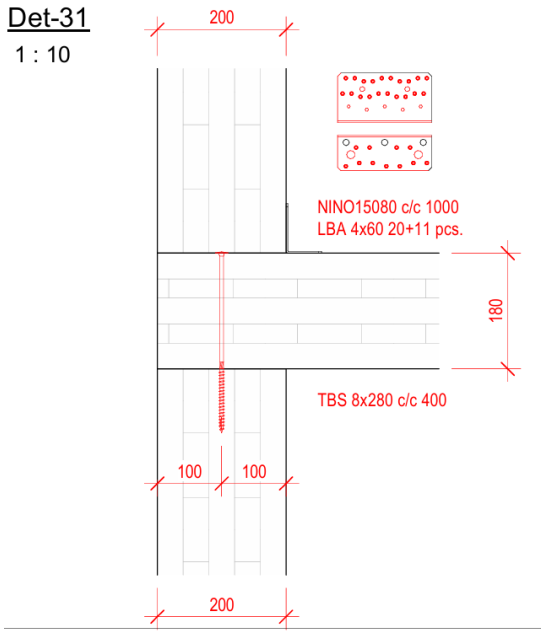

Figure C.7: Connection roof slab to core, Detail 31 from the technical drawings (CLT-S NV 2024)

The supports of the core are explained in Section A.2. The two different supports are modelled in two different ways. The big groups of dowels are modelled as a Nodal support with a stiffness in the vertical direction existing out of the stiffness of the dowels and the foundation, and it is given the Nonlinearity ”Failure if negative pz. This Nonlinearity means that the Nodal support fails if there is compression at the node, meaning it only takes up a tension force. The second type of supports are modelled as a Line support with a spring constant in the x- and z-directions. The stiffness in the x-direction is the lateral slip modulus of the dowels of the connection and the stiffness in the z-direction is a smeared stiffness of the foundation. For the z-direction the Nonlinearity ”Failure if positive pz” is given, meaning it fails under tension and only works under compression, the exact opposite of the Nodal support.

All stiffness values modelled in the core models are found in Table C.1. The sliding model only has Line hinges with the values for Cu,x and Cphi,x and not the value for Cu,y. The rocking model does have a value for Cu,y but not for Cu,x and the values for the hinges are added. The complete model has all values stated in the table.

Table C.1: RFEM input for the connections in the core

	Spring constant	Nonlinearity	Built up
Line hinge vertical connection			
Cu,x [kN/m^2]	88 719,50	None	TTP1200: Kser,2/3 / t
Cu,y [kN/m^2]	35 466,10	Fixed if negative vy	VGZ 7x260: Kser,1 / c/c
Cu,z [kN/m^2]	0,00	None	
Cphi,x [kNm rad^{-1} m^{-1}]	0,00	None	
Line hinge floor connection			
Cu,x [kN/m^2]	5 791,29	None	VGZ 7x260: Kser,4/5 / c/c
Cu,y [kN/m^2]	35 466,10	Fixed if negative vy	VGZ 7x260: Kser,1 / c/c
Cu,z [kN/m^2]	35 466,10	None	VGZ 7x260: Kser,1 / c/c
Cphi,x [kNm rad^{-1} m^{-1}]	0,00	None	
Line hinge roof connection			
Cu,x [kN/m^2]	2 637,31	None	TBS 8x280: Kser,1 / c/c
Cu,y [kN/m^2]	906,17	Fixed if negative vy	TBS 8x280: Kser,4/5 / c/c
Cu,z [kN/m^2]	2 637,31	None	TBS 8x280: Kser,2/3 / c/c
Cphi,x [kNm rad^{-1} m^{-1}]	0,00	None	
Hinge steel surface (WHTPT820)			
Cu,x [kN/m]	98 100,00	Fixed if negative N	WHTPT820: Kser,n
Cu,y [kN/m]	0,00	None	
Cu,z [kN/m]	–	None	
Cphi,x [kNm/rad]	–	None	
Cphi,y [kNm/rad]	0,00	None	
Cphi,z [kNm/rad]	0,00	None	
Line Release half-lap joint			
Cu,x [kN/m^2]	72 500,00	None	VGZ 9x280: Kser,1 / c/c
Cu,y [kN/m^2]	14 700,00	Fixed if negative vy	VGZ 9x280: Kser, 4/5 / c/c
Cu,z [kN/m^2]	72 500,00	None	VGZ 9x280: Kser,2/3 / c/c
Cphi,x [kNm rad^{-1} m^{-1}]	0,001	None	
Line Release corner joint			
Cu,x [kN/m^2]	77 480,00	None	VGZ 9x520: Kser,1 / c/c
Cu,y [kN/m^2]	77 480,00	Fixed if negative vy	VGZ 9x520: Kser, 2/3 / c/c
Cu,z [kN/m^2]	11 000,00	None	VGZ 9x520: Kser,4/5 / c/c
Cphi,x [kNm rad^{-1} m^{-1}]	0,001	None	
Nodal support			
Cu,x [kN/m]	0,00	None	
Cu,y [kN/m]	0,00	None	
Cu,z [kN/m]	316 973.00	Failure if negative pz	1/(1/Det3 + 1/Kfoundation)
Cphi,x [kNm/rad]	0,00	None	
Cphi,y [kNm/rad]	0,00	None	
Cphi,z [kNm/rad]	–	None	
Line support			
Cu,x [kN/m^2]	112 271.00	None	Det4 / c/c
Cu,y [kN/m^2]	0,00	None	
Cu,z [kN/m^2]	304 639.00	Failure if positive pz	# Nodal supports * Kfoundation / Total length

Continued on next page

Table C.1 (continued)

	Spring constant	Nonlinearity	Built up
Cphi,x [kNm rad^{-1} m^{-1}]	0,00	None	
Cphi,y [kNm rad^{-1} m^{-1}]	0,00	None	
Cphi,z [kNm rad^{-1} m^{-1}]	–	None	

-t in column “Built up” is thickness of the wall is 200 (mm)
-c/c is the center to center value of that connection

C.3. Urban Woods model

The complete model of the Urban Woods building in Delft combines the models of the facades and core into one and adds the floor system and 10th storey.

C.3.1. Floor system

The general layout of the floor system is illustrated in figure C.8. There are six types of connections modeled in RFEM for the floor slabs, as illustrated in figure C.9. The stiffness values for each connection are listed in table C.2, the built up of each spring constant exists out of a value from table A.2 divided by the center-to-center distance of that type of connection.

- Floor to floor with pairs of VGZ 7x220 (Detail 23)
- Floor to floor with WHPT300
- Floor on top of a beam with a TBS 8x280 (Detail 22)
- Floor on top of a beam at the facade with a TBS 8x280 (Detail 25)
- Floor to floor on top of a beam with WHPT300 and TBS 8x280 (Detail 21)
- Floor to core with VGZ 7x260 (Detail 16)

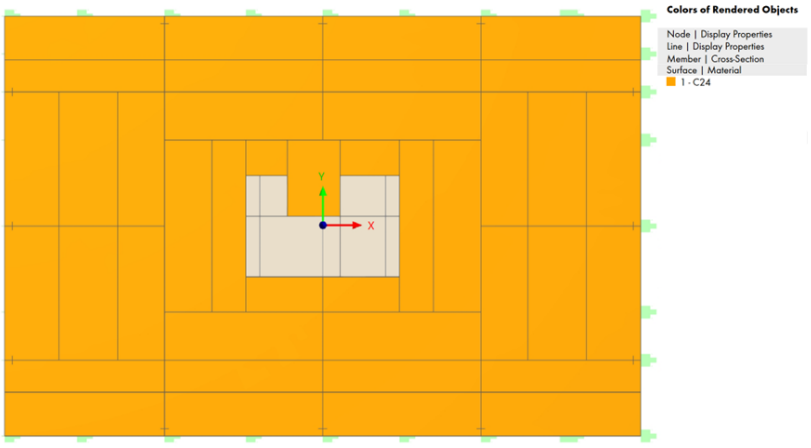

Figure C.8: General layout CLT floor slabs and core

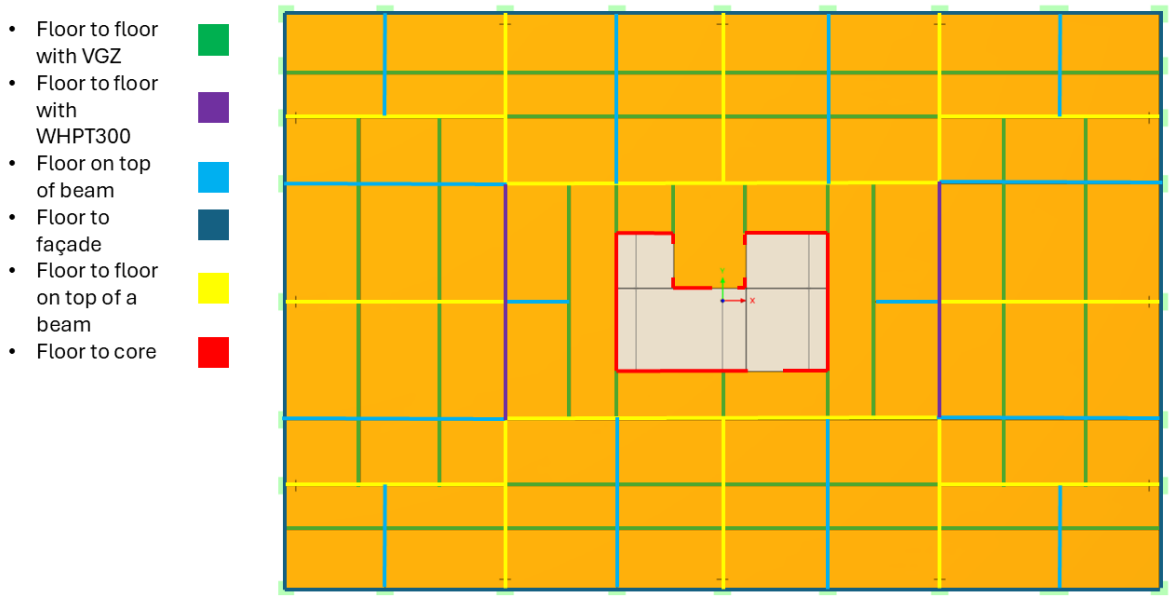

Figure C.9: General layout connections of the floor slabs

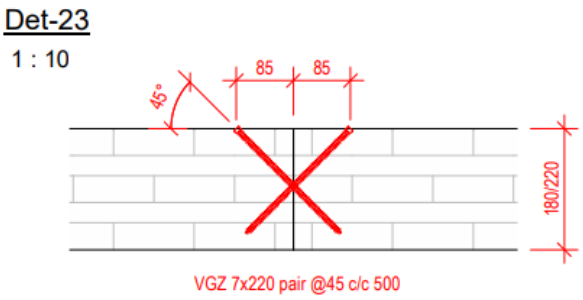

(a) Top (full-width) panel

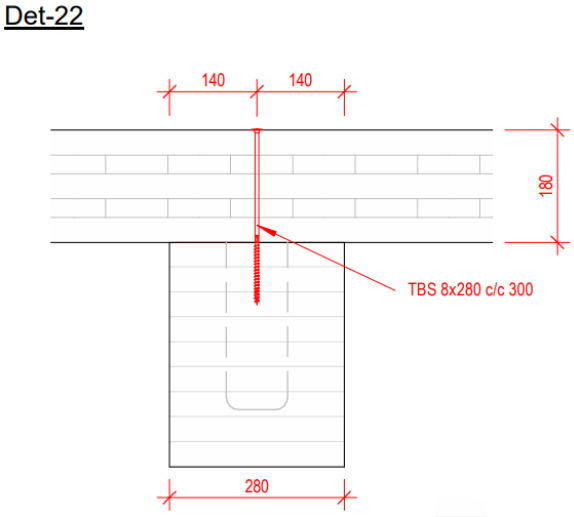

(b) Floor on top a a beam with TBS 8x280 (Detail 22)

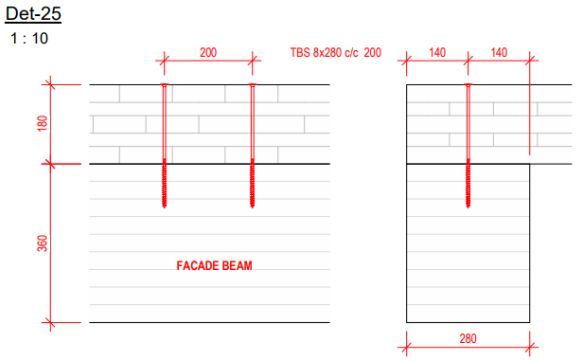

(c) Floor on top of a beam at the facade with TBS 8x280 (Detail 25)

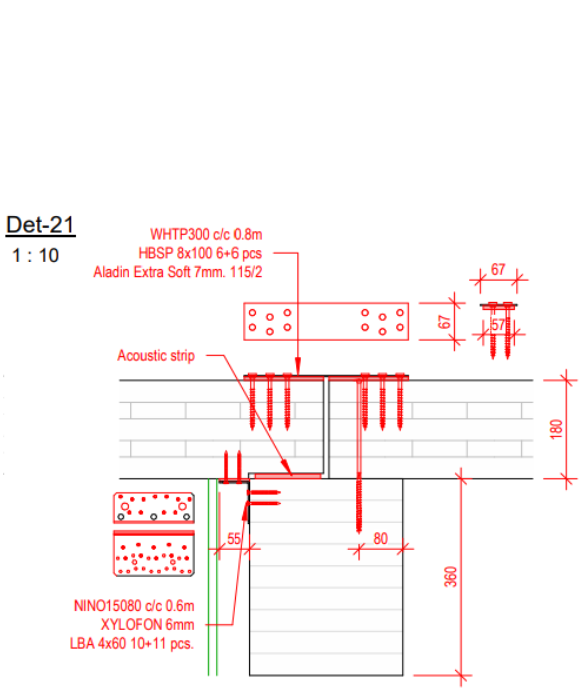

(d) Floor to floor on top of a beam with WHPT300 and TBS 8x280 (Detail 21)

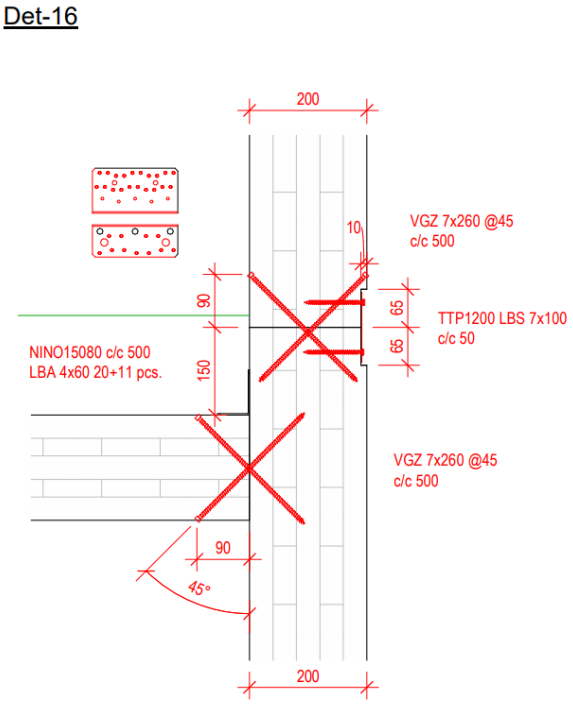

(e) Floor to core with VGZ 7x260 (Detail 16)

Figure C.10: Technical drawings of the connections used with the CLT floor slabs

Table C.2: RFEM input for the connections of the floor slabs

	Spring constant	Nonlinearity	Built up
Line Hinge floor to floor (VGZ)			
Cu,x [kN/m^2]	5 791,29	None	VGZ 7x220: Kser,4/5 / 0,5 [m]
Cu,y [kN/m^2]	32 075,10	Fixed if negative vy	VGZ 7x220: Kser,1 / 0,5 [m]
Cu,z [kN/m^2]	32 075,10	None	VGZ 7x220: Kser,2/3 / 0,5 [m]
Cphi,x [kNm rad^{-1} m^{-1}]	0,00	None	
Line Release floor to floor (WHPT300)			
Cu,x [kN/m^2]	8 907,47	None	WHPT300: Kser,2/3 / 0,8 [m]
Cu,y [kN/m^2]	9 083,31	Fixed if negative vy	WHPT300: Kser,1 / 0,8 [m]
Cu,z [kN/m^2]	0,00	None	
Cphi,x [kNm rad^{-1} m^{-1}]	0,00	None	
Line Release floor on top of a beam			
Cu,x [kN/m^2]	3 516,41	None	TBS 8x280: Kser,1 / 0,3 [m]
Cu,y [kN/m^2]	–	None	
Cu,z [kN/m^2]	–	None	
Cphi,x [kNm rad^{-1} m^{-1}]	–	None	
Line Release floor on top of a beam at the façade			
Cu,x [kN/m^2]	5 274,61	None	TBS 8x280: Kser,1 / 0,2 [m]
Cu,y [kN/m^2]	5 274,61	None	TBS 8x280: Kser,2/3 / 0,2 [m]
Cu,z [kN/m^2]	0,00	None	
Cphi,x [kNm rad^{-1} m^{-1}]	0,00	None	
Line Release floor to floor on top of a beam			
Cu,x [kN/m^2]	3 516,41	None	TBS 8x280: Kser,1 / 0,3 [m]
Cu,y [kN/m^2]	9 083,31	Fixed if negative vy	WHPT300: Kser,1 / 0,8 [m]
Cu,z [kN/m^2]	–	None	
Cphi,x [kNm rad^{-1} m^{-1}]	0,001	None	
Line Hinge floor to core			
Cu,x [kN/m^2]	5 791,29	None	VGZ 7x260: Kser,4/5 / 0,5 [m]
Cu,y [kN/m^2]	35 466,10	Fixed if negative vy	VGZ 7x260: Kser,1 / 0,5 [m]
Cu,z [kN/m^2]	35 466,10	None	VGZ 7x260: Kser,2/3 / 0,5 [m]
Cphi,x [kNm rad^{-1} m^{-1}]	0,00	None	

C.3.2. 10th storey

The third to the ninth floors have identical layouts, with only the differences being the location of the diagonals. The second floor has a slight difference with parts of the floor panels removed to open space with the ground floor. However, more changes are seen for the 10th storey. Firstly, the plan dimensions of the roof are decreased, causing the penthouse to have a balcony running all the way around the building. Secondly, this results in the diagonals in the facades stopping at the ninth floor. Thirdly, the layout of the CLT floor slabs of both the floor of the 10th storey (roof of the 9th) and the roof are different. Lastly, different connections are used to connect the beams in the roof to columns.

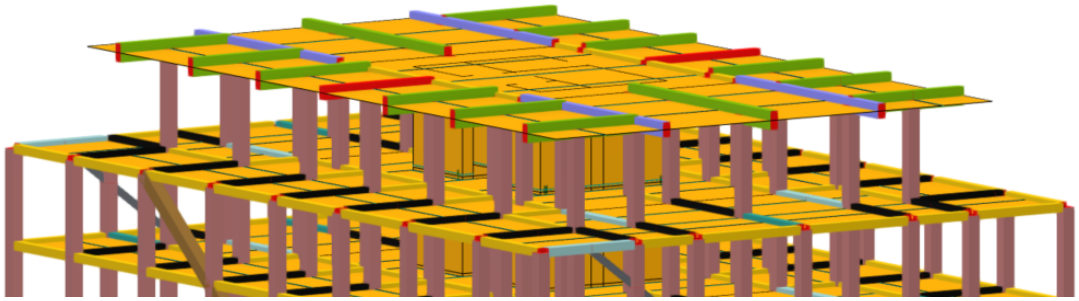

Figure C.11: Structure of the 10th storey

The first three changes can be implemented directly as already used parts are reused but at a different location (for example with the connections of the slabs). However, the last difference introduces a new connection. A version of this type of connection is shown in the technical drawing of figure C.12. The fasteners to focus on here are the four VGS 13x600 fasteners. These fasteners are placed there to prevent the beams and roof being pulled off due to wind load, meaning they take up tension. The stiffness is determined by calculating the axial withdrawal resistances of the two threaded parts, then adding the axial resistance of pull-out by the head of the screw to the withdrawal resistance of the part in the beam. Finally, the stiffness of the part in the beam is added to the part in the column as a series of springs, as described in equations 3.4. This results in a value of 32.54 [kN/mm] for the axial stiffness of one fastener. Per connection 4 fasteners are used, totaling the stiffness to a value of 130.17 [kN/mm]. This stiffness is only activated in case of tension between the beam and the column. In case of compression the load goes directly from timber to timber.

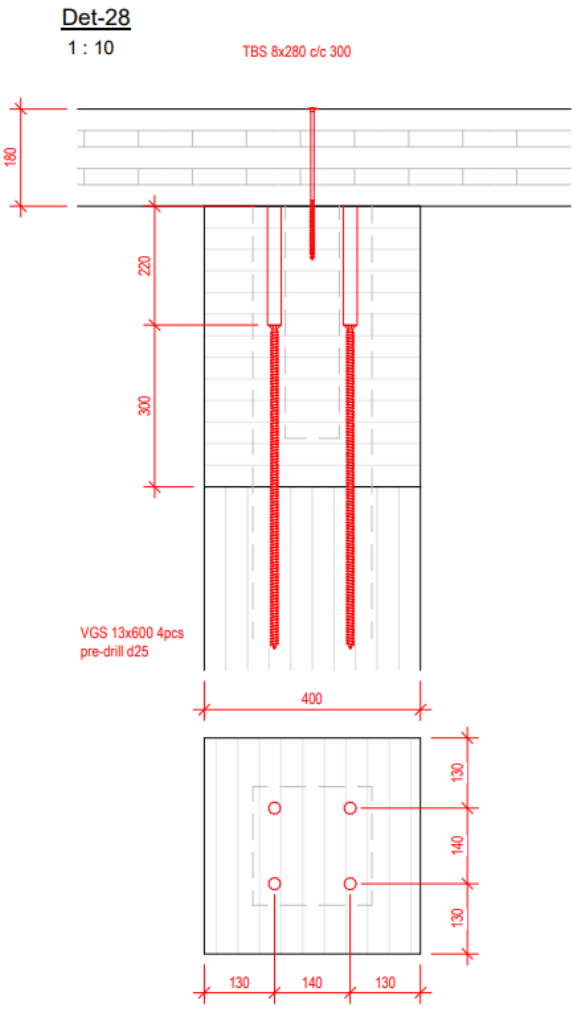

Figure C.12: Connection at the top of the columns of the 10th storey

C.4. Additional results

In this section extra results obtained from the numerical models are presented. These results are similar to those presented in Chapter 5, but for different wind directions.

C.4.1. Deformed shapes

C.4.2. Influence of connection stiffness

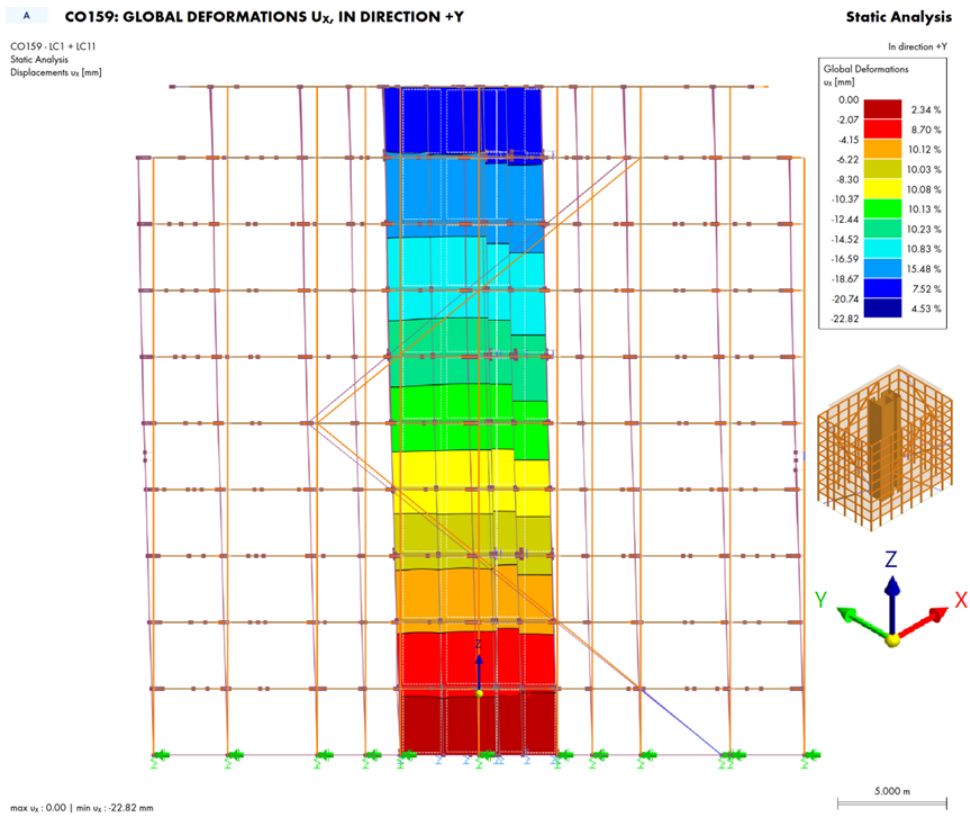

Figure C.13: Side view of the displacement due to wind load X- and self weight, deformation shape scaled by 40

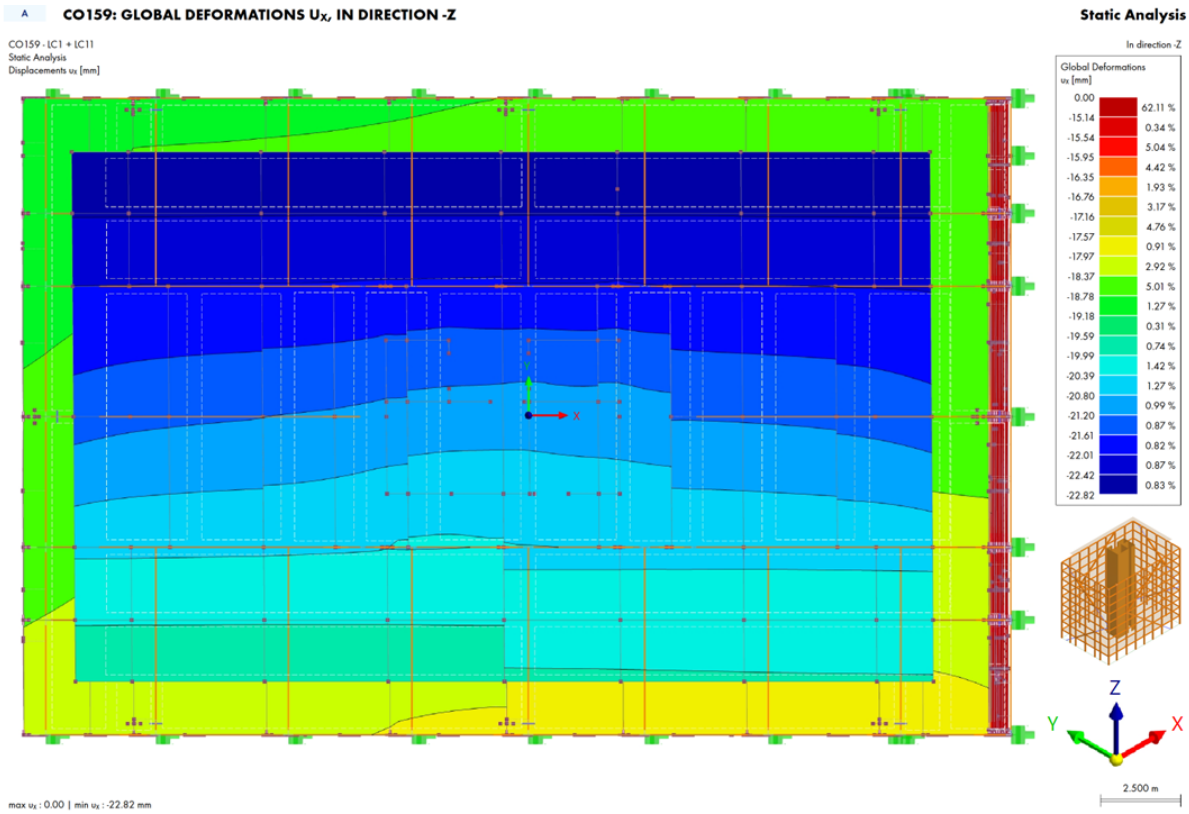

Figure C.14: Top view of the displacement due to wind load X- and self weight, deformation shape scaled by 40

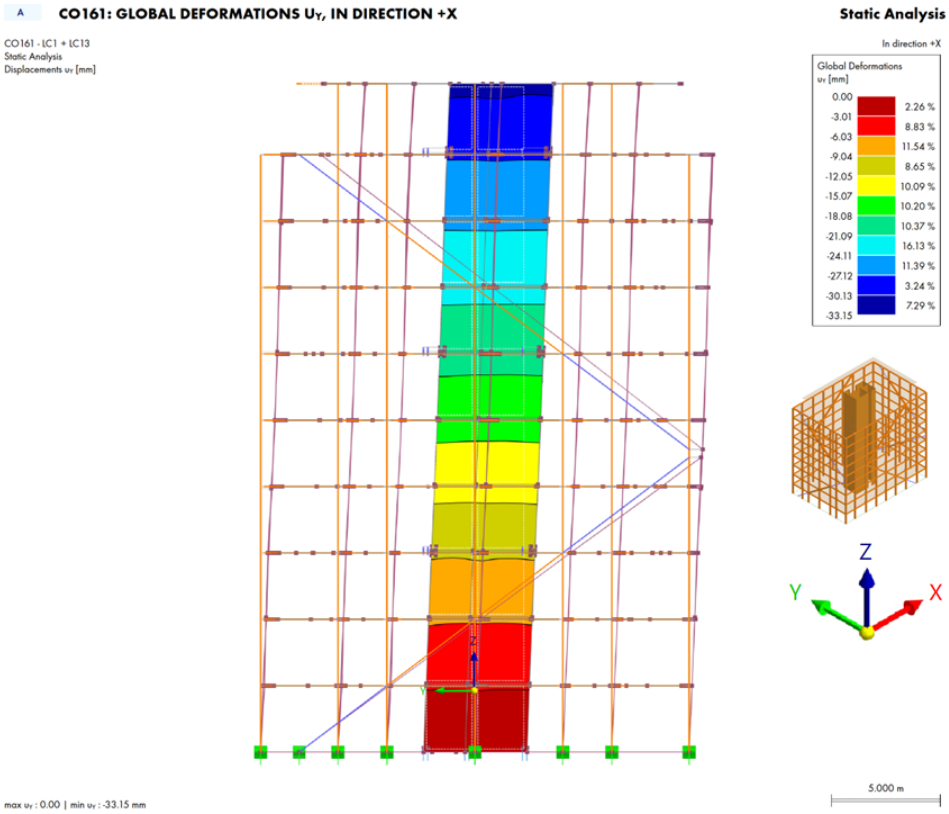

Figure C.15: Side view of the displacement due to wind load Y- and self weight, deformation shape scaled by 40

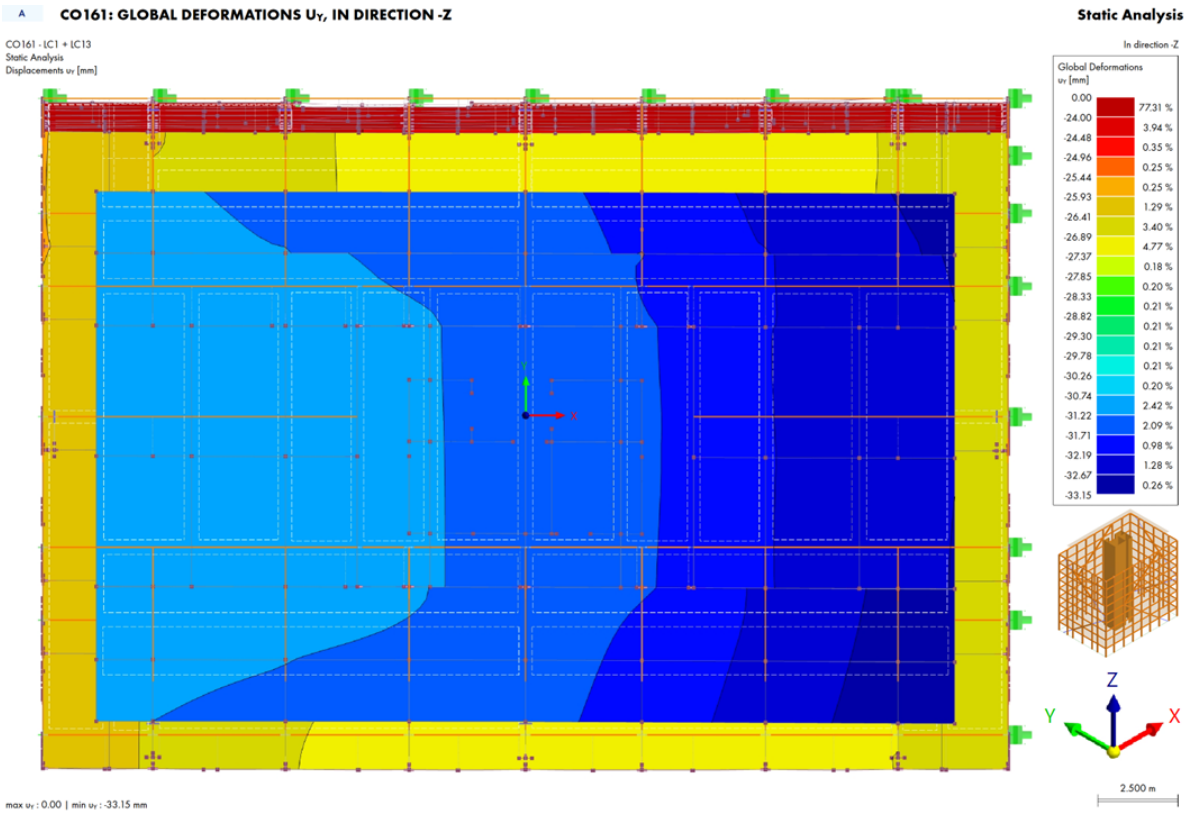

Figure C.16: Top view of the displacement due to wind load Y- and self weight, deformation shape scaled by 40

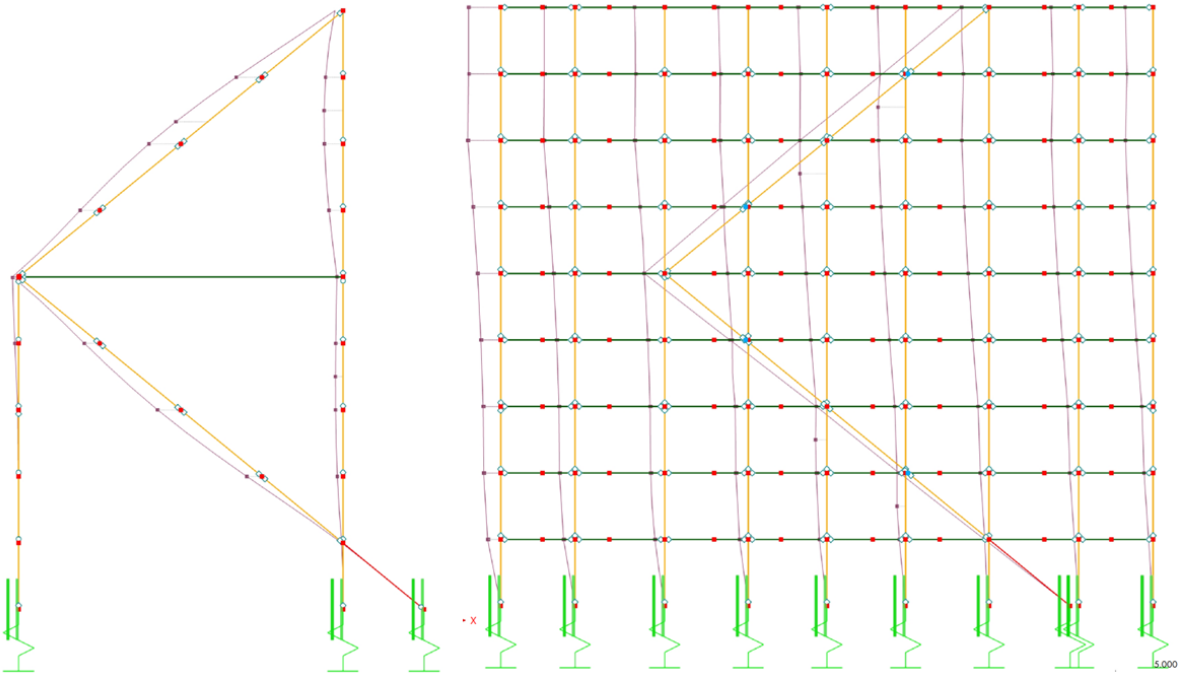

Figure C.17: Horizontally deformed shapes of the RFEM VW model (left) and the RFEM 2D model (right) of the wide facade loaded by the self weight and the wind in direction X-

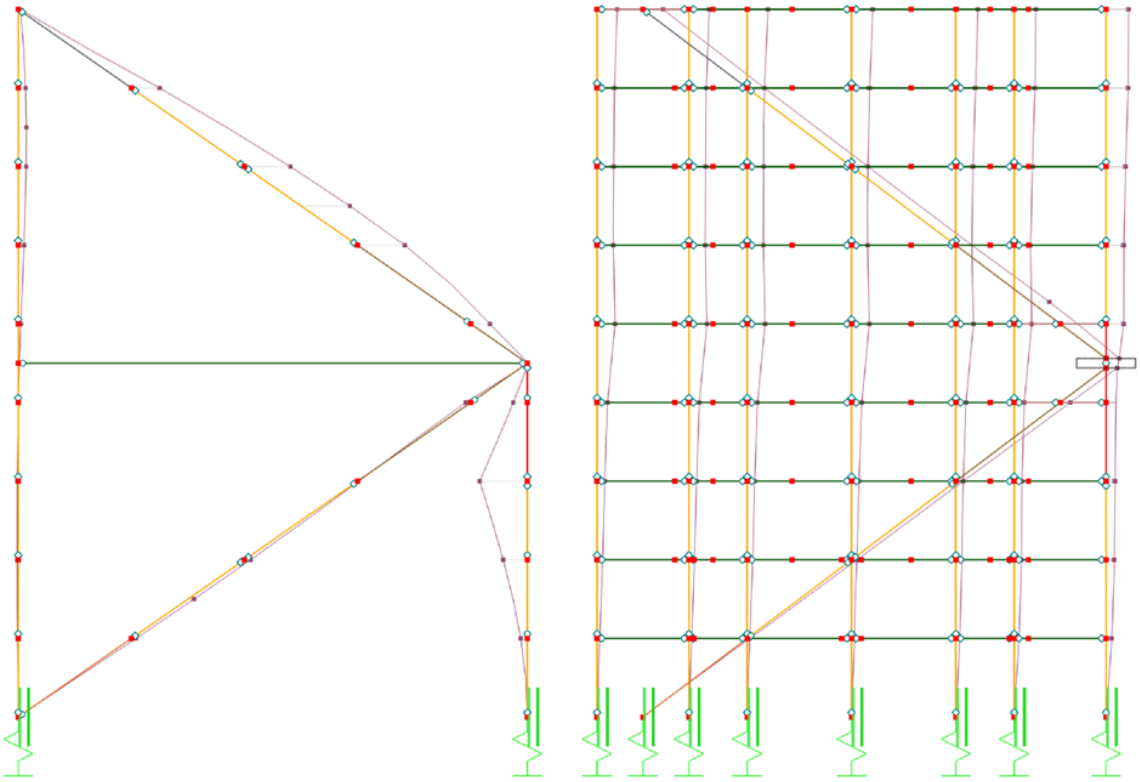

Figure C.18: Horizontally deformed shapes of the RFEM VW model (left) and the RFEM 2D model (right) of the narrow facade loaded by the self weight and the wind in direction Y-

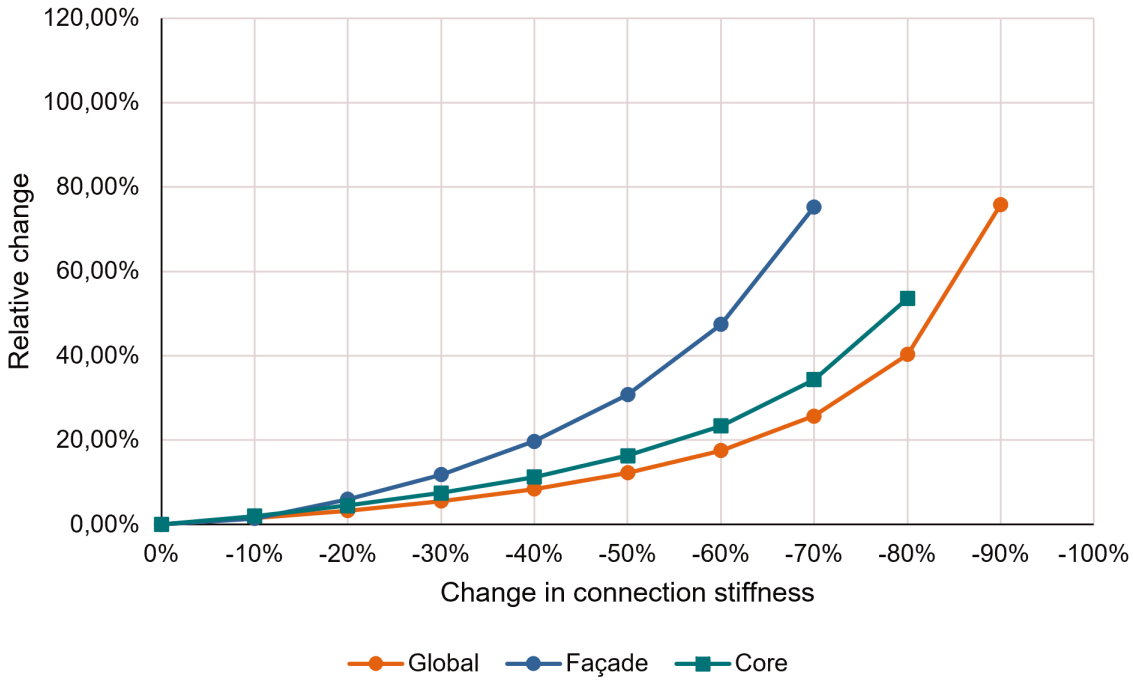

Figure C.19: Relative increase of the maximum horizontal deflection of the 9th storey for the lateral load resisting systems, while subjected to the self weight and the wind load in X- direction

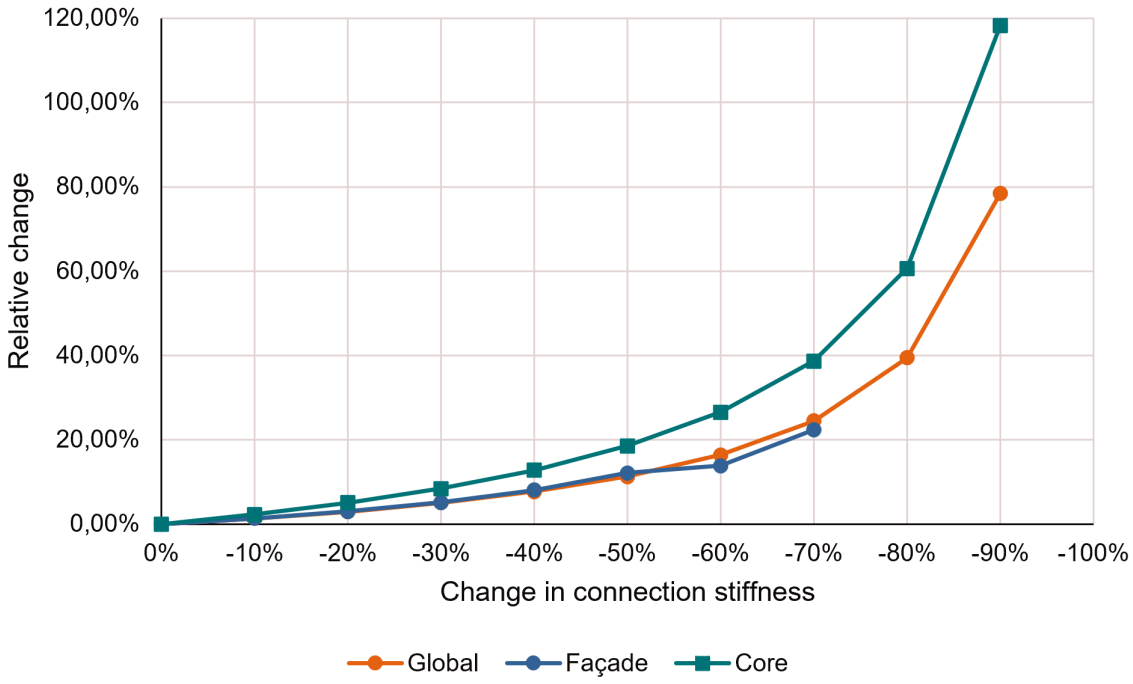

Figure C.20: Relative increase of the maximum horizontal deflection of the 9th storey for the lateral load resisting systems, while subjected to the self weight and the wind load in Y+ direction

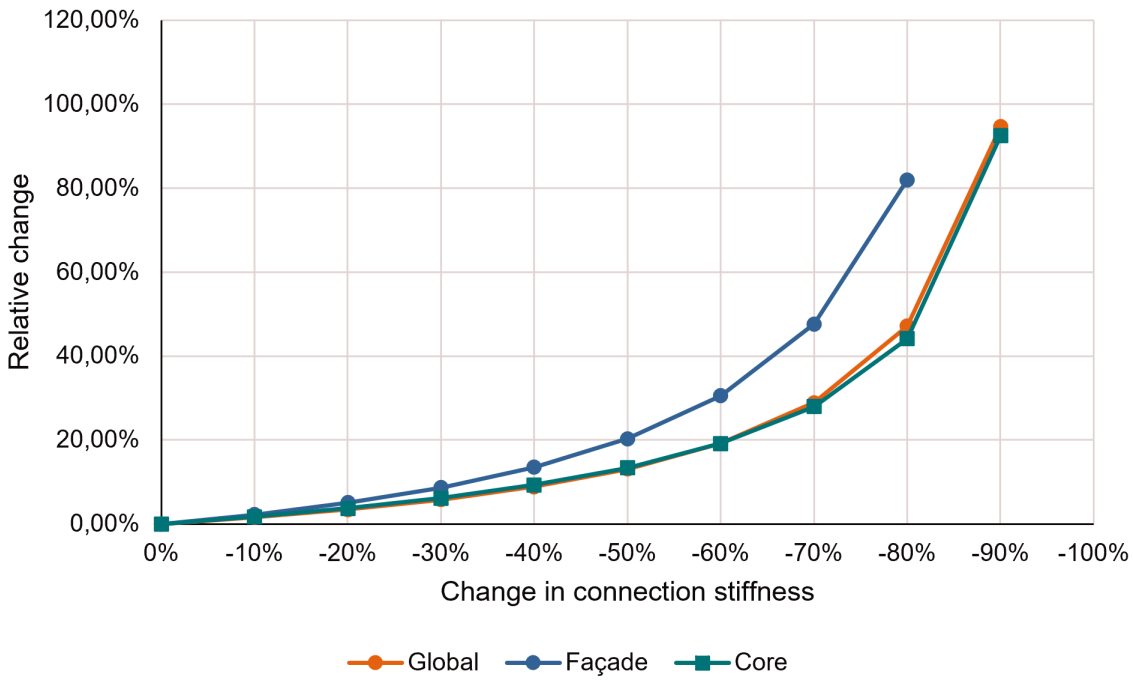

Figure C.21: Relative increase of the maximum horizontal deflection of the 9th storey for the lateral load resisting systems, while subjected to the self weight and the wind load in Y- direction

D

Load cases and combinations

The load cases used in the models are self weight and wind, they are combined according to SLS standards with a factor of 1.0. This Appendix shows detailed information about how these load cases are applied and combined in the models.

D.1. Wind load

The calculations for the wind load are done according to Eurocodes NEN-EN 1991-1-4 Eurocode 1: Actions on structures - Part 1-4: General actions - Wind actions, and the Dutch National Annex: NEN-EN 1991-1-4+A1+C2:2011/NB:2019+C2:2023.

D.1.1. Peak velocity pressure

The result of the appendix is value for the wind pressure per zone of the building for two wind directions. To get there the peak velocity pressure needs to be calculated for the reference heights.

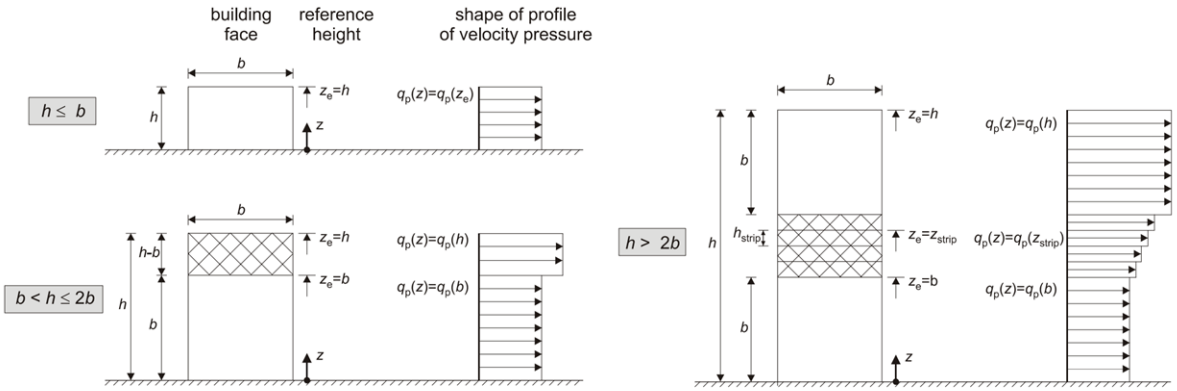

Figure D.1: Reference height, z_e, depending on h and b, and corresponding velocity pressure profile

The Urban Woods building has a narrow face (façade X) and a wide face (façade Y). For the wide façade the h ≤ b, resulting in one peak velocity pressure according to Figure D.1. However, the narrow facade has b < h ≤ 2b, meaning a peak velocity pressure needs to be calculated for reference height h and b. In the upcoming calculations if there is an influence of the reference height the first value corresponds to a reference height of 31.85 m (h) and the second to a reference height of 20.06 m (b). The terrain category is II.

$$k_r = 0,19 \cdot \left(\frac{z_0}{z_{0,II}} \right)^{0,07} \tag{D.1}$$

- z_0 = roughness length = 0,2 m
- $z_{0,II}$ = 0,05 m
- k_r = terrain factor = 0,21

$$c_r(z_e) = k_r \cdot \ln \left(\frac{z_e}{z_0} \right) \tag{D.2}$$

- z_e = height of the structure = 31.85 or 20.06 m
- z_0 = roughness length as described in D.1
- $c_r(z)$ = roughness factor = 1,06 or 0,96

$$v_b = c_{dir} \cdot c_{season} \cdot v_{b,0} \tag{D.3}$$

- c_{dir} = directional factor: Dutch National Annex states c_{dir} = 1,0
- c_{season} = season factor: Dutch National Annex states c_{season} = 1,0
- $v_{b,0}$ = fundamental wind velocity: Dutch National Annex states $v_{b,0}$ = 27 m/s for category II
- v_b = basic wind velocity = 27 m/s

$$v_m(z_e) = c_r(z_e) \cdot c_o(z) \cdot v_b \tag{D.4}$$

- $c_r(z_e)$ = roughness factor as described in D.2
- c_o = orography factor : Dutch National Annex states c_o = 1,0
- v_b = basic wind velocity as described in D.3
- $v_m(z_e)$ = mean wind velocity = 28,66 or 26.05 m/s

$$I_v(z_e) = \frac{k_l}{c_o(z) \cdot \ln(z_e/z_0)} \tag{D.5}$$

- k_l = turbulence factor: Dutch National Annex states k_l = 1,0
- c_o = orography factor as described in D.4
- z_e = reference height = 31.85 or 20.06 m
- z_0 = roughness length as described in D.1
- $I_v(z_e)$ = turbulence intensity = 0.20 or 0.22

$$q_p(z_e) = [1 + 7 \cdot I_v(z_e)] \cdot \frac{1}{2} \cdot \rho \cdot v_m^2(z_e) \tag{D.6}$$

- $I_v(z)$ = turbulence intensity as described in D.5
- ρ = air density: Dutch National Annex states ρ = 1,25 kg/m^3
- $v_m(z)$ = mean wind velocity as described in D.4
- $q_p(z_e)$ = peak velocity pressure = 1222,3 or 1068.30 N/m^2

D.1.2. Wind pressure per zone

Using the peak velocity pressure, the wind pressure per zone can be calculated for the two wind directions.

$$w_e(z_e) = q_p(z_e) \cdot c_{pe} \tag{D.7}$$

- $q_p(z_e)$ = peak velocity pressure as described in D.6
- c_{pe} = external pressure coefficient
- w_e = wind pressure on external surface kN/m^2

The values for the external pressure coefficient depend on the zone of the building, these zones are described in Figure D.2. Their values and the following results are visible in Tables D.2 and D.3. The values for q in the tables are obtained by multiplying the values for the external wind pressure (w_e) with the height of one floor (3.04 m).

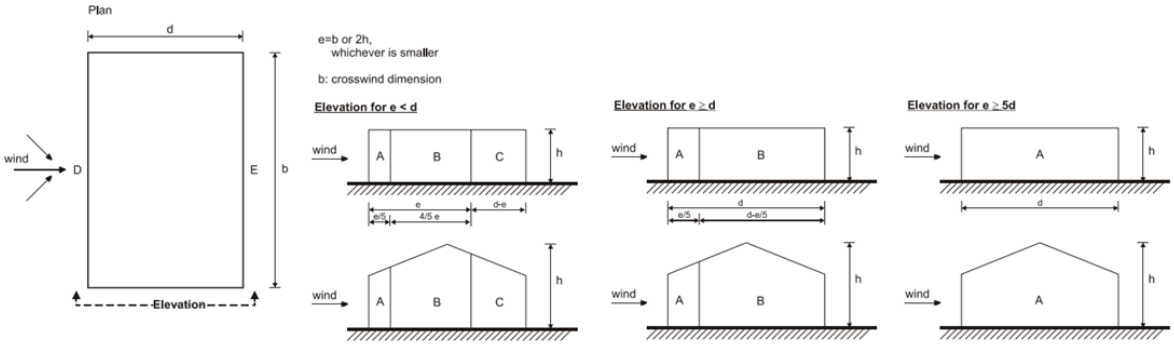

Figure D.2: Wind zones

Geometry	Wide face	Narrow face
d [m]	20.06	30.24
b [m]	30.24	20.06
h [m]	31.85	31.85
e [m]	30.24	20.06
	$e > d$	$e < d$
h/d	1.59	1.05

Table D.1: Geometric data for the wind load in two directions

Zone	$c_{pe,10}$	w_e [kN/m^2]	q [kN/m]	Comments
A	-1.20	-1.47	-4.46	Length of Zone A = 6.05 m
B	-0.80	-0.98	-2.97	Length of Zone B = 14.01 m
C				
D	0.80	0.98	2.97	Full height, one zone
D'				
E	-0.53	-0.65	-1.97	

Table D.2: Wind loads per zone for the wide face of the building

Tables D.2 and D.3 present the wind loads per zone with the values in the column q being used in the main model on each floor. For the roof and the ground floor the values are halved due to the distribution of the wind loads on the façades. For the roof an additional wind load is added to represent the fence on the roof and other parts, such as a roof garden with small trees. It was decided to model the additional load as a fence of 1.5 m high. Resulting in new wind loads that use the same wind pressures as the other loads. For the wind loads in the direction of the wind in normal circumstances, such as the tables

Zone	$c_{pe,10}$	w_e [kN/m^2]	q [kN/m]	Comments
A	-1.20	-1.47	-4.46	Length of Zone A = 4.01 m
B	-0.80	-0.98	-2.97	Length of Zone B = 16.05 m
C	-0.50	-0.61	-1.86	Length of Zone C = 10.18 m
D	0.80	0.98	2.97	Starts from h = 20.06 up to h = 31.85
D'	0.80	0.85	2.60	Starts from h = 0 up to h = 20.06
E	-0.50	-0.61	-1.87	

Table D.3: Wind loads per zone for the narrow face of the building

above, one wall (zone D) is being pushed and the wall on the other side (zone E) is being pulled by the wind. In case of a fence it experiences both zone E and D at the same time. Therefore the q-load is calculated by adding the wind pressures for the two zones and multiplying it by 1.5 m. This results in the values listed in table D.4.

Table D.4: Additional q-load on roof due to 1.5 m high fence [$\mathrm{kN/m^2}$]

Zone	Wide face	Narrow face
D+E	2.44	2.39
A	-2.20	-2.20
B	-1.47	-1.47
C		-0.92

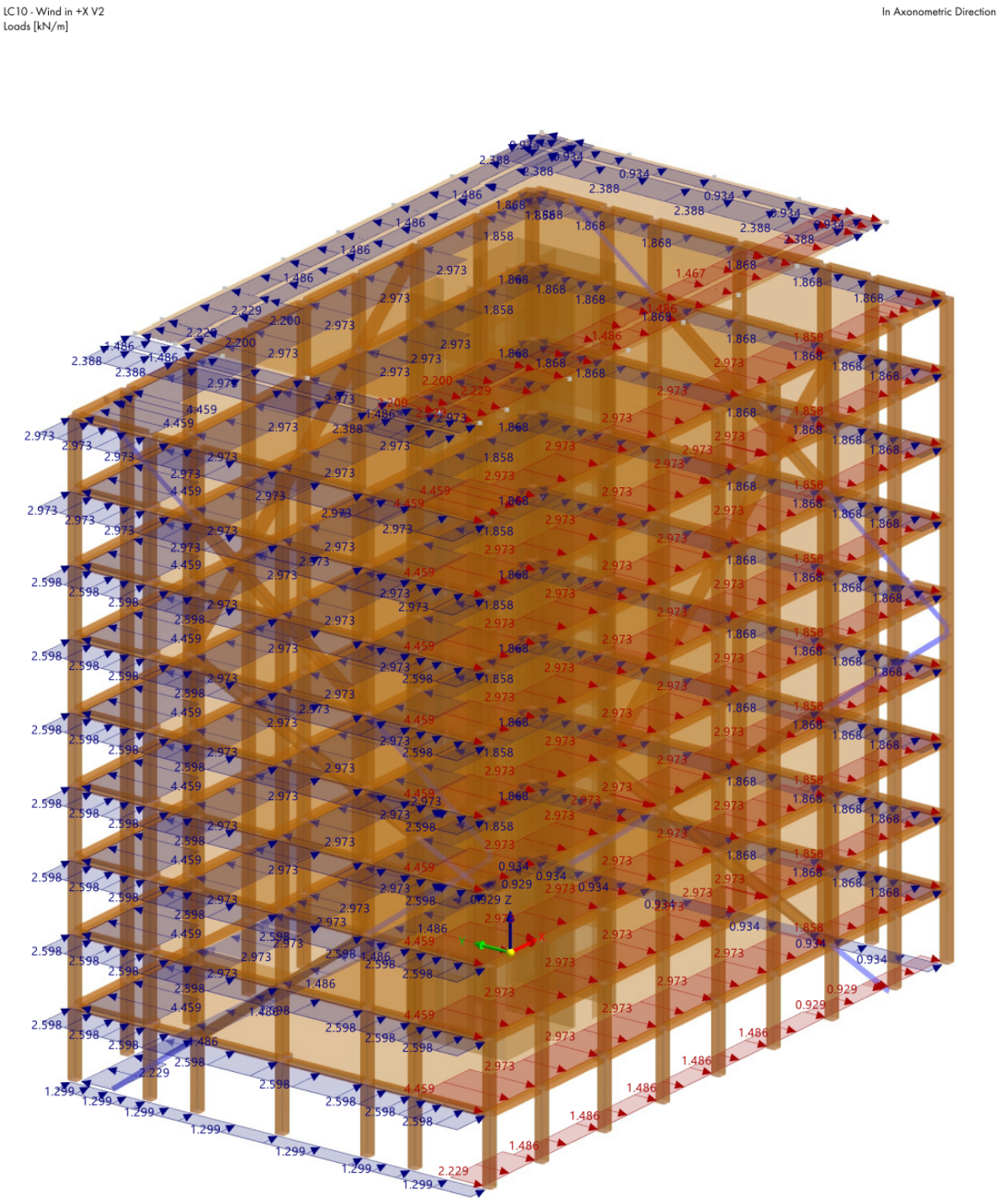

Figure D.3: Wind loads in the +X direction [kN/m]

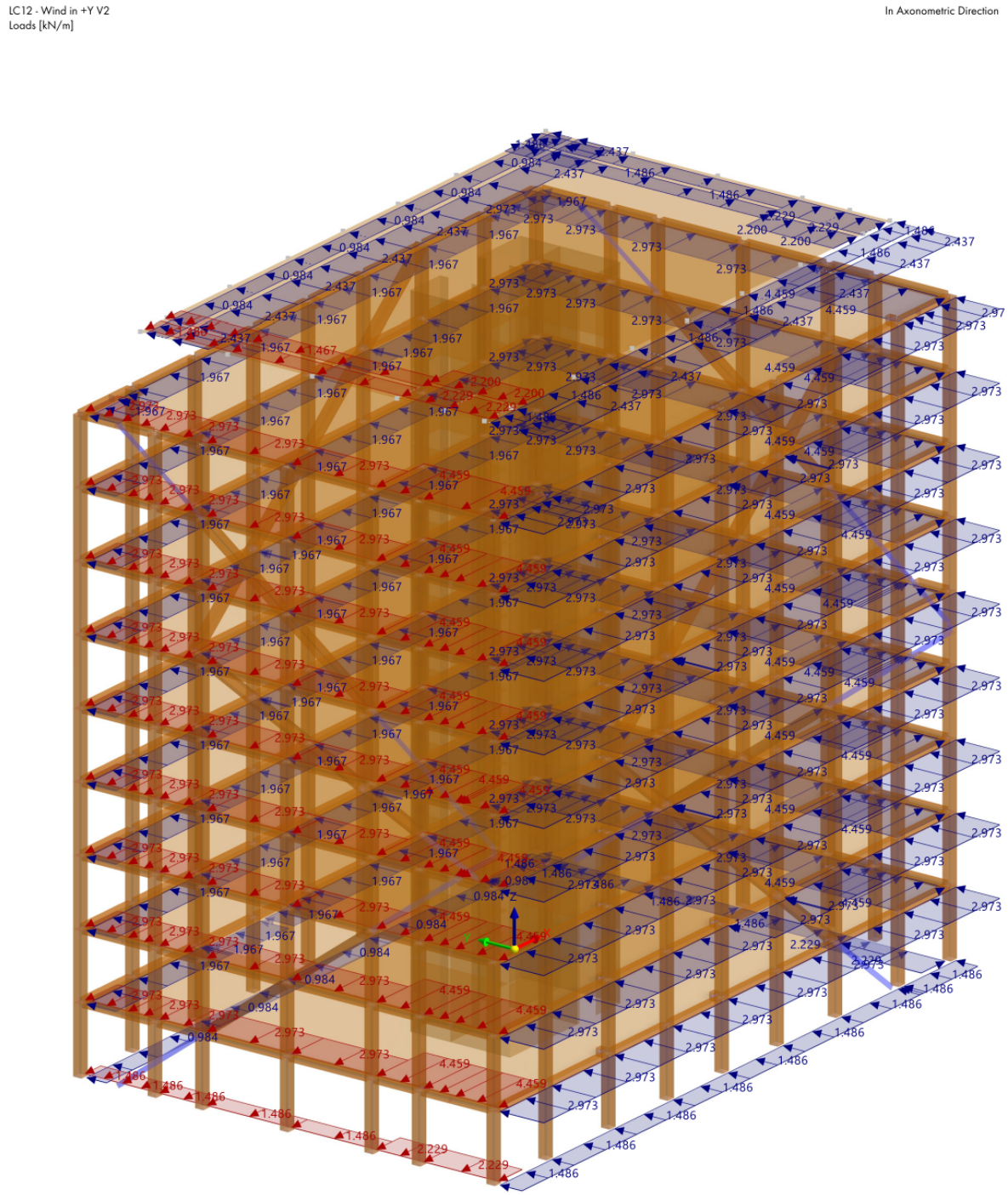

Figure D.4: Wind loads in the +X direction [kN/m]

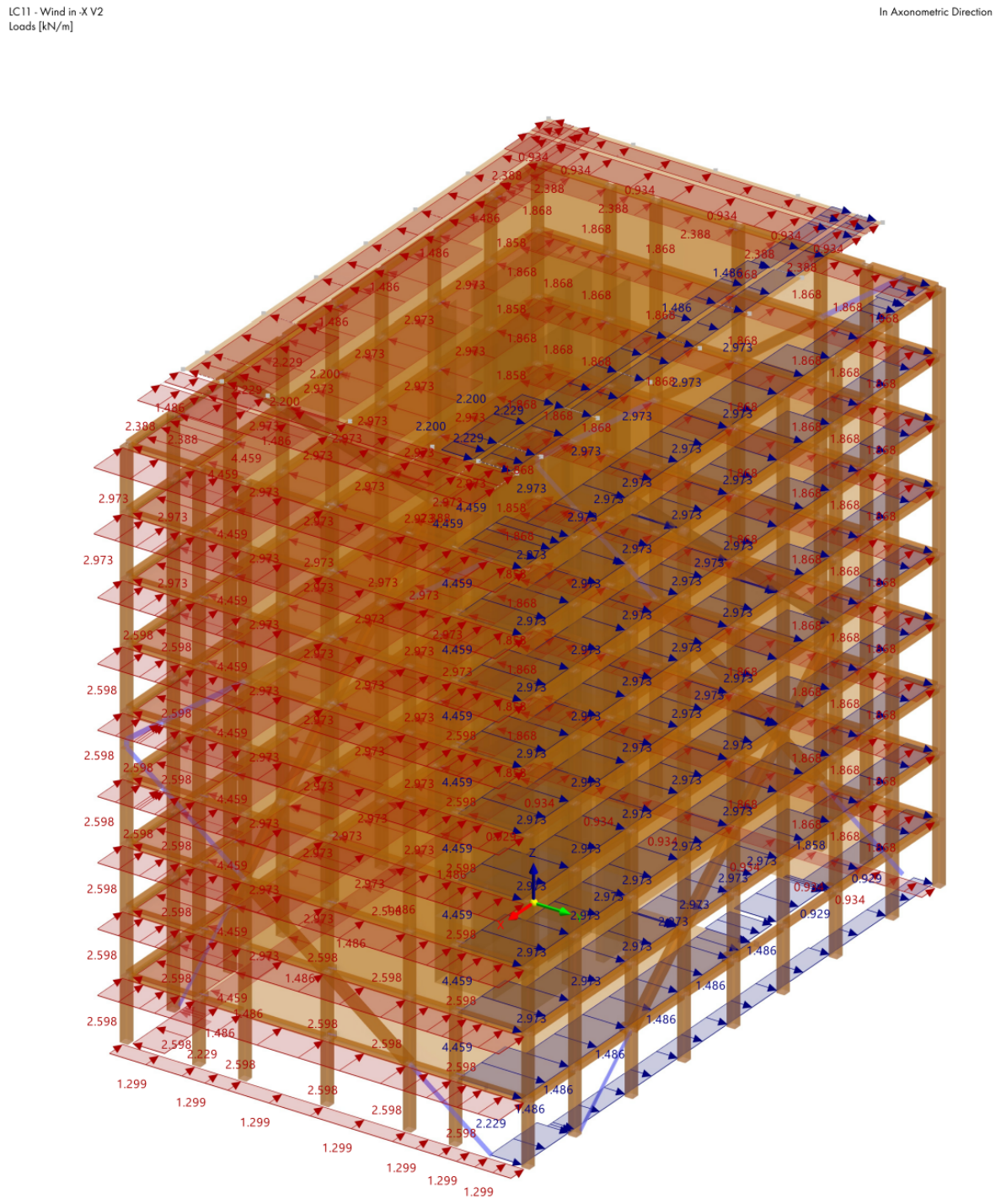

Figure D.5: Wind loads in the +X direction [kN/m]

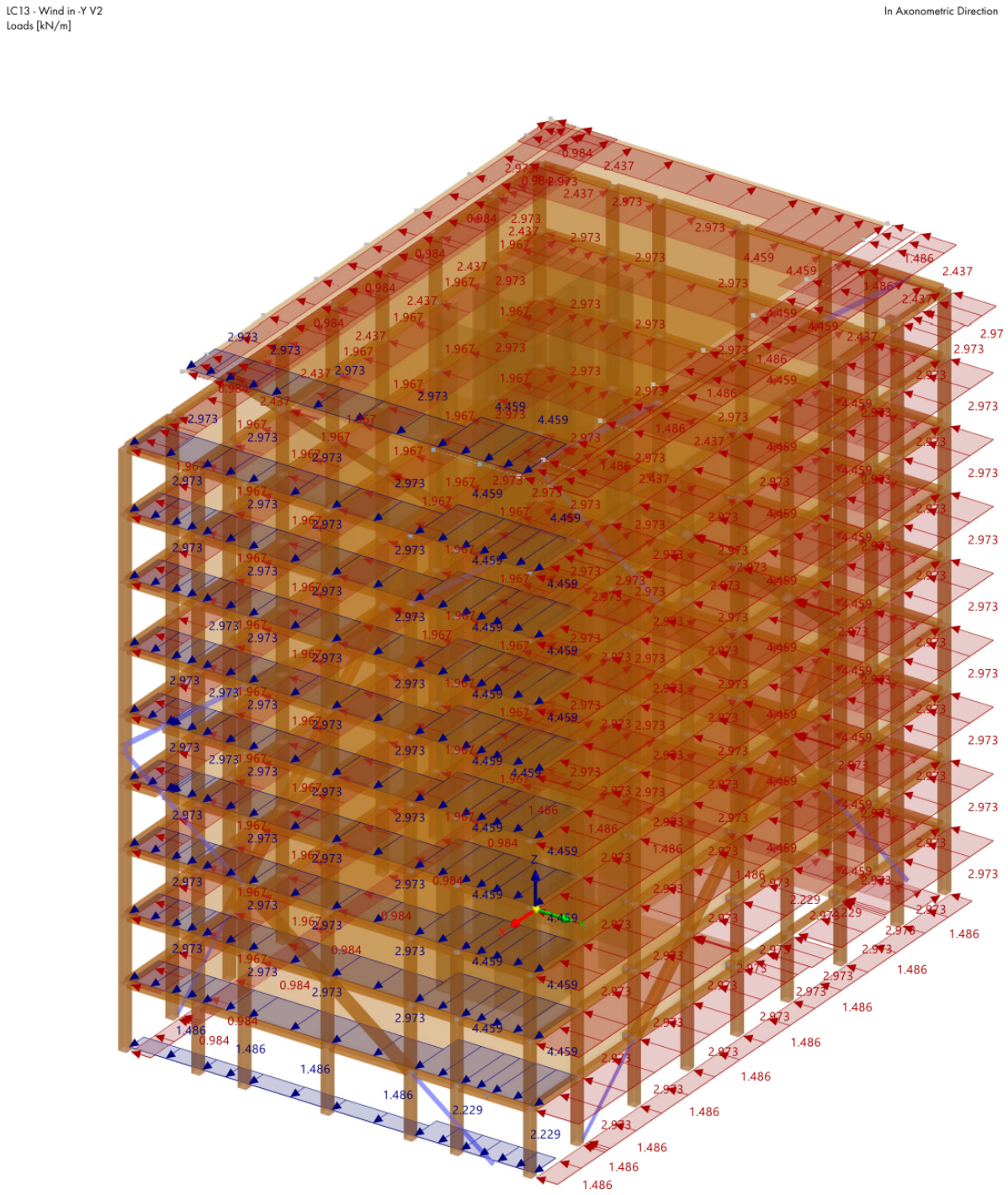

Figure D.6: Wind loads in the +X direction [kN/m]

D.1.3. Wind load 2D and core models

The Tables D.2 and D.3 give the values for the wind loads in the model for the whole building, to get the values for the other models (façades and core) further calculation is needed, which is illustrated in Figure D.7. The illustration is a top view on how the wind load (q_w) is applied on one level of the façade. This q-load is multiplied by the width of the façade and the percentage of what each part takes up. The building was designed with the idea that for the wide face 25% goes to the core and for the narrow face 35%. Meaning each narrow façade (Façade X) takes up 37.5% and wide façade (Façade Y) 32.5% of the wind pressure on the façade perpendicular to theirs. In the model of the core the structure is subjected to a distributed load instead of a point load for the façades. The calculation process is similar with the addition that the whole value needs to be divided by the effective width of the core for that direction. Not just the width of the core, but the effective width. This is because of the openings in the core on which no load can be applied. The effective width (b_{eff}) is 4.74 m for the narrow side and 6.15 or 7.2 m for the wide side, depending on which wide side the load is applied on.

Zone	X-façade [kN]	Y-façade [kN]	Core, Y-direction [kN/m]	Core, X-direction [kN/m]
D	33.71	19.38	3.65 or 3.12	4.40
D'		16.94		3.85
E	-22.31	-12.18	-2.07 or -2.42	-2.77

Note: Core, Y-direction values differ depending on the effective width of the core (b_{eff}).

Table D.5: Wind loads for models of the facades and core

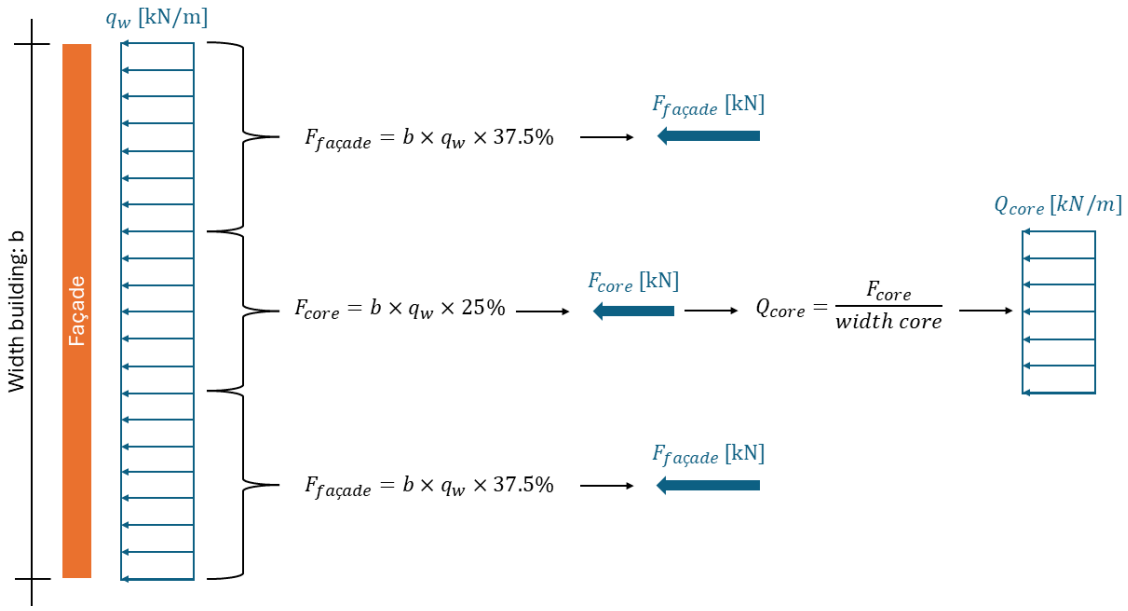

Figure D.7: Illustration on how the wind load on the 2D and core models is based on the load on the global model (Top view)

The roof of the core is however subjected to a significantly higher load, due to two aspects. First the load on the roof of the global model is also higher, due to objects placed on the roof, therefore, the load on the core will be higher. But the more important aspect is, is that the wind bracing system in the façades don't resist the loads applied on the roof, as they are not connected. Therefore, the horizontal wind load on the roof is only laterally supported by the core. The loads for the roof of the core model are listed in Table D.6

Zone	X+ [kN]	X- [kN]	Y+ [kN]	Y- [kN]
D	13.37	13.37	16.93	14.46
E	11.47	11.47	12.61	14.76

Table D.6: Wind loads for the roof of the core model per zone and wind direction

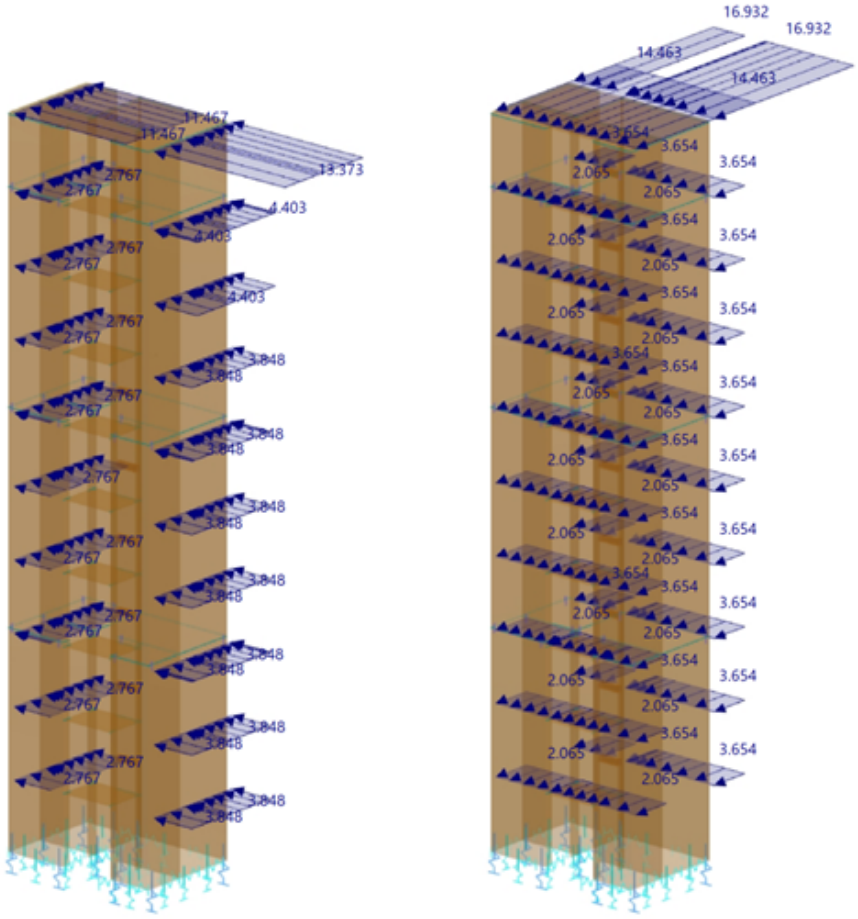

Figure D.8: Wind loads on the structure of the core model for directions X+ (left) and Y+ (right)

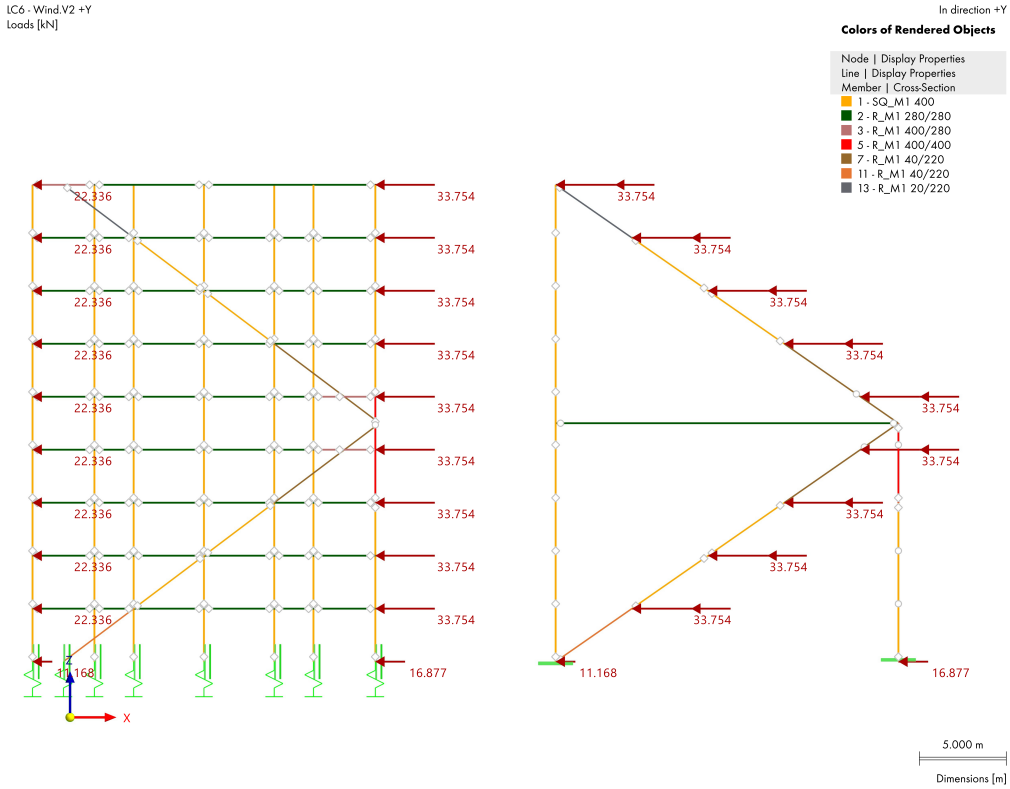

(a) +Y wind loads [kN]

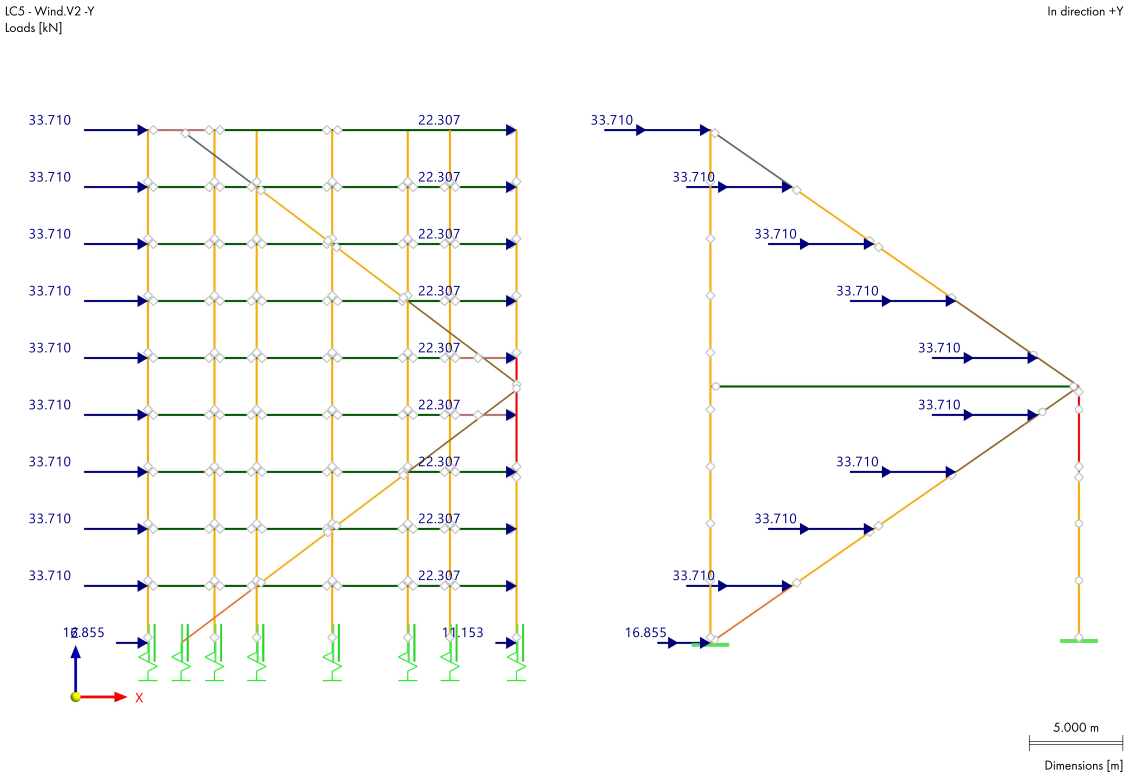

(b) −Y wind loads [kN]

Figure D.9: Wind loads on the façade in the X-plane for both directions.

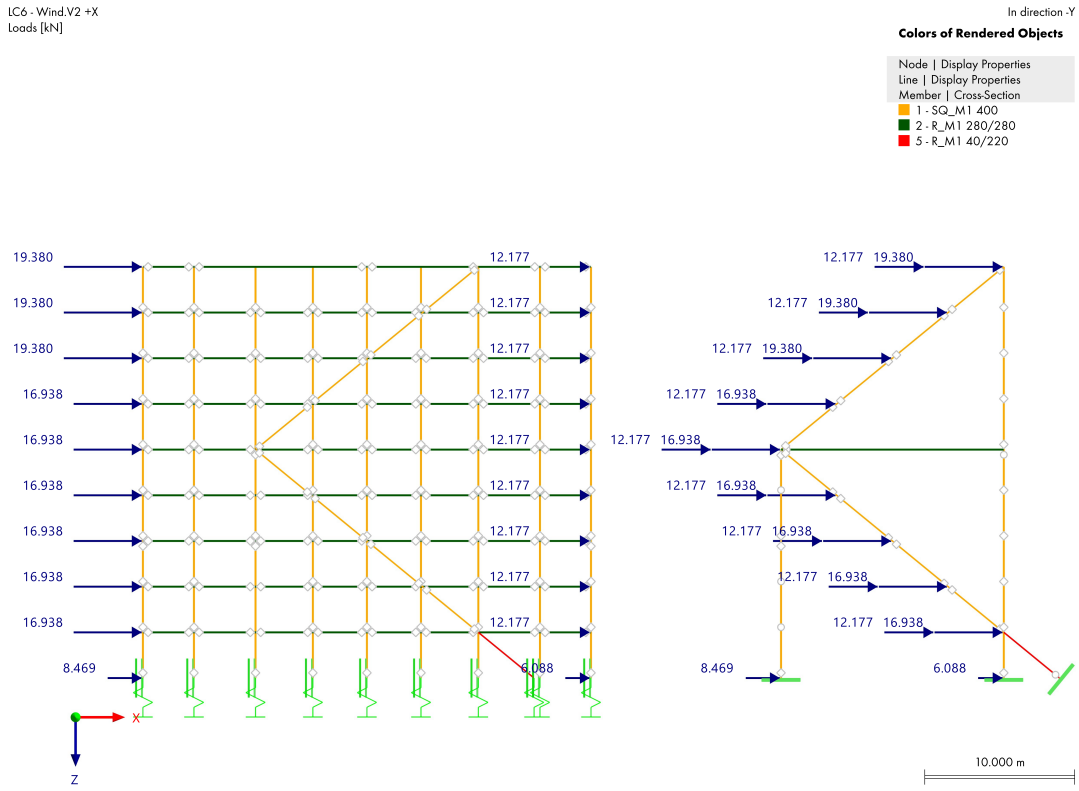

(a) +X wind loads [kN]

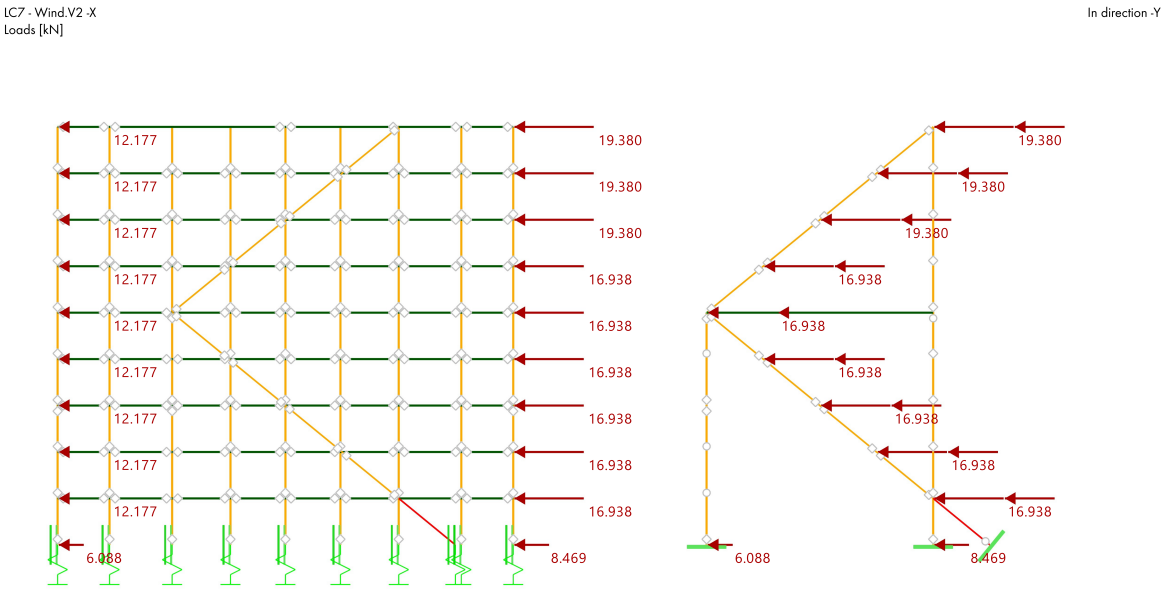

(b) −X wind loads [kN]

Figure D.10: Wind loads on the façade in the Y-plane for both directions.

D.2. Self weight

The self weight used in the RFEM 6 models originates from the RFEM 5 model used in the design of the building and is in correspondence with code NEN-EN 1991-1-1:2002. It exists out of surface loads 1.50 kN/m^2 (outside) and 2.75 kN/m^2 (inside), line loads 1.0 kN/m and 3.0 kN/m depending on the façade, and point loads for the balconies. Visualizations of these loads are found in the Figures below.

The self weight is also applied on the core and 2D models by adding the amount of load that are taken up by the structural parts in these models. For the core models this means that the self weight exists out of the surface loads for the surrounding surfaces, while for the 2D façade models the additional weight of the façades and balconies are also taken into account.

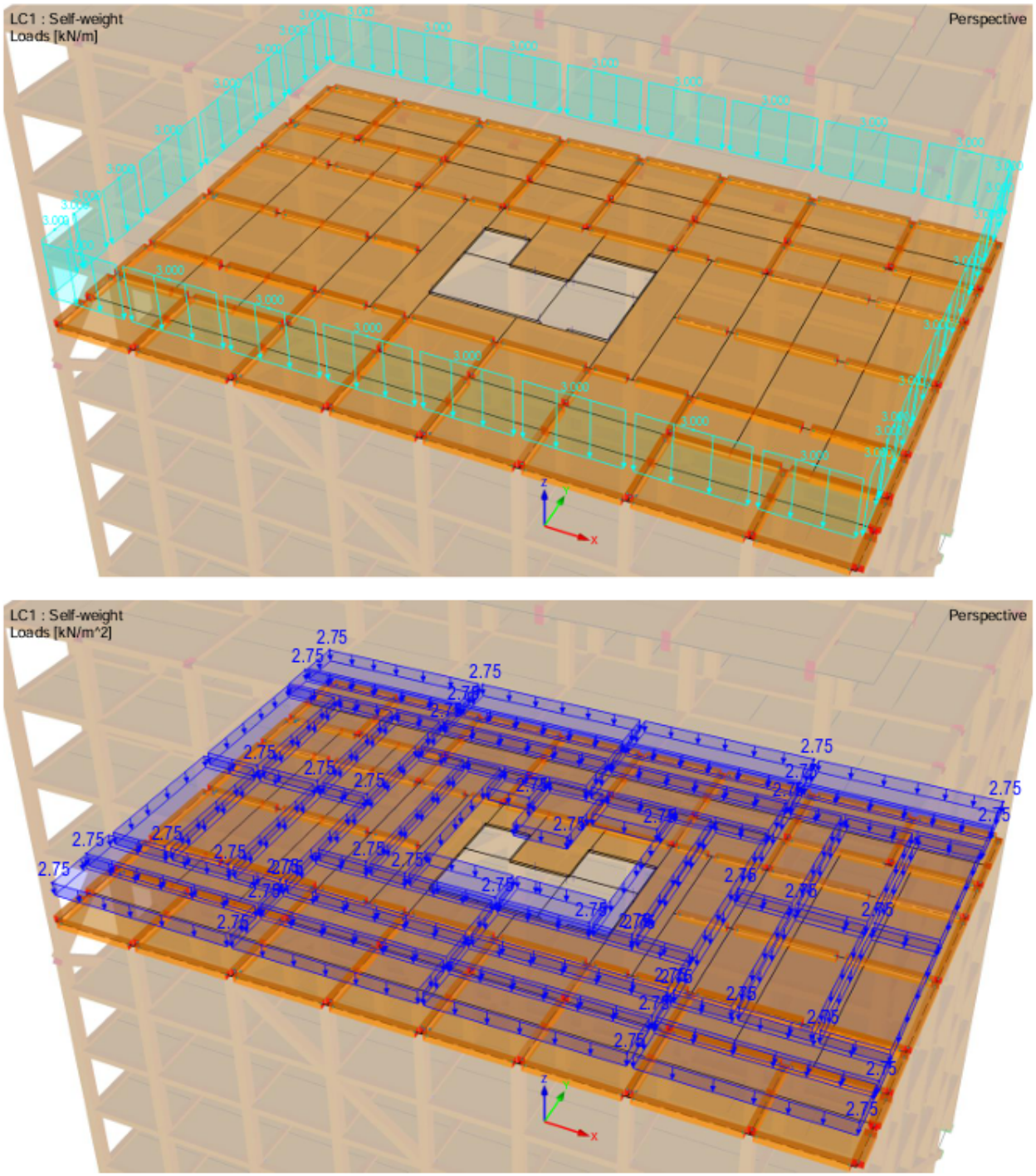

Figure D.11: Self weight on a typical floor [kN/m] by CLT-s

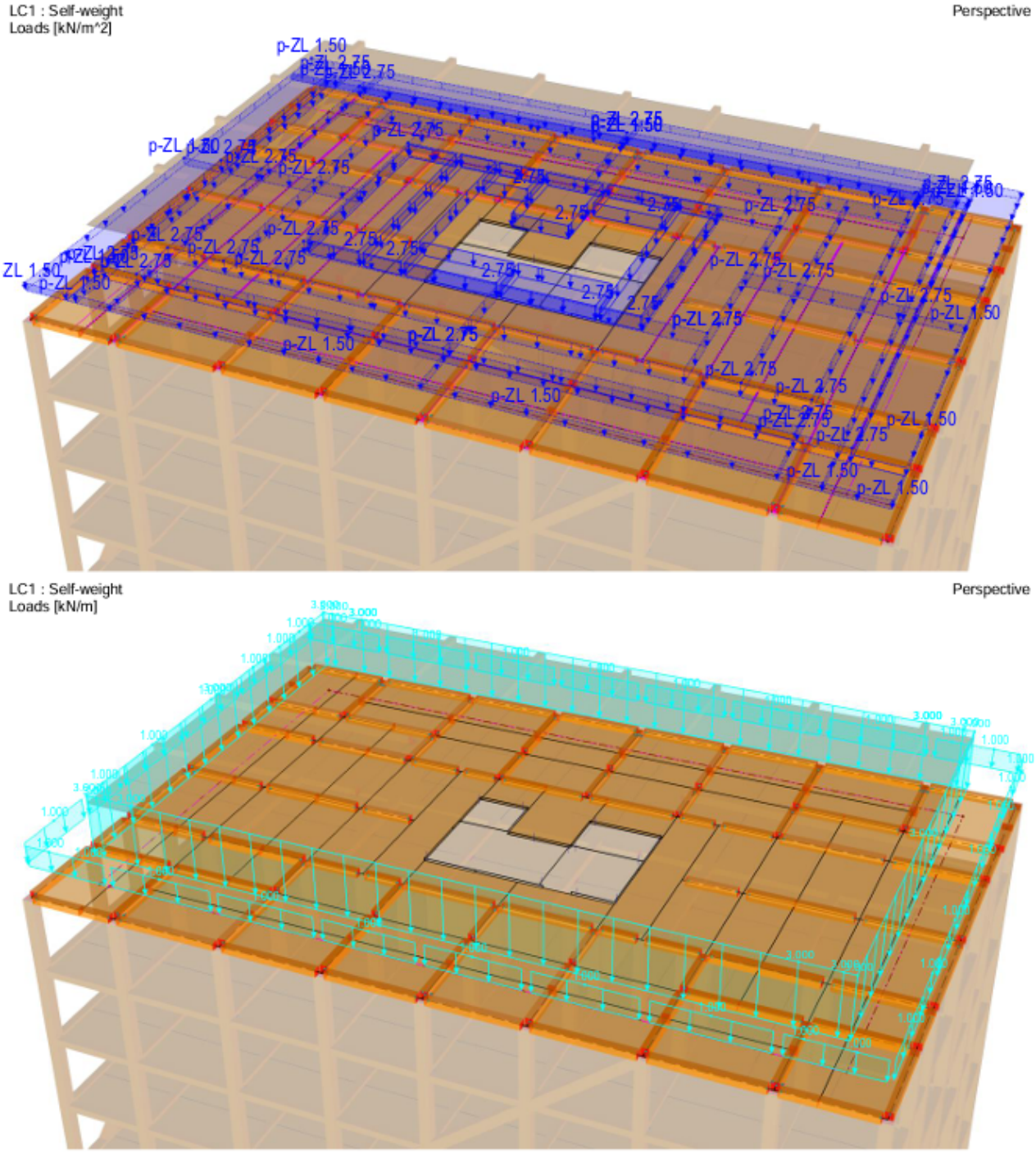

Figure D.12: Self weight on the top level [kN/m] by CLT-s

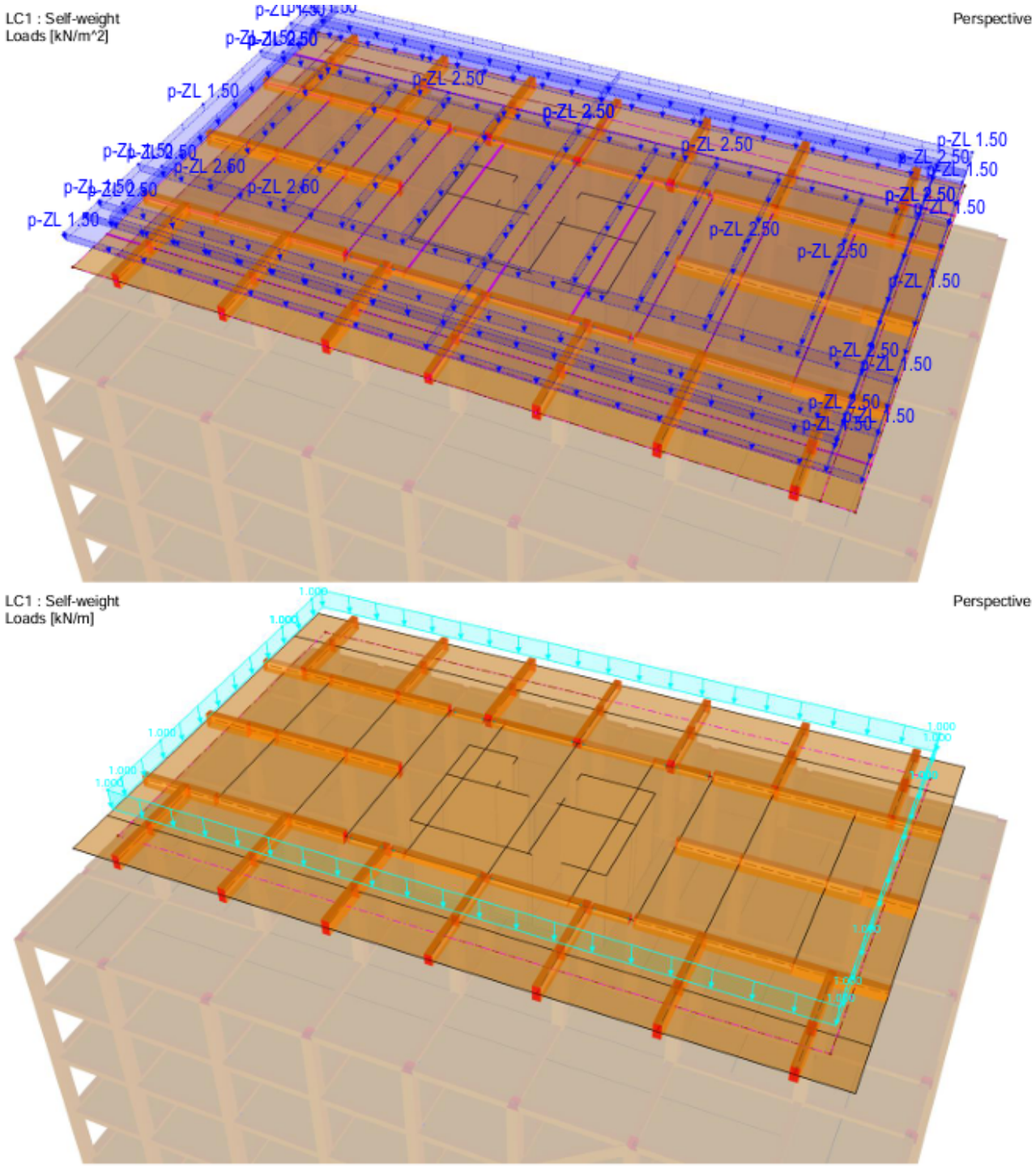

Figure D.13: Self weight on the roof [kN/m] by CLT-s

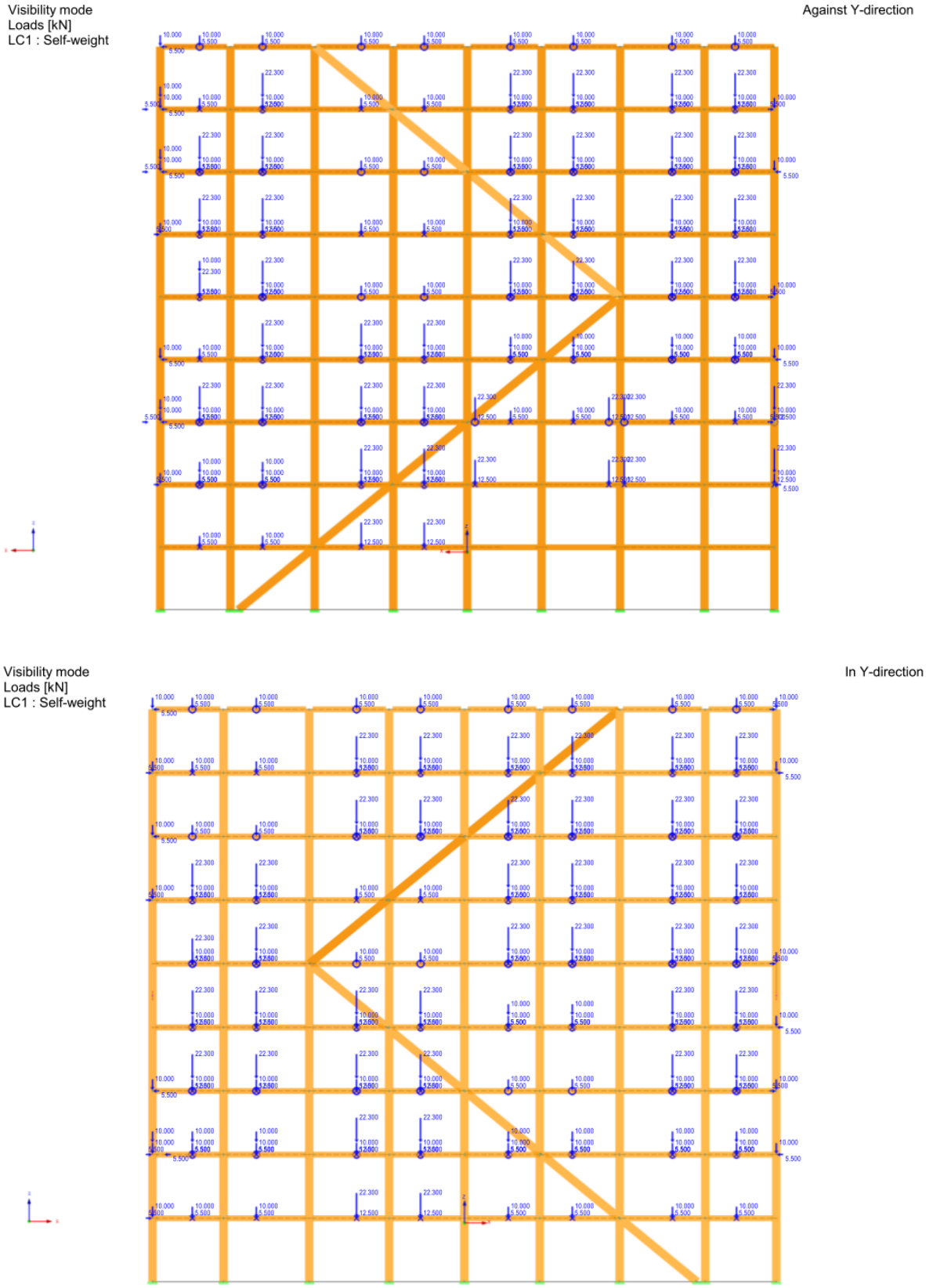

Figure D.14: Point loads caused by the self weight of the balconies on the wide façade [kN] by CLT-s

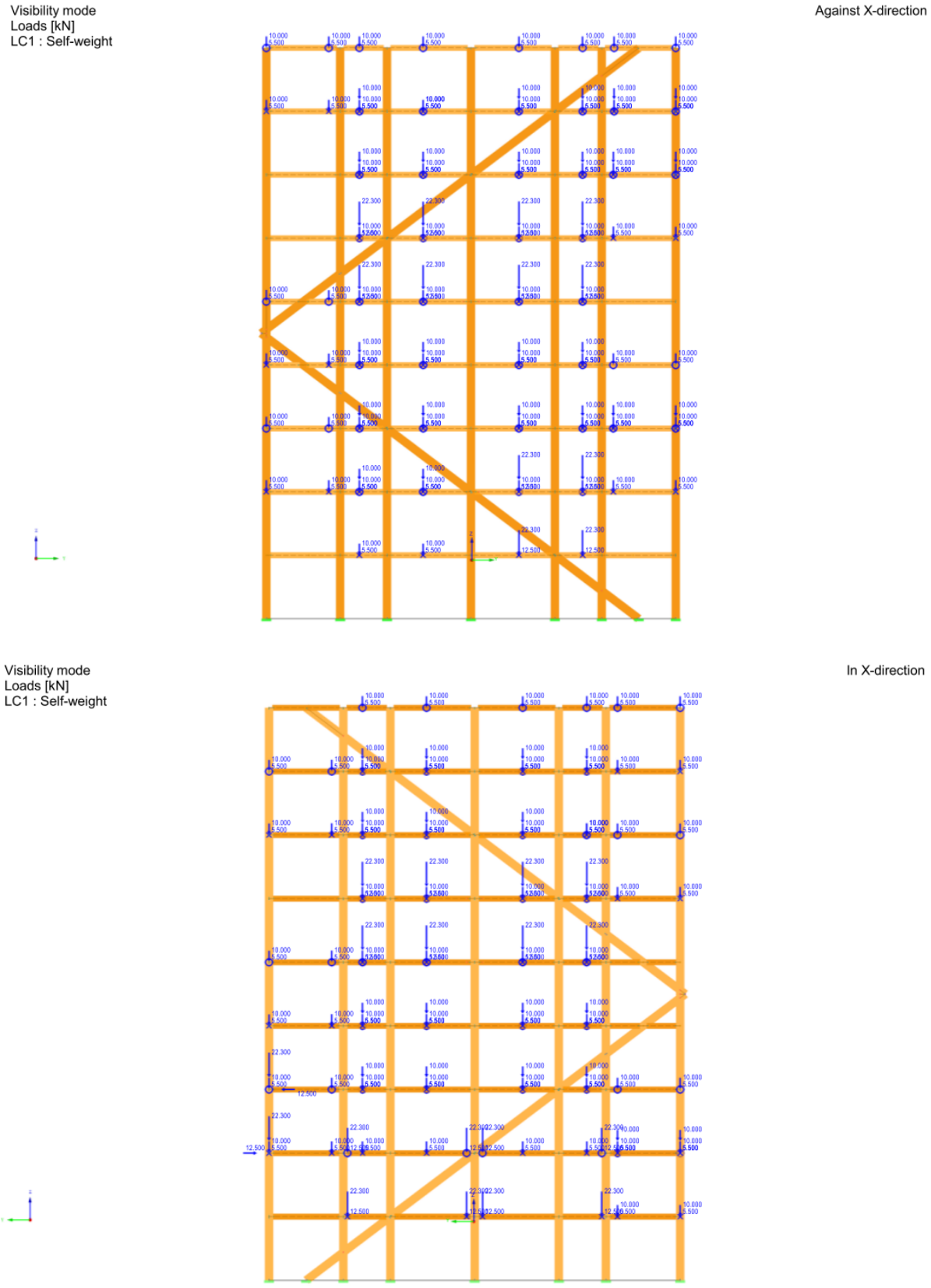

Figure D.15: Point loads caused by the self weight of the balconies on the wide façade [kN] by CLT-s

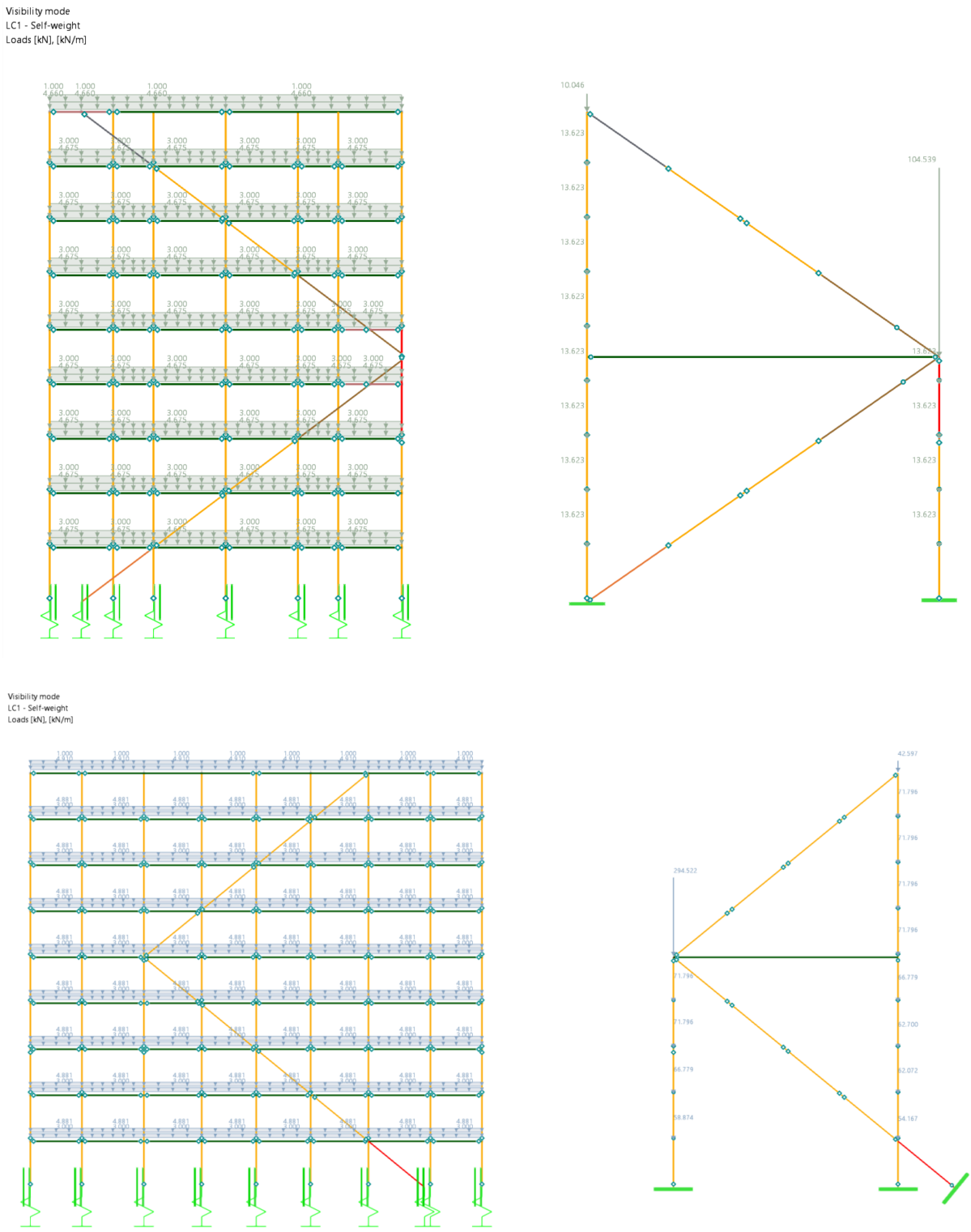

Figure D.16: Self weight on the 2D façade models without the load point loads for the balconies

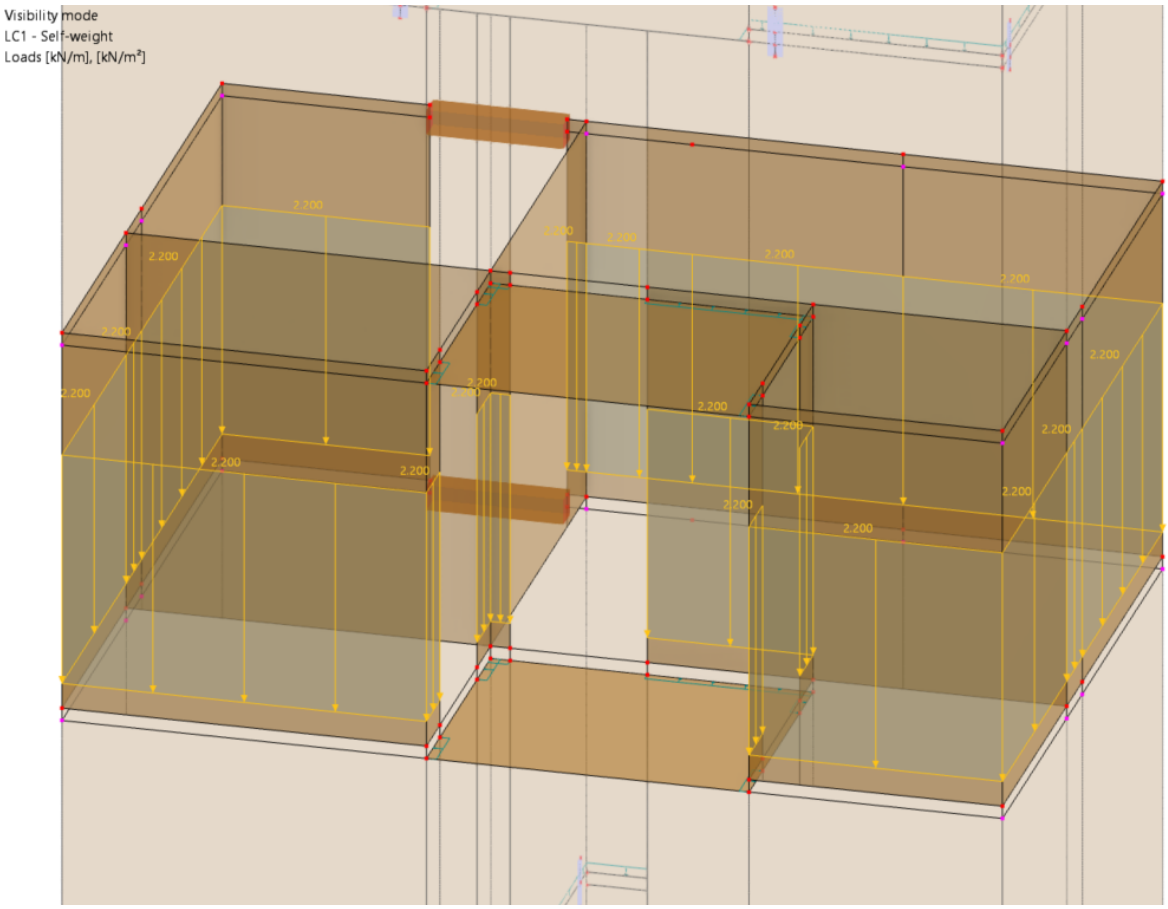

Figure D.17: Self weight of the core [kN/m]